

## **INFORMATION TO USERS**

**This manuscript has been reproduced from the microfilm master. UMI films the text directly from the original or copy submitted. Thus, some thesis and dissertation copies are in typewriter face, while others may be from any type of computer printer.**

**The quality of this reproduction is dependent upon the quality of the copy submitted. Broken or indistinct print, colored or poor quality illustrations and photographs, print bleedthrough, substandard margins, and improper alignment can adversely affect reproduction.**

**In the unlikely event that the author did not send UMI a complete manuscript and there are missing pages, these will be noted. Also, if unauthorized copyright material had to be removed, a note will indicate the deletion.**

**Oversize materials (e.g., maps, drawings, charts) are reproduced by sectioning the original, beginning at the upper left-hand corner and continuing from left to right in equal sections with small overlaps.**

**Photographs included in the original manuscript have been reproduced xerographically in this copy. Higher quality 6" x 9" black and white photographic prints are available for any photographs or illustrations appearing in this copy for an additional charge. Contact UMI directly to order.**

**Bell & Howell Information and Learning  
300 North Zeeb Road, Ann Arbor, MI 48106-1346 USA  
800-521-0600**

**UMI<sup>®</sup>**



UNIVERSITY OF OKLAHOMA

GRADUATE COLLEGE

MECHANISMS OF ELECTROPHILIC AROMATIC SUBSTITUTION REACTIONS OF  
( $\eta^6$ -ARENE)MOLYBDENUM(PHOSPHINE)<sub>3</sub> COMPLEXES

A Dissertation

SUBMITTED TO THE GRADUATE FACULTY

in partial fulfillment of the requirements for the

degree of

Doctor of Philosophy

By

VICTOR SAM ASIRVATHAM

Norman, Oklahoma

2000

UMI Number: 9977947

**UMI**<sup>®</sup>

---

UMI Microform 9977947

Copyright 2000 by Bell & Howell Information and Learning Company.

All rights reserved. This microform edition is protected against  
unauthorized copying under Title 17, United States Code.

---

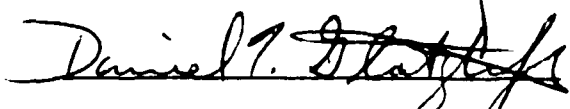
Bell & Howell Information and Learning Company  
300 North Zeeb Road  
P.O. Box 1346  
Ann Arbor, MI 48106-1346

**© Copyright by VICTOR SAM ASIRVATHAM 2000  
All Rights Reserved.**

MECHANISMS OF ELECTROPHILIC AROMATIC SUBSTITUTION REACTIONS OF  
( $\eta^6$ -ARENE)MOLYBDENUM(PHOSPHINE)<sub>3</sub> COMPLEXES

A DISSERTATION APPROVED FOR THE  
DEPARTMENT OF CHEMISTRY AND BIOCHEMISTRY

BY


## REPRODUCTION PERMISSION

Portions of this dissertation have been reported in the following published or submitted papers.

Portions of CHAPTER 2 was published in the article "Electronic Factors for Protonation of an Organometallic Molecule: Photoelectron Spectroscopy and Electron Paramagnetic Resonance Study of  $[(\eta^6\text{-C}_6\text{H}_6)\text{Mo}(\text{TRIPOD})]^{0/+}$ " Asirvatham, V. S.; Gruhn, N. E.; Lichtenberger, D. L.; Ashby, M. T. *Organometallics* **2000**, *19*, 2215-2227. (Reprinted in part with permission from Organometallics. Copyright 2000)

Portions of CHAPTER 3 was published in the article "Stereo-electronic Factors That Influence Kinetic and Thermodynamic Sites of Protonation of  $(\eta^6\text{-Arene})\text{molybdenum}(\text{phosphine})_3$  Complexes" Ashby, M. T.; Asirvatham, V. S.; Kowalski, A. S.; Khan, M. A. *Organometallics* **1999**, *18*, 5004-5016. (Reprinted in part with permission from Organometallics. Copyright 1999)

Portions of CHAPTER 5 was submitted to be published in the article "Synthesis of Bis( $\eta^6\text{-alkylbenzene})\text{molybdenum}$  by Arene Metathesis" Asirvatham, V. S.; Ashby, M. T. *J. Chem. Soc. Chem. Commun.* accepted with revision

## COWORKERS AND COLLABORATORS

This project was initiated by Dr. Angela S. Kowalski, NALCO, Naperville, IL. The mechanism of protonation of  $(\eta^6\text{-C}_6\text{H}_6)\text{Mo}(\text{TRIPOD})$  and related experiments described in Chapter 1 are her contributions.

Photoelectron Spectroscopy was carried out by Dr. Nadine E. Gruhn, Department of Chemistry, University of Arizona, Tucson, AZ. Dr. Gruhn obtained the PES spectra of  $(\eta^6\text{-C}_6\text{H}_6)\text{Mo}(\text{CO})_3$ ,  $(\eta^6\text{-C}_6\text{H}_3\text{Me}_3)\text{Mo}(\text{CO})_3$ ,  $(\eta^6\text{-C}_6\text{H}_6)\text{Mo}(\text{TRIPOD})$ ,  $\text{PPh}_2\text{Me}$  and  $\text{TRIPOD}$ . She also made the assignments of ionizations and related analysis.

Theoretical Calculations were performed by Prof. Dennis L. Lichtenberger, Department of Chemistry, University of Arizona, Tucson, AZ. Prof. Lichtenberger carried out all theoretical calculations described in Chapter 2.

The EPR spectra and simulations were obtained by Prof. Michael T. Ashby, Department Chemistry & Biochemistry, University of Oklahoma, Norman, OK. Prof. Ashby also performed the calculations described in Chapter 3 of this dissertation.

Dr. Masood A. Khan, Department of Chemistry & Biochemistry, University of Oklahoma, Norman, OK determined all the single crystal structures described in this dissertation.

MECHANISMS OF ELECTROPHILIC AROMATIC SUBSTITUTION REACTIONS OF  
( $\eta^6$ -ARENE)MOLYBDENUM(PHOSPHINE)<sub>3</sub> COMPLEXES

TABLE OF CONTENTS

|                             | page   |    |
|-----------------------------|--|----|
| LIST OF ABBREVIATIONS ..... | ix   |    |
| LIST OF FIGURES .....       | x  |    |
| LIST OF SCHEMES .....       | xi   |    |
| LIST OF TABLES .....        | xii  |    |
| ABSTRACT .....              | xiii   |    |
| <br>                        |  |    |
| Chapter 1                   | INTRODUCTION..... 1  |    |
|                             | 1.1 Introduction .....   | 1  |
|                             | 1.2 Literature Overview .....  | 2  |
|                             | 1.3 Mechanism of Protonation of ( $\eta^6$ -C <sub>6</sub> H <sub>6</sub> )Mo(TRIPOD).....   | 4  |
|                             | 1.4 Outlook .....  | 10 |
|                             | 1.5 Bibliography .....   | 12 |
| <br>                        |  |    |
| Chapter 2                   | ELECTRONIC STRUCTURE OF ( $\eta^6$ -C <sub>6</sub> H <sub>6</sub> )Mo(L) <sub>3</sub><br>AND [( $\eta^6$ -C <sub>6</sub> H <sub>6</sub> )Mo(L) <sub>3</sub> ] <sup>+</sup> ..... | 14 |
|                             | 2.1 Introduction .....   | 14 |
|                             | 2.2 Literature Overview .....  | 15 |
|                             | 2.3 Photoelectron Spectra.....   | 16 |
|                             | 2.4 Cyclic Voltammetry .....   | 26 |
|                             | 2.5 Oxidation and EPR.....   | 27 |
|                             | 2.6 Theoretical Calculations .....   | 35 |
|                             | 2.7 Summary .....  | 44 |
|                             | 2.8 Bibliography .....   | 46 |
| <br>                        |  |    |
| Chapter 3                   | EFFECT OF PHOSPHORUS LIGAND VARIATION<br>ON THE MECHANISM OF PROTONATION OF<br>( $\eta^6$ -C <sub>6</sub> H <sub>6</sub> )Mo(PHOSPHINE) <sub>3</sub> COMPLEXES .....             | 48 |
|                             | 3.1 Introduction .....   | 48 |
|                             | 3.2 Literature Overview .....  | 48 |
|                             | 3.3 Synthesis of ( $\eta^6$ -C <sub>6</sub> H <sub>6</sub> )Mo(phosphine) <sub>3</sub> Complexes.....  | 51 |
|                             | 3.4 Isotope Tracer Studies .....   | 52 |

|                  |  |            |
|------------------|--|------------|
|                  | 3.5 Reaction of Acid with ( $\eta^6\text{-C}_6\text{H}_6$ )Mo(TRIPHOS).....  | 62         |
|                  | 3.6 Summary .....  | 74         |
|                  | 3.7 Bibliography .....   | 74         |
| <b>Chapter 4</b> | <b>EFFECT OF ELECTROPHILE VARIATION ON THE<br/>MECHANISM OF AROMATIC ELECTROPHILIC<br/>SUBSTITUTION OF (<math>\eta^6\text{-C}_6\text{H}_6</math>)Mo(TRIPOD).....</b> | <b>77</b>  |
|                  | 4.1 Introduction .....   | 77         |
|                  | 4.2 Literature Overview .....  | 77         |
|                  | 4.3 Reactions with [ $\text{CH}_2=\text{NMe}_2$ ]I .....   | 80         |
|                  | 4.4 Methylation.....   | 81         |
|                  | 4.5 Reactions with Electrophiles other than Proton.....  | 91         |
|                  | 4.6 Summary .....  | 92         |
|                  | 4.7 Bibliography .....   | 92         |
| <b>Chapter 5</b> | <b>EFFECT OF ARENE LIGAND SUBSTITUTION<br/>ON THE MECHANISM OF PROTONATION OF<br/>(<math>\eta^6\text{-ARENE}</math>)Mo(TRIPOD) COMPLEXES.....</b>                    | <b>94</b>  |
|                  | 5.1 Introduction .....   | 94         |
|                  | 5.2 Literature Overview .....  | 94         |
|                  | 5.3 Synthesis .....  | 98         |
|                  | 5.4 Reactions .....  | 102        |
|                  | 5.5 Summary .....  | 102        |
|                  | 5.6 Bibliography .....   | 103        |
| <b>Chapter 6</b> | <b>EXPERIMENTAL.....</b>   | <b>105</b> |
|                  | 6.1 Chemicals and Solvents .....   | 105        |
|                  | 6.2 Instruments and Methods.....   | 111        |
|                  | 6.3 Crystal Structure Data.....  | 115        |
|                  | 6.4 Selected NMR Spectra.....  | 161        |
|                  | 6.5 Bibliography .....   | 175        |
| <b>Chapter 7</b> | <b>CONCLUSIONS .....</b>   | <b>176</b> |
|                  | 7.1 Conclusions .....  | 176        |
|                  | 7.2 Future Work .....  | 178        |
|                  | 7.3 Bibliography .....   | 179        |

## LIST OF ABBREVIATIONS

| Abbreviation | expanded form                                   |
|--------------|---|
| br           | broad   |
| Cp           | cyclopentadienyl                                |
| Cp*          | pentamethylcyclopentadienyl                     |
| d            | doublet   |
| DIP          | direct insertion probe                          |
| dmpe         | 1,2-bis(dimethylphosphino)ethane                |
| dppe         | 1,2-bis(diphenylphosphino)ethane                |
| dt           | doublet of triplets                             |
| EPR          | electron paramagnetic resonance                 |
| FAB          | fast atom bombardment                           |
| IR           | infrared  |
| NMR          | nuclear magnetic resonance                      |
| PES          | photoelectron spectroscopy                      |
| prophos      | 1,2-bis(diphenylphosphino)propane               |
| q            | quartet   |
| s            | singlet   |
| t            | triplet   |
| td           | triplet of doublets                             |
| temp.        | temperature                                     |
| TRIPHOS      | bis(diphenylphosphinoethyl)phenyl phosphine     |
| TRIPOD       | tris(1,1,1-diphenylphosphinoethyl)methyl ethane |
| UV-VIS       | ultraviolet-visible                             |
| °C           | centigrade units                                |
| HOMO         | highest occupied molecular orbital              |
| SOMO         | singly occupied molecular orbital               |
| LUMO         | lowest unoccupied molecular orbital             |
| DFT          | density functional theory                       |
| HF           | Hartree-Fock                                    |
| hfc          | hyperfine coupling                              |

## LIST OF FIGURES

|             |  |    |
|-------------|--|----|
| Figure 2.1  | He I photoelectron spectrum of $(\eta^6\text{-C}_6\text{H}_6)\text{Mo}(\text{CO})_3$ ..... 18  | 18 |
| Figure 2.2  | He I and He II photoelectron spectra of<br>$(\eta^6\text{-1,3,5-C}_6\text{H}_3\text{Me}_3)\text{Mo}(\text{CO})_3$ ..... 20   | 20 |
| Figure 2.3  | He I photoelectron spectra of PPh <sub>2</sub> Me and TRIPOD ..... 21  | 21 |
| Figure 2.4  | He I and He II photoelectron spectra of $(\eta^6\text{-C}_6\text{H}_6)\text{Mo}(\text{TRIPOD})$ ..... 23   | 23 |
| Figure 2.5  | Cyclic voltammogram of $(\eta^6\text{-C}_6\text{H}_6)\text{Mo}(\text{TRIPOD})$ ..... 25  | 25 |
| Figure 2.6  | X-band EPR spectrum (solid line) of $[(\eta^6\text{-C}_6\text{H}_6)\text{Mo}(\text{TRIPOD})]^+$<br>at 4 K in THF and a simulation (broken line) ..... 28   | 28 |
| Figure 2.7  | X-band EPR spectrum of $[(\eta^6\text{-C}_6\text{D}_6)\text{Mo}(\text{TRIPOD})]^+$<br>at 4 K in THF ..... 29   | 29 |
| Figure 2.8  | First harmonic Q-band EPR spectrum of $[(\eta^6\text{-C}_6\text{D}_6)\text{Mo}(\text{TRIPOD})]^+$<br>at 50 K in THF ..... 31   | 31 |
| Figure 2.9  | Second harmonic Q-band EPR spectrum of $[(\eta^6\text{-C}_6\text{D}_6)\text{Mo}(\text{TRIPOD})]^+$<br>at 50 K in THF ..... 32  | 32 |
| Figure 2.10 | Single crystal X-ray structure of $[(\eta^6\text{-C}_6\text{H}_6)\text{Mo}(\text{TRIPOD})]\text{PF}_6$ ..... 33  | 33 |
| Figure 2.11 | Calculated molecular orbitals of $(\eta^6\text{-C}_6\text{H}_6)\text{Mo}(\text{CO})_3$<br>The e symmetry orbital (top) and a <sub>1</sub> symmetry orbital (bottom)..... 38  | 38 |
| Figure 2.12 | The calculated percentage contributions of metal, arene and<br>monodentate ligands to the frontier molecular orbitals of<br>$[(\eta^6\text{-C}_6\text{H}_6)\text{Mo}(\text{CO})_3]^{0/+}$ and $[(\eta^6\text{-C}_6\text{H}_6)\text{Mo}(\text{PH}_3)_3]^{0/+}$ ..... 39 | 39 |
| Figure 2.13 | Calculated conformations of the TRIPOD molecule. <i>anti, anti,</i><br><i>anti</i> (top) and <i>anti, gauche, gauche</i> (bottom) conformations ..... 40   | 40 |
| Figure 2.14 | Intrinsic reaction coordinate diagram for the protonation<br>of $(\eta^6\text{-C}_6\text{H}_6)\text{Mo}(\text{PH}_3)_3$ via direct attack on the metal ( $\square$ , A'→E)<br>and indirect attack on the arene (O, A→B→C→D→E)..... 45                                  | 45 |
| Figure 3.1  | Thermal ellipsoid drawing (50% probability) of<br>$(\eta^6\text{-C}_6\text{H}_6)\text{Mo}(\text{TRIPOD})$ ( <b>1</b> ) sideview (top) and top view (bottom) .... 57  | 57 |
| Figure 3.2  | Thermal ellipsoid drawing (50% probability) of<br>$(\eta^6\text{-C}_6\text{H}_6)\text{Mo}(\text{TRIPHOS})$ ( <b>4</b> ) sideview (top) and top view (bottom) .. 58   | 58 |
| Figure 3.3  | Thermal ellipsoid drawing (50% probability) of<br>$(\eta^6\text{-C}_6\text{H}_6)\text{Mo}(\text{PMePh}_2)_3$ ( <b>7</b> ) sideview (top) and top view (bottom) .... 59   | 59 |
| Figure 3.4  | Thermal ellipsoid drawing (50% probability) of<br>$(\eta^6\text{-C}_6\text{H}_6)\text{Mo}(\text{PMe}_2\text{Ph})_3$ ( <b>8</b> ) sideview (top) and top view (bottom). ... 60  | 60 |

|              |   |     |
|--------------|---|-----|
| Figure 3.5   | CPK models (left) and surface electron density plots of<br>1, 4, 7, 8, and 9 .....  | 63  |
| Figure 3.6   | Plot of [4], [5], [5a], and [6] versus time (sec) at -60 °C.....  | 70  |
| Figure 3.7   | Plot of ln[6] versus time (sec) at -60 °C .....   | 71  |
| Figure 3.8   | Thermal ellipsoid drawing of $[(\eta^6\text{-C}_6\text{H}_6)\text{MoH}(\text{TRIPOD})]\text{PF}_6$<br>(50% probability) sideview (top) and top view (bottom) .....  | 72  |
| Figure 3.9   | Thermal ellipsoid drawing of $[(\eta^6\text{-C}_6\text{H}_6)\text{MoH}(\text{TRIPHOS})]\text{PF}_6$<br>(50% probability) sideview (top) and top view (bottom) ..... | 73  |
| Figure 4.1   | Plot of $^{31}\text{P}$ integrations of resonances around 27, 19, and<br>-28 ppm versus temperature ( °C).....  | 88  |
| Figure 5.1   | Thermal ellipsoid drawing of $(\eta^6\text{-C}_6\text{H}_5\text{SiMe}_3)\text{Mo}(\text{TRIPOD})$ .....   | 102 |
| Figure 6.1.  | $^1\text{H}$ NMR spectrum of $(\eta^6\text{-C}_6\text{D}_6)\text{Mo}(\text{TRIPOD}) + \text{CF}_3\text{SO}_3\text{H}$ .....   | 164 |
| Figure 6.2.  | $^2\text{H}$ NMR spectrum of $(\eta^6\text{-C}_6\text{D}_6)\text{Mo}(\text{TRIPOD}) + \text{CF}_3\text{SO}_3\text{H}$ .....   | 165 |
| Figure 6.3.  | $^1\text{H}$ NMR spectrum of $(\eta^6\text{-C}_6\text{D}_6)\text{Mo}(\text{TRIPHOS}) + \text{CF}_3\text{SO}_3\text{H}$ .....  | 166 |
| Figure 6.4.  | $^2\text{H}$ NMR spectrum of $(\eta^6\text{-C}_6\text{D}_6)\text{Mo}(\text{TRIPHOS}) + \text{CF}_3\text{SO}_3\text{H}$ .....  | 167 |
| Figure 6.5.  | $^{31}\text{P}$ NMR spectrum of $(\eta^6\text{-C}_6\text{D}_6)\text{Mo}(\text{TRIPHOS}) + \text{CF}_3\text{SO}_3\text{H}$ .....                                     | 168 |
| Figure 6.6.  | $^1\text{H}$ NMR spectrum of $(\eta^6\text{-C}_6\text{D}_6)\text{Mo}(\text{PPh}_2\text{Me})_3 + \text{CF}_3\text{SO}_3\text{H}$ .....                               | 169 |
| Figure 6.7.  | $^2\text{H}$ NMR spectrum of $(\eta^6\text{-C}_6\text{D}_6)\text{Mo}(\text{PPh}_2\text{Me})_3 + \text{CF}_3\text{SO}_3\text{H}$ .....                               | 170 |
| Figure 6.8.  | $^1\text{H}$ NMR spectrum of $(\eta^6\text{-C}_6\text{D}_6)\text{Mo}(\text{PMe}_2\text{Ph})_3 + \text{CF}_3\text{SO}_3\text{H}$ .....                               | 171 |
| Figure 6.9.  | $^2\text{H}$ NMR spectrum of $(\eta^6\text{-C}_6\text{D}_6)\text{Mo}(\text{PMe}_2\text{Ph})_3 + \text{CF}_3\text{SO}_3\text{H}$ .....                               | 172 |
| Figure 6.10. | $^1\text{H}$ NMR spectrum of $(\eta^6\text{-C}_6\text{D}_6)\text{Mo}(\text{PMe}_3)_3 + \text{CF}_3\text{SO}_3\text{H}$ .....  | 173 |
| Figure 6.11. | $^2\text{H}$ NMR spectrum of $(\eta^6\text{-C}_6\text{D}_6)\text{Mo}(\text{PMe}_3)_3 + \text{CF}_3\text{SO}_3\text{H}$ .....  | 174 |
| Figure 6.12. | $^1\text{H}$ NMR spectrum of $(\eta^6\text{-C}_6\text{H}_5\text{CH}_3)\text{Mo}(\text{TRIPOD})$ .....   | 175 |
| Figure 6.13. | $^1\text{H}$ NMR spectrum of $(\eta^6\text{-C}_6\text{H}_5\text{SiMe}_3)\text{Mo}(\text{TRIPOD})$ .....   | 176 |

## LIST OF SCHEMES

|            |   |    |
|------------|---|----|
| Scheme 1.1 | Alternate pathways for proton exchange with $(\eta^6\text{-arene})\text{ML}_n$ .....  | 5  |
| Scheme 1.2 | Proposed mechanism for isotope exchange in $(\eta^6\text{-C}_6\text{H}_6)\text{Cr}(\text{CO})_3$ .....                        | 7  |
| Scheme 1.3 | Possible kinetic products upon addition of $\text{D}^+$ to<br>$(\eta^6\text{-C}_6\text{H}_6)\text{Mo}(\text{TRIPOD})$ .....   | 9  |
| Scheme 1.4 | Factors governing the electrophilic aromatic substitution in<br>$(\eta^6\text{-C}_6\text{H}_6)\text{Mo}(\text{TRIPOD})$ ..... | 11 |
| Scheme 3.1 | Possible products upon addition of $\text{H}^+$ to $(\eta^6\text{-C}_6\text{D}_6)\text{Mo}(\text{P})_3$ .....                 | 55 |
| Scheme 3.2 | Reaction of acid with $(\eta^6\text{-C}_6\text{H}_6)\text{Mo}(\text{TRIPHOS})$ .....  | 75 |
| Scheme 4.1 | Alternate pathways for electrophile reaction with $(\eta^6\text{-arene})\text{ML}_n$ .....                                    | 80 |
| Scheme 4.2 | Green's proposed mechanism for the alkylation of<br>$(\eta^6\text{-C}_6\text{H}_6)\text{Mo}(\text{dmpe})(\text{PMe}_3)$ ..... | 84 |
| Scheme 4.3 | Reaction of $\text{MeI}$ with $(\eta^6\text{-C}_6\text{H}_6)\text{Mo}(\text{TRIPOD})$ .....                                   | 86 |
| Scheme 4.4 | Proposed mechanism for the addition of $\text{Me}^+$ to<br>$(\eta^6\text{-C}_6\text{H}_6)\text{Mo}(\text{TRIPOD})$ .....      | 91 |
| Scheme 5.1 | Preferred sites of nucleophilic and electrophilic substitutions .....   | 99 |

## LIST OF TABLES

|              |   |     |
|--------------|---|-----|
| Table 2.1    | Assignments of photoelectron ionizations and labels of primary characters .....   | 17  |
| Table 2.2    | Selected interatomic distances (Å) and bond angles (deg) for <b>1</b> ·PF <sub>6</sub> and <b>1</b> .....   | 34  |
| Table 2.3    | Selected interatomic distances (Å) and angles (deg) for [(η <sup>6</sup> -C <sub>6</sub> H <sub>6</sub> )Mo(CO) <sub>3</sub> ] <sup>0+</sup> and energies (eV) to lowest cation states.....               | 36  |
| Table 2.4    | Modeled vertical ionization energies to lowest positive ion states of (η <sup>6</sup> -C <sub>6</sub> H <sub>6</sub> )Mo(CO) <sub>3</sub> .....   | 37  |
| Table 2.5    | Selected interatomic distances (Å) and angles (deg) for [(η <sup>6</sup> -C <sub>6</sub> H <sub>6</sub> )Mo(PH <sub>3</sub> ) <sub>3</sub> ] <sup>0+</sup> and energies (eV) to lowest cation states..... | 41  |
| Table 2.6    | Modeled vertical ionization energies to lowest positive ion states of (η <sup>6</sup> -C <sub>6</sub> H <sub>6</sub> )Mo(PH <sub>3</sub> ).....   | 42  |
| Table 3.1    | Percentages of isotopic distribution in tracer studies .....  | 55  |
| Table 3.2    | Selected interatomic distances (Å) and bond angles (deg) for <b>1</b> , <b>4</b> , <b>7</b> , and <b>8</b> .....  | 61  |
| Table 3.3    | Calculated interatomic distances (Å) and bond angles (deg) for <b>1</b> , <b>4</b> , <b>7</b> , <b>8</b> , and <b>9</b> .....   | 62  |
| Table 3.4    | <sup>1</sup> H NMR data for the protonation of (η <sup>6</sup> -C <sub>6</sub> H <sub>6</sub> )Mo(TRIPHOS).....   | 65  |
| Table 3.5    | <sup>31</sup> P NMR data for the protonation of (η <sup>6</sup> -C <sub>6</sub> H <sub>6</sub> )Mo(TRIPHOS).....  | 66  |
| Table 3.6    | Selected interatomic distances (Å) and bond angles (deg) for <b>3</b> ·PF <sub>6</sub> and <b>6</b> ·PF <sub>6</sub> .....  | 74  |
| Table 4.1    | <sup>31</sup> P Integrations from reactions of (η <sup>6</sup> -C <sub>6</sub> H <sub>6</sub> )Mo(TRIPOD) with MeI .....  | 87  |
| Table 5.1    | Isomer ratios for acetylations of (η <sup>6</sup> -C <sub>6</sub> H <sub>5</sub> R)Cr(CO) <sub>3</sub> .....  | 99  |
| Table 5.2    | Selected interatomic distances (Å) and bond angles (deg) for <b>35</b> and <b>1</b> .....   | 103 |
| Table 6.1.1. | Crystal data and structure refinement for [(η <sup>6</sup> -C <sub>6</sub> H <sub>6</sub> )Mo(TRIPOD)]PF <sub>6</sub> ( <b>1</b> ·PF <sub>6</sub> ).....  | 118 |
| Table 6.1.2. | Atomic coordinates (x 10 <sup>4</sup> ) and equivalent isotropic displacement parameters (Å <sup>2</sup> x 10 <sup>3</sup> ) for <b>1</b> ·PF <sub>6</sub> .....  | 119 |
| Table 6.1.3. | Anisotropic displacement parameters (Å <sup>2</sup> x 10 <sup>3</sup> ) for <b>1</b> ·PF <sub>6</sub> .....   | 122 |

|              |   |     |
|--------------|---|-----|
| Table 6.2.1. | Crystal data and structure refinement for<br>( $\eta^6$ -C <sub>6</sub> H <sub>6</sub> )Mo(TRIPHOS) ( <b>4</b> ) .....  | 123 |
| Table 6.2.2. | Atomic coordinates (x 10 <sup>4</sup> ) and equivalent isotropic displacement<br>parameters (Å <sup>2</sup> x 10 <sup>3</sup> ) for <b>4</b> . .....                  | 124 |
| Table 6.2.3. | Anisotropic displacement parameters (Å <sup>2</sup> x 10 <sup>3</sup> ) for <b>4</b> . .....  | 127 |
| Table 6.2.4. | Hydrogen coordinates (x 10 <sup>4</sup> ) and isotropic displacement<br>parameters (Å <sup>2</sup> x 10 <sup>3</sup> ) for <b>4</b> .....                             | 130 |
| Table 6.3.1. | Crystal data and structure refinement for<br>( $\eta^6$ -C <sub>6</sub> H <sub>6</sub> )Mo(PMePh <sub>2</sub> ) <sub>3</sub> ( <b>7</b> ).....                        | 133 |
| Table 6.3.2. | Atomic coordinates (x 10 <sup>4</sup> ) and equivalent isotropic displacement<br>parameters (Å <sup>2</sup> x 10 <sup>3</sup> ) for <b>7</b> .....                    | 134 |
| Table 6.3.3. | Anisotropic displacement parameters (Å <sup>2</sup> x 10 <sup>3</sup> ) for <b>7</b> . .....  | 135 |
| Table 6.3.4. | Hydrogen coordinates (x 10 <sup>4</sup> ) and isotropic displacement<br>parameters (Å <sup>2</sup> x 10 <sup>3</sup> ) for <b>7</b> .....                             | 136 |
| Table 6.4.1. | Crystal data and structure refinement for<br>( $\eta^6$ -C <sub>6</sub> H <sub>6</sub> )Mo(PPhMe <sub>2</sub> ) <sub>3</sub> ( <b>8</b> ).....                        | 137 |
| Table 6.4.2. | Atomic coordinates (x 10 <sup>4</sup> ) and equivalent isotropic displacement<br>parameters (Å <sup>2</sup> x 10 <sup>3</sup> ) for <b>8</b> .....                    | 138 |
| Table 6.4.3. | Anisotropic displacement parameters (Å <sup>2</sup> x 10 <sup>3</sup> ) for <b>8</b> . .....  | 140 |
| Table 6.4.4. | Hydrogen coordinates (x 10 <sup>4</sup> ) and isotropic displacement<br>parameters (Å <sup>2</sup> x 10 <sup>3</sup> ) for <b>8</b> .....                             | 142 |
| Table 6.5.1. | Crystal data and structure refinement for<br>[( $\eta^6$ -C <sub>6</sub> H <sub>6</sub> )MoH(TRIPHOS)]PF <sub>6</sub> ( <b>6</b> ·PF <sub>6</sub> ) .....             | 144 |
| Table 6.5.2. | Atomic coordinates (x 10 <sup>4</sup> ) and equivalent isotropic displacement<br>parameters (Å <sup>2</sup> x 10 <sup>3</sup> ) for <b>6</b> ·PF <sub>6</sub> . ..... | 145 |
| Table 6.5.3. | Anisotropic displacement parameters (Å <sup>2</sup> x 10 <sup>3</sup> ) for <b>6</b> ·PF <sub>6</sub> . .....   | 148 |
| Table 6.5.4. | Hydrogen coordinates (x 10 <sup>4</sup> ) and isotropic displacement<br>parameters (Å <sup>2</sup> x 10 <sup>3</sup> ) for <b>6</b> ·PF <sub>6</sub> . .....          | 151 |
| Table 6.6.1. | Crystal data and structure refinement for<br>( $\eta^6$ -C <sub>6</sub> H <sub>5</sub> SiMe <sub>3</sub> )Mo(TRIPOD) ( <b>35</b> ).....                               | 153 |
| Table 6.6.2. | Atomic coordinates (x 10 <sup>4</sup> ) and equivalent isotropic displacement<br>parameters (Å <sup>2</sup> x 10 <sup>3</sup> ) for <b>35</b> .....                   | 154 |
| Table 6.6.3. | Anisotropic displacement parameters (Å <sup>2</sup> x 10 <sup>3</sup> ) for <b>35</b> .....   | 157 |
| Table 6.6.4. | Hydrogen coordinates (x 10 <sup>4</sup> ) and isotropic displacement<br>parameters (Å <sup>2</sup> x 10 <sup>3</sup> ) for <b>35</b> .....                            | 160 |

## ABSTRACT

The mechanism of protonation of  $(\eta^6\text{-C}_6\text{H}_6)\text{Mo}(\text{TRIPOD})$  (**1**) (TRIPOD = tris(1,1,1-diphenylphosphinoethyl)methyl ethane) to give  $[(\eta^6\text{-C}_6\text{H}_6)\text{MoH}(\text{TRIPOD})]^+$  was reported to involve a cyclohexadienyl intermediate. In this project, the basis of this unusual mechanism was probed by studying the electronic structure of  $(\eta^6\text{-C}_6\text{H}_6)\text{Mo}(\text{TRIPOD})$  using experimental and theoretical methods. Gas phase photoelectron spectra indicate that the highest occupied molecular orbital of  $(\eta^6\text{-C}_6\text{H}_6)\text{Mo}(\text{TRIPOD})$  is metal based with sizable arene character. The theoretical calculations augment the experimental results. One electron oxidation of **1** yields  $[(\eta^6\text{-C}_6\text{H}_6)\text{Mo}(\text{TRIPOD})]^+$  (**1**<sup>+</sup>), the electron paramagnetic resonance spectra of which shows phosphorus and arene hyperfine coupling (hfc). The presence of arene hfc indicates arene character in the singly occupied molecular orbital of **1**<sup>+</sup>. Experimental and theoretical studies of **1** and related model compounds reveal the initial protonation of these compounds takes place at the metal-based frontier orbital with substantial arene character. The TRIPOD ligand makes the metal center of **1** electron-rich while sterically protecting it from electrophilic attack. The TRIPOD ligand in **1** was replaced by four different phosphines with differing steric and electronic requirements. Unlike TRIPOD, some monodentate phosphines and other chelating phosphines do not sterically protect the metal center. This fact was verified by studying the protonation mechanism of  $(\eta^6\text{-C}_6\text{H}_6)\text{Mo}(\text{TRIPHOS})$  (**4**),  $(\eta^6\text{-C}_6\text{H}_6)\text{Mo}(\text{PMePh}_2)_3$  (**7**),  $(\eta^6\text{-C}_6\text{H}_6)\text{Mo}(\text{PMe}_2\text{Ph})_3$  (**8**), and  $(\eta^6\text{-C}_6\text{H}_6)\text{Mo}(\text{PMe}_3)_3$  (**9**). Complexes **7**, **8**, **9** and **4** are protonated at the metal 0%, 22%, 37% and 88%, respectively. The pathways of protonation of the phosphine complexes were followed by isotope tracer studies. The initial site of protonation is partitioned between metal and ring, and is governed by the phosphine size. In general, as the phosphine becomes less bulkier a higher percent of protonation at the metal was observed. The  $(\eta^6\text{-C}_6\text{H}_6)\text{Mo}(\text{TRIPHOS})$  (TRIPHOS = bis(diphenylphosphinoethyl)phenyl phosphine) complex, despite having a bulkier

TRIPHOS ligand shows an anomaly in the trend of ring to metal protonation ratio. Theoretical calculations and CPK models predict the orientation of the TRIPHOS ligand around the metal is the factor for the lower ring to metal protonation ratio. Electrophilic substitution reactions of **1** with various electrophiles were attempted to understand the effect on the mechanism by electrophiles bulkier than proton. The electrophilic methylation of **1** was studied in detail. There are indications the mechanism of methylation is different from that of protonation. A mixture of methylated hydride,  $[(\eta^6\text{-C}_6\text{H}_5\text{Me})\text{MoH}(\text{TRIPOD})]^+$  and unmethylated hydride,  $[(\eta^6\text{-C}_6\text{H}_6)\text{MoH}(\text{TRIPOD})]^+$  were formed in methylation reactions. The origin of the unmethylated hydride in methylation (and in other alkylation) reactions is not well understood. Electrophilic reaction of  $[\text{CH}_2=\text{NMe}_2]^+$  with **1** gives the ring substituted product,  $[(\eta^6\text{-C}_6\text{H}_5\text{CH}_2\text{NMe}_2)\text{MoH}(\text{TRIPOD})]^+$ . Although attempts to isolate the product proved unsuccessful, spectroscopic evidence shows the ring-substituted complex as the only product. The effect of arene ring functionalization on the aromatic electrophilic substitution was studied by protonation of alkylarene derivatives of  $(\eta^6\text{-C}_6\text{H}_6)\text{Mo}(\text{TRIPOD})$ . An effort was made to synthesize  $(\eta^6\text{-C}_6\text{H}_5\text{R})\text{Mo}(\text{TRIPOD})$  [R = Me, Et, i-Pr, t-Bu or SiMe<sub>3</sub>] complexes. The precursors for tripodal complexes,  $(\eta^6\text{-alkylbenzene})_2\text{Mo}$  complexes were synthesized by arene displacement reactions. Heating  $(\eta^6\text{-C}_6\text{H}_6)_2\text{Mo}$  with C<sub>6</sub>H<sub>5</sub>R (R = Me, Et, i-Pr, or t-Bu) at 160 °C and 0.1 torr for 48 hours gives  $(\eta^6\text{-C}_6\text{H}_5\text{R})_2\text{Mo}$ . Reaction of one equivalent of CF<sub>3</sub>SO<sub>3</sub>D with  $(\eta^6\text{-C}_6\text{H}_5\text{Me})\text{Mo}(\text{TRIPOD})$  (**31**) gives  $[(\eta^6\text{-C}_6\text{H}_5\text{DMe})\text{MoH}(\text{TRIPOD})]^+$  with approximately equal distribution of *ortho*, *meta*, *para* isomers. The complex  $(\eta^6\text{-C}_6\text{H}_5\text{SiMe}_3)\text{Mo}(\text{TRIPOD})$  was synthesized and its X-ray structure was determined. Reaction of  $(\eta^6\text{-C}_6\text{H}_5\text{SiMe}_3)\text{Mo}(\text{TRIPOD})$  with one equivalent of acid gives  $(\eta^6\text{-C}_6\text{H}_6)\text{Mo}(\text{TRIPOD})$ , which is the product of C-Si bond cleavage. In conclusion, the mechanism of protonation observed for **1** is governed by its stereoelectronic factors, but not general for  $(\eta^6\text{-arene})\text{M}(\text{phosphine})_3$  complexes.

# CHAPTER 1

## INTRODUCTION

### 1.1 INTRODUCTION

Metal phosphine complexes have been studied for more than a century. In the first half of this century, the study of phosphine complexes was exploratory in nature.<sup>1</sup> The complexes were synthesized in an effort to understand coordination chemistry, and to obtain knowledge of ligands that would render metal ions soluble in organic solvents, dipole-moments, etc. The use of metal phosphine complexes in homogenous catalysis was realized in the 1950's. The discovery of Wilkinson's catalyst in 1965 has led to study of reactions that are catalyzed by transition metal phosphine complexes. The study of homogenous catalysis has advanced enormously owing to the ability of phosphines to form stable complexes with a variety of transition metals. The great strength of homogenous catalysis involving phosphine ligands is the possibility of tuning the ligands to enhance the reactivity and selectivity of the metal centered reactions. The nature and size of the substituents on the phosphine can control catalytic activity of the metal center due to their different electronic and steric properties.

Transition metal arene complexes are also known to catalyze homogenous reactions. Several ( $\eta^6$ -arene)nickel complexes were shown to be active homogenous catalysts of the dimerization of ethylene and propylene.<sup>2</sup> One of the key features in the catalysis involving ( $\eta^6$ -arene)M complexes is the tendency of the arene ligand to undergo reversible slippage  $\eta^6$  to the  $\eta^4$ -binding mode. However, at least two

$(\eta^6\text{-arene})\text{Mo}(\text{phosphine})_3$  complexes were inert towards hydrogenation due the reluctance of  $\eta^6\text{-arene}$  to slip to the  $\eta^1$ -binding fashion.<sup>3</sup> The arene is more strongly bound to the metal possibly due to  $\sigma$ -acid character of the phosphine ligands, donating to the metal which in turns binds strongly with the arene ligand.

The strong binding of arene to the metal and the resistance of the arene ligand towards hydrogenation make  $(\eta^6\text{-arene})\text{Mo}(\text{phosphine})_3$  complexes good candidates for studying the chemistry of these type of complexes. These complexes do not decompose on oxidation and protonated complexes are stable which are desirable properties for this kind of study.

## 1.2 LITERATURE OVERVIEW

The first example of an hexahapto arene metal complex,  $(\eta^6\text{-C}_6\text{H}_6)_2\text{Cr}$  was reported<sup>4</sup> soon after the synthesis of ferrocene was published. Afterwards half-sandwich arene complexes of the type  $(\eta^6\text{-C}_6\text{H}_6)\text{M}(\text{CO})_3$  were reported for group 6 metals.<sup>5</sup> Existence of a complex of the type  $(\eta^6\text{-arene})\text{M}(\text{phosphine})_3$  was first reported in 1964.<sup>6</sup> A paper by Kruck in 1967 states the two  $(\eta^6\text{-arene})\text{M}(\text{phosphine})_3$  complexes known at that time were  $(\eta^6\text{-C}_6\text{H}_6)\text{Cr}(\text{PF}_3)_3$  and  $(\eta^6\text{-1,3,5-C}_6\text{H}_3\text{Me}_3)\text{Mo}(\text{PF}_3)_3$ .<sup>7</sup> These two complexes were synthesized by the reaction of the corresponding bis( $\eta^6\text{-arene})\text{M}$  complexes with excess  $\text{PF}_3$  gas at 300 °C.<sup>7</sup> The chromium chemistry did not expand owing to the inertness of the arene ligands of the accessible precursor,  $(\eta^6\text{-C}_6\text{H}_6)_2\text{Cr}$ . On the other hand,  $(\eta^6\text{-arene})_2\text{Mo}$  is suited because one or both arene ligands can be smoothly displaced to synthesize a variety of derivatives. In phosphine substitution of the arene reactions, the lability of the one or two arene ligands is dependent on the steric and electronic properties of the phosphine. Both arene ligands are displaced at elevated temperatures by  $\text{PF}_3$ ,  $\text{F}_2\text{PC}_6\text{H}_{10}\text{PF}_2$ , or  $\text{R}_2\text{PC}_2\text{H}_4\text{PR}_2$  ( $\text{R} = \text{Me}, \text{H}$ ) to form  $\text{Mo}(\text{P})_6$  complexes.<sup>8,9</sup> One arene ligand is displaced to give  $(\eta^6\text{-arene})\text{Mo}(\text{PR}_3)_3$  when  $\text{PR}_3$  is  $\text{PPhMe}_2$ ,  $\text{PPh}_2\text{Me}$ ,  $\text{PPh}_2(\text{OMe})$ ,  $\text{P}(\text{OMe})_3$  or  $\text{P}(\text{OPh})_3$ .<sup>10-13</sup> Bulky phosphines like  $\text{PPh}_3$

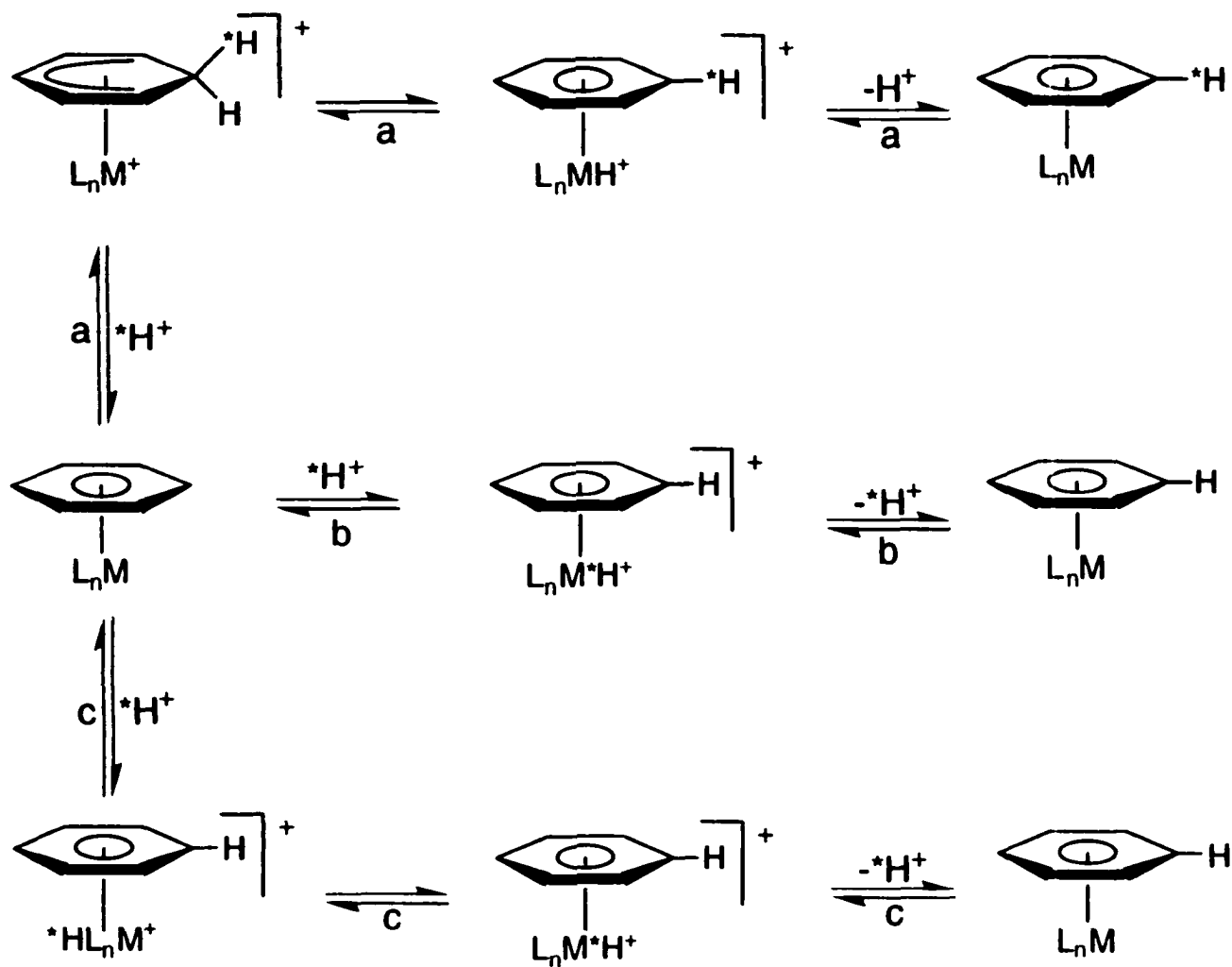
or more basic phosphines such as  $\text{PMe}_3$  and  $\text{PEt}_3$  do not react with  $(\eta^6\text{-arene})_2\text{Mo}$  under similar conditions. The arene complexes with more basic phosphines are accessible via reduction of the allyl dimer,  $[(\eta^6\text{-arene})\text{Mo}(\eta^3\text{-C}_3\text{H}_5)\text{Cl}]_2$  which in turn was synthesized by the reaction of  $(\eta^6\text{-arene})_2\text{Mo}$  with allyl chloride.<sup>11,14-16</sup> Green's group has extensively studied the  $(\eta^6\text{-arene})\text{M}(\text{phosphine})_3$  systems, especially the molybdenum and tungsten complexes, in their effort towards to explore the activation of dinitrogen. In 1971, Green and Silverthorn reported the first entry into group of  $(\eta^6\text{-arene})\text{Mo}(\text{phosphine})_3$  complexes, where the phosphine is an alkylaryl phosphine rather than trifluorophosphine.<sup>14</sup> Chatt and Wedd isolated a compound of the formula  $\text{Mo}(\text{PPhMe}_2)_4$  by reducing  $\text{MoCl}_5$  in the presence of excess phosphine.<sup>17</sup> The complex,  $\text{Mo}(\text{PPhMe}_2)_4$  was later characterized to be  $(\eta^6\text{-PhPMe}_2)\text{Mo}(\text{PPhMe}_2)_3$  by single crystal X-ray crystallography.<sup>18</sup> Morris and coworkers reported the synthesis of  $(\eta^6\text{-PhPMePh})\text{Mo}(\text{PMePh}_2)_3$  by a reduction method.<sup>19</sup> Reduction of  $[(\eta^6\text{-arene})\text{Mo}(\text{dmpe})(\eta^3\text{-C}_3\text{H}_5)]\text{PF}_6$  with  $\text{Na}/\text{Hg}$  in the presence of dmpe yields the dimer,  $[(\eta^6\text{-arene})\text{Mo}(\text{dmpe})]_2(\mu\text{-dmpe})$ , while reduction in the presence of monophosphine  $\text{PMe}_3$  gives the monomeric,  $(\eta^6\text{-arene})\text{Mo}(\text{dmpe})(\text{PMe}_3)$ .<sup>20</sup> Morris and coworkers have described the synthesis of a variety of  $(\eta^6\text{-phenylphosphine})\text{Mo}$  complexes by the reduction of  $\text{MoCl}_5$  with the appropriate phosphine using different reducing agents. The reversible binding of  $\text{N}_2$  and  $\text{H}_2$  by  $(\eta^6\text{-PhPMePh})\text{Mo}(\text{PMePh}_2)_3$  was reported.<sup>21</sup> The synthesis of  $(\eta^6\text{-PhPMePh})\text{Mo}(\text{PMePh}_2)_2(\text{P}(\text{OMe})_3)$  and  $(\eta^6\text{-PhPMePh})\text{Mo}(\text{PMePh}_2)(\text{dppe})$  and their binuclear rhodium complexes were reported.<sup>22</sup> Morris and Luck reported the synthesis of heterobimetallic quadruple-bonded complex,  $(\text{PhMePh}_2)_4\text{MoWCl}_4$  by reacting  $(\eta^6\text{-PhPMePh})\text{Mo}(\text{PMePh}_2)_3$  with  $(\text{PPh}_3)_2\text{WCl}_4$ .<sup>23</sup> The reduction of  $\text{MoCl}_4(\text{dppe})$  with  $\text{Mg}$  or  $\text{Na}/\text{Hg}$  in the presence of  $\text{PR}_2\text{Ph}$  ( $\text{R} = \text{Ph}$  or  $\text{Et}$ ) results in the complex,  $(\eta^6\text{-PhPR}_2)\text{Mo}(\text{PPhR}_2)(\text{dppe})$ .<sup>24</sup> Synthesis and single crystal X-ray structure was reported for  $(\eta^6\text{-PhPMePh})\text{Mo}(\text{PMePh}_2)(\text{prophos})$  complex.<sup>25</sup> Photosubstitution of group 6 hexacarbonyls with  $(\eta^6\text{-PhPRPh})\text{Mo}(\text{L})(\text{dppe})$  ( $\text{R} = \text{Me}, \text{Ph}$ ;  $\text{L} = \text{CO}, \text{PMe}_3$ ) yields the

bimetallic complexes  $M(CO)_5(\eta^6\text{-PhPRPh})Mo(L)(dppe)$ .<sup>26</sup> In 1989, Morris and coworkers found a high yield synthesis of  $(\eta^6\text{-PhPMe}_2)Mo(PPhMe_2)_3$  and its dimerization to  $[Mo(\mu\text{-}\eta^1, \eta^6\text{-PhPMe}_2)(PPhMe_2)]_2$ .<sup>27</sup> George and Hammund prepared  $(\eta^6\text{-arene})Mo(TRIPHOS)$  by reducing  $Cl_3Mo(TRIPHOS)$  with Na/Hg in the presence of arenes such as benzene, toluene, anisole or naphthalene.<sup>28</sup> Synthesis of  $(\eta^6\text{-arene})Mo(TRIPOD)$  (from  $(\eta^6\text{-C}_6\text{H}_6)_2Mo$  and TRIPOD) and its protonation mechanism was reported by Kowalski and Ashby in 1995.<sup>29</sup>

### 1.3 MECHANISM OF PROTONATION OF $(\eta^6\text{-C}_6\text{H}_6)M(L_n)$

Alternative mechanistic pathways (Scheme 1.1) can be envisioned for the proton exchange with the arene metal complexes.<sup>30</sup> Path *a* involves an addition of the proton to the less hindered *exo*-face of the arene to give an  $\eta^5$ -cyclohexadienyl-type intermediate followed by an *endo*-transfer to the metal center to give a metal hydride species which can revert back to the proton exchanged complex by losing a proton from the metal. Another possible pathway (path *b*) is direct attack of the proton on the metal followed by an *endo* proton transfer to the ring and *exo* proton loss to lead to the proton exchanged complex. Pathway *b* is exactly the reverse of the reaction pathway *a*. By the principle of microscopic reversibility<sup>31</sup> under equilibrium conditions, paths *a* and *b* would be indistinguishable. Isolation of kinetic intermediates in the paths *a* and *b* would help to differentiate between the two paths. In the case of path *c*, when the proton attaches to ligand L that is more basic than the metal, the reaction is usually irreversible. Since path *c* is very unusual and characteristic, it can be identified from the products formed. The key to distinguish between the two pathways *a* and *b* is the interception of the intermediates.

Setkina et al. proposed a mechanism of acid exchange with  $(\eta^6\text{-C}_6\text{H}_6)Cr(CO)_3$  (Scheme 1.2).<sup>32</sup> The mechanism involves an initial protonation of the metal on **A** to yield **B**, followed by an *endo* transfer to the arene to form an  $\eta^5$ -cyclohexadienyl species **C**, which in turn loses a proton in an *exo* fashion to give the acid exchanged product **D**.



Scheme 1.1 Alternate pathways for proton exchange with  $(\eta^6\text{-arene})\text{ML}_n$

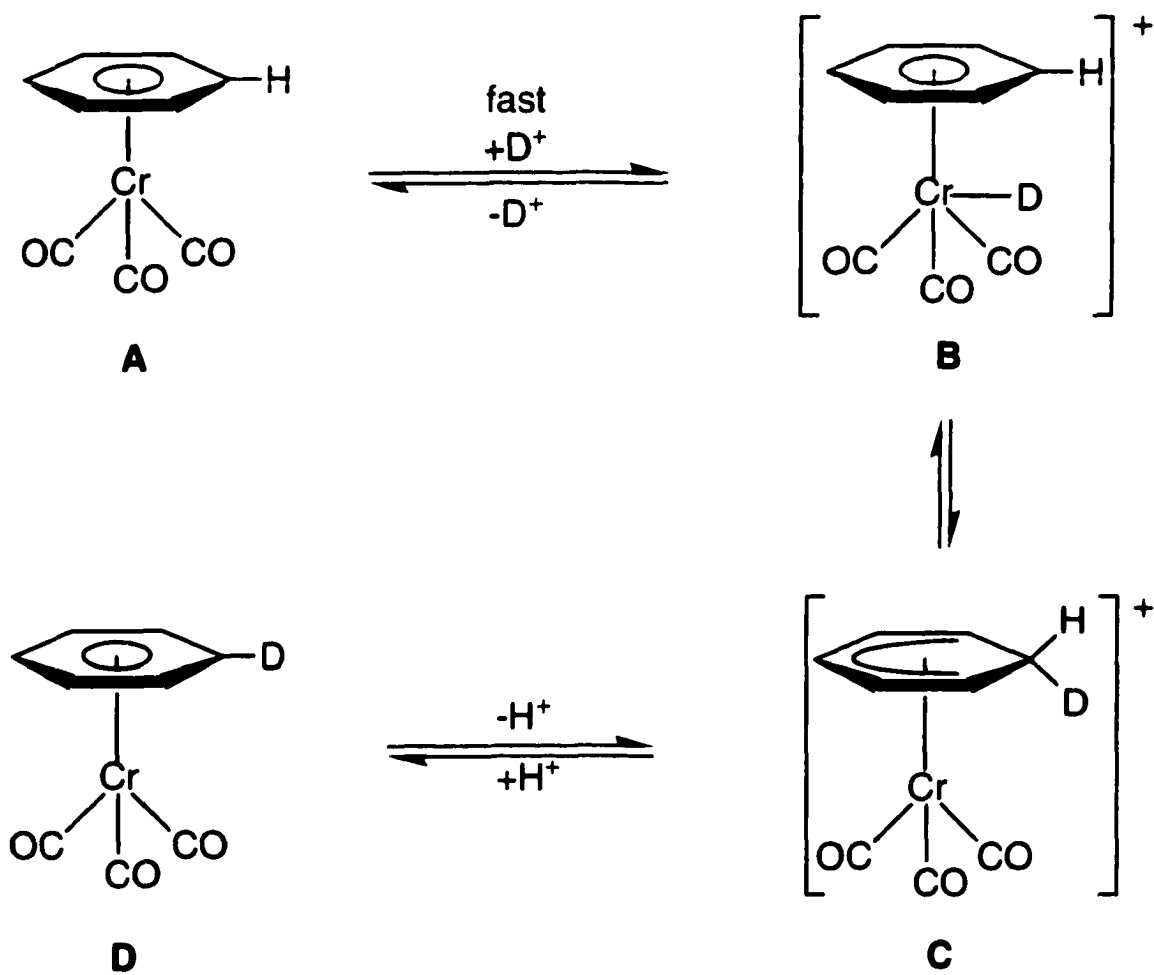
Though the intermediate species having Cr-H bond was observed spectroscopically, it was not isolable. The reaction is under equilibrium conditions making it not possible to distinguish between the two pathways, similar to *a* and *b* in Scheme 1.1. Therefore, the principle of microscopic reversibility dictates that both pathways are operable in this system. In the case of the  $(\eta^6\text{-C}_6\text{H}_6)\text{Mo}(\text{TRIPOD})$  reaction with acid, the kinetic intermediate was isolated thereby differentiating the two different pathways.

#### Mechanism of protonation of $(\eta^6\text{-C}_6\text{H}_6)\text{Mo}(\text{TRIPOD})$

Several mechanistic studies on the protonation/acid exchange have been reported for metal bound cyclic aromatics. The first mechanism of electrophilic aromatic substitution of  $(\eta^6\text{-arene})\text{Mo}(\text{phosphine})_3$  complexes was reported by our group in 1995.<sup>29</sup>

Compound **1** is protonated upon addition of one equivalent of  $\text{H}^+$  to yield the red crystalline product  $[(\eta^6\text{-C}_6\text{H}_6)\text{MoH}(\text{TRIPOD})]^+$  (**3**). The protonated complex **3** exhibits dynamic  $^1\text{H}$ ,  $^{13}\text{C}$ , and  $^{31}\text{P}$  NMR spectra and apparent peaks decoalesce when the sample is cooled. The hydride ligand apparently does not lie along the axis of the parent compound **1** (in the pocket of the TRIPOD ligand), but in an equatorial position between two phosphorus atoms. This geometry was confirmed when the solid-state structure of  $\mathbf{3}\cdot\text{PF}_6$  was determined (Figure 3.7). The hydride ligand was located in the final difference map as the largest peak. The location of the hydride ligand is also indicated by the observed distortion of the metal's coordination sphere.

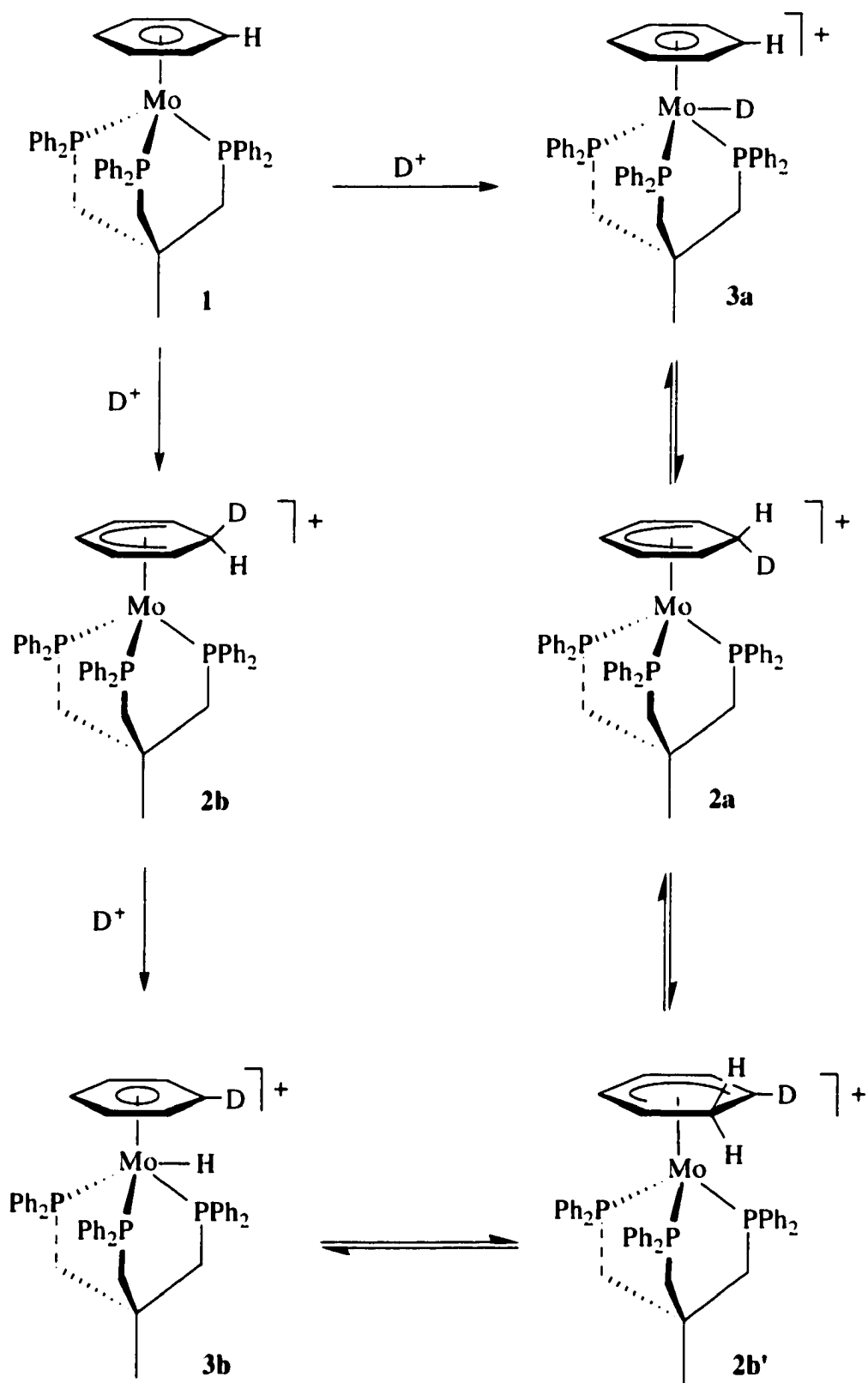
One equivalent of deuterioacid reacts with  $(\eta^6\text{-C}_6\text{H}_6)\text{Mo}(\text{TRIPOD})$  to give the product  $[(\eta^6\text{-C}_6\text{H}_5\text{D})\text{MoH}(\text{TRIPOD})]^+$ , which was confirmed by  $^1\text{H}$  and  $^{31}\text{P}$  NMR spectroscopy. The  $^1\text{H}$  NMR spectrum shows a Mo-H resonance at -5.84 ppm indicating the absence of a Mo-D in the product. Further evidence to the isotopic substitution of one deuterium on the ring was obtained by deprotonating the  $[(\eta^6\text{-C}_6\text{H}_5\text{D})\text{MoH}(\text{TRIPOD})]^+$  with NaOMe followed by high-accuracy FAB mass spectrum shows that the product is one mass unit higher than the starting  $(\eta^6\text{-C}_6\text{H}_6)\text{Mo}(\text{TRIPOD})$ . Though the FAB mass spectrum



Scheme 1.2 Proposed mechanism for isotope exchange in  $(\eta^6\text{-C}_6\text{H}_6)\text{Cr}(\text{CO})_3$

results indicate the initial deuteration occurs on arene ring, this does not explain the source of hydride of Mo-H, since there is a possibility of proton coming from the solvent. To demonstrate the *endo* transfer of proton following an initial ring protonation, the complementary experiment with the C<sub>6</sub>D<sub>6</sub> derivative **1-d<sub>6</sub>** was carried out. One equivalent of protium triflic acid reacts with (η<sup>6</sup>-C<sub>6</sub>D<sub>6</sub>)Mo(TRIPOD) to yield [(η<sup>6</sup>-C<sub>6</sub>D<sub>5</sub>H)MoD(TRIPOD)]<sup>+</sup>, which was characterized by <sup>1</sup>H, <sup>2</sup>H and <sup>31</sup>P NMR spectroscopy. Further, confirmation of the product was obtained when [(η<sup>6</sup>-C<sub>6</sub>D<sub>5</sub>H)MoD(TRIPOD)]<sup>+</sup> was treated with NaOMe to give (η<sup>6</sup>-C<sub>6</sub>D<sub>5</sub>H)Mo(TRIPOD), characterized by DIP and FAB mass spectra. The complementary experiments indicate the hydride on the metal was *endo* transferred from the ring.

Two pathways are possible for the reaction of D<sup>+</sup> with (η<sup>6</sup>-C<sub>6</sub>H<sub>6</sub>)Mo(TRIPOD) (Scheme 1.3) (i) direct protonation on the metal (**1** → **3a**) and (ii) indirect protonation via an η<sup>5</sup>-cyclohexadienyl ion complex (**1** → **2b** → **3b**). While the origin of the hydride ligand is demonstrated by the tracer studies, these experiments do not unambiguously demonstrate that the initial site of protonation is the *exo* (**1** → **2** → **3b**) addition. The equilibria (**3a** = **2a** = **2b'** = **3b**) could explain the incorporation of deuterium into the arene ligand even if the initial protonation is at the metal (**1** → **3a**). If the hydride ligand exchanges rapidly with the hydrogens of the arene ligand (**3a** = **2a** = **2b'** = **3b**) and ignoring isotope effects, statistics dictate a 1:6 ratio of **3a**:**3b**. But only **3b** is observed experimentally. Moreover, it was possible to differentiate these two pathways experimentally using qualitative kinetic information that rules out the **1** → **3a** → **2a** → **2b'** → **3b** pathway. In equimolar solutions of **1** and CF<sub>3</sub>SO<sub>3</sub>D at -150 °C in CDCl<sub>2</sub>F protonation does not occur until the solution is warmed to ca. -85 °C. The first product that is observed in these experiments is **3b**. Selective spin inversion transfer (SSIT) NMR experiments at 25 °C indicate that no spin exchange takes place between the arene ligand hydrogens and the metal hydride on the time-scale of nuclear relaxation (*T*<sub>1</sub> ≈ 1 s) which rules out step **3a** = **2a**. Extrapolating to -85 °C, the rate of formation of **3b** must be much



Scheme 1.3 Possible kinetic products upon addition of  $D^+$  to  $(\eta^6\text{-C}_6\text{H}_6)\text{Mo}(\text{TRIPOD})$

faster than the rate of intramolecular chemical exchange (**3a** = **2a** = **2b'** = **3b**).

Based on the above discussed mechanistic studies it was concluded that  $(\eta^6\text{-C}_6\text{H}_6)\text{Mo}(\text{TRIPOD})$  is protonated at the metal via a mechanism that involves initial protonation of the arene ligand to give the transient  $\eta^5$ -cyclohexadienyl complex.

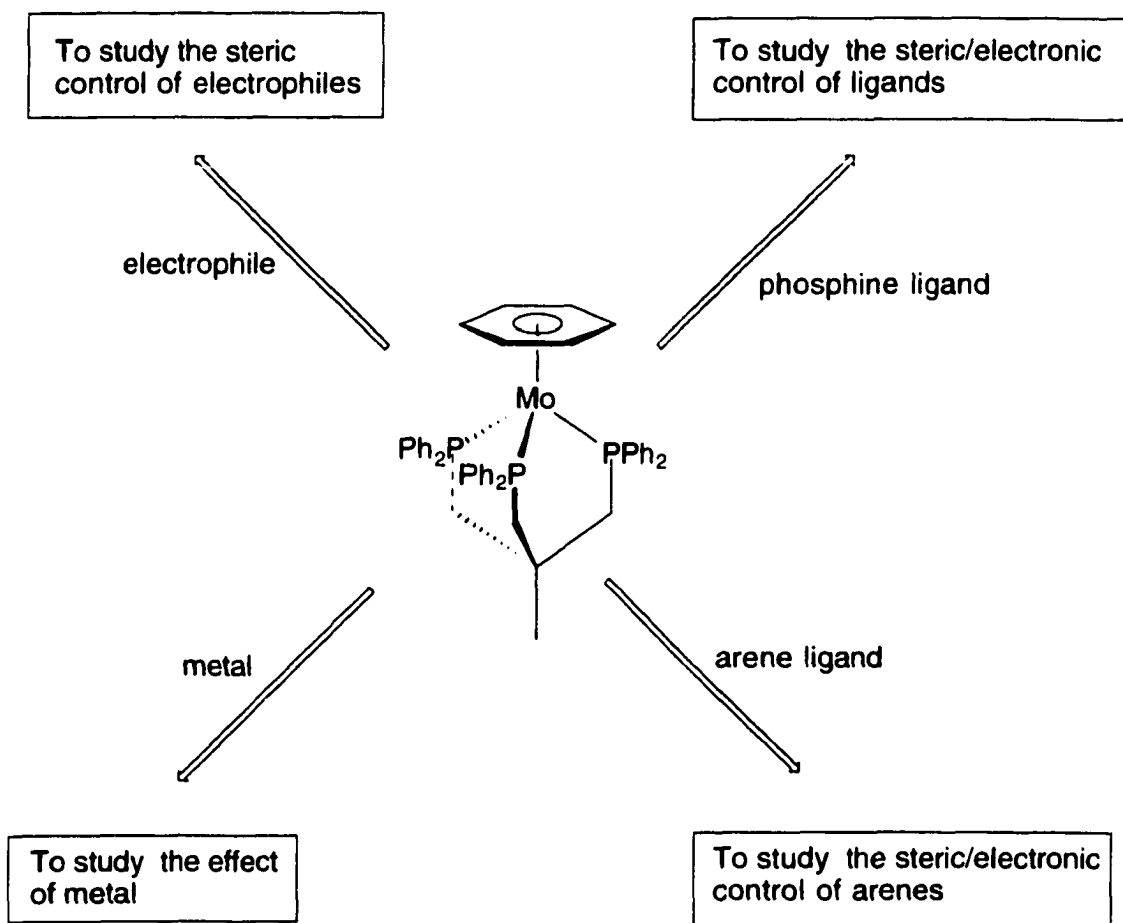
## 1.4 OUTLOOK

It is clear from the earlier study by Kowalski and Ashby that the arene of  $(\eta^6\text{-C}_6\text{H}_6)\text{Mo}(\text{TRIPOD})$  is the kinetic site of protonation and the metal is the thermodynamic site. Why? This project was initiated to explore the factors that govern the unusual mechanism. The themes of the project are depicted in Scheme 1.4.

In chapter 2, the electronic structures of  $(\eta^6\text{-C}_6\text{H}_6)\text{Mo}(\text{CO})_3$  and  $(\eta^6\text{-C}_6\text{H}_6)\text{Mo}(\text{TRIPOD})$  are discussed. The results from CV, PES, EPR of the oxidized complex  $[(\eta^6\text{-C}_6\text{H}_6)\text{Mo}(\text{TRIPOD})]^+$ , and theoretical calculations are described.

Since protonation is an acid base reaction, the stereoelectronic factors of the metal complex might play a role in the regiochemical preferences of protonation. To understand the stereoelectronic effects of the phosphine ligands, several complexes with alkyl and aryl phosphines were synthesized and their protonation studied in chapter 3. In changing from one phosphine ligand to another, electronic and steric factor affect the sites of protonation on the complexes. Single crystal X-ray structures were obtained to establish the steric demands of the phosphine ligands. To rationalize the observed protonation results, surface density maps based on the crystal structures and quantum chemical methods were calculated.

The proton is the smallest electrophile possible. Does the unusual mechanism observed for protonation of **1** hold for bulkier electrophiles as well? Carbon-centered electrophiles might react differently than protons. Attempted reactions of various electrophiles with **1** are described in chapter 4.



Scheme 1.4 Factors governing the electrophilic aromatic substitution in  $(\eta^6\text{-C}_6\text{H}_6)\text{Mo}(\text{TRIPOD})$

After establishing that the initial protonation takes place on the ring of  $(\eta^6\text{-C}_6\text{H}_6)\text{Mo}(\text{TRIPOD})$ , the study of regiochemistry of electrophilic aromatic substitution in  $(\eta^6\text{-C}_6\text{H}_5\text{R})\text{Mo}(\text{TRIPOD})$  complexes was initiated. Does ring substitution have an effect on the protonation mechanism? Syntheses of different alkyl substituted arene ligand complexes and their protonation reactions are presented in chapter 5 of this dissertation.

## 1.5 BIBLIOGRAPHY

- (1) Chatt, J. In *Homogenous Catalysis by Metal Phosphine Complexes*; Pignolet, L. H., Ed.; Plenum Press: New York, 1983, pp. 1-11.
- (2) Choe, S.-B.; Kanai, H.; Klabunde, K. J. *J. Am. Chem. Soc.* **1989**, *111*, 2875-2882.
- (3) Muetterties, E. L.; Schaeffer, H.; Mink, R. I.; Darensbourg, M. Y.; Millar, M.; Groshens, T.; Klabunde, K. J. *Inorg. Chem.* **1979**, *18*, 883-884.
- (4) Fischer, E. O.; Stahl, H. O. *Chem. Ber.* **1956**, *89*, 1805-1808.
- (5) Fischer, E. O.; Ofele, K.; Essler, H.; Frohlich, W.; Mortensen, J. P.; Semmlinger, W. *Chem. Ber.* **1958**, *91*, 2753.
- (6) Clark, R. J. *Chem. Engg. News* **1964**, *42*, 52.
- (7) Kruck, T. *Angew. Chem. Int. Ed. Engl.* **1967**, *6*, 53-67.
- (8) Gallup, D. L.; Morse, J. G. *Inorg. Chem.* **1978**, *17*, 3438-3446.
- (9) Ernst, M. F.; Roddick, D. M. *Organometallics* **1990**, *9*, 1586.
- (10) Green, M. L. H.; Mitchard, L. C.; Silverthorn, W. E. *J. Chem. Soc., Sec. A* **1971**, 2929-2931.
- (11) Green, M. L. H.; Silverthorn, W. E. *J. Chem. Soc., Dalton Trans.* **1973**, 301-306.
- (12) Green, M. L. H.; Mitchard, L. C.; Silverthorn, W. E. *J. Chem. Soc., Dalton Trans.* **1974**, 1361-1363.
- (13) Green, M. L. H.; Knight, J. *J. Chem. Soc., Dalton Trans.* **1974**, 311-319.
- (14) Green, M. L. H.; Silverthorn, W. E. *J. Chem. Soc. Chem. Commun.* **1971**, 557-558.
- (15) Green, M. L. H.; Knight, J.; Mitchard, L. C.; Roberts, G. G.; Silverthorn, W. E. *J. Chem. Soc. Chem. Commun* **1971**, 1619-1621.
- (16) Green, M. L. H.; Knight, J. *J. Chem. Soc., Dalton trans.* **1975**, 213-216.
- (17) Chatt, J.; Wedd, A. G. *J. Organomet. Chem.* **1970**, *27*, C15-C16.

- (18) Mason, R.; Thomas, K. M.; Heath, G. K. *J. Organomet. Chem.* **1975**, *90*, 195-202.
- (19) Azizian, H.; Luck, R.; Morris, R. H.; Wong, H. *J. Organomet. Chem.* **1982**, *238*, C24-C26.
- (20) Cantestari, M.; Green, M. L. H.; Izquierdo, A. *J. Chem. Soc., Dalton Trans.* **1984**, 2795-2801.
- (21) Luck, R.; Morris, R. H. *Inorg. Chem.* **1984**, *23*, 1489-1491.
- (22) Luck, R.; Morris, R. H. *J. Organomet. Chem.* **1983**, *255*, 221-230.
- (23) Luck, R.; Morris, R. H. *J. Am. Chem. Soc.* **1984**, *106*, 7978-7979.
- (24) Frizzell, J. J.; Luck, R. L.; Morris, R. H.; Peng, S. H. *J. Organomet. Chem.* **1985**, *284*, 243-255.
- (25) Morris, R. H.; Sawyer, J. F.; Sella, A. *Acta Crystallogr., Sect. C: Cryst. Struct. Commun.* **1988**, *C44*, 23-27.
- (26) Luck, R. L.; Morris, R. H. *J. Organomet. Chem.* **1988**, *347*, 349-364.
- (27) Cotton, F. A.; Luck, R. L.; Morris, R. H. *Organometallics* **1989**, *8*, 1282-1287.
- (28) George, T. A.; Hammud, H. H. *J. Organomet. Chem.* **1995**, *503*, C1-C3.
- (29) Kowalski, A. S.; Ashby, M. T. *J. Am. Chem. Soc.* **1995**, *117*, 12639-12640.
- (30) Watts, W. E. In *Comprehensive Organometallic Chemistry*; Wilkinson, G., Stone, F. G. A., Abel, E. W., Ed.; Pergamon Press: Oxford, 1982; Vol. 8, pp. 1013-1026.
- (31) Atkins, P. *Physical Chemistry*; 5 ed.; W. H. Freeman: New York, 1994.
- (32) Setkina, V. N.; Baranetskaya, N. K.; Ginzburg, A. G.; Zdanovich, V. I.; Nefedova, M. N.; Kursanov, D. N. *J. Organomet. Chem.* **1973**, *61*, 287-300.

## CHAPTER 2

# ELECTRONIC STRUCTURE OF $(\eta^6\text{-C}_6\text{H}_6)\text{Mo}(\text{TRIPOD})$ AND $[(\eta^6\text{-C}_6\text{H}_6)\text{Mo}(\text{TRIPOD})]^+$

### 2.1 INTRODUCTION

In Chapter 1, the mechanism for protonation of  $(\eta^6\text{-C}_6\text{H}_6)\text{Mo}(\text{TRIPOD})$  (**1**) was depicted as evidenced by the isotope tracer studies and kinetic measurements. The protonation of **1** (see Scheme 1.3) involves *exo* protonation of the arene to give the transient  $[(\eta^5\text{-C}_6\text{H}_7)\text{Mo}(\text{TRIPOD})]^+$  (**2b**) followed by *endo* proton transfer to the metal forming the metal hydride complex, **3b**.

While the metal is the site where the proton eventually ends up, why does the reaction take place initially at the arene? Three possible reasons are (1) the relatively small intrinsic barrier that is needed to protonate a main-group element (carbon) compared to a transition metal.<sup>1</sup> It has been suggested that protonation could be slower at transition metal centers compared to main-group elements under similar reaction conditions due to the large reorganization energy required at the metal, (2) the protonation is under steric control, and the bulky TRIPOD ligand makes the metal inaccessible, or (3) if electronic factors play an important role in the protonation and it is charge- or frontier-orbital controlled, the arene could be the electronically favored site of initial reaction.<sup>2</sup>

The basis for the protonation mechanism of **1**, explored using a combination of experimental and theoretical techniques, forms the subject of this chapter. Photoelectron Spectroscopy (PES) was employed to understand the electronic structure of **1**. The

monocation  $[(\eta^6\text{-C}_6\text{H}_6)\text{Mo}(\text{TRIPOD})]^+$  ( $1^+$ ), which is the one-electron oxidized product of **1** was formed by electrochemical and chemical oxidation methods. The electronic structure of  $1^+$  was interpreted using EPR spectra. Quantum chemical calculations have been performed to understand the energy and site of protonation of **1**.

## 2.2 LITERATURE OVERVIEW

The PES of many  $(\eta^6\text{-arene})\text{M}(\text{CO})_3$  complexes have been investigated previously. He I PES have been obtained for group 6 metals arenetricarbonyl complexes.<sup>3</sup> The metal d-orbital and ligand  $\pi$ -orbital ionization energies were assigned. Worley and Webb have studied the PES of mesitylene tricarbonyl complexes of group 6 metals and noted that the electronic structure of arene ligand does not vary with the choice of the metal.<sup>4</sup> A comparative study of the PES, MO calculations and X-ray crystal structure data of complexes of the type  $(\eta^6\text{-arene})\text{M}(\text{CO})_3$  (arene =  $\text{C}_6\text{H}_6$ ,  $\text{C}_6\text{H}_3\text{Me}_3$ , or  $\text{C}_6\text{Me}_6$ ; M = Cr, Mo, or W) was reported by Byers and Hall.<sup>5</sup> They have determined the changes in ionization potential of the first two bands in the PES are related to the changes in the electronic structure and the arene ring distortion observed in the X-ray structures of these complexes.

Electrochemical studies have been reported for metal arene tricarbonyls, but are very rare for triphosphine complexes. Connelly et al. have studied the electrochemistry of  $(\eta^6\text{-C}_6\text{Me}_6)\text{Cr}(\text{CO})_2\text{L}$  (L =  $\text{PPh}_3$ ,  $\text{PPh}_2\text{Me}$ ,  $\text{PPhMe}_2$ ,  $\text{P}(\text{OPh})_3$ , or  $\text{P}(\text{OMe})_3$ ) and reported the oxidation to be an one-electron reversible process.<sup>6</sup> Energetics of one electron transfer processes by CV was reported for group 6 metals arene tricarbonyls.<sup>7</sup> Van Order et al. have studied binuclear chromium arene complexes by CV, IR, and EPR methods.<sup>8</sup> The binuclear complexes show two successive one-electron oxidations. In this study, some monocations have displayed IR and EPR spectra indicative of a charge- and spin-localized mixed valent state. Morris and coworkers have published a compilation of data correlating

electrochemical or PES data with IR force constants of  $d_6$  octahedral complexes.<sup>9</sup> Richter-Addo and Hunter have reported that the fluoroarene complexes of chromium exhibit one-electron reversible oxidations in  $\text{CH}_2\text{Cl}_2$  solutions. It was shown that in  $\text{CH}_3\text{CN}$  solutions,  $(\eta^6\text{-arene})\text{M}(\text{CO})_3$  (arene =  $\text{C}_6\text{H}_6$ ,  $\text{C}_6\text{H}_3\text{Me}_3$ , or  $\text{C}_6\text{Me}_6$ ; M = Cr, Mo, or W) complexes have different electrochemical oxidation reactions dependent upon the metal.<sup>10</sup> The unsymmetric sandwich complexes of the type  $\text{Cp}^*\text{Cr}(\eta^6\text{-arene})$  (arene =  $\text{C}_6\text{H}_6$ ,  $\text{C}_6\text{H}_3\text{Me}$ ,  $\text{C}_6\text{H}_3\text{Et}$ ,  $\text{C}_6\text{H}_3\text{Me}_3$ , or  $\text{C}_6\text{Me}_6$ ) were synthesized and studied by NMR, CV and EPR methods.<sup>11</sup> From spectroscopic results a  $^2A_1$  ( $e_2^4, a_1^1$ ) ground state was deduced for these complexes. Appreciable spin density was found on the ligands. The ligand  $\pi$  orbitals had a negative spin density, with more spin on the arene than on  $\text{Cp}^*$ .

Though many  $(\eta^6\text{-arene})\text{Mo}(\text{phosphine})_3$  complexes are reported (Chapter 1) in the literature, very few physical studies such as PES, CV, EPR and MO calculations have been done on these complexes. Electrochemical generation of  $[(\eta^6\text{-PhPPH}_2)\text{Mo}(\text{TRIPHOS})]^+$  has been reported, however the product was not isolated.<sup>12</sup> The ionization energy for  $(\eta^6\text{-PhCH}_3)\text{Mo}(\text{PMe}_3)_3$  has been mentioned without much experimental detail.<sup>13</sup>

### 2.3 PHOTOELECTRON SPECTRA

The photoelectron spectra of  $(\eta^6\text{-C}_6\text{H}_6)\text{Mo}(\text{TRIPOD})$  and related molecules were obtained and their assignments are given in Table 2.1. Assignments of the spectral peaks were made by comparing previously reported spectra for related molecules. The labels assigned to the ionizations correspond to the predominant character of the orbital from which the ionization arises; however, additional character likely exists in these orbitals.

**Photoelectron spectrum of  $(\eta^6\text{-arene})\text{Mo}(\text{CO})_3$  complexes.** The PES of  $(\eta^6\text{-C}_6\text{H}_6)\text{Mo}(\text{CO})_3$  and  $(\eta^6\text{-1,3,5-C}_6\text{H}_3\text{Me}_3)\text{Mo}(\text{CO})_3$  were obtained for a direct comparison with that of  $(\eta^6\text{-C}_6\text{H}_6)\text{Mo}(\text{TRIPOD})$ . Since the PES of many  $(\eta^6\text{-arene})\text{M}(\text{CO})_3$  complexes have been studied previously, the assignments were made by

Table 2.1. Assignments of photoelectron ionizations and labels of primary characters.

| Compound   | Position<br>(eV) | Average<br>width | Relative Peak Area |       | Label               |
|--|------------------|------------------|--------------------|-------|---------------------|
|  |                  |                  | He I               | He II |                     |
| TRIPOD   | 7.46             | 0.46             | 1.0                | --    | P 1.p.              |
|  | 7.92             | 0.60             |                    |       |                     |
|  | 8.88             | 0.87             | 4.9                | --    | Ph $\pi$            |
|  | 10.08            | 0.53             |                    |       |                     |
|  | 10.54            | 0.60             | 9.8                | --    | P-C $\sigma$        |
|  | 11.52            | 1.04             |                    |       |                     |
| PPh <sub>2</sub> Me  | 8.0              |                  |                    |       | P 1.p.              |
|  | 9.0              |                  |                    |       | Ph $\pi$            |
|  | 9.3              |                  |                    |       |                     |
|  | 9.6              |                  |                    |       |                     |
|  | 10.5             |                  |                    |       | P-C $\sigma$        |
| $(\eta^6\text{-C}_6\text{H}_6)\text{Mo}(\text{CO})_3$            | 7.43             | 0.28             | 1.0                | --    | Mo d                |
|  | 7.65             | 0.38             |                    |       |                     |
|  | 10.58            | 0.47             | 0.8                | --    | arene $\pi$         |
|  | 11.13            | 0.82             |                    |       |                     |
| $(\eta^6\text{-C}_6\text{H}_3\text{Me}_3)\text{Mo}(\text{CO})_3$ | 7.16             | 0.37             | 1.0                | 1.0   | Mo d                |
|  | 7.36             | 0.40             |                    |       |                     |
|  | 9.89             | 0.35             | 1.0                | 0.7   | arene $\pi$         |
|  | 10.25            | 0.48             |                    |       |                     |
| $(\eta^6\text{-C}_6\text{H}_6)\text{Mo}(\text{TRIPOD})$          | 5.12             | 0.38             | 1.0                | 1.0   | Mo d                |
|  | 5.37             | 0.38             |                    |       |                     |
|  | 5.62             | 0.46             |                    |       |                     |
|  | 7.93             | 0.38             | 16.1               | 9.6   | Mo-P $\sigma$ ,     |
|  | 8.48             | 0.60             |                    |       | Ph $\pi$ , Bz $\pi$ |
|  | 8.99             | 0.86             |                    |       |                     |
|  | 10.08            | 0.66             |                    |       |                     |
|  | 10.73            | 0.95             | 9.4                | 4.6   | P-C $\sigma$        |
|  | 11.44            | 1.00             |                    |       |                     |

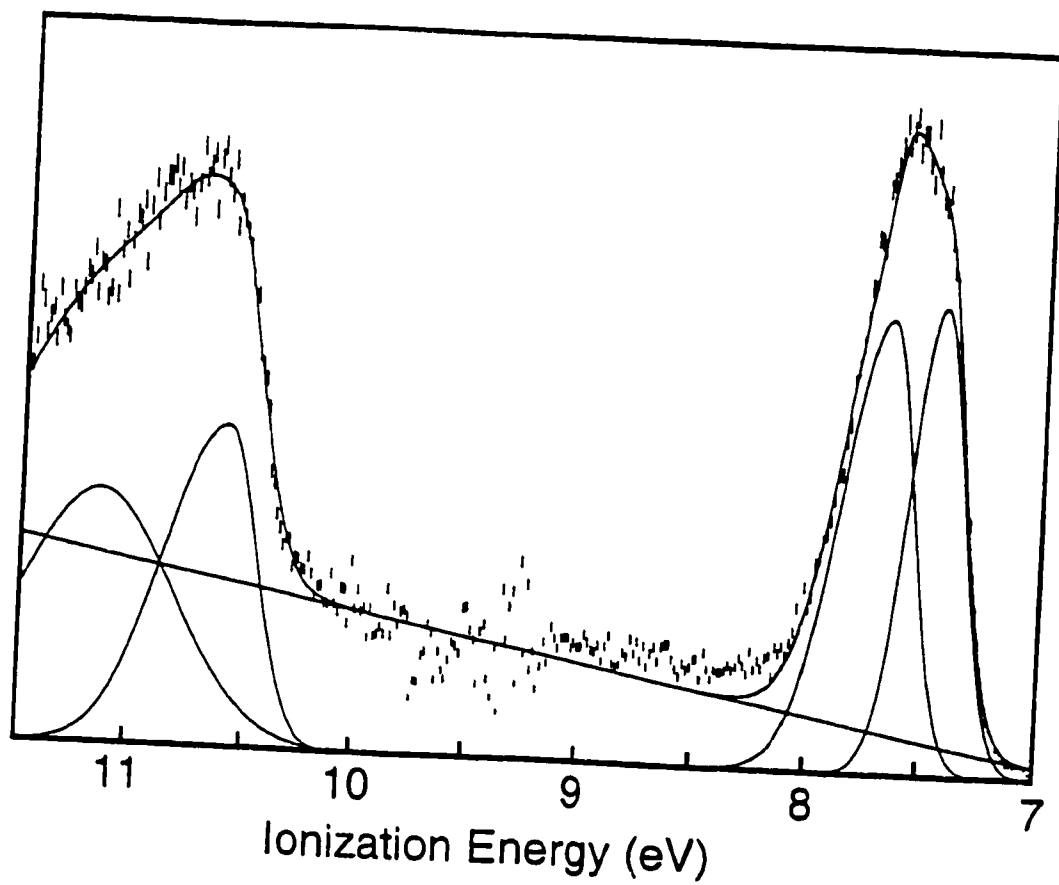


Figure 2.1. He I photoelectron spectrum of  $(\eta^6\text{-C}_6\text{H}_6)\text{Mo}(\text{CO})_3$ .

comparison with reported spectra. The He I spectrum of  $(\eta^6\text{-C}_6\text{H}_6)\text{Mo}(\text{CO})_3$  is shown in Figure 2.1. Two Gaussians at 7.43 and 7.65 eV are used to model the shape of the band at 7-8 eV. These are metal d-orbital based ionizations. The pseudo-octahedral three-legged piano stool complex,  $(\eta^6\text{-C}_6\text{H}_6)\text{Mo}(\text{CO})_3$  has  $C_{3v}$  symmetry in which the filled valence orbitals are e and  $a_1$  as derived from the  $t_{2g}$  orbitals in  $O_h$  symmetry. Therefore the bands can be assigned to the  ${}^2E$  and  ${}^2A_1$  ion states, corresponding to ionizations from the e and  $a_1$  set of filled metal orbitals. It is not possible to absolutely assign the peaks to the orbitals because the e and  $a_1$  orbitals are very close in energy. The band located between 10.5 and 11.5 eV is assigned as ionization from the predominantly arene orbital descended from the  $e_{2g}$  orbital of free benzene. This orbital has been stabilized by about 1 eV from the  ${}^2E_{2g}$  ionization of free benzene due to electron-donation from this orbital to the metal. It can be noted that the intensity of the benzene-based ionization is approximately the same as the metal-based ionization.

The He I and He II spectra of  $(\eta^6\text{-1,3,5-C}_6\text{H}_3\text{Me}_3)\text{Mo}(\text{CO})_3$  between 6 and 11 eV are very similar (Figure 2.2). Two bands at 7-8 eV and 9-11 eV represent the metal and mesitylene ligand ionizations, respectively. The band at 7-8 eV may be modeled with two Gaussians at 7.16 and 7.36 eV representing the metal-based e and  $a_1$  orbitals and the 9-11 eV band can be modeled with two Gaussians at 9.89 and 10.25 eV for the ionizations of  $e_{2g}$  orbitals of the mesitylene ligand. The metal and ligand ionizations have decreased from those of  $(\eta^6\text{-C}_6\text{H}_6)\text{Mo}(\text{CO})_3$  by about 0.3 eV and 0.7 eV, respectively.

The intensity of metal-based ionizations has increased compared to the arene-based ionizations in He II spectrum of  $(\eta^6\text{-1,3,5-C}_6\text{H}_3\text{Me}_3)\text{Mo}(\text{CO})_3$  from that of He I spectrum. It is expected from theoretical photoionization cross-sections of Mo and C that the metal-based ionizations would decrease in intensity relative to the primarily carbon-based ionizations. However, in metal carbonyl complexes the reverse is observed and has been attributed to a resonance enhancement of the metal-based ionizations.<sup>14</sup>

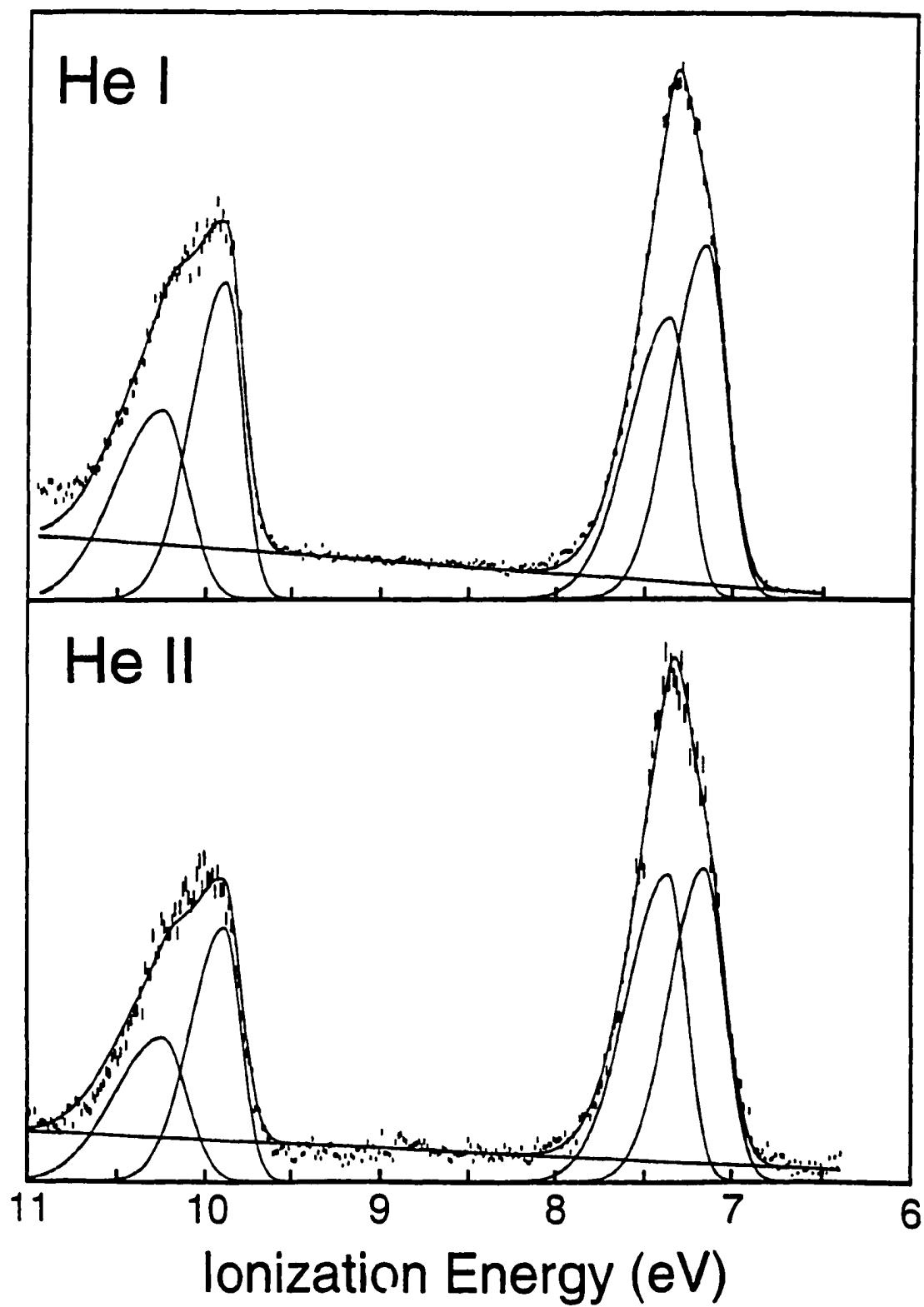


Figure 2.2. He I and He II photoelectron spectra of  $(\eta^6\text{-}1,3,5\text{-C}_6\text{H}_3\text{Me}_3)\text{Mo}(\text{CO})_3$ .

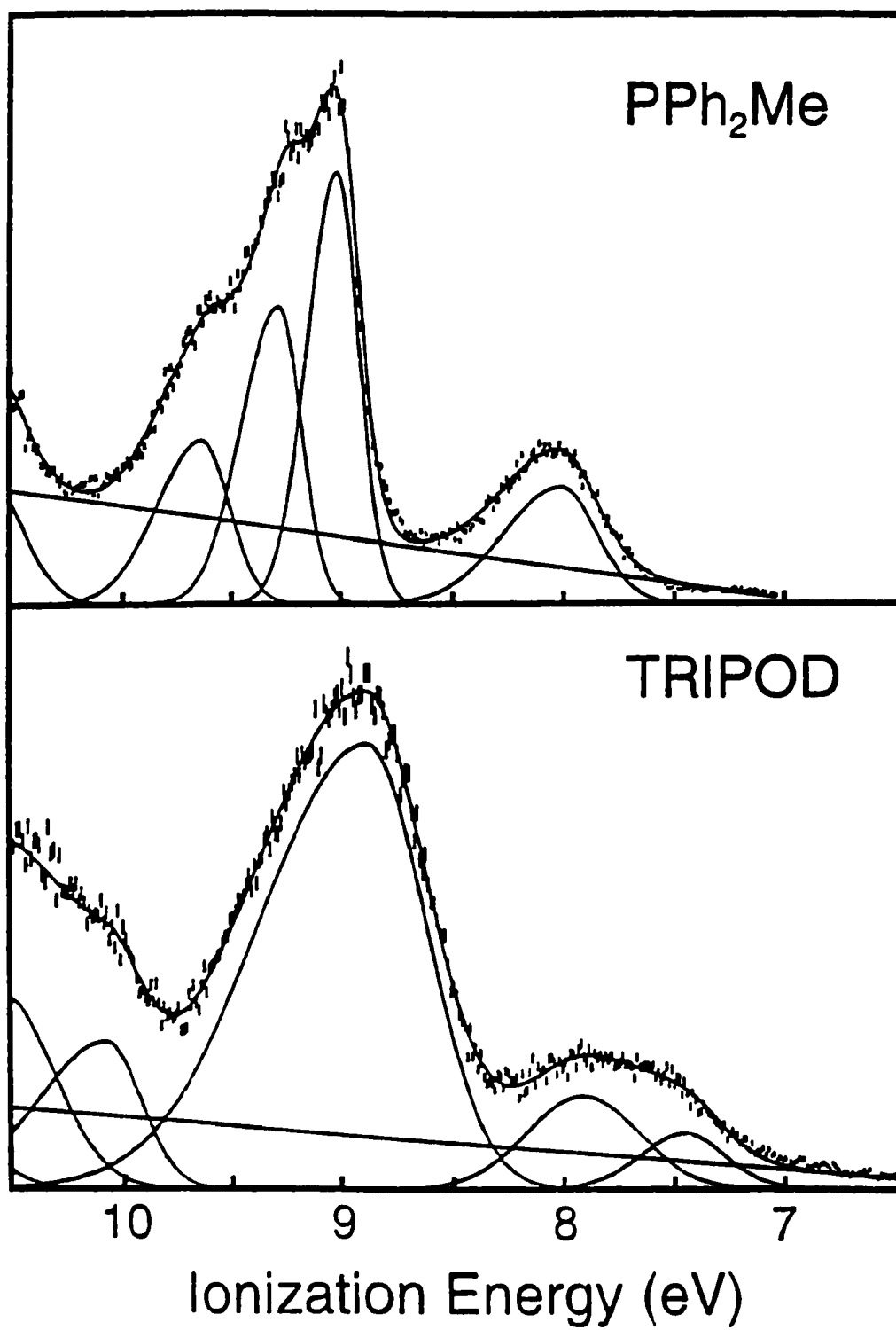


Figure 2.3. He I photoelectron spectra of PPh<sub>2</sub>Me and TRIPOD.

**PES spectra of TRIPOD and PPh<sub>2</sub>Me.** He I spectrum of the TRIPOD molecule and PPh<sub>2</sub>Me (Figure 2.3) were collected to compare with that of ( $\eta^6$ -C<sub>6</sub>H<sub>6</sub>)Mo(TRIPOD). The ionizations in the range 5 to 11 eV in these phosphines arise from phosphorus lone pairs and phenyl  $\pi$ -based a<sub>2</sub> and b<sub>1</sub> orbitals. There is appreciable interaction at 7.43 and 7.65 eV between the phosphorus lone pairs and the phenyl b<sub>1</sub> orbitals. The lower energy ionization at 8.0 eV in the spectrum of PPh<sub>2</sub>Me predominantly contains phosphorus lone pair character. The band between 8.5-10 eV was modeled with three Gaussian peaks. The peak at 9.3 eV is assigned to the phenyl a<sub>2</sub> ionization. The shoulder at 9.6 eV on the phenyl a<sub>2</sub> ionization band is from 'phenyl b<sub>1</sub>  $\pi$ ', and it shares the phosphorus character.

The He I spectrum of TRIPOD has a band in the 7-8.5 eV region. This band, which can be modeled with two Gaussians with an approximate intensity ratio of 1:2, is assigned to phosphorus lone pair ionizations. The slight splitting of the band suggests that one phosphorus might be in a different environment from the other two. Another reason for splitting a band may be due to the interaction between the phosphorus atoms. However, the band at 9 eV assigned to phenyl b<sub>1</sub> and a<sub>2</sub> ionizations is modeled with a single Gaussian indicating there is no interaction between the twelve phenyl groups present in the molecule. Since there is no interaction between the phenyl groups it can be concluded that there is no interaction between the phosphorus atoms, but the splitting is due to the different environments. Theoretical calculations on the TRIPOD molecule conformations support the PES observation that there is little interaction between the phosphorus atoms (see Section 2.6).

**Photoelectron spectra of ( $\eta^6$ -C<sub>6</sub>H<sub>6</sub>)Mo(TRIPOD).** The He I and He II PES spectra of ( $\eta^6$ -C<sub>6</sub>H<sub>6</sub>)Mo(TRIPOD) along with the He I PES of TRIPOD are shown in Figure 2.4. The band at 5-6 eV in the spectrum of ( $\eta^6$ -C<sub>6</sub>H<sub>6</sub>)Mo(TRIPOD), is assigned to the metal d ionizations. The first Gaussian at 5.12 eV is 2.4 eV lower than that of ( $\eta^6$ -C<sub>6</sub>H<sub>6</sub>)Mo(CO)<sub>3</sub>. The 2.4 eV destabilization is normal for the substitution of three carbonyls by three phosphines based on the literature precedence.<sup>15,16</sup> The band at

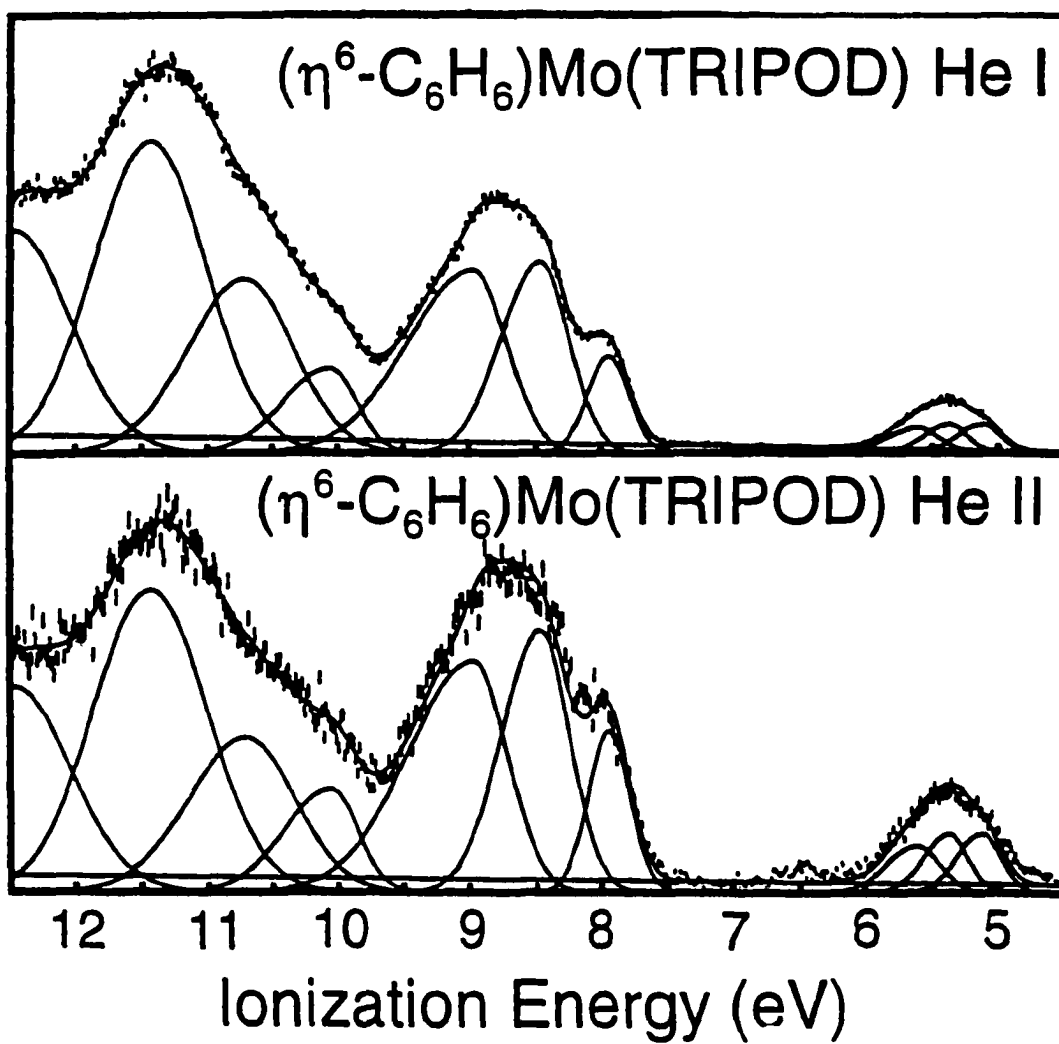


Figure 2.4. He I and He II photoelectron spectra of  $(\eta^6\text{-C}_6\text{H}_6)\text{Mo}(\text{TRIPOD})$ .

5-6 eV assigned to the metal d-orbitals can be modeled with three Gaussians. In  $C_{3v}$  symmetry,  $^2A_1$  and  $^2E$  are the two ion states. The  $^2E$  state is split due to Jahn-Teller distortion to lower the symmetry to  $C_s$ . This gives rise to three metal based peaks. The ionization of  $(\eta^6\text{-C}_6\text{H}_6)\text{Mo}(\text{TRIPOD})$  at 5.12 eV can be compared to that of 5.3 eV for  $(\eta^6\text{-C}_6\text{H}_6)\text{Mo}(\text{PMe}_3)_3$ . The latter complex bears electron donating methyl substituents on the phosphines yet it has an higher ionization energy than the  $(\eta^6\text{-C}_6\text{H}_6)\text{Mo}(\text{TRIPOD})$  complex. This would indicate that the TRIPOD ligand despite having phenyl groups might be expected to be a better donor than the three  $\text{PMe}_3$  ligands. This suggests that the  $(\eta^6\text{-C}_6\text{H}_6)\text{Mo}(\text{TRIPOD})$  is more susceptible to electrophilic attack. The TRIPOD ligand bearing six phenyl groups is expected to be a poor donor compared to phosphines bearing methyl groups based on their  $\text{p}K_b$  values. However, PES studies of alkyl and aryl phosphines confirm that the latter are better donors in the gas phase.<sup>17,18</sup> The reason for this donor ability of aryl phosphines is due to the interaction between the phosphorus lone pairs and the phenyl  $b_1$   $\pi$  electrons.

As discussed for carbonyl complexes, the metal ionization intensities are expected to increase in He II compared to He I spectra. Accordingly, the intensity of the 5-6 eV band has increased in intensity in the He II spectrum of  $(\eta^6\text{-C}_6\text{H}_6)\text{Mo}(\text{TRIPOD})$  compared the He I spectrum. Specifically the two Gaussians on the lower energy side have increased in intensity in the He II spectrum. This suggests that the  $^2E$  state is the low energy side of metal ionization. This trend in intensities is reasonable because the  $a_1$  orbital has poor overlap with the arene ligand while the e orbitals have better overlap and are expected to have more carbon character. The  $a_1$  orbital contains the  $d_z^2$  orbital, which is essentially orthogonal to the arene and hence the poor overlap. On the other hand, the e set contains the  $d_{xy}$  and  $d_{x^2-y^2}$  orbitals, which are parallel to the arene and are better suited for overlap. The band at 7-10 eV that is modeled using three peaks is assigned to Mo-P  $\sigma$ , phenyl  $\pi$ , and arene  $\pi$  ionizations. The phosphorus lone pairs and phenyl  $b_1$   $\pi$  are stabilized by 0.8 eV upon coordination to the metal. Based on that value, the 7.93 ionization can be

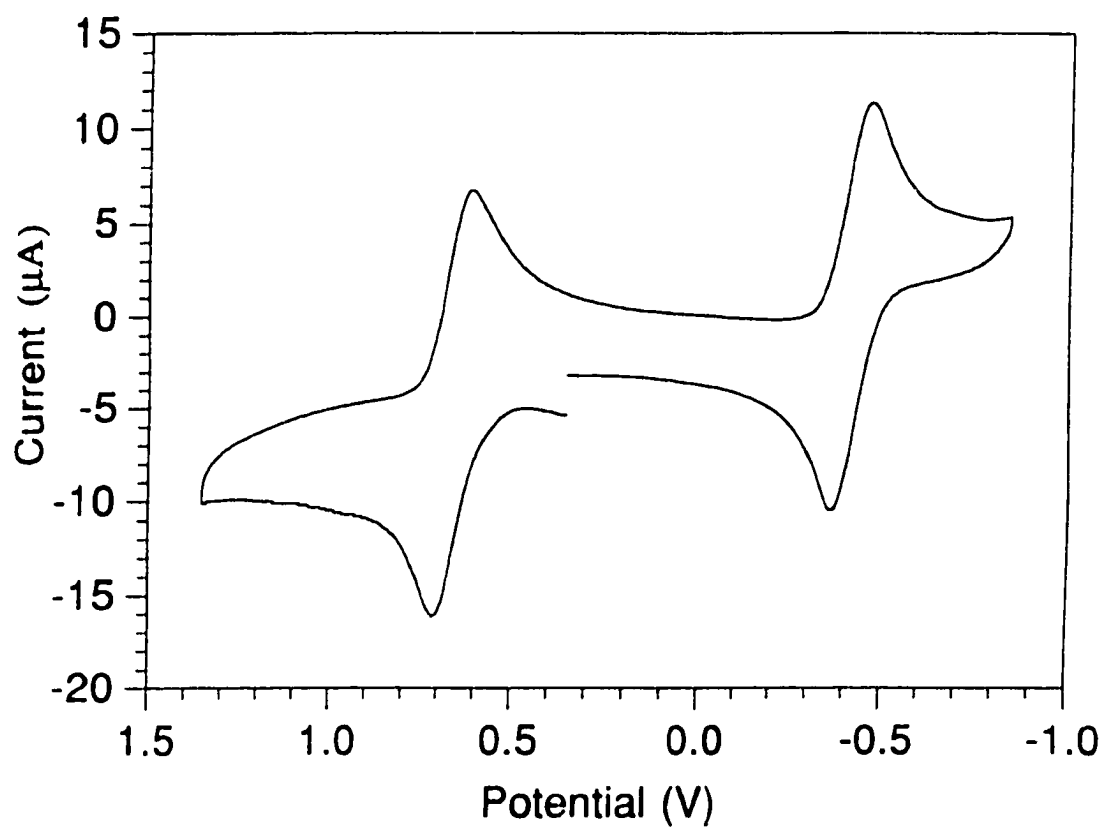


Figure 2.5. Cyclic voltammogram of  $(\eta^6\text{-C}_6\text{H}_6)\text{Mo}(\text{TRIPOD})$ .

assigned to Mo-P  $\sigma$  ionization. The peaks at 8.48 and 8.99 are assigned to the arene  $\pi$  and phenyl  $a_2$  ionizations. The ionization at 10.08 eV arises from the phenyl  $b_1$  ionization because it is stabilized with respect to phenyl  $a_2$  due to the phosphorus lone pair character interaction with the metal. The band above 11 eV is assigned to the P-C  $\sigma$  bonds.

In conclusion, the PES studies of  $(\eta^6\text{-C}_6\text{H}_6)\text{Mo}(\text{TRIPOD})$  and related molecules provide some useful information in understanding the site of initial protonation. The substitution of three carbonyls by TRIPOD shifts the first ionizations by more than 2 eV, which makes  $(\eta^6\text{-C}_6\text{H}_6)\text{Mo}(\text{TRIPOD})$  an electron rich molecule. The e set of orbitals are split slightly due to Jahn-Teller distortion. Since the He I and He II PES indicate a significant amount of arene character on the low energy side of the metal d-orbitals, the orbitals derived from the e-set are believed to be at slightly higher energy than the a. Nonetheless, the  ${}^3\text{E}$  and  ${}^2\text{A}_1$  states are close in energy. Since the energies of these two states are similar, the relative energies might switch or spread depending on the environment. That is to say, exact assignments of the ion states are not always possible when they are in close in energy.

## 2.4 CYCLIC VOLTAMMETRY

Under the conditions that the CV (Figure 2.5) was measured (+1.5 to -2.0 V at a scan rate of 100 mV/s), the redox couple of an internal reference, ferrocene was at +0.25 V. The first and second oxidation potentials of  $(\eta^6\text{-C}_6\text{H}_6)\text{Mo}(\text{TRIPOD})$  occurred at -0.77 and +0.33 V, respectively. No reduction waves were observed down to -2.0 V. The scale of Figure 2.5 assumes the ferrocene/ferrocenium couple in  $\text{CH}_2\text{Cl}_2$  occurs at 0.46 V versus SCE.<sup>19</sup> Thus,  $E(\text{Mo}^{I/0}) = -0.56$  V with  $\Delta_p = 99$  mV and  $E(\text{Mo}^{II/I}) = +0.56$  V with  $\Delta_p = 100$  mV versus SCE.

In  $\text{CH}_2\text{Cl}_2$  solution,  $(\eta^6\text{-C}_6\text{H}_6)\text{Mo}(\text{TRIPOD})$  exhibits two reversible one-electron oxidation waves at all scan rates. The first oxidation potential for  $(\eta^6\text{-C}_6\text{H}_6)\text{Mo}(\text{TRIPOD})$  of  $E_{1/2}(\text{Mo}^{I/0}) = -0.56$  V is quite low compared to those of other  $(\eta^6\text{-arene})\text{MoL}_3$  complexes

in  $\text{CH}_2\text{Cl}_2$  solvent. Oxidation potentials for related  $(\eta^6\text{-arene})\text{MoL}_3$  complexes in various solvents range from about -1 to +1 V.<sup>20</sup> Not surprisingly, complexes such as  $(\eta^6\text{-C}_6\text{H}_3\text{Me})\text{Mo}(\text{pyridine})_3$  with hard donors tend to exhibit very negative potentials<sup>9</sup> while derivatives such as  $(\eta^6\text{-C}_6\text{H}_6)\text{Mo}(\text{CO})_3$  with soft ligands are more positive.<sup>10</sup>

A relevant comparison with respect to the present study is the redox potentials of  $(\eta^6\text{-C}_6\text{H}_6)\text{Mo}(\text{CO})_3$  and  $(\eta^6\text{-C}_6\text{H}_6)\text{Mo}(\text{TRIPOD})$ . Unfortunately,  $(\eta^6\text{-C}_6\text{H}_6)\text{Mo}(\text{CO})_3$  does not exhibit a reversible cyclic voltammogram in  $\text{CH}_2\text{Cl}_2$ . It does exhibit quasi-reversible oxidation waves in  $\text{CH}_3\text{CN}$ , but  $(\eta^6\text{-C}_6\text{H}_6)\text{Mo}(\text{TRIPOD})$  is not soluble in  $\text{CH}_3\text{CN}$ . Assuming about 100 mV negative shift in the oxidation potential in  $\text{CH}_3\text{CN}$  as compared with  $\text{CH}_2\text{Cl}_2$ ,<sup>19</sup> the estimated  $\text{Mo}^1/\text{Mo}^0$  couple for  $(\eta^6\text{-C}_6\text{H}_6)\text{Mo}(\text{TRIPOD})$  is roughly 1.5 V more negative than that for  $(\eta^6\text{-C}_6\text{H}_6)\text{Mo}(\text{CO})_3$ . Using the empirical relationship of the form  $E_{1/2} = (0.6 \text{ to } 0.8)\text{IP} - (3.5 \text{ to } 4.5)$ , that correlates between electrochemical and photoionization data, a difference of 2.4 eV is calculated for the HOMO IP of  $(\eta^6\text{-C}_6\text{H}_6)\text{Mo}(\text{CO})_3$ ,<sup>7,9,21,22</sup> The HOMO IP of  $(\eta^6\text{-C}_6\text{H}_6)\text{Mo}(\text{TRIPOD})$  should correspond to a difference of  $E_{1/2}$  in the range of 1.4 - 1.9 V.

## 2.5 OXIDATION AND EPR SPECTRA

Chemical oxidation of  $(\eta^6\text{-C}_6\text{H}_6)\text{Mo}(\text{TRIPOD})$  can be achieved by one-electron oxidants such as  $\text{Ag}^+$ , ferrocenium and iodine. Silver salts were normally used because of the ease in the separation of the reduced oxidant. The EPR spectra of the oxidized species were obtained to probe its electronic structure.

The X-band EPR spectrum of  $[(\eta^6\text{-C}_6\text{H}_6)\text{Mo}(\text{TRIPOD})]^+$  and a simulation are illustrated in Figure 2.6. The X-band EPR spectrum of the isotopomer  $[(\eta^6\text{-C}_6\text{D}_6)\text{Mo}(\text{TRIPOD})]^+$  is presented in Figure 2.7. The first- and second harmonic Q-band spectra of  $[(\eta^6\text{-C}_6\text{D}_6)\text{Mo}(\text{TRIPOD})]^+$  are illustrated in Figure 2.8 and Figure 2.9, respectively.

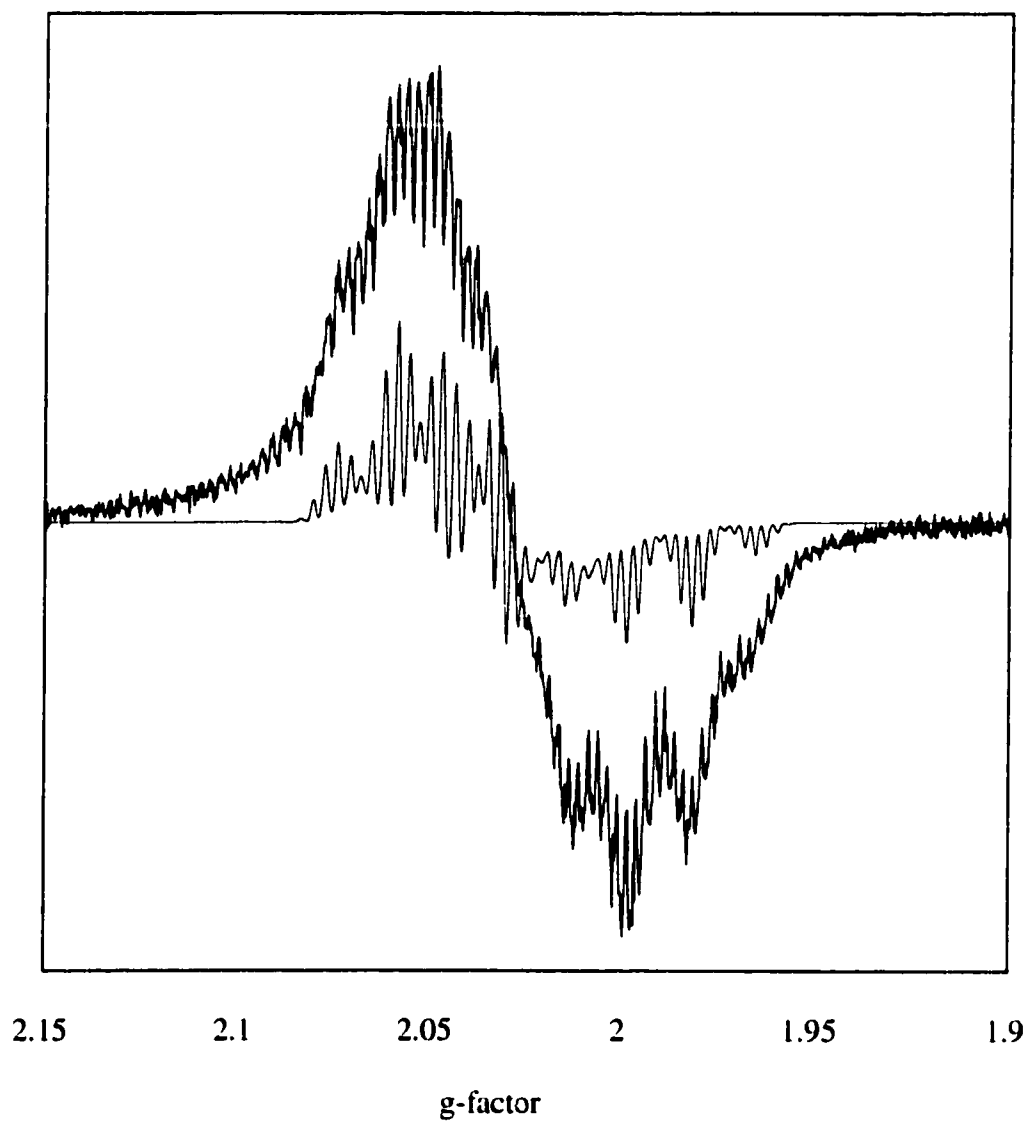


Figure 2.6. X-band EPR spectrum (solid line) of  $[(\eta^6\text{-C}_6\text{H}_6)\text{Mo}(\text{TRIPOD})]^+$  at 4 K in THF and a simulation (broken line)

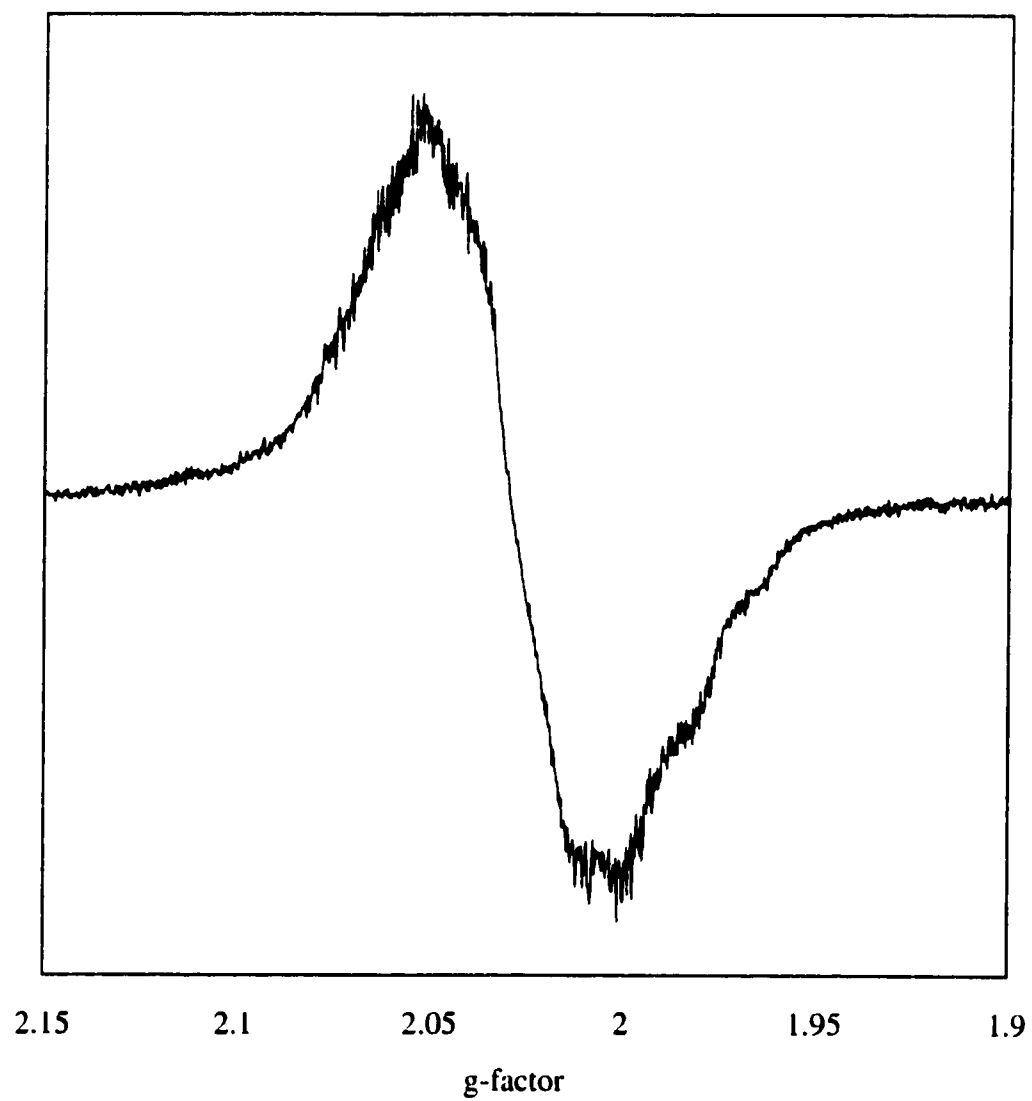


Figure 2.7. X-band EPR spectrum of  $[(\eta^6\text{-C}_6\text{D}_6)\text{Mo}(\text{TRIPOD})]^+$  at 4 K in THF

Two distinctive hfc's that are attributed to the  $^{31}\text{P}$  and  $^1\text{H}$  nuclei coupled to the unpaired electron are observed in the spectrum of  $[(\eta^6\text{-C}_6\text{H}_6)\text{Mo}(\text{TRIPOD})]^+$  (Figure 2.6). The larger hfc of  $a_{xx} = a_{yy} = 25\text{ G}$ ,  $a_{zz} = 29\text{ G}$  is assigned to three  $^{31}\text{P}$  nuclei, and the smaller hfc of  $a = 5\text{ G}$  to the  $^1\text{H}$  nuclei on the arene. The larger hfc of  $^{31}\text{P}$  nuclei is suggested by the quartets that are observed in the second harmonic Q-band spectrum (Figure 2.9). The larger hfc that is observed is also in the range of  $a$  values (25-30 G) that have been reported for related metal complexes.<sup>23</sup> The assignment of the smaller hfc to the  $^1\text{H}$  nuclei is supported by the X-band spectrum of the deuterio derivative  $[(\eta^6\text{-C}_6\text{D}_6)\text{Mo}(\text{TRIPOD})]^+$  (Figure 2.7). An  $a = 5\text{ G}$  observed for the  $^1\text{H}$  hfc is comparable to the values reported for benzene cation radical<sup>24</sup> ( $a = 3.8\text{ G}$ ) and benzene anion radical<sup>25</sup> ( $a = 6.4\text{ G}$ ). The proton hfc that is observed can be attributed to  $\sigma$ - $\pi$  spin polarization. Proton hfc is possible via  $\sigma$ - $\pi$  spin polarization when the SOMO has a significant amount of arene  $\pi$  character. Therefore, the proton hfc observed indicates that the SOMO of  $1^+$  has substantial arene character.

**X-Ray Structure of  $[(\eta^6\text{-C}_6\text{H}_6)\text{Mo}(\text{TRIPOD})]\text{PF}_6 \cdot (1 \cdot \text{PF}_6)$**  Yellow-brown crystals of  $[(\eta^6\text{-C}_6\text{H}_6)\text{Mo}(\text{TRIPOD})]\text{PF}_6$  were obtained and a X-ray structure analysis was performed. The data were corrected for Lorentz and polarization effect. Absorption correction was not applied since it was judged to be insignificant. The intensity statistics and the lack of any systematic absences suggested the choice of two space groups, C2 and Cm. Based on the successful structure solution and the subsequent refinement the space group C2 was selected as the correct choice. The structure was solved by the direct method using SHELXTL (Siemens) system, and refined by full-matrix least-squares on  $F^2$  using all reflections. The data quality was very poor and the  $\text{PF}_6$  anion is highly disordered. As a consequence, the refinement is extremely poor and needed extensive use of restraints (SHELXTL, "SAME", SADI, and FLAT) for stabilizing the refinement.

The structure of the cation was established unambiguously, and shows the unsymmetric environment of the Mo atom with respect to the coordination of the three P

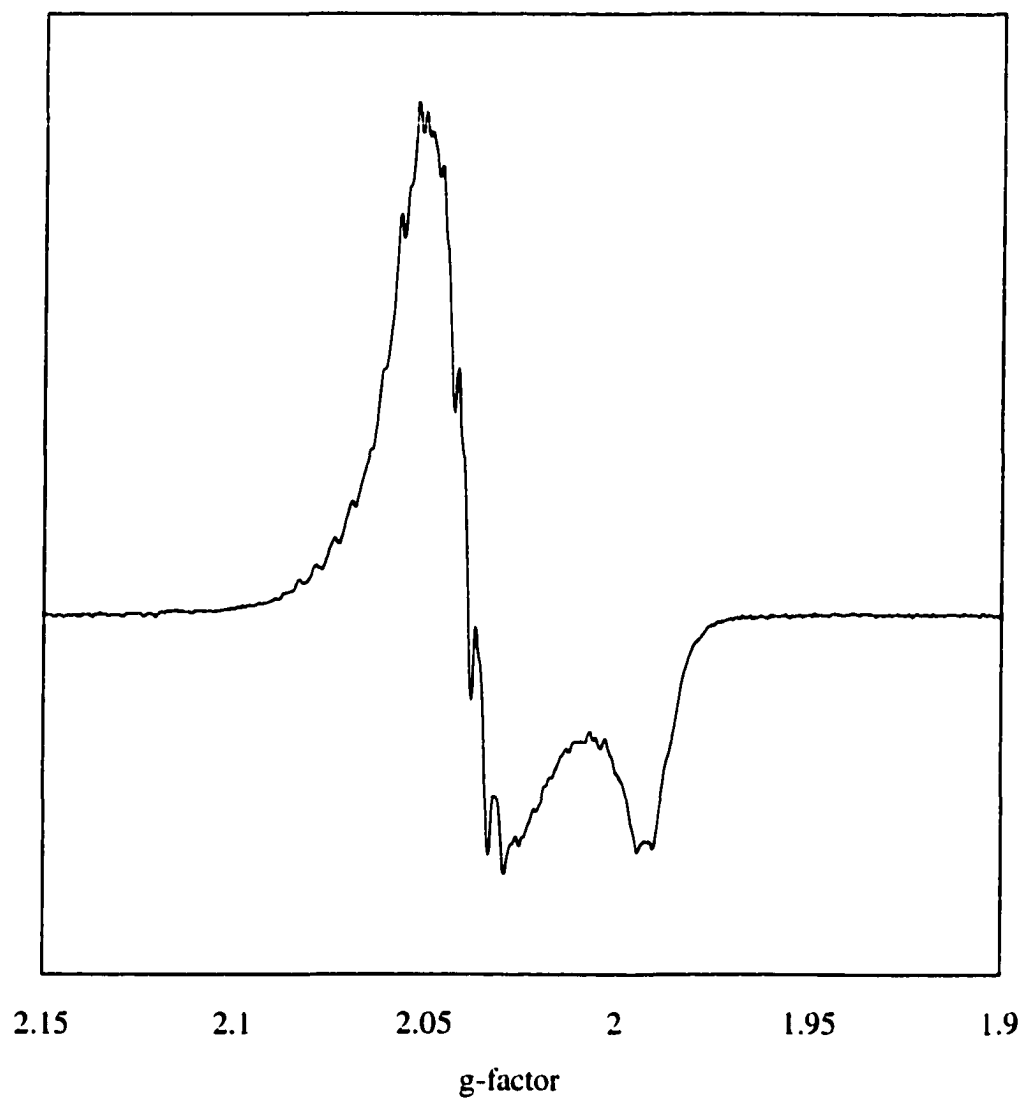


Figure 2.8. First harmonic Q-band EPR spectrum of  $[(\eta^6\text{-C}_6\text{D}_6)\text{Mo}(\text{TRIPOD})]^+$  at 50 K in THF

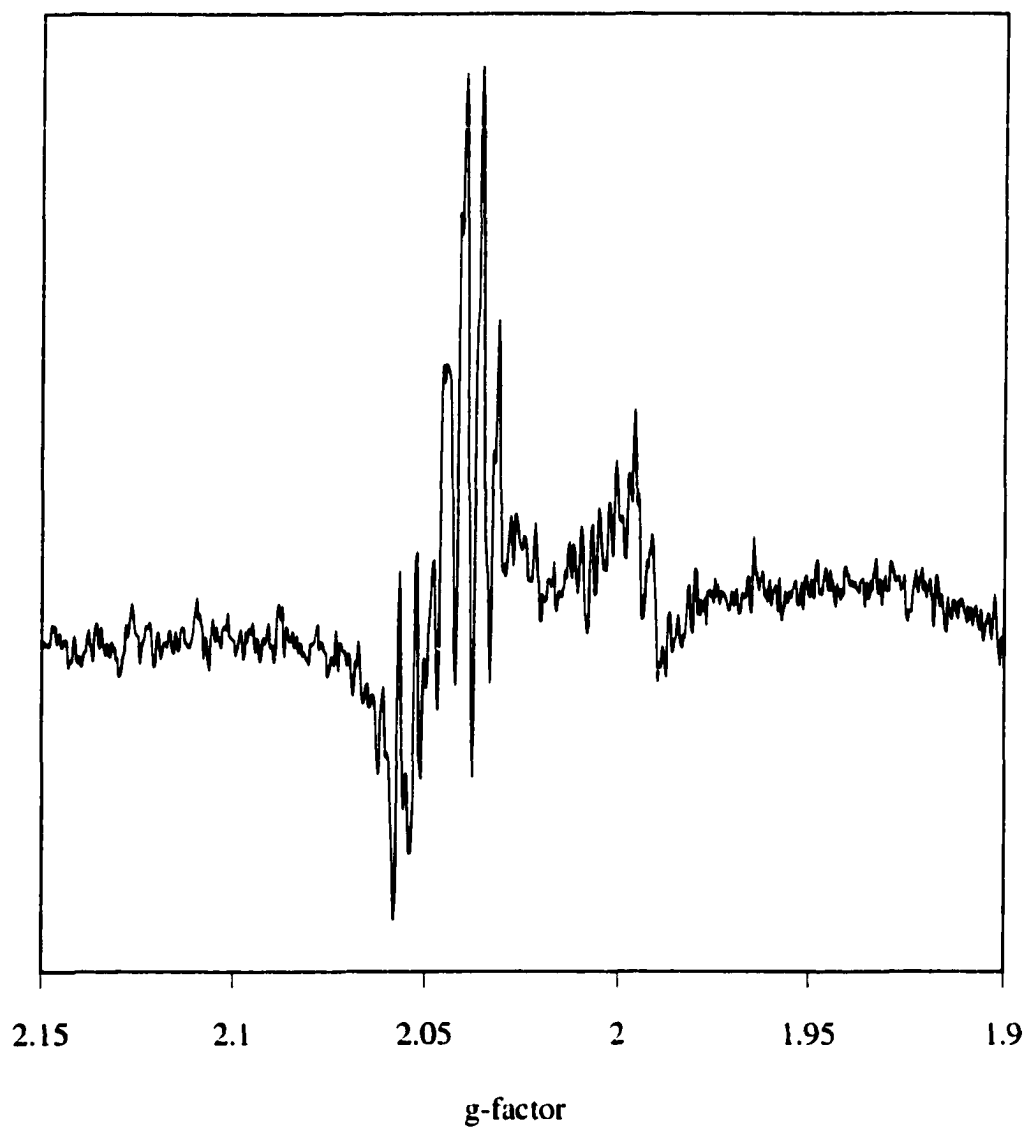


Figure 2.9. Second harmonic Q-band EPR spectrum of  $[(\eta^6\text{-C}_6\text{D}_6)\text{Mo}(\text{TRIPOD})]^+$  at 50 K in THF

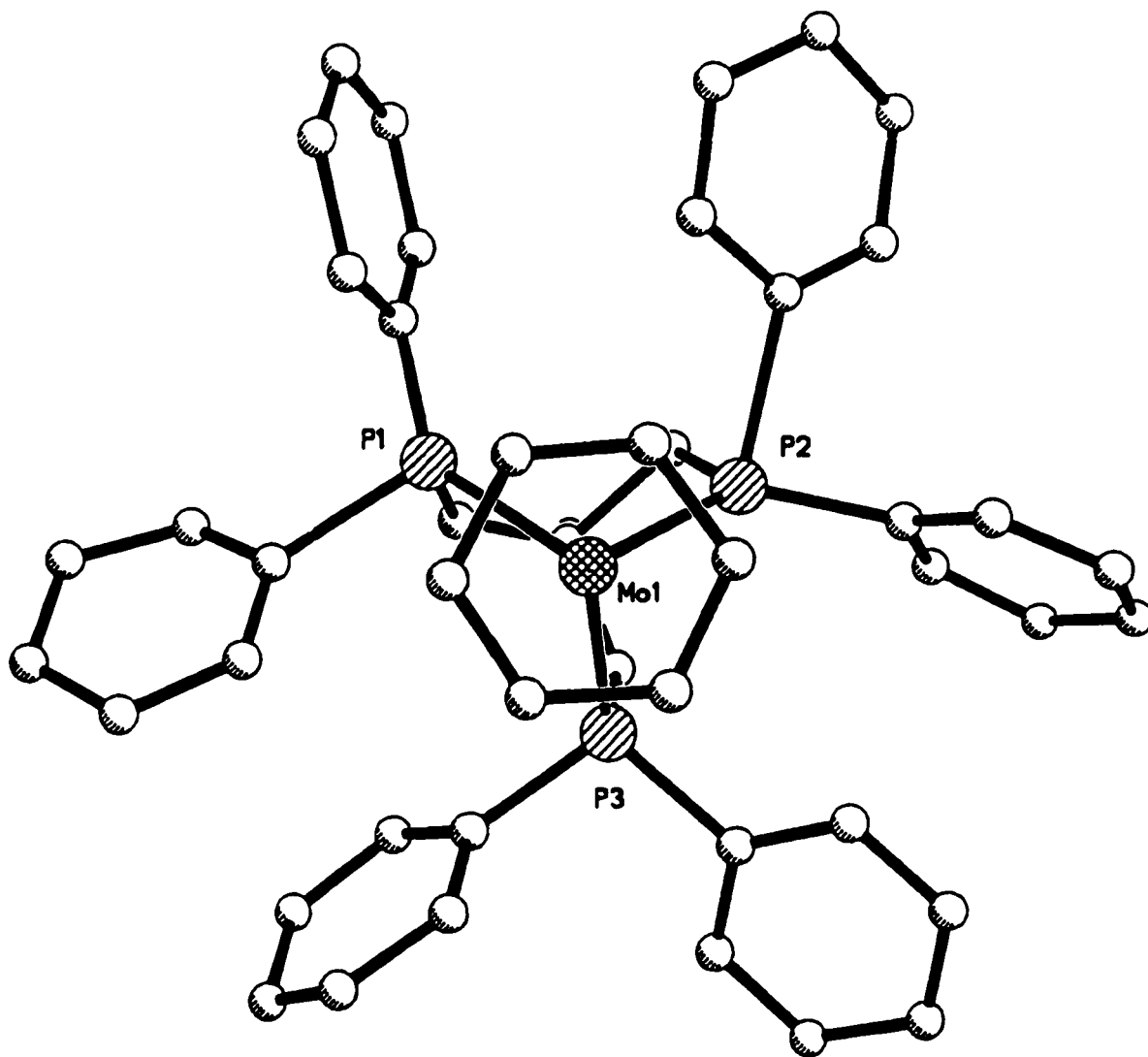


Figure 2.10. Thermal ellipsoid drawing of  $[(\eta^6\text{-C}_6\text{H}_6)\text{Mo}(\text{TRIPOD})]\text{PF}_6$ .

Table 2.2. Selected interatomic distances (Å) and bond angles (deg) for **1**·PF<sub>6</sub> and **1**.

| Bond/Angle | <b>1</b> ·PF <sub>6</sub> | <b>1</b>   |
|------------|---------------------------|------------|
| Mo-P1      | 2.452(6)                  | 2.4118(13) |
| Mo-P2      | 2.427(7)                  | 2.3856(10) |
| Mo-P3      | 2.489(5)                  | 2.3846(10) |
| Mo-X       | 1.789(2)                  | 1.816(5)   |
| P1-Mo-P2   | 86.7(2)                   | 84.82(4)   |
| P2-Mo-P3   | 75.6(3)                   | 83.12(4)   |
| P3-Mo-P1   | 91.9(2)                   | 83.50(3)   |
| P1-Mo-X    | 124.1(6)                  | 129.2(1)   |
| P2-Mo-X    | 131.5(6)                  | 128.4(1)   |
| P3-Mo-X    | 131.1(6)                  | 131.0(1)   |

X - centroid of the arene

atoms, as reflected by the significantly different bond angles involving the arene-centroid and the three P atoms. The asymmetric unit contains one cation and two independent halves of the  $\text{PF}_6^-$  ions, which are located very close to the C2 symmetry axis, hence the resulting disorder. The phosphorus (P4 and P5) and the twelve fluorine atoms were refined with 50% occupancy factor. Because of the poor state of refinement only the Mo and the three P atoms of the cation (P1, P2, P3) were refined anisotropically, all other atoms were refined isotropically, and no attempt was made to include the hydrogen atoms. Table 2.2 lists the comparison of selected bond lengths and bond angles  $\mathbf{1} \cdot \text{PF}_6^-$  and  $\mathbf{1}$ . Further details of the crystal data are given in Section 6.3.

## 2.6 THEORETICAL CALCULATIONS

Theoretical calculations were carried out to determine the frontier orbitals and structures of  $(\eta^6\text{-C}_6\text{H}_6)\text{Mo}(\text{CO})_3$  and  $(\eta^6\text{-C}_6\text{H}_6)\text{Mo}(\text{TRIPOD})$  complexes, and energies and electron distributions of the lowest positive ion states.

$(\eta^6\text{-C}_6\text{H}_6)\text{Mo}(\text{CO})_3$ . Table 2.3 summarizes the crystal structure geometry of  $(\eta^6\text{-C}_6\text{H}_6)\text{Mo}(\text{CO})_3$  and the geometries that were optimized using the DFT and *ab initio* methods. Both calculation methods converge to  $C_{3v}$  geometry, in agreement with the crystal structure of  $(\eta^6\text{-C}_6\text{H}_6)\text{Mo}(\text{CO})_3$ . The DFT method provides bond distances and angles that are in good agreement with the experimental structure. The computed distances of  $\text{Mo-C(arene)}_{\text{avg.}} = 2.41$  and  $\text{Mo-CO} = 2.00$  Å are comparable with the distances of  $\text{Mo-C(arene)}_{\text{avg.}} = 2.37$  and  $\text{Mo-CO} = 1.97$  Å from the crystal structure.<sup>26</sup> The computed and experimental OC-Mo-CO bond angles are both 87°. The *ab initio* calculation also agrees with the experimental bond distances and angles except the arene molybdenum distance is longer. Based on the computed models, the metal-based orbitals are the frontier orbitals, with the e-set orbitals slightly above  $a_1$  orbital. Earlier EHMO calculations predicted the opposite ordering.<sup>27</sup> Figure 2.11 shows the calculated frontier molecular e symmetry orbital (top) and  $a_1$  symmetry orbital (bottom). The e orbital is significantly

**Table 2.3. Selected interatomic distances (Å) and angles (deg) for  $(\eta^6\text{-C}_6\text{H}_6)\text{Mo}(\text{CO})_3$  and  $[(\eta^6\text{-C}_6\text{H}_6)\text{Mo}(\text{CO})_3]^+$  energies (eV) to lowest cation states.**

| molecular charge         | 0                 | 0        | 0        | +1                                       | +1               |
|--------------------------|-------------------|----------|----------|--|------------------|
|                          | Expt <sup>b</sup> | DFT      | RHF      | DFT                                      | UHF              |
| Symmetry                 | $C_{3v}$          | $C_{3v}$ | $C_{3v}$ | $C_s$                                    | $C_s$            |
| Mo-centroid <sup>a</sup> | 1.91              | 1.95     | 2.11     | 1.98                                     | 2.20             |
| C-C (arene)avg.          | 1.41(1)           | 1.43     | 1.41     | 1.42                                     | 1.41             |
| Mo-C(arene)avg.          | 2.38(1)           | 2.41     | 2.54     | 2.43                                     | 2.61             |
| Mo-CO                    | 1.96(1)           | 2.00     | 2.00     | 2 x 2.04<br>2.02                         | 2 x 2.11<br>2.09 |
| C-O                      | 1.161(1)          | 1.15     | 1.16     | 1.13                                     | 1.13             |
| Centroid-Mo-CO           | 127(2)            | 128      | 126      | 2 x 129<br>121                           | 2 x 127<br>122   |
| OC-Mo-CO                 | 87(1)             | 87       | 89       | 1 x 82<br>96                             | 2 x 85<br>96     |
|                          |                   |          |          | Distortion <sup>c</sup> stabilization => |                  |
|                          |                   |          |          | 10 kcal/mol                              | 22 kcal/mol      |

<sup>a</sup> Averaged center of arene ring.

<sup>b</sup> Average crystal geometric parameters (and standard deviations from three-fold symmetry from the carbonyls and six-fold symmetry for the arene).

<sup>c</sup> From  $C_{3v}$  vertical position ion.

Table 2.4. Modeled vertical ionization energies to lowest positive ion states of  $(\eta^6\text{-C}_6\text{H}_6)\text{Mo}(\text{CO})_3$ .

| Method       |                   | Energy(eV)     |              |
|--------------|-------------------|----------------|--------------|
|              |                   | $^2\text{A}_1$ | $^2\text{E}$ |
| DFT          | orbital energies  | 5.72           | 5.65         |
| DFT          | E(ion)-E(neutral) | –              | 7.68         |
| HF           | orbital energies  | 8.45           | 7.75         |
| HF           | E(ion)-E(neutral) | 6.33           | 5.97         |
| MP2          | E(ion)-E(neutral) | 7.41           | 7.40         |
| EXPERIMENTAL |                   | 7.43-7.65      |              |

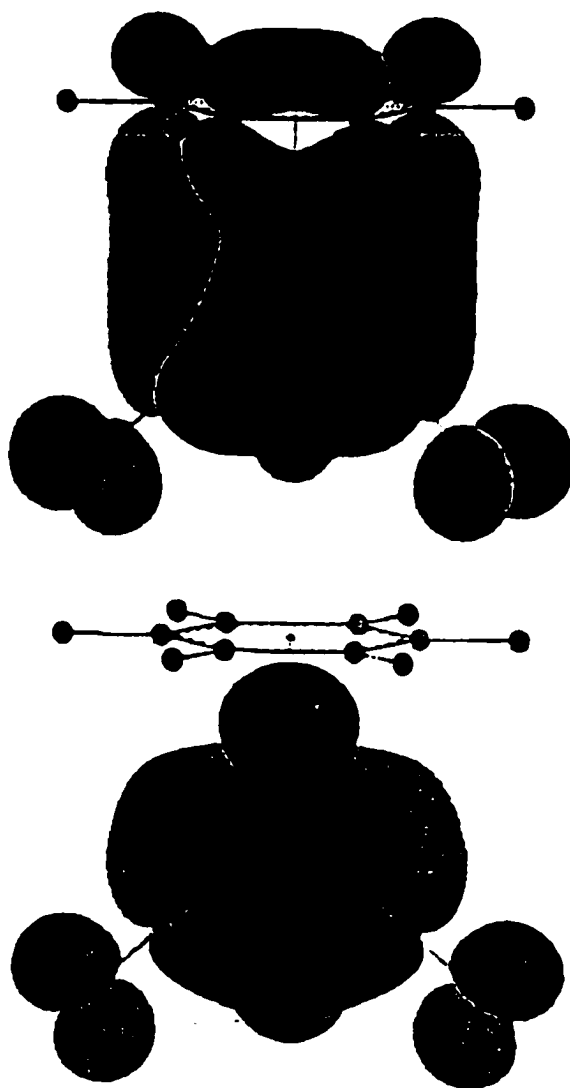


Figure 2.11. Frontier molecular orbitals of  $(\eta^6\text{-C}_6\text{H}_6)\text{Mo}(\text{CO})_3$ . The e symmetry orbital (top) and a<sub>1</sub> symmetry orbital (bottom).

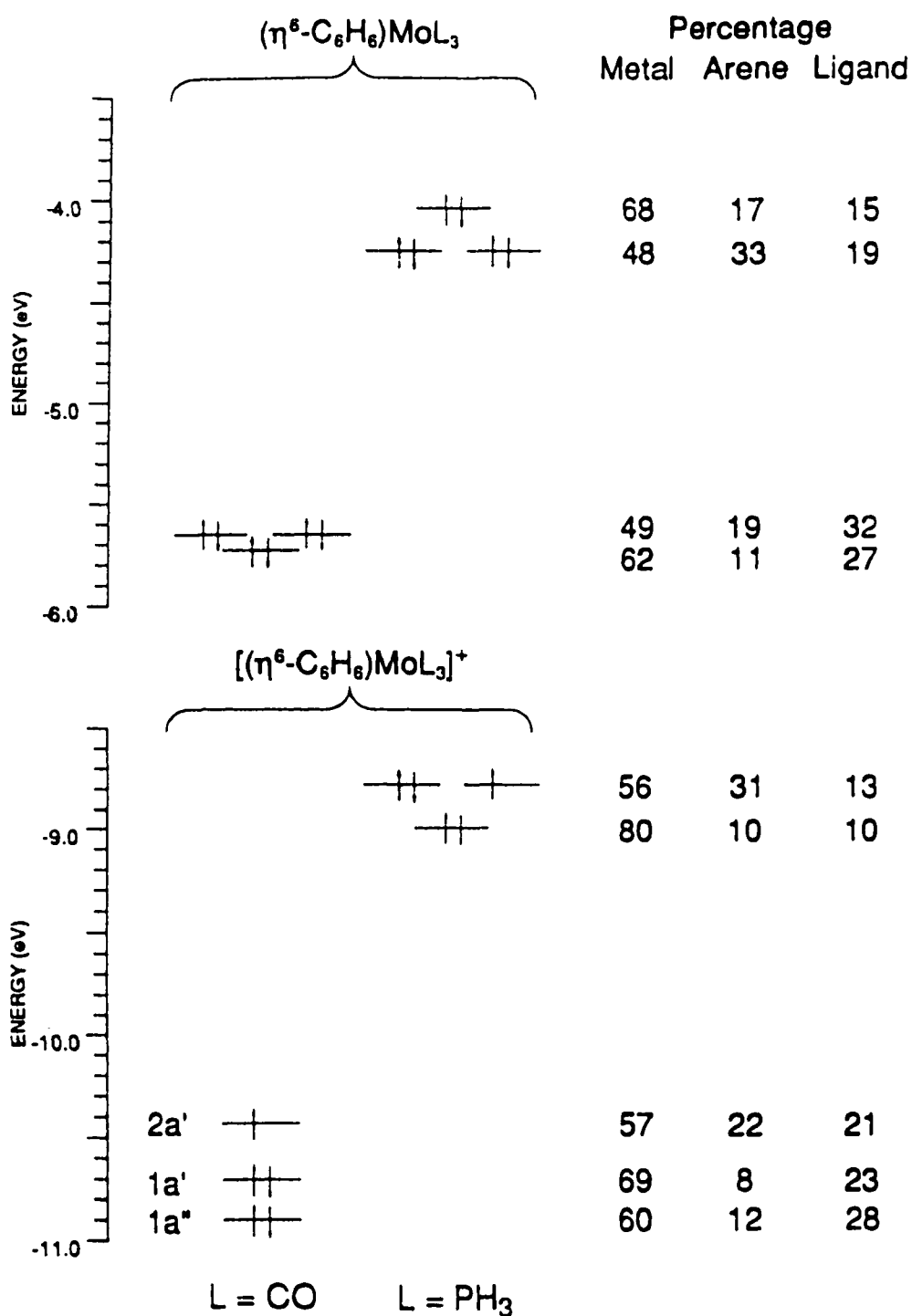


Figure 2.12. The calculated percentage contributions of metal, arene and monodentate ligands to the frontier molecular orbitals of  $(\eta^6\text{-C}_6\text{H}_6)\text{Mo}(\text{CO})_3$ ,  $[(\eta^6\text{-C}_6\text{H}_6)\text{Mo}(\text{CO})_3]^+$ ,  $(\eta^6\text{-C}_6\text{H}_6)\text{Mo}(\text{PH}_3)_3$  and  $[(\eta^6\text{-C}_6\text{H}_6)\text{Mo}(\text{PH}_3)_3]^+$ .



Figure 2.13. Calculated conformations of the TRIPOD molecule. *anti, anti, anti* (top) and *anti, gauche, gauche* (bottom) conformations.

Table 2.5. Selected interatomic distances (Å) and angles (deg) for  $[(\eta^6\text{-C}_6\text{H}_6)\text{Mo}(\text{PH}_3)_3]$  and  $[(\eta^6\text{-C}_6\text{H}_6)\text{Mo}(\text{PH}_3)_3]^+$ , and energies (eV) to lowest cation states.

| molecular charge         | 0                 | 0  | 0        | +1           | +1             |
|--------------------------|-------------------|--|----------|--------------|----------------|
|                          | Expt <sup>b</sup> | DFT                                      | RHF      | DFT          | UHF            |
| Symmetry                 | $C_{3v}$          | $C_{3v}$                                 | $C_{3v}$ | $C_s$        | $C_s$          |
| Mo-centroid <sup>a</sup> | 1.82              | 1.84                                     | 1.86     | 1.84         | 2.12           |
| C-C (arene)avg.          | 1.41(1)           | 1.43                                     | 1.43     | 1.43         | 1.41           |
| Mo-C(arene)avg.          | 2.30(2)           | 2.33                                     | 2.34     | 2.33         | 2.55           |
| Mo-P                     | 2.39(1)           | 2.41                                     | 2.61     | 2.48         | 2.69           |
| P-H                      | -                 | 1.45                                     | 1.42     | 1.43         | 1.41           |
| Centroid-Mo-P            | 1.30(1)           | 128                                      | 125      | 124          | 2 x 127<br>123 |
| P-Mo-P                   | 84(1)             | 87                                       | 90       | 92           | 2 x 87<br>95   |
|                          |                   | distortion <sup>c</sup> stabilization => |          | 4.5 kcal/mol | 12 kcal/mol    |

<sup>a</sup> Averaged center of arene ring.

<sup>b</sup> Average crystal geometric parameters and deviations from three-fold symmetry from the phosphorus atoms and six-fold symmetry for the arene for  $(\eta^6\text{-C}_6\text{H}_6)\text{Mo}(\text{TRIPOD})$ .

<sup>c</sup> From  $C_{3v}$  vertical position ion.

Table 2.6. Modeled vertical ionization energies to lowest positive ion states of  $(\eta^6\text{-C}_6\text{H}_6)\text{Mo}(\text{PH}_3)_3$ .

| Method       |                   | Energy(eV) |       |
|--------------|-------------------|------------|-------|
|              |                   | $^2A_1$    | $^2E$ |
| DFT          | orbital energies  | 4.23       | 4.04  |
| DFT          | E(ion)-E(neutral) | 6.20       | -     |
| HF           | orbital energies  | 6.88       | 5.88  |
| HF           | E(ion)-E(neutral) | 4.15       | 3.98  |
| MP2          | E(ion)-E(neutral) | 5.47       | 5.79  |
| EXPERIMENTAL |                   | 5.12-5.42  |       |

delocalized to the benzene  $\pi$  orbital framework while the  $a_1$  symmetry orbital is not. The  $e$ -orbital has more arene character than the  $a_1$  orbital as shown in Figure 2.12. Table 2.4 summarizes metal orbital energies and the vertical ionization energies to the lowest positive ion states. The results of calculations suggest that the energies of the  ${}^2E$  and  ${}^2A_1$  states are similar as seen in the PES studies.

The computed molecular structure of  $[(\eta^6\text{-C}_6\text{H}_6)\text{Mo}(\text{CO})_3]^+$  is highly distorted from the  $C_{3v}$  symmetry, as is typically observed for  $d_5(\eta^6\text{-C}_6\text{H}_6)\text{ML}_3$  complexes. The DFT and HF theoretical calculations both predict lengthening of the Mo-arene distance, short C-O distances due to reduced backbonding and opening of one OC-Mo-CO angles. There are no experimental crystal structures of  $[(\eta^6\text{-C}_6\text{H}_6)\text{M}(\text{CO})_3]^+$  complexes available, but the structure of  $(\eta^5\text{-C}_5\text{H}_5)\text{Cr}(\text{CO})_3$  shows distortion similar to the one calculated for  $[(\eta^6\text{-C}_6\text{H}_6)\text{Mo}(\text{CO})_3]^+$ .<sup>28</sup> The distortion might be attributed to a Jahn-Teller effect, which breaks the degeneracy of a  ${}^2E$  state in  $C_{3v}$  symmetry to form  ${}^2A'$  and  ${}^2A''$  states in  $C_s$  symmetry.<sup>29,30</sup>

The calculated geometry energy differences between the  ${}^2E$  positive ion and the neutral molecule are about 10 kcal/mole by DFT and 22 kcal/mole by *ab initio* Hartree-Fock method, respectively. The DFT value is more reliable because it closely reproduces the structure and Hartree-Fock value represents an upper limit.

**1,1,1-tris(diphenylphosphinomethyl)ethane.** Calculations for the TRIPOD molecule yield different structures within 10 kcal/mole of the most stable structure. Figure 2.13 (bottom) shows the space filling model of the most stable conformation that has two of the phosphines in *gauche* positions and one phosphine in the *anti* position with respect to the ethane bridge. All three phosphines are in an *anti* position with respect to the ethane bridge (Figure 2.13, top), when the TRIPOD ligand is coordinated to the Mo atom. The most stable conformation observed is consistent with the results of PES, which suggested that two phosphines are in a similar environment different from the third one. The other conformations observed are grouped according to one, two or all three phosphines in

basically *gauche* orientations with respect to the ethane bridge. Regardless of the particular conformation, the TRIPOD ligand is flexible enough to adapt to different coordinating environments.

$(\eta^6\text{-C}_6\text{H}_6)\text{Mo}(\text{PH}_3)_3$ .  $(\eta^6\text{-C}_6\text{H}_6)\text{Mo}(\text{PH}_3)_3$  was used as a model for  $(\eta^6\text{-C}_6\text{H}_6)\text{Mo}(\text{TRIPOD})$ , since the latter is too large for present computation methods. Both DFT and *ab initio* computational methods for the structure of  $(\eta^6\text{-C}_6\text{H}_6)\text{Mo}(\text{PH}_3)_3$  display  $C_{3v}$  symmetry with expected bond distances and angles. The density functional calculation is particularly successful. The computed distances of  $\text{Mo-C(arene)}_{\text{avg.}} = 2.33$  and  $\text{Mo-P} = 2.41$  are in agreement with those of known  $(\eta^6\text{-arene})\text{Mo}(\text{phosphine})_3$  complexes (also see Chapter 3).<sup>31,32</sup> The molecular structure from the Hartree-Fock calculation is also reasonable except for the Mo-P distance, which is 0.2 Å longer.

The various calculated metal-based ionization energies are listed in Table 2.6. The first ionization of  $(\eta^6\text{-C}_6\text{H}_6)\text{Mo}(\text{PH}_3)_3$  is shifted 2.2 eV to lower energy from that of  $(\eta^6\text{-C}_6\text{H}_6)\text{Mo}(\text{CO})_3$ . The calculations shows reasonable shifts of 1.5 to 2.0 eV, given the model of  $(\text{PH}_3)_3$  for the TRIPOD ligand. Although both methods find the e-set orbitals as the HOMO's, they were unable to predict the state that represents the lowest ionization energy and the most stable ion state. A  $^2A_1$  ground state was predicted for the positive ion constrained to the  $C_{3v}$  geometry of neutral molecule by DFT calculations and by MP2 correlation estimates on the Hartree-Fock calculations.

The DFT calculations show about 33% total arene character (primarily derived from the arene  $e_{2u}$  orbital) in the predominantly metal e orbital for the model complex  $(\eta^6\text{-C}_6\text{H}_6)\text{Mo}(\text{PH}_3)_3$ . Because the TRIPOD ligand is expected to be a better donor than  $\text{PH}_3$ , even more arene character would be expected in this orbital of the TRIPOD complex.

The molecular structures and energies along different paths of the potential energy surface for protonation were studied. The intrinsic reaction coordinates for the protonation of  $(\eta^6\text{-C}_6\text{H}_6)\text{Mo}(\text{PH}_3)_3$  is shown in Figure 2.15. The calculation assumes gas-phase conditions for protonation and ignores the effect of solvent and conjugate base of the acid.

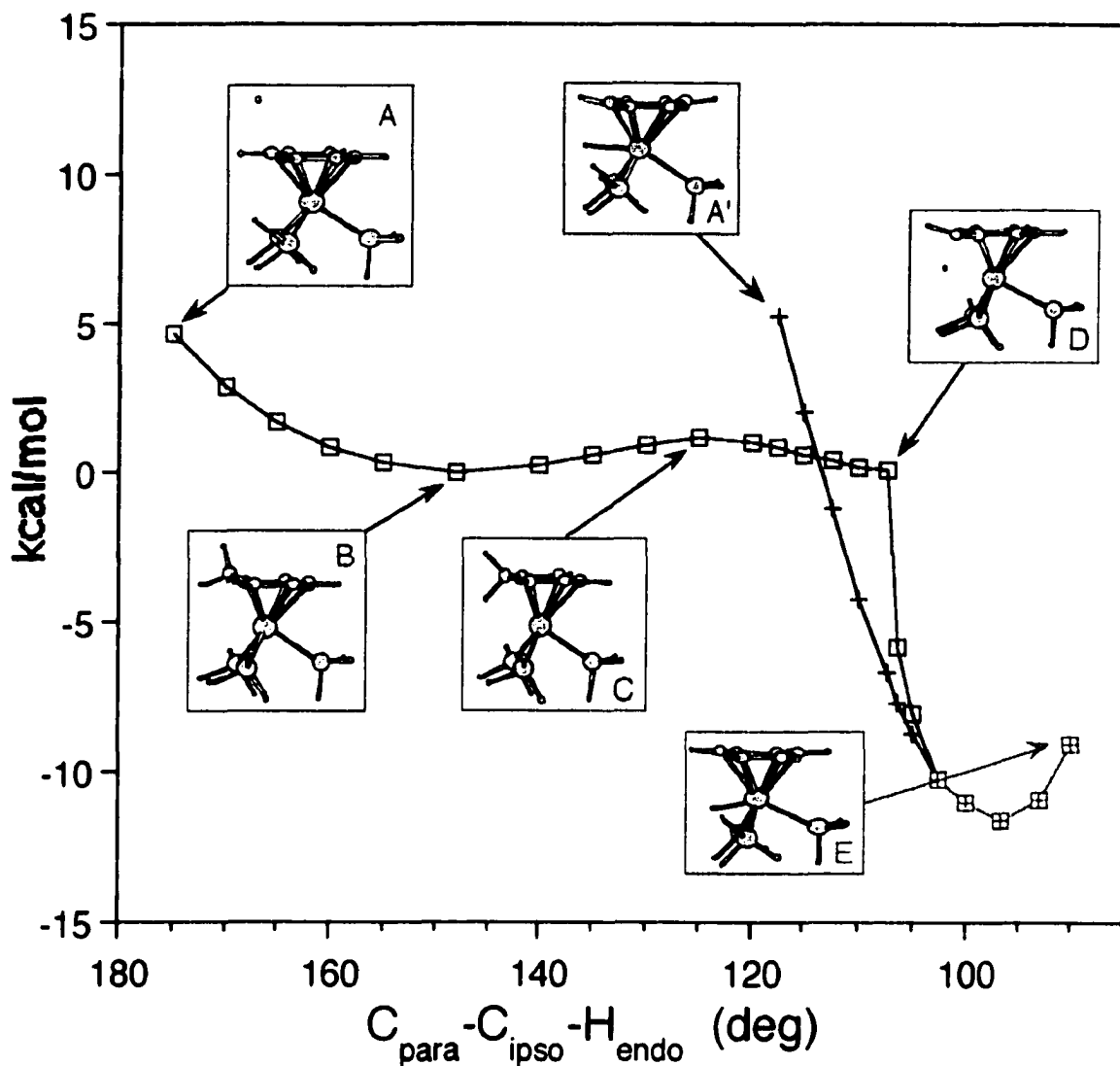


Figure 2.14. Intrinsic reaction coordinate diagram for the protonation of  $(\eta^6\text{-C}_6\text{H}_6)\text{Mo}(\text{PH}_3)_3$  via direct attack on the metal ( $\square$ ,  $A' \rightarrow E$ ) and indirect attack on the arene ( $\circ$ ,  $A \rightarrow B \rightarrow C \rightarrow D \rightarrow E$ ). The two pathways merge at  $H\text{-C}_{ipso}\text{-C}_{para} = 105^\circ$ .

There are two pathways in the potential energy surface that would lead to protonation of the complex. The direct metal attack pathway and indirect arene attack pathway have potential energy minimums for protonation. The  $\text{H-C}_{\text{ipso}}-\text{C}_{\text{para}}$  angle (where H is the incoming proton the in the direct metal attack pathway and the endo proton in the indirect arene pathway) was used as a measurement of the reaction coordinate. The two pathways merge at an angle of  $105^\circ$ .

At point A (in Figure 2.14) arene ring is nearly planar, as the proton is yet not bonded to the complex. At this point, the complex is oxidized through an electron transfer to the proton, which is due to the strong attraction (13.6 eV) between the proton and the electron. At point B, the C-H bond is formed, creating a 16 electron ( $\eta^5$ -cyclohexadienyl) metal complex with a +II,  $d^4$  metal center. Point C is the transition state that brings the endo C-H bond to the metal to satisfy the electron deficiency, which needs only about 2 kcal/mol from point B. The formation of Mo-H begins at point D that dramatically lowers the energy and quickly breaks the C-H bond. The direct metal attack pathway ( $A' \rightarrow E$ ) merges with the indirect pathway between points D and E at around  $105^\circ$ .

## 2.8 SUMMARY

Both experiments and calculations indicate that the HOMO's of  $(\eta^6\text{-C}_6\text{H}_6)\text{Mo}(\text{L})_3$  complexes are the  $a_1$  and e orbitals. The energies of the two orbitals are very close and ionizations of these lead to  $^2A_1$  and  $^2E$  positive ion states that are similar in energy. PES and calculations suggest that the  $^2E$  state is split by Jahn-Teller distortion reducing the overall symmetry of the molecule to  $C_2$ . The  $^2E$  ion state has delocalized more electron spin on to the benzene ring. The PES and the EPR results suggest that the first electron is ejected from the e-set orbital.

Protonation of organic compounds<sup>2</sup> and nucleophilic reaction of some organometallics<sup>33</sup> are believed to take place under frontier orbital control. If the present case is also frontier orbital controlled and the  $a_1$  orbital is the HOMO, then  $a_1$  should be the

site of electrophilic attack. An earlier EHMO study of  $(\eta^6\text{-arene})\text{Mo}(\text{CO})_3$  predicts the  $a_1$  orbital as the HOMO for sterically demanding arene ligands (e.g.  $\text{C}_6\text{Et}_6$ ) and electrophilic attack is preferred along the z-axis opposite from the arene ligand to give a metal-hydride complex of  $C_{3v}$  symmetry.<sup>27</sup> However, for less demanding arene ligands (e.g.  $\text{C}_6\text{H}_6$ ), the proton is favored in a lateral location to give a metal-hydride complex of  $C_s$  symmetry. The  $a_1$  orbital (the  $d_{z^2}$  orbital) projects electron density in both directions.

In the present case of  $(\eta^6\text{-C}_6\text{H}_6)\text{Mo}(\text{TRIPOD})$ , the ethane linkage of the TRIPOD ligand protects the area of the  $a_1$  orbital that is localized along the z axis. Furthermore, the portions of the e symmetry orbitals in the x-y plane are protected by the phenyl groups of the TRIPOD ligand. Since the metal is encapsulated, the solvated proton cannot gain direct access to the metal center. Instead the proton gains access to the metal based e orbital which has a sizable arene  $\pi$  electron density.

In the case of  $(\eta^6\text{-C}_6\text{H}_6)\text{Mo}(\text{CO})_3$ , the e orbital contains less arene character than the  $a_1$  orbital because of the poor energy matching of the arene LUMO. Moreover,  $\pi$ -backbonding of CO ligands with the metal orbitals reduces metal-arene overlap. The metal orbitals are destabilized when the CO's are replaced by phosphines due to good  $\sigma$ -donor ability and lack of back bonding in phosphines. The result is better overlap and better energy matching of the e metal orbital with the arene  $e_{2u}$  orbital, and therefore a substantial amount of arene-character in this metal-based orbital.

In conclusion, the TRIPOD ligand, while rendering the metal center very electron-rich, also encapsulates the metal center, sterically protecting it from direct attack by electrophiles. The proton is presumably delivered as a tight ion pair with the acid's conjugate base in non-polar solvents like  $\text{CH}_2\text{Cl}_2$ , and is therefore unable to be delivered directly to the metal. The initial step in the mechanism likely involves electrophilic attack at a more kinetically accessible site to the frontier orbital density. This study of  $(\eta^6\text{-C}_6\text{H}_6)\text{Mo}(\text{TRIPOD})$  has shown the HOMO is primarily metal in character although it contains a sizable amount of arene character. The initial proton attack on the arene takes

place at the same frontier orbital as the direct attack on the metal except on a different portion of the molecular orbital. These results indicate that this mechanism of protonation requires certain steric and electronic features in the molecule. The arenium mechanism of protonation displayed by ( $\eta^6$ -C<sub>6</sub>H<sub>6</sub>)Mo(TRIPOD) is assisted by a highly electron rich metal center, but is not expected to be general.

## 2.9 BIBLIOGRAPHY

- (1) Kristjansdottir, S. S.; Norton, J. R. In *Transition Metal Hydrides*; Dedieu, A., Ed.; VCH: Weinheim, 1992, pp 309-355.
- (2) DeKock, R. L. *J. Am. Chem. Soc.* **1975**, *97*, 5592.
- (3) Gower, M.; Kane-Maguire, L. A.; Maier, J. P.; Sweigart, D. A. *J. Chem. Soc., Dalton Trans.* **1977**, 316.
- (4) Worley, S. D.; Webb, T. R. *J. Organomet. Chem.* **1980**, *192*, 139-145.
- (5) Byers, B. P.; Hall, M. B. *Organometallics* **1987**, *6*, 2319-2325.
- (6) Connelly, N. G.; Demidowicz, Z.; Kelly, R. L. *J. Chem. Soc., Dalton Trans.* **1975**, 2335.
- (7) Howell, J. O.; Goncalves, J. M.; Amatore, C.; Klasinc, L.; Wightman, R. M.; Kochi, J. K. *J. Am. Chem. Soc.* **1984**, *106*, 3968-3976.
- (8) Van Order, N.; Geiger, W. E.; Bitterwolf, T. E.; Rheingold, A. L. *J. Am. Chem. Soc.* **1987**, *109*, 5680.
- (9) Morris, R. H.; Earl, K. A.; Luck, R. L.; Lazarowych, N. J.; Sella, A. *Inorg. Chem.* **1987**, *26*, 2674-2683.
- (10) Rourke, F.; Gash, R.; Crayston, J. A. *J. Organomet. Chem.* **1992**, *423*, 223-239.
- (11) Kohler, F. H.; Metz, B.; Strauss, W. *Inorg. Chem.* **1995**, *34*, 4402-4413.
- (12) Talarmin, J.; Al-Salih, T. I.; Pickett, C. J.; Bossard, G. E.; George, T. A.; Duff-Spence, C. M. *J. Chem. Soc., Dalton Trans.* **1992**, 2263-2269.
- (13) Green, M. L. H.; Hughes, A. K.; Lincon, P.; Martin-Polo, J. J.; Mountford, P.; Sella, A.; Wong, L.-L.; Bandy, J. A.; Banks, T. W.; Prout, K.; Watkin, D. J. *J. Chem. Soc., Dalton Trans.* **1992**, 2063-2069.
- (14) Cooper, G.; Green, J. C.; Payne, M. P.; Dobson, B. R.; Hillier, I. H. *J. Am. Chem. Soc.* **1987**, *109*, 3836.
- (15) Hubbard, J. L.; Lichtenberger, D. L. *J. Chem. Phys.* **1981**, *75*, 2560.

- (16) Bursten, B. E.; Darensbourg, D. J.; Kellogg, G. E.; Lichtenberger, D. L. *Inorg. Chem.* **1984**, *23*, 4361.
- (17) Puddephatt, R. J.; Bancroft, G. M.; Chan, T. *Inorg. Chim. Acta* **1983**, *73*, 83.
- (18) Puddephatt, R. J.; Dignard-Bailey, L.; Bancroft, G. M. *Inorg. Chim. Acta* **1985**, *96*, L91.
- (19) Connelly, N. G.; Geiger, W. E. *Chem. Rev.* **1996**, *96*, 887.
- (20) Ernst, M. F.; Roddick, D. M. *Organometallics* **1990**, *9*, 1586.
- (21) Loufty, R. O. *J. Chem. Phys.* **1963**, *18*, 4781.
- (22) Pysh, E. S.; Yang, N. C. *J. Am. Chem. Soc.* **1963**, *85*, 2124.
- (23) Pleune, B.; Poli, R.; Fettinger, J. C. *J. Am. Chem. Soc.* **1998**, *120*, 3257.
- (24) Feldman, V. I.; Sukhov, F. F.; Orlov, A. Y. *Chem. Phys. Lett.* **1999**, *300*, 713.
- (25) Atkins, P. *Physical Chemistry*; 5 ed.; W. H. Freeman: New York, 1994.
- (26) Burgi, H.-B.; Raselli, A.; Braga, D.; Griponi, F. *Acta Crystallogr., Sect. B* **1992**, *48*, 428.
- (27) Mailvaganam, B.; Sayer, B. G.; McGlinchey, M. J. *Organometallics* **1990**, *9*, 1089-1093.
- (28) Fortier, S.; Baird, M. C.; Preston, K. F.; Morton, J. R.; Ziegler, T.; Jaeger, T. J.; Watkins, W. C.; Macneil, J. H.; Watson, K. A.; Hensel, K.; Page, Y. L.; Charland, J. P.; Williams, A. J. *J. Am. Chem. Soc.* **1991**, *113*, 542.
- (29) Krusic, P. J.; McLain, S. J.; Morton, J. R.; Preston, K. F.; Page, Y. L. *J. Magn. reson.* **1987**, *74*, 72.
- (30) Morton, J. R.; Preston, K. F.; Cooley, N. A.; Baird, M. C. *J. Chem. Soc., Faraday Trans. 1* **1987**, *83*, 3535.
- (31) Morris, R. H.; Sawyer, J. F.; Sella, A. *Acta Crystallogr., Sect. C: Cryst. Struct. Commun.* **1988**, *C44*, 23-27.
- (32) Mason, R.; Thomas, K. M.; Heath, G. K. *J. Organomet. Chem.* **1975**, *90*, 195
- (33) Block, T. F.; Fenske, R. F.; Casey, C. P. *J. Am. Chem. Soc.* **1976**, *98*, 441.

## CHAPTER 3

# EFFECT OF PHOSPHORUS LIGAND VARIATION ON THE MECHANISM OF PROTONATION OF $(\eta^6\text{-C}_6\text{H}_6)\text{Mo}(\text{PHOSPHINE})_3$ COMPLEXES

### 3.1 INTRODUCTION

The reactions of acids with organometallic complexes have been known for nearly four decades now.<sup>1</sup> Protonations of metal complexes have been investigated from both fundamental and practical perspectives.<sup>2</sup> From the fundamental view, protonation is one of the simplest yet important electrophilic reaction with the metal complexes. The protonation causes a change in the metal complex without altering its electron count. Practical interests arise from the fact that protonation is related to the biological pathways such as nitrogen fixation and metal-ion catalyzed hydrogen evolution by metalloenzymes.<sup>3</sup> Protonation of metal complexes are also related to catalytic processes<sup>4</sup> such as hydrogenation of unsaturated organic ligands which involve heterolytic activation of hydrogen.

### 3.2 LITERATURE OVERVIEW

The mechanism of protonation of transition metal complexes with arene ligands has been the subject of many studies. Detailed investigations of the mechanisms of electrophilic substitution have been carried for the ferrocene and benzotrene series.<sup>5</sup> The protonation of  $\eta^6$ -arene metal complexes was first studied by Wilkinson et al. in 1962.<sup>1</sup> In that study, a series of  $(\eta^6\text{-arene})\text{Cr}$  complexes in  $\text{BF}_3\cdot\text{H}_2\text{O}/\text{CF}_3\text{COOH}$  mixture were shown to have protonated metal centers as characterized by high field  $^1\text{H}$  NMR resonances. The

complex  $(\eta^6\text{-arene})\text{Cr}(\text{CO})_3$  and its derivatives have been thoroughly studied owing to the ease of their syntheses. Lillya and Sahatjian<sup>6</sup> have studied the protonation of  $(\eta^6\text{-arene})\text{Cr}(\text{CO})_3$  (arene = benzene, mesitylene, hexamethylbenzene and 1,3,5-trimethoxybenzene) using variable temperature <sup>1</sup>H NMR and proposed possible mechanisms for proton exchange. Olah and Yu<sup>7</sup> have demonstrated using <sup>13</sup>C NMR studies that the metal is the most probable site of protonation in the reaction of FSO<sub>3</sub>H/SO<sub>3</sub> with  $(\eta^6\text{-C}_6\text{H}_5\text{OMe})\text{Cr}(\text{CO})_3$ . Green and coworkers have synthesized various  $(\eta^6\text{-arene})\text{Mo}(\text{PR}_3)_3$  (arene = benzene, mesitylene; R = Me, Et, Ph, OMe, OPh) complexes and have isolated the mono- and di- protonated species.<sup>8,9</sup> The PR<sub>3</sub> ligands are more basic and less  $\pi$ -accepting than CO ligands, which makes the metal complexes more basic allowing the isolation of protonated products. Kursanov et al. have carried out several studies on protonation of  $(\eta^6\text{-arene})\text{CrL}_3$  system over a period of two decades. They have shown that electron releasing groups on the arene enhance while electron-attracting groups hinder protonation of these complexes.<sup>10</sup> In a solution of BF<sub>3</sub>·D<sub>2</sub>O/CF<sub>3</sub>COOH,  $(\eta^6\text{-C}_6\text{H}_6)\text{Cr}(\text{CO})_3$  undergoes electrophilic hydrogen isotope exchange (HIE) to give  $(\eta^6\text{-C}_6\text{D}_6)\text{Cr}(\text{CO})_3$ .<sup>11</sup> Substitution of a carbonyl ligand of  $(\eta^6\text{-arene})\text{Cr}(\text{CO})_3$  by a PPh<sub>3</sub> ligand results in increased basicity of the complex and facilitates its protonation. The HIE's for various arenes have been compared.<sup>12</sup> The complexes  $(\eta^6\text{-arene})\text{Cr}(\text{Ph}_2\text{CH}_2\text{CH}_2\text{PPh}_2)(\text{CO})$  (arene = benzene, mesitylene) have faster rates of HIE compared with the tricarbonyl complex.<sup>13</sup> The ligand C<sub>4</sub>H<sub>2</sub>O<sub>3</sub> was protonated in the case of the complex  $(\eta^6\text{-arene})\text{Cr}(\text{CO})_2(\eta^2\text{-C}_4\text{H}_2\text{O}_3)$ , where C<sub>4</sub>H<sub>2</sub>O<sub>3</sub> = maleic anhydride, when reacted with CF<sub>3</sub>COOH.<sup>14</sup> The HIE was measured for these complexes and found to be similar to that of  $(\eta^6\text{-C}_6\text{H}_6)\text{Cr}(\text{CO})_3$  under identical conditions. No mechanism was proposed for the HIE process. In another study, protonation of the complexes M-( $\eta^6\text{-PPh}_2\text{C}_6\text{H}_5$ )Cr(CO)<sub>3</sub> where M =  $(\eta^6\text{-C}_6\text{H}_6)\text{Cr}(\text{CO})_2$ ,  $(\eta^5\text{-C}_5\text{H}_5)\text{Mn}(\text{CO})_2$ , Cr(CO)<sub>5</sub>, Mo(CO)<sub>5</sub> and W(CO)<sub>5</sub> was reported.<sup>15</sup> Setkina et al. have studied the protonation of  $(\eta^6\text{-arene})\text{Cr}(\text{CO})_2\text{L}$  in which L=Pf<sub>2</sub>PhH and Pf<sub>2</sub>H (where Fc=ferrocenyl) and found

that the Cr atom is protonated.<sup>16</sup> It was concluded that M does not have an effect on the HIE process. Protonation of  $(\eta^6\text{-arene})\text{Cr}(\text{CO})_2(\text{PMe}_2\text{Ph})$  (arene =  $\text{C}_6\text{H}_6$ ,  $\text{C}_6\text{H}_3\text{Me}_3$ ; M = Cr, Mo, W) was studied<sup>17</sup> using variable temperature NMR spectroscopy. Two isomers of the metal protonated complexes were observed to undergo rapid nondissociative interconversion. The reaction of acid with  $(\eta^6\text{-PPh}_2\text{C}_6\text{H}_5)\text{Mo}(\text{Ph}_2\text{CH}_2\text{CH}_2\text{PPh}_2)(\text{PPh}_3)$  yields a MoH complex.<sup>18</sup> The proposed mechanism involves an initial attack of protons at both the metal and  $\eta^0$ -phosphine ligand leading to P-C bond cleavage and formation of a  $(\eta^6\text{-C}_6\text{H}_6)\text{MoH}$  type complex. McGlinchey et al. have studied the protonation of  $(\eta^6\text{-C}_6\text{H}_6)\text{M}(\text{CO})_3$  (M = Cr, Mo, W) using  $^{13}\text{C}$  NMR and theoretical methods.<sup>19</sup> They found that the protonated metal center is fluxional between  $\text{C}_{3v}$  and  $\text{C}_s$  geometries. For the biphenyl and diphenylmethane complexes of  $\text{Cr}(\text{CO})_3$ , neighboring group assistance of electrophilic substitution was reported.<sup>20</sup> Green and co-workers have protonated  $(\eta^6\text{-toluene})\text{WL}_3$  [ $\text{L}_3 = 3\text{PMe}_3$  and  $\text{MeSi}(\text{CH}_2\text{PMe}_2)_3$ ] using  $\text{NH}_4\text{BF}_4$  and HCl gas to give the mono- and di- protonated salts, respectively.<sup>21</sup> George and Hammund have synthesized and protonated molybdenum complexes of the formula  $(\eta^6\text{-C}_6\text{H}_5\text{R})\text{Mo}(\text{TRIPHOS})$  in which R = H, Me, and OMe and  $\text{TRIPHOS} = \text{PhP}(\text{CH}_2\text{CH}_2\text{PPh}_2)_2$ .<sup>22</sup>

Electrophilic reactions with arene complexes that are  $\eta^4$  and  $\eta^2$  bound are also known. Cooper et al. have protonated  $[(\eta^4\text{-benzene})\text{Cr}(\text{CO})_3]^{2-}$  and  $[(\eta^4\text{-benzene})\text{Mn}(\text{CO})_3]^-$  complexes to form the respective cyclohexadienyl species and in the former case protonation was shown to be metal mediated.<sup>23,24</sup> Dihapto coordinated aromatic hydrocarbons have been protonated to form the cyclohexadienyl cations.<sup>25</sup> In a recent study by Harman et al.,  $[\text{Os}(\text{NH}_3)_5(\eta^2\text{-L})](\text{OTf})_2$  (where L = various arenes) were protonated to form the  $[\text{Os}(\text{NH}_3)_5(\eta^3\text{-LH})](\text{OTf})_3$  complexes, in which the LH is the  $\eta^3$  bound arenium cation.<sup>26</sup> In a communication, Kowalski and Ashby reported the first evidence of a electrophilic aromatic protonation of  $(\eta^6\text{-arene})\text{metal}$  complex leading to metal hydride product.<sup>27</sup>

When  $(\eta^6\text{-C}_6\text{H}_6)\text{Mo}(\text{TRIPOD})$  (**1**) was treated with acid, the metal hydride complex was formed via a cyclohexadienyl transient species (see Chapter 1 for the details of the mechanism). The electronic properties studies (see Chapter 2) of  $(\eta^6\text{-C}_6\text{H}_6)\text{Mo}(\text{TRIPOD})$  indicate that the metal should be the site of protonation on the basis of electronic properties alone and the mechanistic studies of protonation clearly demonstrate (as seen in Chapter 1) that the initial site of protonation is the arene ring. The bulky phosphine TRIPOD ligand was seen to envelop the metal, thereby preventing equatorial approach of a proton for direct protonation at the metal. By replacing TRIPOD ligand with other less bulkier phosphines, the site of initial protonation may change. Therefore, to check the generality of the mechanism and to deduce the steric and electronic factors governed by the phosphine ligands in the electrophilic aromatic protonations of  $(\eta^6\text{-arene})\text{Mo}(\text{phosphine})_3$  complexes, four known complexes were synthesized and their protonation and studied. In this chapter the protonation mechanisms of closely related complexes  $(\eta^6\text{-C}_6\text{H}_6)\text{Mo}(\text{TRIPHOS})$  (**4**),  $(\eta^6\text{-C}_6\text{H}_6)\text{Mo}(\text{PMePh}_2)_3$  (**7**),  $(\eta^6\text{-C}_6\text{H}_6)\text{Mo}(\text{PMe}_2\text{Ph})_3$  (**8**) and  $(\text{C}_6\text{H}_6)\text{Mo}(\text{PMe}_3)_3$  (**9**) are described.

### 3.3 SYNTHESIS OF $(\eta^6\text{-C}_6\text{H}_6)\text{Mo}(\text{PHOSPHINE})_3$ COMPLEXES

Complexes **7** and **8** were reported as synthesized by refluxing xylenes (120 °C) solution of phosphine and  $(\eta^6\text{-C}_6\text{H}_6)_2\text{Mo}$ .<sup>28</sup> Neat melt reaction of TRIPOD and  $(\eta^6\text{-C}_6\text{H}_6)_2\text{Mo}$  was employed for the synthesis of **1**. Complex **4** was obtained in an impure form by a reduction route. George and Hammund have synthesized **4** in 40% yield by reducing  $\text{Cl}_3\text{Mo}(\text{TRIPHOS})$  with Na/Hg in benzene.<sup>22</sup> Green et al. have previously shown that complexes **7**, **8**, and **9** that bear monodentate phosphine ligands can be protonated to give metal-hydride complexes.<sup>29</sup>

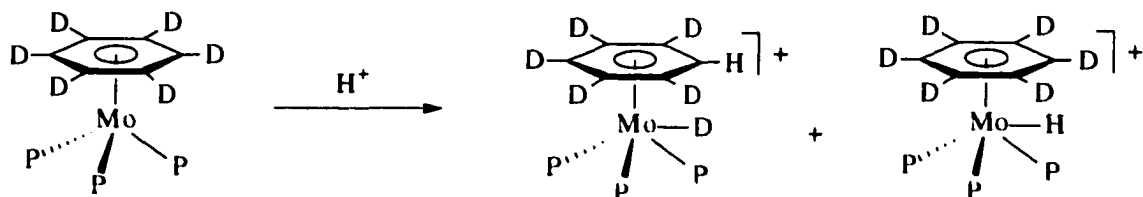
In this project, **1** and **4** were originally obtained through neat melt reactions at 160 °C. Later on, complexes **1**, **4**, **7**, **8** and **9** were synthesized by refluxing at 160 °C the benzene solution of the appropriate phosphine and  $(\eta^6\text{-C}_6\text{H}_6)_2\text{Mo}$  under vacuum. The

arene displacement route provides cleaner) product in higher yield than the reduction procedure reported for **4**.

### 3.4 ISOTOPE TRACER STUDIES

Initial isotope tracer studies of the  $C_6H_6$  derivatives with  $CF_3SO_3D$  did not give reproducible results due to exchange of acid with adventitious  $H_2O$  (moisture) in the solvent or glassware. However, tracer studies that were carried out for  $C_6D_6$  derivatives with  $CF_3SO_3H$ , gave reproducible results. The complexes  $(\eta^6-C_6D_6)Mo(P)_3$ , ((P)<sub>3</sub> = TRIPOD, (PPh<sub>2</sub>Me)<sub>3</sub>, (PPhMe<sub>2</sub>)<sub>3</sub>, (PMe<sub>3</sub>)<sub>3</sub> and TRIPHOS) were reacted with one equivalent of  $CF_3SO_3H$  in  $CD_2Cl_2$  and  $CH_2Cl_2$  solutions to give the corresponding protonated complexes as depicted in Scheme 3.4. The results of the tracer studies, as measured by  $^1H$  and  $^3H$  NMR spectra peak integrations, are summarized in Table 3.1. The NMR spectra are shown in Section 6.4.

Initial protonation of **1** and **7** occurs on the ring. Considering **1** and **7** having similar ligand environments (diarylalkylphosphines), it is not unexpected that the initial sites of protonation are similar for the two. Calculations have predicted that protonation of the metal does not occur along the z-axis.<sup>30</sup> Single crystal X-ray structure of **7** shows that the three Me groups of the phosphines are pointing opposite from the arene creating a vacant space along the z-axis. Though **7**, unlike **1**, has an open end access to the metal from the opposite side of the arene ligand, initial protonation still occurs at the ring. Thus initial protonation of **7** on the ring, suggests that the proton prefers to approach the metal along the equatorial axis, perpendicular to the metal-arene centroid. Since for **1** and in **7** the phenyl groups on the phosphorus block the equatorial axis, the acid reacts with the ring initially. For **8**, the phosphine ligand bears two alkyl and one aryl substituents, which makes it less sterically demanding than **1** or **7**. However **8**, shows a high (80%) percentage of ring protonation. This would mean that the aryl group on the phosphorus atoms covers the metal, but not as effective as in **7** which has two aryl groups on the



Scheme 3.1 Possible products upon addition of  $\text{H}^+$  to  $(\eta^6\text{-C}_6\text{D}_6)\text{Mo}(\text{P})_3$

Table 3.1 Percentages of isotopic distribution from the tracer studies

| Complex                | Ligand                  | % by $^1\text{H}$ NMR spectra |       | % by $^2\text{H}$ NMR spectra |       |
|------------------------|-------------------------|-------------------------------|-------|-------------------------------|-------|
|                        |                         | Metal                         | Arene | Metal                         | Arene |
| <b>1-d<sub>6</sub></b> | TRIPOD                  | 0                             | 100   | 0                             | 100   |
| <b>7-d<sub>6</sub></b> | $\text{PPh}_2\text{Me}$ | 0                             | 100   | 0                             | 100   |
| <b>8-d<sub>6</sub></b> | $\text{PPhMe}_2$        | 22                            | 78    | 16                            | 84    |
| <b>9-d<sub>6</sub></b> | $\text{PMe}_3$          | 37                            | 63    | 39                            | 61    |
| <b>4-d<sub>6</sub></b> | TRIPHOS                 | 88                            | 12    | 72                            | 28    |

phosphorus atoms. It should be also noted that the Mo-P bond in **8** can, in principle, rotate allowing it to exist in more than one conformation. The electronic factors are comparable for  $(\eta^6\text{-C}_6\text{D}_6)\text{Mo}(\text{TRIPOD})$  and  $(\eta^6\text{-C}_6\text{D}_6)\text{Mo}(\text{TRIPHOS})$ , yet they have strikingly different sites of initial protonations. This result suggests that the steric factors may play a dominant role. Initial protonation of **4** takes place about 80% on the metal. For **4**, the TRIPHOS ligand has one unique P atom, in the middle, bearing one phenyl group and two equivalent terminal P atoms having two phenyl groups each. It might seem that there is an open access to metal between the two terminal P atoms. But the space filling model suggests that the space inbetween the two P atoms is sterically protected by the phenyl groups. Instead there is a void over the methylene bridges that connect the two terminal P atoms with the middle P atom. This void can provide some evidence for the low arene protonation percentage of **4**. However, protonation of **9** shows a different picture. Complex **9** has the smallest phosphines which should make them less sterically crowded and the metal more accessible to the incoming  $\text{H}^+$  and direct metal attack percentage would be expected to be higher than for **4**. Nevertheless, the reverse is observed. About a 60:40 ratio of arene versus metal protonation was observed for **9**. Simple steric models do not explain this entire trend. Therefore, to rationalize these observed protonation trends, calculations based on single crystal X-ray structures for **1**, **4**, **7** and **8** were carried out. The single crystal X-ray structures were obtained for complexes **4**, **7** and **8**. Table 3.2 presents a comparison of the metric parameters for the complexes **1**, **4**, **7** and **8**. Theoretical calculations based on single crystal X-ray structures were carried out for **1**, **4**, **7**, **8**, and **9** and the results are tabulated in Table 3.3. Attempts to obtain X-ray quality crystals of **5** were not successful. Semi-empirical calculations essentially predict the conformations of **1**, **4**, **7**, and **8** that are displayed by the crystal structures. The phenyl groups in **1** and **7** are pointing toward the arene ligand as seen in the respective crystal structures. The calculations show that the thermodynamically preferred structure for **7** is the same as the one observed in the crystal structure, though other orientations of the

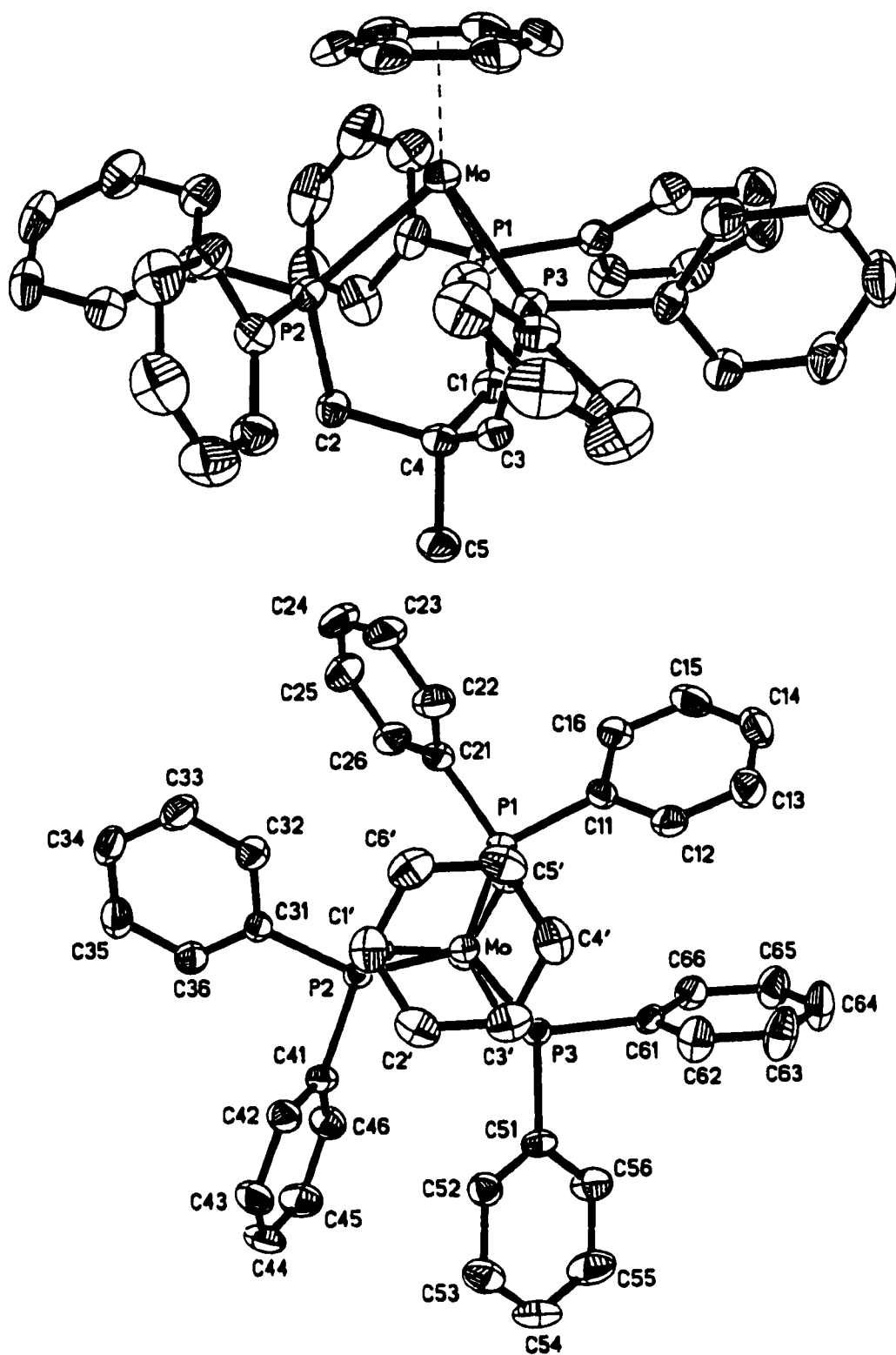


Figure 3.1. Thermal ellipsoid drawing (50% probability) of  $(\eta^6\text{-C}_6\text{H}_6)\text{Mo}(\text{TRIPOD})$  (1) sideview (top) and top view (bottom).

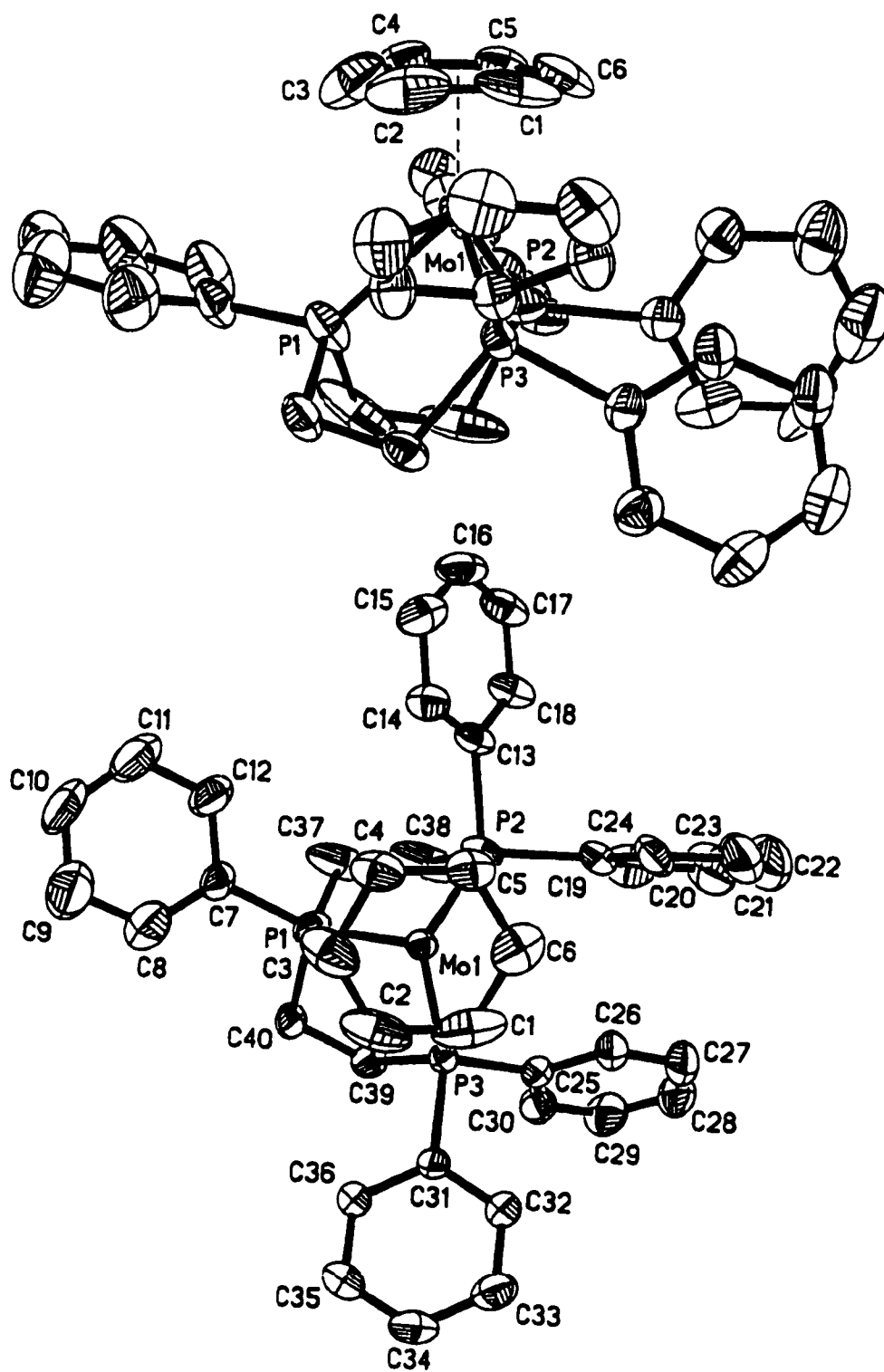


Figure 3.2. Thermal ellipsoid drawing (50% probability) of  $(\eta^6\text{-C}_6\text{H}_6)\text{Mo}(\text{TRIPHOS})$  (4) sideview (top) and top view (bottom).

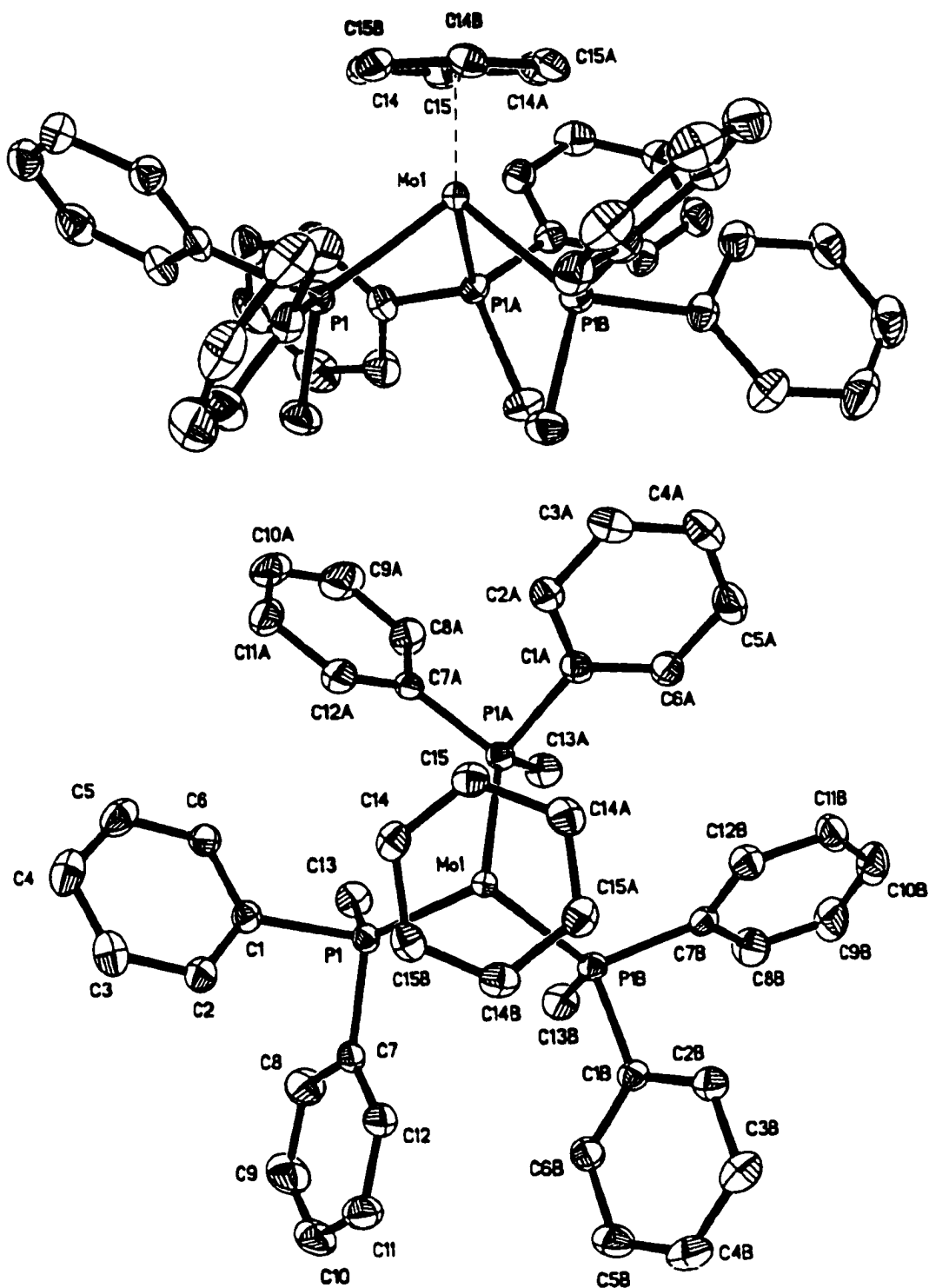


Figure 3.3. Thermal ellipsoid drawing (50% probability) of  $(\eta^6\text{-C}_6\text{H}_6)\text{Mo}(\text{PMePh}_2)_3$  (**7**) sideview (top) and top view (bottom).

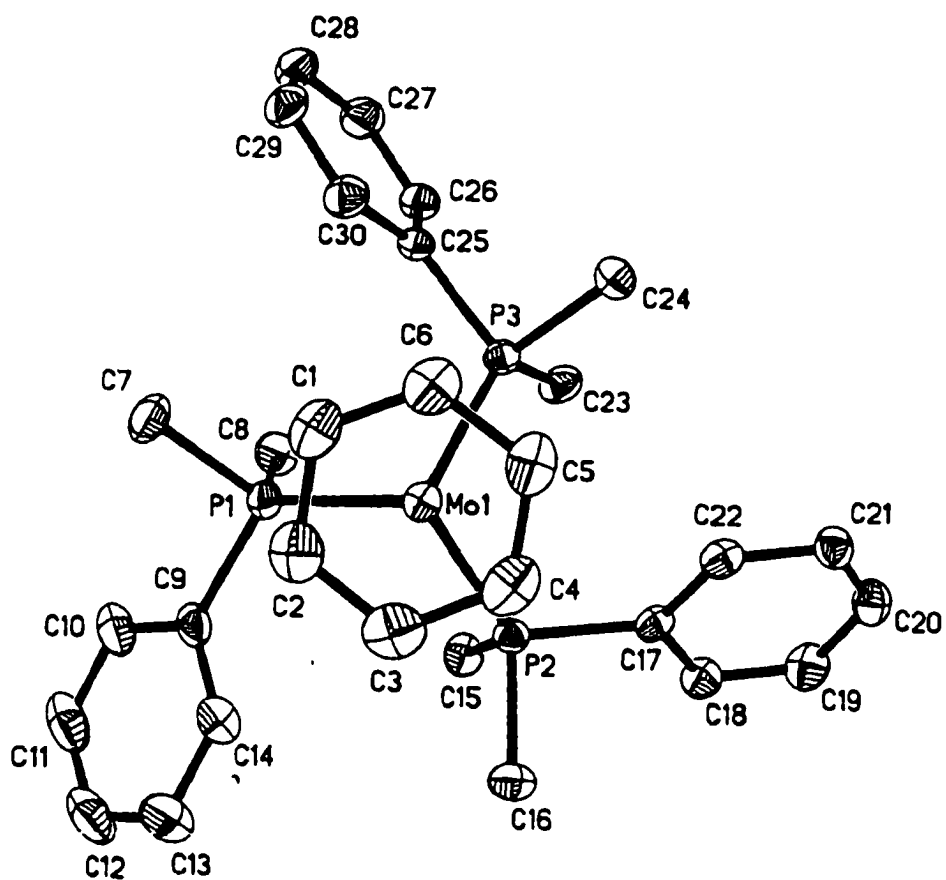
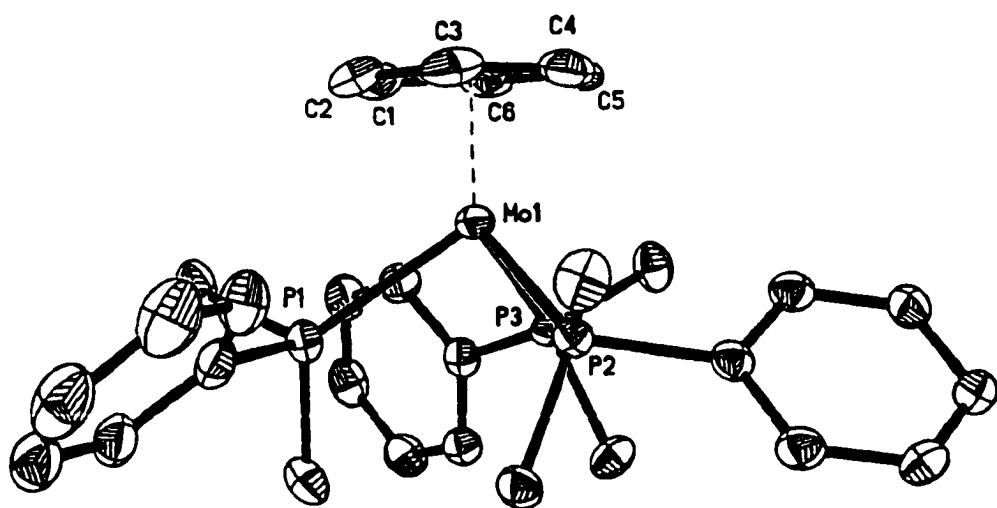


Figure 3.4. Thermal ellipsoid drawing (50% probability) of  $(\eta^6\text{-C}_6\text{H}_6)\text{Mo}(\text{PMe}_2\text{Ph})_3$  (**8**) sideview (top) and top view (bottom).

Table 3.2. Selected interatomic distances (Å) and bond angles (deg) for **1**, **4**, **7** and **8**.

| Bond/Angle | <b>1</b>       | <b>4</b>       | <b>7</b>       | <b>8</b>       |
|------------|----------------|----------------|----------------|----------------|
|            | C <sub>1</sub> | C <sub>1</sub> | C <sub>3</sub> | C <sub>1</sub> |
| Mo-P1      | 2.4118(13)     | 2.3687(8)      | 2.4438(5)      | 2.4431(7)      |
| Mo-P2      | 2.3856(10)     | 2.3926(8)      |                | 2.4431(6)      |
| Mo-P3      | 2.3846(10)     | 2.4045(8)      |                | 2.4428(7)      |
| Mo-X       | 1.816(5)       | 1.789(4)       | 1.788(2)       | 1.781(3)       |
| P1-Mo-P2   | 84.82(4)       | 78.91(3)       | 92.37(2)       | 92.32(2)       |
| P2-Mo-P3   | 83.12(4)       | 92.74(3)       |                | 92.25(2)       |
| P3-Mo-P1   | 83.50(3)       | 79.80(3)       |                | 90.49(2)       |
| P1-Mo-X    | 129.2(1)       | 131.8(1)       | 123.6(1)       | 123.6(1)       |
| P2-Mo-X    | 128.4(1)       | 132.3(1)       |                | 123.6(1)       |
| P3-Mo-X    | 131.0(1)       | 124.0(1)       |                | 124.9(1)       |

X is the centroid of the arene ligand

**Table 3.3. Calculated interatomic distances (Å) and bond angles (deg) for **1**, **4**, **7**, **8**, and **9**.**

| Bond/Angle | <b>1</b>       | <b>4</b>       | <b>7</b>       | <b>8</b>       | <b>9</b>       |
|------------|----------------|----------------|----------------|----------------|----------------|
|            | C <sub>3</sub> | C <sub>1</sub> | C <sub>3</sub> | C <sub>3</sub> | C <sub>3</sub> |
| Mo-P1      | 2.389          | 2.400          | 2.407          | 2.389          | 2.386          |
| Mo-P2      |                | 2.383          |                |                |                |
| Mo-P3      |                | 2.369          |                |                |                |
| Mo-X       | 1.883          | 1.886          | 1.903          | 1.886          | 1.878          |
| P1-Mo-P2   | 85.76          | 79.11          | 93.44          | 93.97          | 93.30          |
| P2-Mo-P3   |                | 99.05          |                |                |                |
| P3-Mo-P1   |                | 79.16          |                |                |                |
| P1-Mo-X    | 128.21         | 128.01         | 122.79         | 122.43         | 122.90         |
| P2-Mo-X    |                | 133.66         |                |                |                |
| P3-Mo-X    |                | 122.75         |                |                |                |

**X is the centroid of the arene ligand**

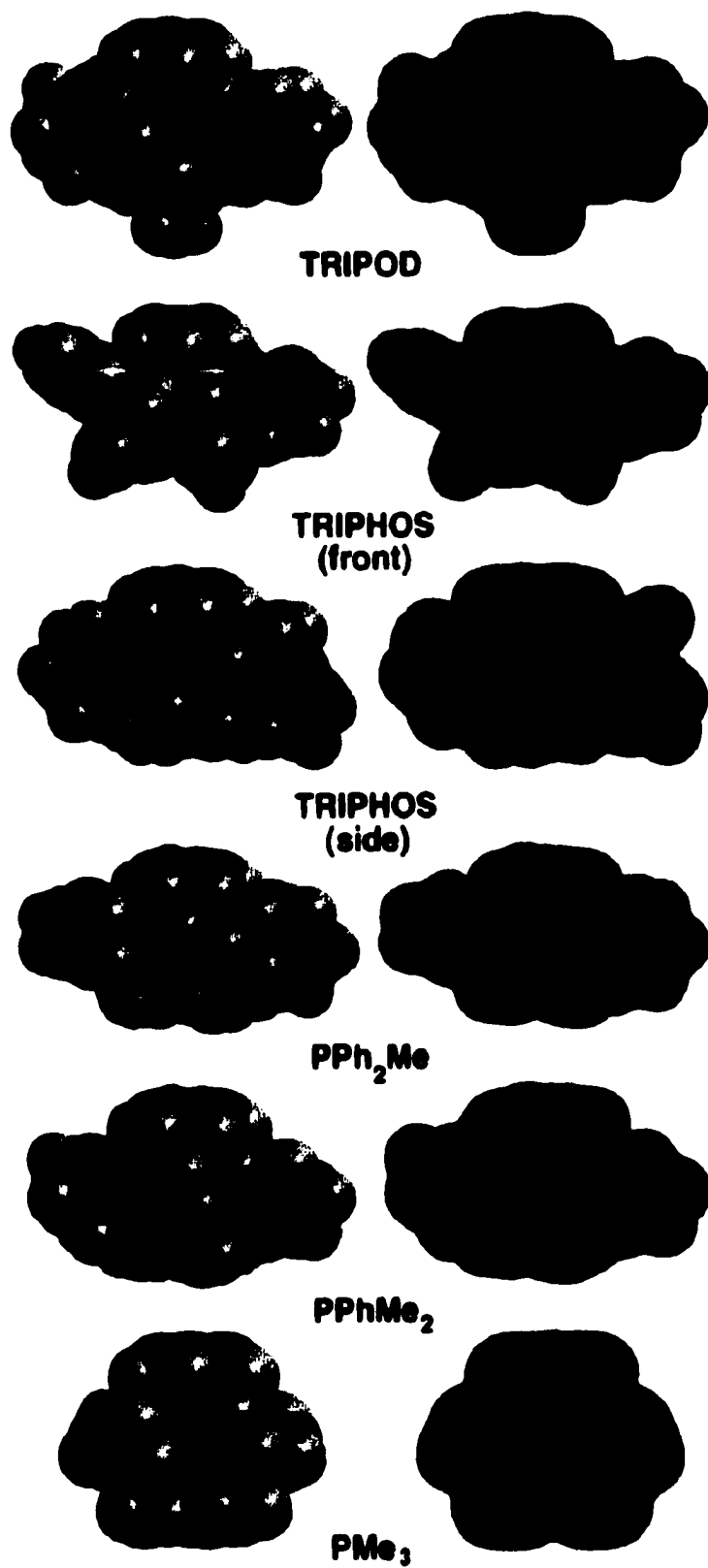


Figure 3.5. CPK models (left) and electron density plots (right) of 1, 4, 7, 8 and 9.

phosphine are possible. Mapping the occupied metal-containing frontier orbitals onto the calculated surface electron densities provides a convenient model for predicting the initial site of protonation (Figure 3.5). The models of **1** and **7** show no available metal electron density except on the arene ligands. Accordingly, the two complexes are protonated at the arene. The models of **4**, **8**, and **9** reveal varying amounts of direct access to the metal center. Although, these models predict the direct access to the metal center is feasible, they do not indicate the relative amounts of metal versus arene protonation. The CPK models reveal the steric accessibility to the metal is in the order **8** < **9** < **4**. Experimentally, the same order is observed for the extent of direct metal protonation. More direct metal protonation is observed for **4**, despite the fact that TRIPHOS ligand on **4** is bulkier than  $\text{PMe}_3$  on **9**. This observation is clearly explained by the CPK model. The model of **4** suggests there would be less steric hindrance for the proton to approach the metal in-between the terminal P atoms and bridging P atom.

### 3.5 REACTION OF ACID WITH $(\eta^6\text{-C}_6\text{H}_6)\text{Mo}(\text{TRIPHOS})$

Since **4** has  $C_3$  symmetry, unlike the complexes **1**, **8**, and **9** that have an approximate  $C_{3v}$  symmetry, the protonation at the metal would be expected to be different for **4** compared with the rest of the complexes. Protonation of  $(\eta^6\text{-C}_6\text{H}_6)\text{Mo}(\text{TRIPHOS})$  was studied using low temperature NMR spectroscopy and our observations are summarized in Tables 3.3 and 3.4.

When one equivalent of acid is reacted with **4** at  $-90^\circ\text{C}$ , a doublet of triplets is observed in the  $^1\text{H}$  NMR spectrum at  $-7.2$  ppm, which is assigned to the kinetic monohydride (**5**). On warming up above  $-60^\circ\text{C}$ , **5** irreversibly converts to the thermodynamic monohydride (**6**) with high field resonances of a triplet of doublets at  $-6.2$  ppm. Complex **6** has a static spectrum even at temperatures as low as  $-125^\circ\text{C}$ . The  $^{31}\text{P}$  NMR signals for **5** are a sharp singlet at 99 ppm and two broad singlets at 76 and 69 ppm measured at  $-94^\circ\text{C}$ . The  $^{31}\text{P}$  resonances of complex **6** are a triplet at 110 ppm for the

Table 3.4.  $^1\text{H}$  NMR data for the protonation of  $(\eta^6\text{-C}_6\text{H}_6)\text{Mo}(\text{TRIPHOS})$  (**4**).

| com       | name                         | structure | $^1\text{H}$ NMR ( $\delta$ )<br>peak<br>(temp. $^\circ\text{C}$ ) | multiplicity |
|-----------|------------------------------|-----------|--|--------------|
| <b>5</b>  | kinetic<br>monohydride       |           | -7.21<br>(-90)   | dt           |
| <b>6</b>  | thermodynamic<br>monohydride |           | -6.21<br>(20)  | td           |
| <b>5a</b> | kinetic<br>dihydride         |           | -5.24<br>(-90)   | dt           |
| <b>6a</b> | thermodynamic<br>dihydride   |           | -4.73<br>(20)  | dt           |

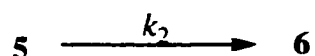
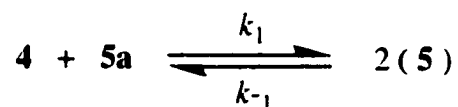
Table 3. 5.  $^{31}\text{P}$  NMR data for the protonation of  $(\eta^6\text{-C}_6\text{H}_6)\text{Mo}(\text{TRIPHOS})$  (4).

| com | name                         | structure | $^{31}\text{P}$ NMR ( $\delta$ )<br>peaks<br>(temp. $^\circ\text{C}$ ) | multiplicity |
|-----|------------------------------|-----------|--|--------------|
| 5   | kinetic<br>monohydride       |           | 99, 76, 69<br>(-125)   | dd, t, dd    |
| 6   | thermodynamic<br>monohydride |           | 110, 89<br>(20)  | t, d         |
| 5a  | kinetic<br>dihydride         |           | 87, 67<br>(-90)  | s, s         |
| 6a  | thermodynamic<br>dihydride   |           | 88, 65<br>(20)   | s, s         |

unique phosphorus atom and doublet at 89 ppm for the two terminal phosphorus atoms. Upon cooling a sample of **5** in CDCl<sub>2</sub>F down to -125 °C, the <sup>31</sup>P NMR singlet at 99 ppm sharpens to a quartet and the two broad singlets at 76 and 69 decoalesces to triplet (79 ppm) and quartet (71 ppm), respectively. The hydride region in the <sup>1</sup>H NMR spectra of **5** at -125 °C consists of a doublet of doublet of doublets around -7.2 ppm, which indicates three different phosphorus atoms couple. In a few instances, a doublet of triplet at -5.0 ppm (**5a**, kinetic dihydride) was noticed when one equivalent acid was reacted, which eventually disappears to monohydrides. This was presumed due to the local high concentration of acid as the solution begins to melt at -90 °C. When two equivalent of acid were reacted with **4**, diprotonation occurs at the metal. The diprotonation at -90 °C produces the kinetic dihydride (**5a**), which upon warming up above -30 °C irreversibly converts to the thermodynamic dihydride (**6a**). Complex **5a** has a <sup>1</sup>H NMR hydride resonance consisting of a doublet of triplets at -5.0 ppm and <sup>31</sup>P resonances as 87 and 67 ppm. Compound **6a** displays an overlapping doublet of triplets at -4.3 ppm for the hydrides in the <sup>1</sup>H NMR spectrum and 88 and 65 ppm resonances in the <sup>31</sup>P NMR spectrum. The two hydride ligands of **6a** are apparently exchanging positions rapidly at room temperature making them equivalent on the NMR time-scale. Cooling **6a** down to -125 °C does not convert it back to **5a**, but the doublet of triplet broadens to what appears to be two triplets. The two hydride ligands in **6a** are interchanging possibly via an η<sup>2</sup>-H<sub>2</sub> complex, based on the fact **6a** was found to exchange with D<sub>2</sub> gas over a period of one week. Only **6** was isolated, when an attempt was made to isolate **6a** from solution.

**Interconversion of Isomers of Protonated (η<sup>6</sup>-C<sub>6</sub>H<sub>6</sub>)Mo(TRIPHOS).** (Scheme 3.2) In order to understand the interconversion of protonated isomers, reactions were followed by <sup>1</sup>H and <sup>31</sup>P NMR spectroscopy. A sample of **5** was prepared at -94 °C and its conversion to **6** was monitored at -60 °C. The plot of peak integrations of [**4**], [**5**], [**5a**] and [**6**] present in solution against time is shown in Figure 3.6. As suggested by the plot, the rate of formation of **6** depends only on the concentration of **5**.<sup>31</sup> The equilibrium

constant  $K_1$  can be calculated by integration of the components at  $t = 0$ .



$$K_1 = \frac{[5]^2}{[4][5a]} = 77$$

The rate of formation of **6** can be obtained using the equation below.

$$\frac{d[6]}{dt} = \frac{k_2 \sqrt{K_1}}{2 + \sqrt{K_1}} [5]$$

From the  $k_{\text{obs}}$  value of  $5.0 \times 10^{-4} \text{ s}^{-1}$ ,  $k_2$  was calculated to be  $6.1 \times 10^{-4} \text{ s}^{-1}$ . The  $\Delta G^\ddagger$  for the process is calculated to be 15.5 kcal at  $-60^\circ \text{C}$ . The energy of interconversion of the two regioisomers of **5** was obtained by measuring the coalescence temperature ( $T_c$ ) of the  $^{31}\text{P}$  NMR spectra. A sample of **5** was prepared at  $-94^\circ \text{C}$  and the spectra obtained as the sample warmed up every 2 degree were used to determine the  $T_c$  of  $87^\circ \text{C}$ . Using the equation<sup>32</sup> below, the rate constant was estimated to be  $6.4 \times 10^3 \text{ s}^{-1}$ .

$$k_{180k} = 2\pi(\Delta\delta)/\sqrt{2}$$

where  $\Delta\delta$  is the difference in frequency in Hz of the resonances of the P atoms in the static spectrum. The corresponding energy barriers were estimated at  $T_c$  by the equation<sup>33,34</sup>

$$\Delta G^\ddagger = -RT_c [\ln(k/T_c) + \ln(h/K)]$$

where  $R = 8.314 \text{ J mol}^{-1} \text{ K}^{-1}$  is the gas constant,  $h = 6.626 \times 10^{-34} \text{ J}$  is Planck's constant, and  $K = 1.381 \times 10^{-23} \text{ J K}^{-1}$  is Boltzmann's constant. The energy barrier for the fluxional

process is 7.5 kcal/mol. For **3**, the hydride on the metal is in similar surroundings as that of **6**. The coalescence temperature was determined to be -70 °C for **3**. A rate constant calculation for the rotational barrier of **3** was estimated using the equation for two-site exchange with a 2:1 population.<sup>35</sup>

$$k_{203K} = \frac{2\pi \cdot \Delta\delta}{e^z + e^{-z}} \approx 3.01 \cdot \Delta\delta$$

$$z = \frac{1}{6} \ln\{3 + 2\sqrt{2}\}$$

The activation barrier for the fluxional process in **3** is calculated to be 8.3 kcal/mol

The kinetic hydrides (**5** and **5a**) are formed preferentially due to accessibility of the metal. It is evident from the space filling model of **4**, that the region over the methylene bridges of the ligand are more open compared to the space in-between the two terminal phosphorus atoms. The terminal phosphorus atoms bear two phenyl groups that orient parallel to each other along the metal arene axis. Presumably, the orientation of the two phenyl groups creates a steric congestion for an incoming proton to attach to the metal. Therefore, the kinetic hydrides are formed by the protonation of the metal at the more accessible site. The similar energies of interconversion between the regioisomers of **5** and those of **3** suggests that in both cases the barrier for the Mo-H bond to pass across is the P-Ph region. The hydride(s) of **6(6a)** are located in the space between the two terminal P atoms. That space is the sterically less demanding position. The crystal structure of **6·PF<sub>6</sub>** reveals that the angle between two terminal P atoms (94°) is more than that between terminal P atoms and the bridging P atom (78°). A similar distortion is also found in the case of **3·PF<sub>6</sub>**, where it is less pronounced due the fact the P atoms of the TRIPOD ligand are connected in a tripodal fashion. A comparison of the metric parameters of **3·PF<sub>6</sub>** and **6·PF<sub>6</sub>** are listed in Table 3.6. Based on the available data, proposed reaction pathways for for **4** and proton are given in Scheme 3.2.

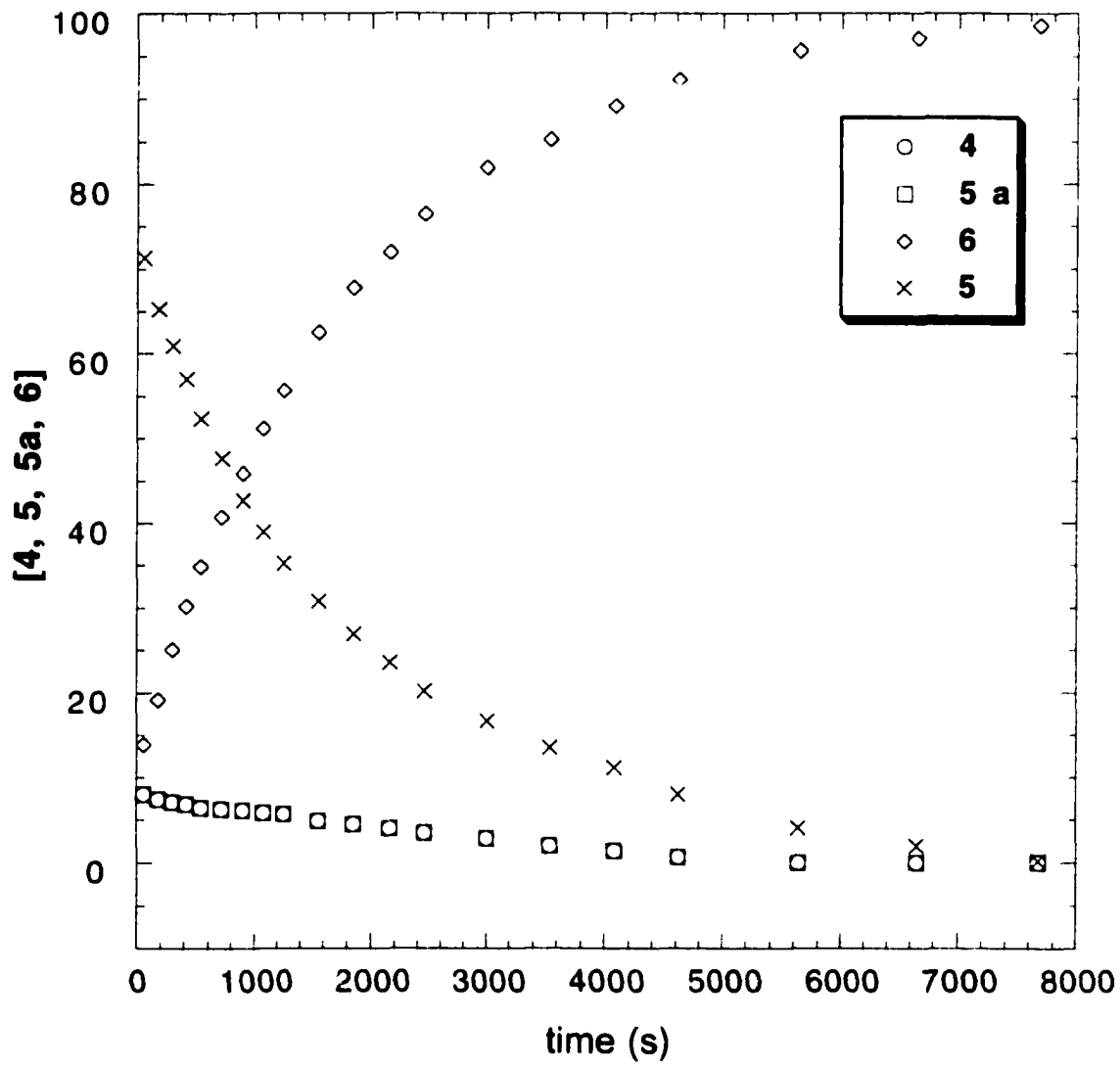


Figure 3.6. Plot of [4], [5], [5a], and [6] versus time (sec) at -60 °C.

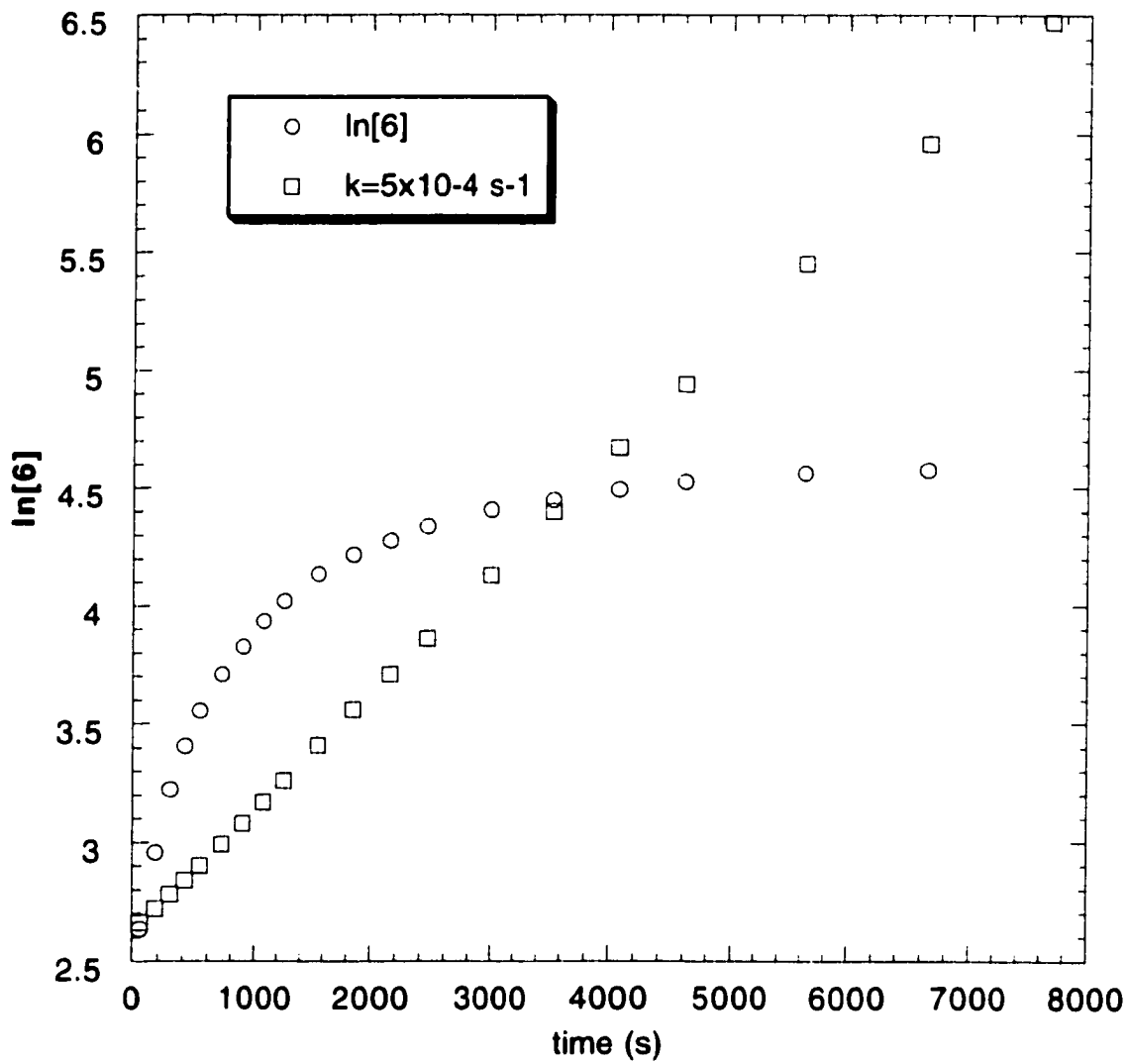


Figure 3.7. Plot  $\ln[6]$  versus time (sec) at  $-60 \text{ }^\circ\text{C}$ .

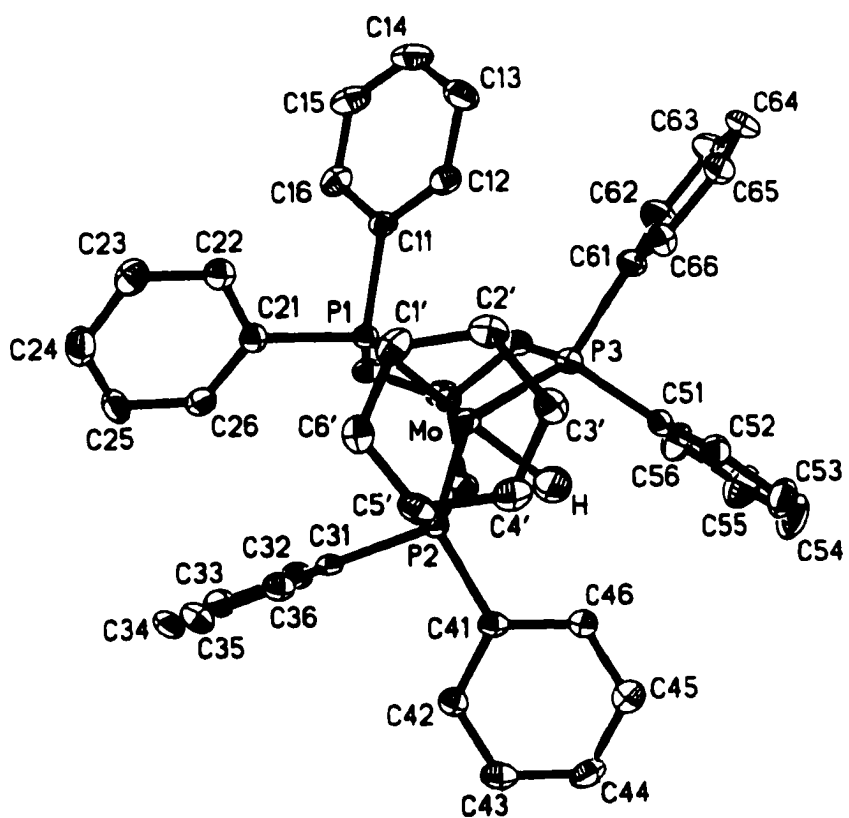
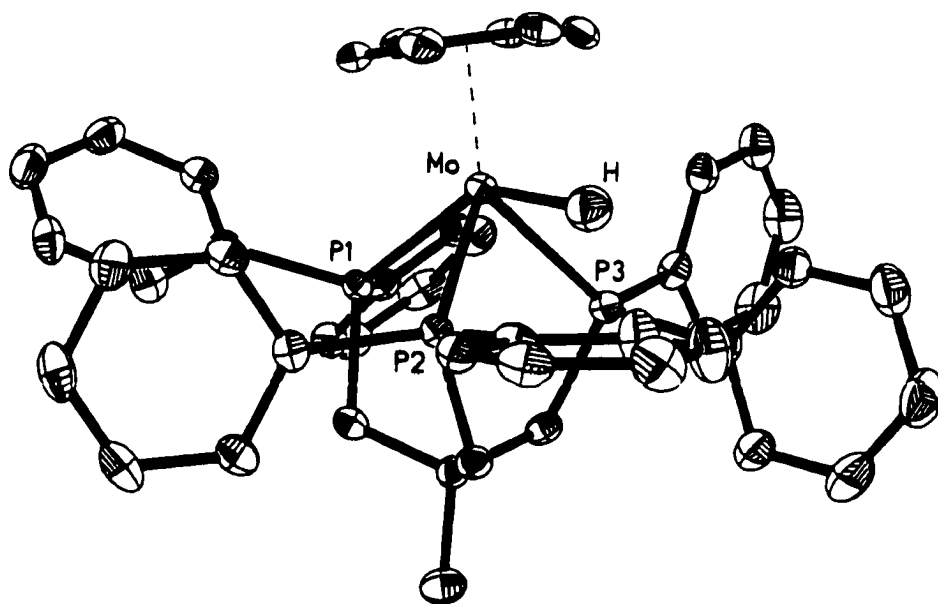


Figure 3.8. Thermal ellipsoid drawing (50% probability) of  $3 \cdot \text{PF}_6$  sideview (top) and top view (bottom)

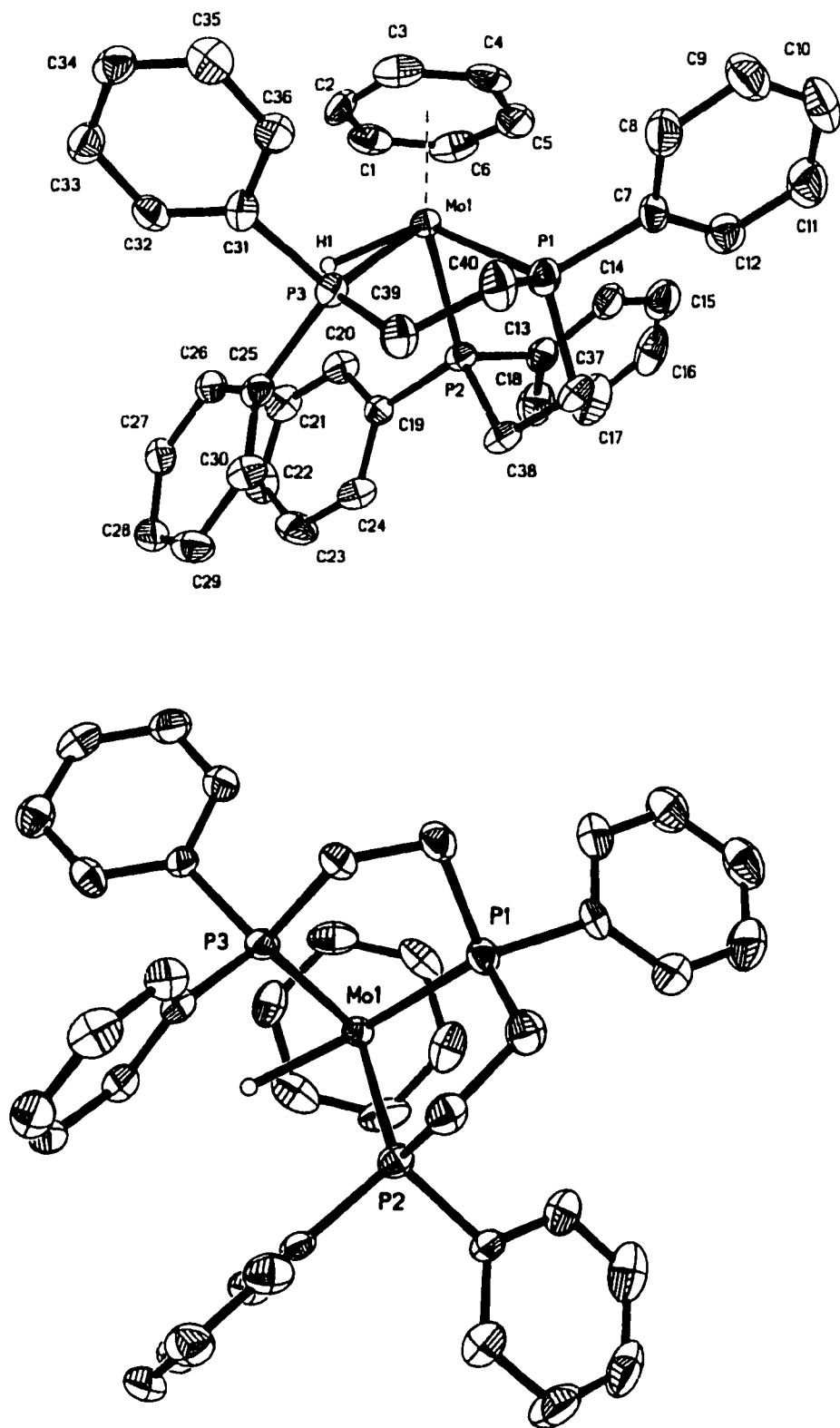
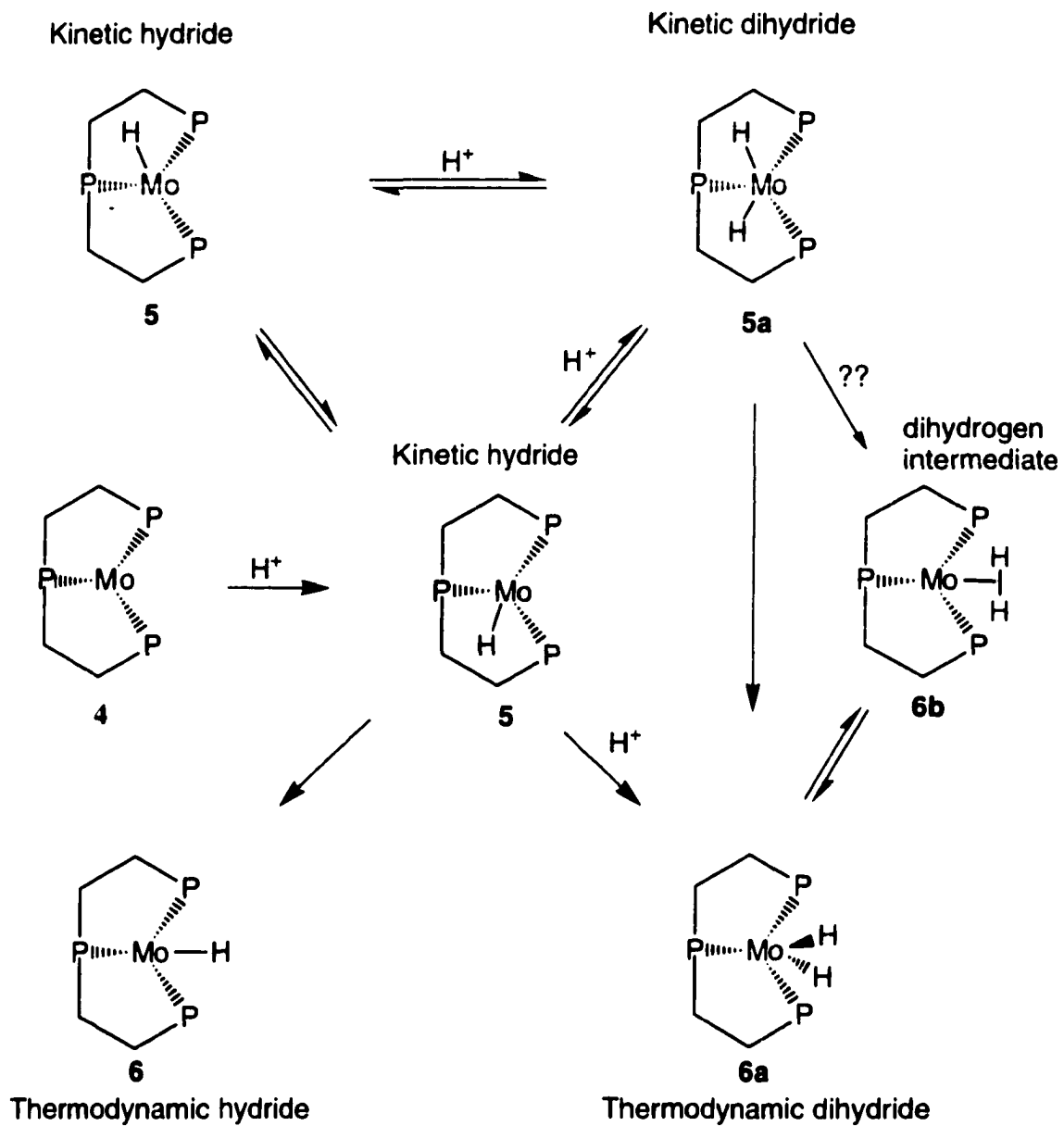


Figure 3.9. Thermal ellipsoid drawing (50% probability) of **6·PF<sub>6</sub>** sideview (top) and top view (bottom)

Table 3.6. Selected interatomic distances (Å) and bond angles (deg) for **3·PF<sub>6</sub>** and **6·PF<sub>6</sub>**.

| Bond/Angle | <b>3·PF<sub>6</sub></b> | <b>6·PF<sub>6</sub></b> |
|------------|-------------------------|-------------------------|
| Mo-P1      | 2.5127(9)               | 2.454(2)                |
| Mo-P2      | 2.4298(10)              | 2.416(2)                |
| Mo-P3      | 2.4568(9)               | 2.416(14)               |
| Mo-X       | 1.843(3)                | 1.848(5)                |
| Mo-H       | 1.66(4)                 | 1.76(6)                 |
| P1-Mo-P2   | 83.03(3)                | 78.74(5)                |
| P2-Mo-P3   | 87.41(3)                | 94.56(5)                |
| P3-Mo-P1   | 81.29(3)                | 78.26(5)                |
| P1-Mo-X    | 117.7(3)                | 122.2(2)                |
| P2-Mo-X    | 131.4(3)                | 131.8(2)                |
| P3-Mo-X    | 136.2(3)                | 130.0(2)                |
| P1-Mo-H    | 139.6(12)               | 133(2)                  |
| P2-Mo-H    | 68.7(13)                | 75(2)                   |
| P3-Mo-H    | 69.6(12)                | 67(2)                   |
| X-Mo-H     | 102.7(4)                | 103(3)                  |



Scheme 3.2 Reaction of acid with (η<sup>6</sup>-C<sub>6</sub>H<sub>6</sub>)Mo(TRIPHOS) (4)

### 3.6 SUMMARY

Effect of phosphine ligand variation on the mechanism of protonation of ( $\eta^6$ -arene)Mo(phosphine)<sub>3</sub> complexes was shown to depend on both steric and electronic factors. The size and orientation of the phosphine ligand dictates the site of initial protonation. Decreasing the size of phosphine effects a decrease in the relative percentage of ring protonation. However, the bulkier ligand TRIPHOS has an orientation that allows a greater percentage of metal protonation than expected. Calculations have provided a model to visualize the steric encumbrance and thereby predict the initial sites of protonation. We conclude that the steric factors play a dominant role in determining the initial site of protonation in these complexes.

### 3.7 BIBLIOGRAPHY

- (1) Davison, A.; McFarlane, W.; Pratt, L.; Wilkinson, G. *J. Chem. Soc.* **1962**, 3653-3666.
- (2) Kristjansdottir, S. S.; Norton, J. R. In *Transition Metal Hydrides*; Dedieu, A., Ed.; VCH: Weinheim, 1992, pp 309-359.
- (3) Evans, D. J.; Henderson, R. A.; Smith, B. E. *Catalysis by Nitrogenases and Synthetic Analogs*; Reedijk, J., Ed.; Marcel Dekker: New York, 1993, pp 89-130.
- (4) Gates, B. C. *Catalytic Chemistry*; John Wiley: New York, 1991.
- (5) Watts, W. E. In *Comprehensive Organometallic Chemistry*; Wilkinson, G., Stone, F. G. A., Abel, E. W., Ed.; Pergamon Press: Oxford, 1982; Vol. 8, pp 1013-1026.
- (6) Lillya, C. P.; Sahatjian, R. A. *Inorg. Chem.* **1972**, *11*, 889-890.
- (7) Olah, G. A.; Yu, S. H. *J. Org. Chem.*, **1975**, *41*, 717-719.
- (8) Green, M. L. H.; Mitchard, L. C.; Silverthorn, W. E. *J. Chem. Soc., Sec. A* **1971**, 2929-2931.
- (9) Green, M. L. H.; Mitchard, L. C.; Silverthorn, W. E. *J. Chem. Soc., Dalton Trans.* **1974**, 1361-1363.
- (10) Kursanov, D. N.; Setkina, V. N.; Petrovskii, P. V.; Zdanovich, V. I.; Baranetskaya, N. K.; Rubin, I. D. *J. Organomet. Chem.* **1971**, *37*, 339-345.
- (11) Setkina, V. N.; Baranetskaya, N. K.; Ginzburg, A. G.; Zdanovich, V. I.; Nefedova, M. N.; Kursanov, D. N. *J. Organomet. Chem.* **1973**, *61*, 287-300.

- (12) Tsoy, A. A.; Baranetskaya, N. K.; Setkina, V. N.; Kursanov, D. N. *J. Organomet. Chem.* **1981**, *212*, 377-387.
- (13) Losilkina, V. I.; Petrovskii, P. V.; Baranetskaya, N. K.; Setkina, V. N.; Kursanov, D. N. *Bull. Acad. Sci. USSR, Div. Chem. Sci. (Engl. Trans.)* **1983**, *32*, 2537.
- (14) Losilkina, V. I.; Petrovskii, P. V.; Baranetskaya, N. K.; Setkina, V. N. *Bull. Acad. Sci. USSR, Div. Chem. Sci. (Engl. Trans.)* **1984**, *33*, 723.
- (15) Losilkina, V. I.; Estekhina, M. N.; Baranetskaya, N. K.; Setkina, V. N. *J. Organomet. Chem.* **1986**, *299*, 187-195.
- (16) Losilkina, V. I.; Baranetskaya, N. K.; Tolkunova, V. S.; Krylova, A. I.; Vil'chevskaya, V. D.; Setkina, V. N. *J. Gen. Chem. USSR. (Engl. Trans.)* **1987**, *57*, 753-758.
- (17) Flood, T. C.; Rosenberg, E.; Sarhangi, A. *J. Am. Chem. Soc.* **1977**, *99*, 4334-4340.
- (18) Morris, R. H.; Sawyer, J. F.; Schweitzer, C. T.; Sella, A. *Organometallics* **1989**, *8*, 2099-2106.
- (19) Mailvaganam, B.; Sayer, B. G.; McGlinchey, M. J. *Organometallics* **1990**, *9*, 1089-1093.
- (20) Rosca, S.; Chiraleu, F.; Rosca, S. I. *Rev. Roumaine Chim.* **1991**, *36*, 693-705.
- (21) Green, M. L. H.; Hughes, A. K.; Lincon, P.; Martin-Polo, J. J.; Mountford, P.; Sella, A.; Wong, L.-L.; Bandy, J. A.; Banks, T. W.; Prout, K.; Watkin, D. J. *J. Chem. Soc., Dalton Trans.* **1992**, 2063-2069.
- (22) George, T. A.; Hammud, H. H. *J. Organomet. Chem.* **1995**, *503*, C1-C3.
- (23) Leong, V. S.; Cooper, N. J. *J. Am. Chem. Soc.* **1988**, *110*, 2644-2646.
- (24) Thompson, R. L.; Lee, S.; Rheingold, A. L.; Cooper, N. J. *Organometallics* **1991**, *10*, 1657-1659.
- (25) Winemiller, M. D.; Kopach, M. E.; Harman, W. D. *J. Am. Chem. Soc.* **1997**, *119*, 2096-2102.
- (26) Winemiller, M. D.; Kelsch, B. A.; Sabat, M.; Harman, W. D. *Organometallics* **1997**, *16*, 3672-3678.
- (27) Kowalski, A. S.; Ashby, M. T. *J. Am. Chem. Soc.* **1995**, *117*, 12639-12640.
- (28) Silverthorn, W. E. *Inorg. Synth.* **1977**, *17*, 54.
- (29) Green, M. L. H.; Knight, J.; Mitchard, L. C.; Roberts, G. G.; Silverthorn, W. E. *J. Chem. Soc. Chem. Commun.* **1971**, 1619-1621.
- (30) Ashby, M. T.; Asirvatham, V. S.; Kowalski, A. S.; Khan, M. A. *Organometallics* **1999**, *18*, 5004-5016.

- (31) Schmid, R.; Sapunov, V. N. *Non-formal kinetics*; Verlag Chemie: Weinheim, 1982.
- (32) Green, M. L. H.; Wong, L.-L.; Sella, A. *Organometallics* **1992**, *11*, 2660.
- (33) Allerhand, A.; Gutowsky, H. S.; Jonas, J.; Meinzer, R. A. *J. Am. Chem. Soc.* **1966**, *79*, 3185.
- (34) Faller, J. W. *Adv. Organomet. Chem.* **1977**, *16*, 211-239.
- (35) Shanan-Atidi, H.; Bar-Eli, K. H. *J. Phys. Chem.* **1970**, *74*, 961.

## CHAPTER 4

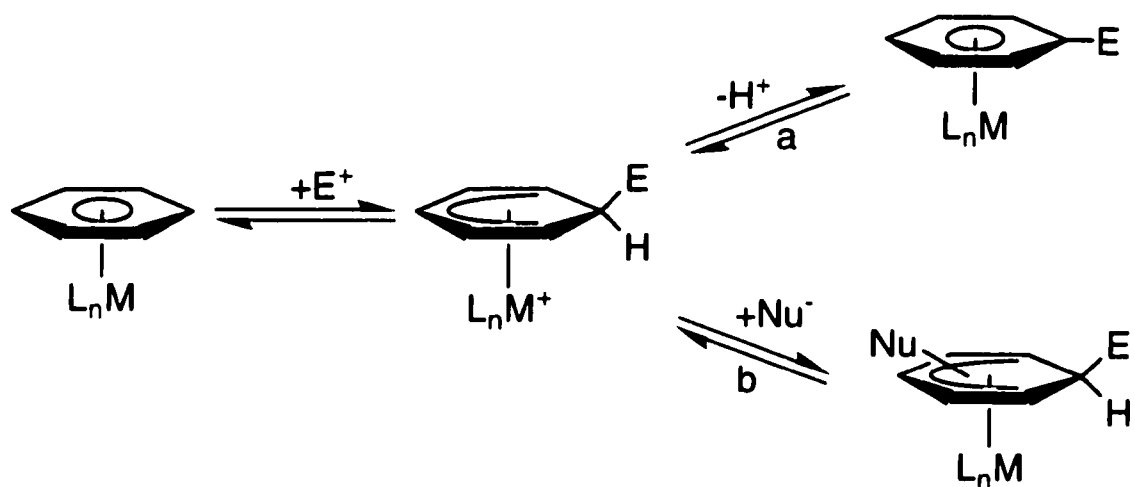
# EFFECT OF ELECTROPHILE VARIATION ON THE MECHANISM OF AROMATIC ELECTROPHILIC SUBSTITUTION OF $(\eta^6\text{-C}_6\text{H}_6)\text{Mo}(\text{TRIPOD})$

### 4.1 INTRODUCTION

The reaction of electrophiles with aromatic hydrocarbon can proceed via two distinct pathways. An electrophile can add to an arene carbon atom thereby forming a cationic intermediate (Wheland intermediate in the case of benzene) followed by 1. proton loss, or 2. an addition of a nucleophile. The proton loss process is energetically more favorable because the product formed is stabilized by the aromatic  $\pi$ -system. The same kind of situation arises for neutral organometallic complexes in which a metal with an eighteen electron configuration bears an  $\pi$ -hydrocarbon ligand (Scheme 4.1).<sup>1</sup> The reaction of electrophiles with the  $\pi$ -hydrocarbon ligand can proceed via two distinct pathways. The addition of electrophile  $\text{E}^+$  produces a sixteen electron intermediate with a coordinatively unsaturated metal. The intermediate can result in a stable product either by a proton loss (path a) (electrophilic substitution) or by addition (path b) of an available two electron donor (nucleophile) ligand.

### 4.2 LITERATURE OVERVIEW

The electrophilic substitution of eighteen-electron Cp-metal complexes have been studied widely. Friedel-Crafts acetylation of these complexes has been the most commonly studied reaction for the Cp-metal complexes.<sup>2</sup> Examples of electrophilic substitutions of



Scheme 4.1 Alternate pathways for electrophile reaction with arene $ML_n$

$\eta^6$ -arene complexes are sparse compared to those of Cp complexes. The first known electrophilic substitution of an  $\eta^6$ -arene complex is the Friedel-Crafts acylation of the  $(\eta^6\text{-C}_6\text{H}_6)\text{Cr}(\text{CO})_3$  reported in 1959 by three independent groups.<sup>3-5</sup> The Friedel-Crafts acetylation of  $(\eta^6\text{-C}_6\text{H}_6)\text{Cr}(\text{CO})_3$  and its derivatives was examined in some detail,<sup>6</sup> although the ligand is less reactive than benzene itself due to the deactivating effect of electron-withdrawing  $\text{Cr}(\text{CO})_3$  moiety.  $(\eta^6\text{-arene})_2\text{Cr}$  was found to react with alkyl halides (RX) to give mixture of products,  $(\eta^6\text{-arene})_2\text{CrX}$  and  $\text{R}_2$  and/or ring alkylated product and HX. Mixed sandwich complexes were also shown to undergo electrophilic substitutions.<sup>7</sup> The rhenium complex,  $(\eta^6\text{-C}_6\text{H}_6)\text{Re}(\eta^5\text{-C}_5\text{H}_5)$  substitutes on either ring, while analogous Mn and Cr complexes ring expand to give the tropylium cation upon acetylation.<sup>8,9</sup> Some unusual substitutions have been reported for Cp complexes. The compound  $\text{CpCo}(\text{PMe}_3)_2$  reacts with alkyl bromides (RBr, R = i-Pr or t-Bu) to give a mixture of ring alkylated hydrido complexes  $[(\text{Cp-R})\text{CoH}(\text{PMe}_3)_2]^+$  and  $[\text{CpCoH}(\text{PMe}_3)_2]^+$ . It is believed that the former complex results from initial addition of  $\text{R}^+$  to the nucleophilic metal center, followed by migration of R to the ring, and *endo* proton transfer to the metal.<sup>10,11</sup> When R = Me or Et, the metal alkyl complex  $[\text{CpCoR}(\text{PMe}_3)_2]^+$  is the only product. A similar reaction was reported with  $[\text{CpM}(\text{CO})_3]^+$  (M = Mo and W) reacting with tri-*t*-butylcyclopropenium cation to give the ring substituted product.<sup>12</sup> Such ring substitution accompanied by metal protonation in  $\eta^6$ -arene complexes was first realized by Green and coworkers when  $[(\eta^6\text{-C}_6\text{H}_6)\text{MoH}(\eta^2\text{-C}_2\text{H}_4)(\text{dppe})]^+$  was reacted with a monophosphine  $\text{PMe}_3$ , to give the ethyl migrated  $[(\eta^6\text{-C}_6\text{H}_5\text{Et})\text{MoH}(\text{PMe}_3)(\text{dmpe})]^+$ .<sup>13</sup> Later on, Green et al. verified their mechanism by the reaction of  $(\eta^6\text{-C}_6\text{H}_6)\text{Mo}(\text{PMe}_3)(\text{dmpe})$  with  $\text{CF}_3\text{SO}_3\text{Me}$  and  $\text{Et}_3\text{OBF}_4$  giving  $[(\eta^6\text{-C}_6\text{H}_5\text{Me})\text{MoH}(\text{PMe}_3)(\text{dmpe})]^+$  and  $[(\eta^6\text{-C}_6\text{H}_5\text{Et})\text{MoH}(\text{PMe}_3)(\text{dmpe})]^+$ , respectively.<sup>14</sup> The mixed sandwich complexes of the type  $(\eta^6\text{-arene})\text{Fe}(\eta^5\text{-Cp})$  were shown to react with alkyl halides to form a mixture of ring substituted products.<sup>15</sup> Activated benzene complexes that are  $\eta^4$  and  $\eta^2$  bound can also undergo electrophilic additions. Cooper et al. have shown that  $[(\eta^4\text{-benzene})\text{Cr}(\text{CO})_3]^{2-}$  and

$[(\eta^1\text{-benzene})\text{Mn}(\text{CO})_3]^+$  undergo electrophilic additions to form the respective cyclohexadienyl species.<sup>16-18</sup> *Exo* addition of  $\text{PhCH}_2\text{Cl}$  to  $[(\eta^1\text{-benzene})\text{Cr}(\text{CO})_3]^2+$  was realized. Carbon dioxide adds to  $[(\eta^1\text{-benzene})\text{Cr}(\text{CO})_3]^2+$  to give an intermediate cyclohexadienyl carboxylate complex, which can be oxidized and silylated to form  $[(\eta^6\text{-C}_6\text{H}_5\text{CO}_2\text{SiMe}_3)\text{Cr}(\text{CO})_3]$ . Iminium salts are known to add to the benzene ligand of  $[(\eta^1\text{-benzene})\text{Mn}(\text{CO})_3]^+$  giving the *exo*-aminoalkyl-substituted cyclohexadienyl complexes.<sup>19</sup> Harman and coworkers have utilized the electrophilic reactions of  $\eta^2$ -arene osmium complexes for organic synthesis.<sup>20</sup> Complexes of the type  $[(\eta^2\text{-arene})\text{Os}(\text{NH}_3)_5](\text{OTf})_2$  were treated with electrophiles followed by oxidative work up to yield substituted arenes.<sup>21,22</sup> The dihapto coordination localizes the  $\pi$ -electron system, allowing the arene to react like dienes with various different electrophiles. The reactions were of great synthetic utility owing to the wide list of aromatics with reactive functional groups such as thiophenes, phenols, anilines that can be tolerated under the reaction conditions.

#### 4.3 REACTION OF $(\eta^6\text{-C}_6\text{H}_6)\text{Mo}(\text{TRIPOD})$ WITH $[\text{CH}_2=\text{NMe}_2]\text{I}$

Iminium salts are widely used as electrophiles in organic chemistry.<sup>23</sup> The methyliminium iodide (Eschenmoser's salt) and other iminium salts were shown to add to activated benzene complexes.<sup>19</sup> The iminium salts are known to add to  $\eta^1$ -benzene ring in an *exo*-fashion.  $(\eta^6\text{-C}_6\text{H}_6)\text{Mo}(\text{TRIPOD})$  (**1**) reacted with  $[\text{CH}_2=\text{NMe}_2]\text{I}$  to form the metal hydride complex,  $[(\eta^6\text{-C}_6\text{H}_5\text{CH}_2\text{NMe}_2)\text{MoH}(\text{TRIPOD})]\text{I}$  (**10**). The  $^1\text{H}$  NMR spectrum of **10** reveals at 5.47 ppm an *o*, *m*, *p* pattern for the metal bound arene, a Mo-H resonance at -6.13 ppm, and other relevant peaks. The arene resonance indicates that the ring is mono substituted. The chemical shift of the Mo-H is very similar to that of  $[(\eta^6\text{-C}_6\text{H}_6)\text{MoH}(\text{TRIPOD})]^+$  (**3**) which suggests that there is negligible interaction between the amine nitrogen and the hydride. A single  $^{31}\text{P}$  resonance at 37.7 ppm for **10** suggests that the arene on the metal is rotating freely along the metal-arene centroid.

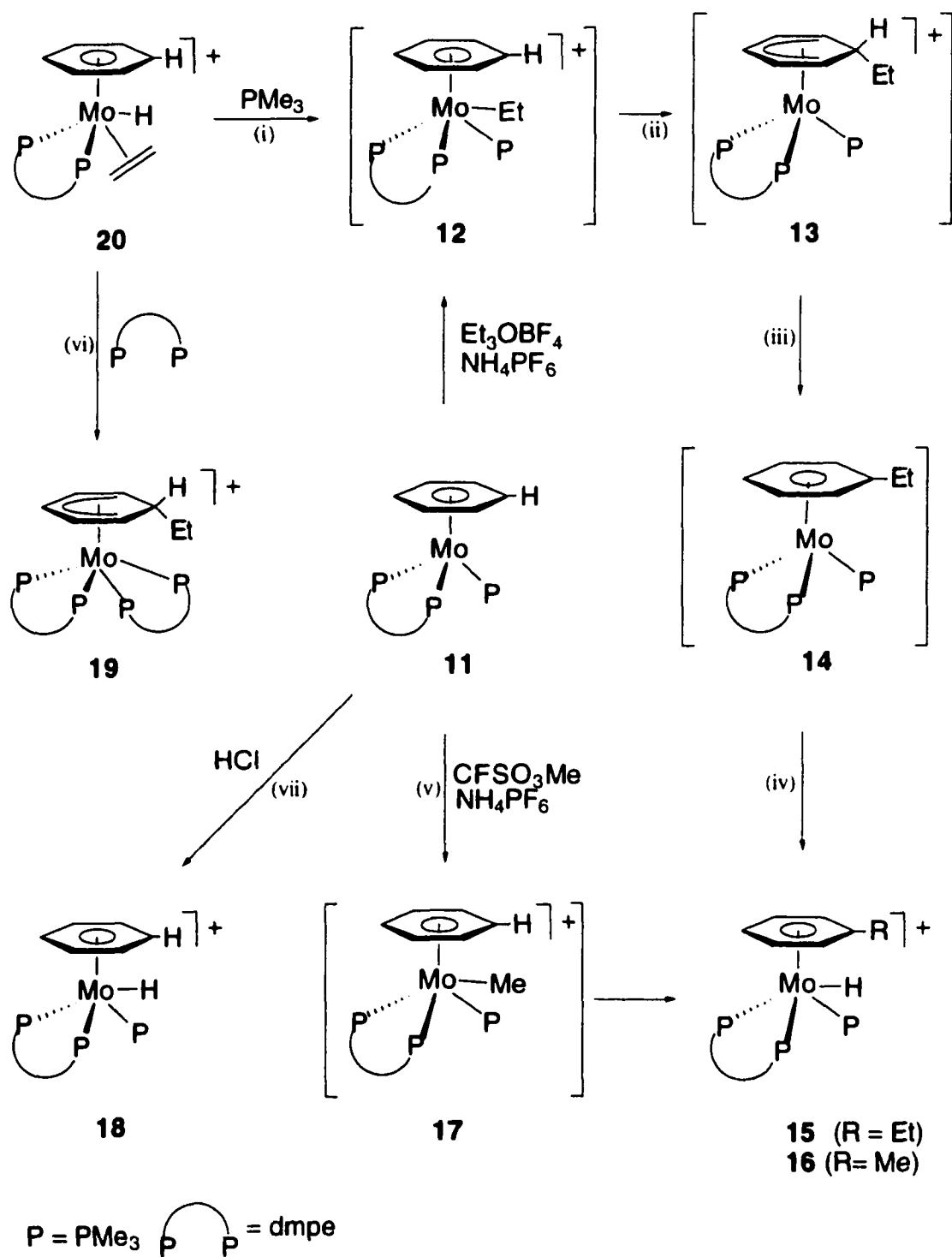
Unlike the methylation reactions (Section 4.4) only a single product is obtained in the reaction of **1** with  $[\text{CH}_2=\text{NMe}_2]\text{I}$ . Unfortunately, **10** is not stable in polar solvents in which it is soluble. It is stable enough to allow spectral characterization within a few hours, but attempts to grow crystals in  $\text{CH}_2\text{Cl}_2$  or MeOH gave paramagnetic species. It was found to be fairly stable in  $\text{CH}_3\text{CN}$ , but attempts to isolate a clean product was unsuccessful.

#### 4.4 METHYLATION

**Analysis of Green's mechanism for  $(\eta^6\text{-C}_6\text{H}_6)\text{Mo}(\text{dmpe})(\text{PMe}_3)$  (**11**).** Green and coworkers have carried out a mechanistic study on the alkylation of **11**. Scheme 4.2 outlines the proposed mechanism.<sup>14</sup> Alkylation of **11** with  $\text{Et}_3\text{OBF}_4$  yields a 40:60 mixture of **18** and **15**.  $\text{CF}_3\text{SO}_3\text{Me}$  reacts with **11** to give **17** and **18** initially and after three days **17** converts to **16**. It was assumed that the formation of **18** in both these reactions was due to "adventitious acid" in the reagents. A detailed mechanistic study was carried out for this reaction which is reproduced here for comparison with the methylation reaction of **1**. The four steps from **20** to **15** are:

- (i) The electrophile initially reacts at the nucleophilic metal center of **20** to yield **12**.
- (ii) **12** converts to **13** by an *endo* alkyl migration from metal to the ring.
- (iii) **13** loses a proton by an *exo*-fashion to yield **14**
- (iv) **14** reprotonates at the metal to give **15**.

Evidence for step (i) is provided by the isolation of the intermediate **17** in the reaction of **11** with  $\text{CF}_3\text{SO}_3\text{Me}$ . When the reaction of **11** with  $\text{CF}_3\text{SO}_3\text{Me}$  is quenched in five minutes a mixture of **17** and **16** was obtained (step (v)). There are also other precedents for electrophiles reacting at the metal.<sup>24,25</sup> Evidence for *endo* alkyl migration in step (ii) is provided by the formation of the *endo* ethyl substituted ring in **19**, when a chelating phosphine is added to **20** (step (vi)). Examples of metal-to-ring alkyl migration are known in the literature.<sup>26-28</sup> It was suggested that the *exo* proton loss by **13** to give **14** is

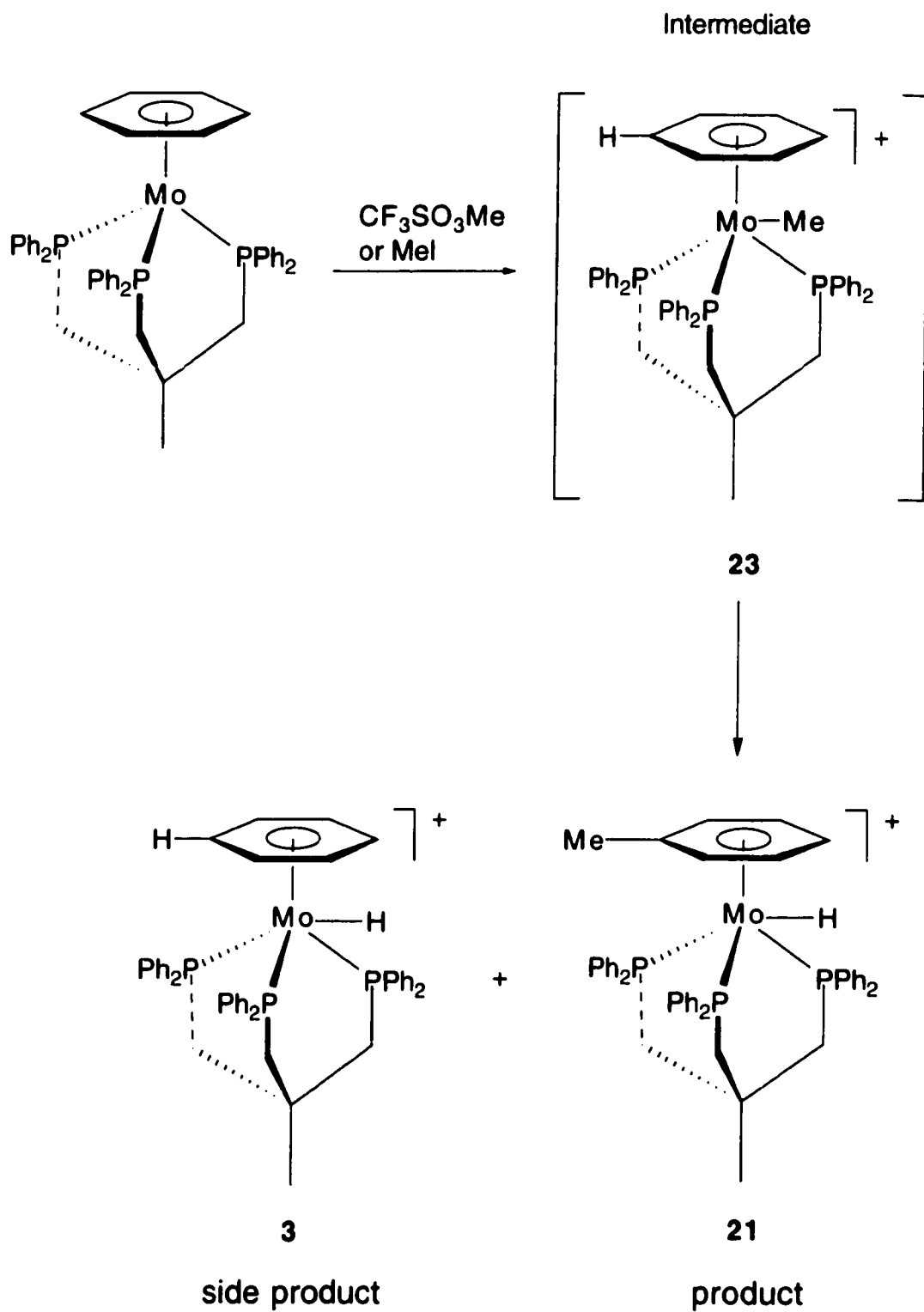


Scheme 4.2 Green's proposed mechanism for the alkylation of  $(\eta^6\text{-C}_6\text{H}_6)\text{Mo}(\text{dmpe})(\text{PMe}_3)$

intermolecular (possibly assisted by the solvent). A control experiment was carried out to support step (iii). When **20** was treated with  $\text{PMe}_3$  in 10%  $\text{D}_2\text{O}$ /acetone- $\text{d}_6$  mixture, the product **15** has more than 70% deuterium on the metal. In a complimentary reaction,  $[(\eta^6\text{-C}_6\text{D}_6)\text{MoH}(\eta^2\text{-C}_2\text{H}_4)(\text{dmpe})]^+$  (**20-d<sub>6</sub>**) with  $\text{PMe}_3$  in 10% aqueous acetone gives  $[(\eta^6\text{-C}_6\text{D}_5\text{Et})\text{MoH}(\text{dmpe})(\text{PMe}_3)]^+$  (with no deuterium on the metal). The isotopic exchange of **11** and **15** in 10-20% aqueous acetone is slow under these experimental conditions. The protonation of **14** to form **15** in step (iv) was expected to occur readily by comparison to the protonation of **11** with acid to give **18**.

As mentioned before, the authors have assumed the formation of **18** in their reactions, is due to adventitious acid present in the reagents. However, 40% of **18** arising from acid impurity in the electrophilic reagents is very unlikely. The methylation reactions of **1** suggest that the proton arises from within the mechanism. Two possibilities could be reasoned for the formation of a high percentage of **18**. It is probable that (1) the *exo* proton that is lost in step (iii) could protonate a neutral molecule of **11** to produce **18**, and/or (2) the *exo* proton lost could hydrolyze any unreacted electrophilic reagent to the produce acid, which could protonate **11** to give **18**. Since **18** was not found in the reaction of **20** converting to **15**, the latter reason is most probably the cause for the formation of **18**. It should be also mentioned that the authors have ruled out the concept of initial ring alkylation mechanism citing electron richness of the metal. Nevertheless, **9** (a complex analogous to **11**) was shown (Chapter 3) to protonate at the metal and the ring in a ratio of 40 to 60.

Methylation is one of the most common electrophilic reaction studied. In order to compare the mechanism of protonation with that of alkylation, some methylating agents were reacted with **1**. Since a clean methylation reaction was not observed, the reaction of  $\text{MeI}$  was studied in detail. Attempts with methylating agents such as  $\text{CF}_3\text{SO}_3\text{Me}$  and  $\text{Me}_3\text{OBF}_4$  were also made. In order to understand the mechanism of this methylation, several different conditions were used and the results are summarized in Table 4.1. All the



Scheme 4.3. Reaction of MeI with  $(\eta^6\text{-C}_6\text{H}_6)\text{Mo}(\text{TRIPOD})$

Table 4.1  $^{31}\text{P}$  Integrations from the reactions of  $(\eta^6\text{-C}_6\text{H}_6)\text{Mo}(\text{TRIPOD})$  with MeI.

| No.            | $^{\circ}\text{C}$ | Conditions       | Relative $^{31}\text{P}$ integrations around 38, 37, 19 ppms |     |     |          |     |     |          |     |     |
|----------------|--------------------|------------------|--|-----|-----|----------|-----|-----|----------|-----|-----|
|                |                    |                  | 1 hour   |     |     | 24 hours |     |     | 72 hours |     |     |
|                |                    |                  | 21   | 3   | 23  | 21       | 3   | 23  | 21       | 3   | 23  |
| 1              | 50                 | none             | 5  | 7   | 50  | 81       | 31  | 25  | 169      | 150 | 17  |
| 2              | 25                 | LA               | 0  | 147 | 7   | 0        | 147 | 10  | -        | -   | -   |
| 3 <sup>a</sup> | 50                 | PS               | br   | 5   | 15  | 53       | 77  | 138 | 177      | 65  | 132 |
| 4              | 25                 | PS and LA        | 6  | 55  | 46  | 177      | 43  | 31  | 186      | 23  | 29  |
| 5              | 50                 | PS and LA        | 51   | 15  | 106 | 173      | 34  | 47  | 183      | 58  | 41  |
| 6              | 50                 | PS pretreated LA | 18   | 168 | 68  | -        | -   | -   | 174      | 69  | 31  |
| 7 <sup>b</sup> | 50                 | AIBN             | br   | br  | 88  | 50       | 92  | 126 | 123      | 80  | 161 |

LA = Lewis acid  $\text{BF}_3$ .etherate; PS = Proton sponge (1,8-dimethylaminonaphthalene)

AIBN = radical initiator (2,2'-Azobisisobutyronitrile)

<sup>a</sup> other unidentified peaks at 25, 36, 39, and 40 ppms

<sup>b</sup> other unidentified peaks at 25, 31 and 36 ppms

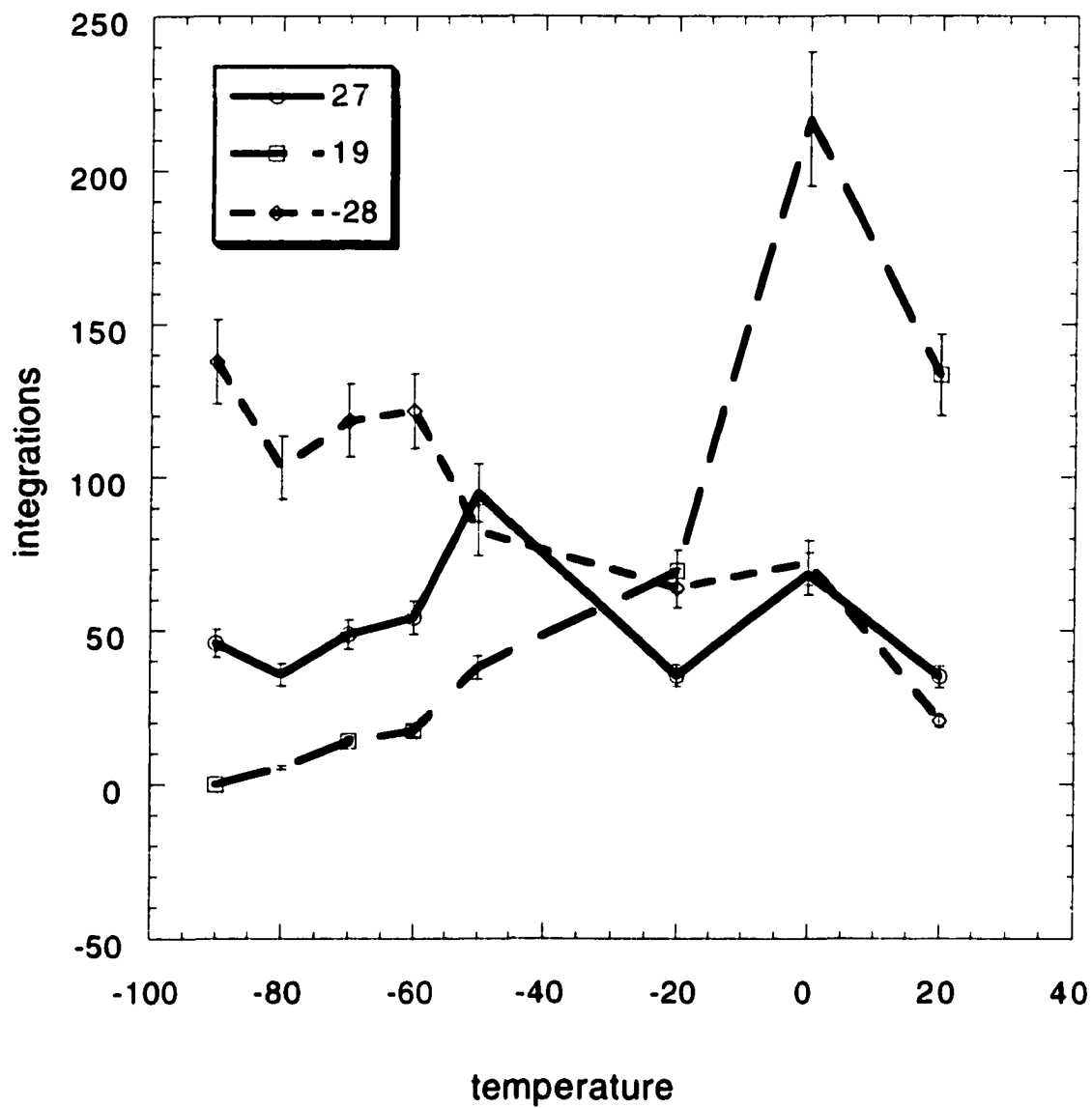


Figure 4.1. Plot of  $^{31}\text{P}$  integrations of resonances around 27, 19, and -28 ppm versus temperature ( $^{\circ}\text{C}$ ).

reactions were carried out in NMR tubes in neat MeI as the solvent and monitored by  $^{31}\text{P}$  NMR spectroscopy. The most common feature of all these reactions is three  $^{31}\text{P}$  signals around 19, 37 and 38 ppm. The peaks at 37 and 38 ppm are attributed to **21** and **3** (Scheme 4.3) respectively. This assignment was confirmed by independent synthesis of **21** and **3**. The peak at 19 ppm is believed due to **23**. Extra precaution (silylated glassware and proton sponge) was taken in removing of any proton in MeI or on the glassware surface. Nevertheless, **3** was present in the product mixture. It became clear that the unmethylated hydride is formed by proton in the mixture or produced during the reaction.

A reaction of **1** and MeI was monitored every 3 hours by  $^1\text{H}$  and  $^{31}\text{P}$  NMR spectroscopy to determine the time at which **21** and **3** are produced. In a 0.16 M solution reaction, resonances for **21** and **3** grew after 9 hours while in the 0.04 M case, resonances for **21** and **3** grew after 6 hours. Based on the results summarized in Tables 4.1 and other studies, the following qualitative observations can be made.

- (i) Use of Lewis acid catalyst  $\text{BF}_3\cdot\text{etherate}$  increases the relative amount of **3**.
- (ii) The reaction rate appears to increase with temperature, from 20 to 70 °C.
- (iii) Addition of proton sponge increases the relative amount of **21**.
- (iv) Complexes **21** and **3** are formed simultaneously.
- (v) 0.04 M solution of **1** produced **21** and **3** faster than 0.16 M solution.

The reaction of  $\text{CF}_3\text{SO}_3\text{Me}$  with **1** was studied to understand the mechanism of methylation. The  $^1\text{H}$  NMR spectra of these reactions were not very useful due to overlap of resonances from different species. However,  $^{31}\text{P}$  NMR spectra reveals some useful information based on which the results will be discussed. When **1** was reacted with  $\text{CF}_3\text{SO}_3\text{Me}$  in  $\text{CD}_2\text{Cl}_2$  at -80 °C and  $^{31}\text{P}$  NMR spectra was monitored as a function of temperature, four distinct resonances are seen at different periods of the experiment. The resonances are .

- I broad hump around 45-50 ppm
- II multiplets 27 and -28 ppm

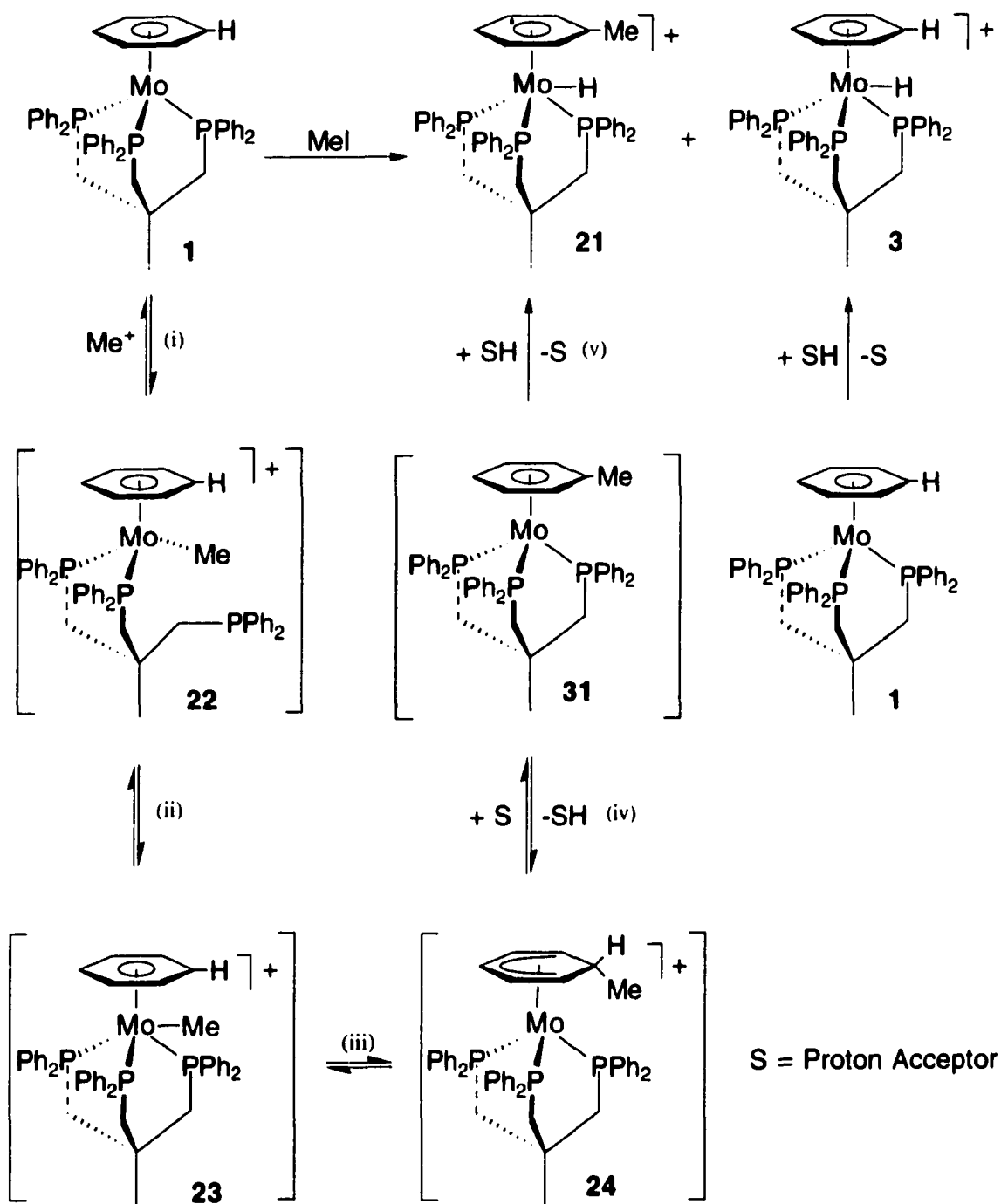
- III multiplet at 19 ppm, and
- IV two singlets at 38 and 37 ppm

At -80 °C, I and II are the two sets of resonances, with I approximately five times more abundant than II. As the temperature is raised to -60 °C, I diminishes and III begins to grow together with II. When the sample is at -20 °C, III has increased while II begins to diminish in height. At 20 °C, II is very small, and III is the major resonance. After sitting at 20 °C for 24 hours, IV grows as III diminishes in abundance. A plot of the <sup>31</sup>P NMR spectra integrations of II (27 and -28 peaks plotted separately) and III as a function of temperature is shown in Figure 4.1. The plot clearly indicates that II and III increase and decrease in intensity during course of the reaction. A very similar pattern is observed for the reaction of **1** with MeI at low temperatures.

A reasonable mechanism (Scheme 4.4) that can be proposed for the reaction of Me<sup>+</sup> as an electrophile with **1** is as follows:

- (i) one of the P arm of the TRIPOD ligand comes off in the presence of Me cation to give the intermediate **22**,
- (ii) the Me group attaches to the metal with the reformation of Mo-P bond to give **23**,
- (iii) an *endo* transfer of the Me group to the ring to yield **24**,
- (iv) followed by an *exo* proton loss to S (another molecule of **1** or solvent), and
- (v) protonation at the metal to give **21**.

To begin with, the results clearly point to different mechanisms for methylation and protonation. Though acids react predominantly by an electrophilic pathway, MeI is known to react by either electrophilic or single electron transfer (SET) mechanisms.<sup>29</sup> A reaction of **1** with 6-hexenyl iodide failed to yield cyclized products. Formation of cyclized products would have been an indication of radical mechanism, though the failure to observe such species does not eliminate a radical pathway.<sup>30</sup> It could be noted that MeI reaction (Table 4.1) in the presence of radical initiator AIBN gave several unidentified products. A



Scheme 4.4 Proposed mechanism for the addition of  $\text{Me}^+$  to  $(\eta^6\text{-C}_6\text{H}_6)\text{Mo}(\alpha\text{-TRIPOD})$

radical pathway should have been accelerated by the addition of AIBN, but instead several unidentified products are formed along with the desired products. Based on these two results, a SET mechanism for methylation is a very unlikely one.

An arm-off mechanism for the tripodal ligand has been encountered for Rh, Ru and Ir complexes.<sup>31-33</sup> The high field <sup>31</sup>P NMR peak at -28 ppm (of II) indicates a dangling phosphine arm of the TRIPOD ligand, which is similar to the chemical shift observed for the free arm of the TRIPOD of [RhMe<sub>2</sub>(MeCN)(TRIPOD)]Cl.<sup>31</sup> Therefore, II can be assigned to **22**, with 27 ppm and -28 ppm peaks due to attached and unattached P atoms to the metal, respectively. At this stage, it is not clear whether the Me group is attached to metal or not. However, it seems reasonable that the Me group is attached to metal in the vacancy created by arm-off of the phosphine. As the temperature is raised, the free phosphine arm attaches again to the metal to form the intermediate **23**, which is similar to **17** that Green and coworkers have isolated and characterized in their study. In the <sup>1</sup>H NMR spectrum at -20 °C, a broad peak at -0.9 ppm is tentatively assigned to the Mo-Me in **23**, which is similar to Green's **17** Mo-Me resonance at -1.29 ppm. The Me group then *endo* transfers to the ring to give **24** which subsequently loses a proton to form a known (Chapter 5) toluene complex, **31**. Complex **31** may be readily protonated from the surrounding media to give **21**. The species **24** is believed to be a transient species based on the precedence from protonation studies. Complex **31** is not observed since its protonation is instantaneous even at -80 °C. Therefore, **21** is observed at the disappearance of **23**. If **24** loses the Me<sup>+</sup> instead of H<sup>+</sup>, then it reverts back to **1**, which can be protonated to produce **3**. The probable reason for observing more **21** than **3** in the mixture is because the *endo* loss of Me<sup>+</sup> from **24** is less favorable compared to the *exo* loss of a proton.

The postulated mechanism for methylation of **1** raises an important question. Why does Me<sup>+</sup> react at the metal while H<sup>+</sup> reacts at the ring in **1**? While the metal is the

nucleophilic site in the molecule, and steric crowding of the TRIPOD ligand prevents the acid from directly reacting at the metal, which necessitates the proton to attack the ring. If steric crowding of the ligand is the primary reason then  $\text{Me}^+$  should react at the ring. However, initial methylation at the metal is observed. One plausible explanation is that in the halogenated solvents the arm-off equilibrium is initiated. Acids are stronger electrophiles than carbocations, which enables acids to react at the arene, a lesser nucleophilic site. On the other hand, carbocations are less electrophilic and therefore seeks a more nucleophilic site such as the metal. The comparative electrophilic character of acids and carbocations are reflected in their reaction durations. The reaction of acid with **1** at  $-85^\circ\text{C}$ , is essentially complete within seconds, while methylation reactions at room temperature are complete in longer than 24 hours. This point is further confirmed by the reaction of Eschenmoser's salt with **1** at  $25^\circ\text{C}$ , where the only product formed is the initial ring substituted complex. Since the iminium salt is a better electrophile than MeI it reacts exclusively at the ring.

#### 4.5 REACTIONS WITH ELECTROPHILES OTHER THAN PROTON

Many attempts were made to react other electrophiles with  $(\eta^6\text{-C}_6\text{H}_6)\text{Mo}(\text{TRIPOD})$ , but they did not give satisfactory results. The list of electrophiles attempted is as follows:  $\text{Et}_3\text{OBF}_4$ ,  $\text{Me}_3\text{SiCl}$ ,  $\text{CF}_3\text{SO}_3\text{SiMe}_3$ , NO,  $\text{NOPF}_6$ ,  $\text{NO}_2\text{BF}_4$ ,  $\text{CH}_3\text{COCl}$ ,  $\text{CH}_3\text{COCl}/\text{AlCl}_3$ ,  $\text{SO}_3$ ,  $\text{C}_6\text{H}_5\text{CH}_2\text{Br}$ , EtI, i-PrI and t-BuI. Highly moisture sensitive reagents simply gave **3** as the product. Attempts to react  $\text{Et}_3\text{OBF}_4$ ,  $\text{Me}_3\text{SiCl}$ ,  $\text{CH}_3\text{COCl}$ , and  $\text{CF}_3\text{SO}_3\text{SiMe}_3$  gave **3** as the only product. Reactions of **1** with NO,  $\text{NOPF}_6$ ,  $\text{NO}_2\text{BF}_4$ ,  $\text{CH}_3\text{COCl}/\text{AlCl}_3$ , and  $\text{SO}_3$  resulted in unidentified products. Since these reagents are known oxidizing agents, probably oxidation of **1** leads to oxidized products. Halogenated reagents such as  $\text{C}_6\text{H}_5\text{CH}_2\text{Br}$ , EtI, i-PrI and t-BuI displayed reactions similar to the MeI reaction discussed above. Separation of the alkylated and unalkylated hydride proved to be difficult with these reaction mixtures.

## 4.6 SUMMARY

Several electrophiles were reacted with the electron rich complex **1**, to understand the electrophilic aromatic substitution with electrophiles other than proton. There are several indications that the mechanism of these electrophile reactions is different from that of the protonation mechanism. The initial site of reaction of carbon-centered electrophiles may be different from that of proton. It appears that the electrophilicity of the reagent dictates the mechanism of alkylation of **1**. It is not clear whether the size of the electrophile plays a role in the mechanism of substitution or not. Methyl cation despite being bulkier than proton does not react exclusively at the ring. It was not possible to extend the result obtained for protonation to more bulkier electrophiles, because of the difficulty in separating the desired electrophilic product from the simply protonated product.

## 4.7 BIBLIOGRAPHY

- (1) Watts, W. E. In *Comprehensive Organometallic Chemistry*; Wilkinson, G., Stone, F. G. A., Abel, E. W., Ed.; Pergamon Press: Oxford, 1982; Vol. 8, pp 1013-1026.
- (2) Fischer, E. O.; von Foerster, M.; Kreiter, C. G.; Schwarzhan, K. E. *J. Organomet. Chem.* **1967**, *7*, 113.
- (3) Nicholls, B.; Whiting, M. C. *J. Chem. Soc.* **1959**, 551-556.
- (4) Ercoli, R.; Calderazzo, F.; Mantica, E. *Chim. Ind. (Milan)* **1959**, *41*, 404.
- (5) Riemschnieder, R.; Becker, O.; Franz, K. *Monatsch. Chem.* **1959**, *90*, 571-572.
- (6) Herberich, G. E.; Fischer, E. O. *Chem. Ber.* **1962**, *95*, 2803-2809.
- (7) Razuvaev, G. A.; Domrachev, G. A. *Tetrahedron* **1963**, *19*, 341-343.
- (8) Fischer, E. O.; Wehner, H. W. *Chem. Ber.* **1968**, *101*, 454-462.
- (9) Fischer, E. O.; Breitschaft, S. *Chem. Ber.* **1966**, *99*, 2213-2221.
- (10) Werner, H.; Hofmann, W. *Chem. Ber.* **1977**, *110*, 3481-3493.
- (11) Werner, H.; Hofmann, W. *Angew. Chem. Int. Ed. Engl.* **1977**, *16*, 794-795.
- (12) Green, M.; Hughes, R. P. *J. Chem. Soc., Chem. Commun.* **1975**, 862-863.
- (13) Cantestari, M.; Green, M. L. H.; Izquierdo, A. *J. Chem. Soc., Dalton Trans.* **1984**, 2795-2801.

- (14) Bunting, H. E.; Green, M. L. H.; Newman, P. A. *J. Chem. Soc., Dalton Trans.* **1988**, 557-577.
- (15) Herberich, G. E.; Klein, W. *Chem. Ber.* **1979**, *122*, 2125-2128.
- (16) Corella, J. A., II; Cooper, N. J. *J. Am. Chem. Soc.* **1990**, *112*, 2832-2834.
- (17) Thompson, R. L.; Lee, S.; Rheingold, A. L.; Cooper, N. J. *Organometallics* **1991**, *10*, 1657-1659.
- (18) Leong, V. S.; Cooper, N. J. *J. Am. Chem. Soc.* **1988**, *110*, 2644-2646.
- (19) Park, S.-H. K.; Geib, S. J.; Cooper, N. J. *J. Am. Chem. Soc.* **1997**, *119*, 8365-8366.
- (20) Harman, W. D. *Chem. Rev.* **1997**, *97*, 1953-1978.
- (21) Kopach, M. E.; Gonzalez, J.; Harman, W. D. *J. Am. Chem. Soc.* **1991**, *113*, 8972-8973.
- (22) Kolis, S. P.; Kopach, M. E.; Liu, R.; Harman, W. D. *J. Org. Chem.* **1997**, *62*, 130-136.
- (23) Heaney, H. In *Comprehensive Organic Synthesis*; Trost, B. M.; Fleming, I., Ed.; Pergamon: Oxford, 1991; Vol. 2, pp 953-973.
- (24) Werner, H.; Feser, R. *J. Organomet. Chem.* **1982**, *232*, 351.
- (25) Benfield, F. W. S.; Cooper, N. J.; Green, M. L. H. *J. Organomet. Chem.* **1974**, *76*, 49.
- (26) Brookhart, M.; Pinhas, A. R.; Lukacs, A. *Organometallics* **1982**, *1*, 2730.
- (27) Fachinetti, G.; Floriani, C. *J. Chem. Soc., Chem. Commun.* **1974**, 516.
- (28) Benfield, F. W. S.; Green, M. L. H. *J. Chem. Soc., Dalton Trans.*, **1973**, 1324-1330.
- (29) Astruc, D. *Chem. Rev.* **1988**, *88*, 1189-1216.
- (30) Tolbert, L. M.; Sun, X.-J.; Ashby, E. C. *J. Am. Chem. Soc.* **1995**, *117*, 2681-2685.
- (31) Landgrafe, C.; Sheldrick, W. S.; Sudfeld, M. *Eur. J. Inorg. Chem.* **1998**, *1*, 407-414.
- (32) Brandt, K.; Sheldrick, W. S. *Chem. Ber.* **1996**, *129*, 1199-1206.
- (33) Rauscher, D. J.; Thaler, E. G.; Huffmann, J. C.; Caulton, K. G. *Organometallics* **1991**, *10*, 2209.

## CHAPTER 5

# EFFECT OF ARENE LIGAND SUBSTITUTION ON THE MECHANISM OF PROTONATION OF ( $\eta^6$ -ARENE)Mo(TRIPOD) COMPLEXES

### 5.1 INTRODUCTION

Regiochemistry of electrophilic aromatic substitution is usually controlled by the substituents on the aromatic ring. Electron-withdrawing substituents retard electrophilic substitution, while electron-releasing substituents cause the reverse. Generally, electron-withdrawing groups are *meta*-directing and electron-releasing groups are *ortho*, *para*-directing in aromatic electrophilic substitutions. This generality can be modified in electrophilic substitutions of arene rings attached to a transition metal. The orientation of the arene ligand in the complexes of the type ( $\eta^6$ -C<sub>6</sub>H<sub>5</sub>R)ML<sub>3</sub> depends on the bulkiness of the substituent group. When the R group is bulky, it is staggered with respect to the ancillary ligands L and is eclipsed when it is small. Since the orientations of the arene ring on the metal is controlled by the ligands, the regiochemistry of substitution is altered compared to that of free arenes.

### 5.2 LITERATURE OVERVIEW

**Synthesis of bis(arene)molybdenum complexes.** Since the first synthesis of ( $\eta^6$ -C<sub>6</sub>H<sub>6</sub>)<sub>2</sub>Mo by Fischer and Stahl in 1956, many routes have been employed to synthesize bis(arene)molybdenum complexes.<sup>1</sup> Synthetic routes to bis(arene)molybdenum can be categorized into two main categories: the reduction route and the metal-atom vapor

route. The Fischer-Hafner synthesis uses Friedel-Crafts reducing conditions namely the use of Al/AlCl<sub>3</sub>.<sup>2</sup> Fischer and Stahl reduced MoCl<sub>5</sub> with Al/AlCl<sub>3</sub> in benzene to give [(η<sup>6</sup>-C<sub>6</sub>H<sub>6</sub>)<sub>2</sub>Mo]AlCl<sub>4</sub> which was further reduced by alkaline Na<sub>2</sub>S<sub>2</sub>O<sub>3</sub> to obtain (η<sup>6</sup>-C<sub>6</sub>H<sub>6</sub>)<sub>2</sub>Mo. Though the Fischer-Hafner synthesis works well with benzene to prepare (η<sup>6</sup>-C<sub>6</sub>H<sub>6</sub>)<sub>2</sub>Mo, it is not suitable for substituted arenes. Alkyl substituents on the ring migrate forming a mixture of isomers under Friedel-Crafts conditions.<sup>3</sup> Timms and coworkers have used potassium<sup>4</sup> and magnesium<sup>5</sup> atoms as reducing agents. Bis(arene)molybdenum complexes were synthesized by condensing K or Mg atoms into solutions containing MoCl<sub>5</sub> and arene in THF at -100°C. Recently, Pampaloni and coworkers reported the synthesis of (η<sup>6</sup>-C<sub>6</sub>H<sub>5</sub>Me)<sub>2</sub>Mo by a one-pot procedure, which is essentially Fischer-Hafner synthesis with toluene and THF as solvents.<sup>6</sup>

The metal-vapor atom technique is a clean method widely used for synthesizing bis(arene)metal complexes.<sup>7</sup> Unlike reduction synthesis, the metal-vapor technique can be used to synthesize complexes of substituted arenes with a variety of different functional groups. The limitation of the technique is the non-traditional and expensive apparatus required. Syntheses of second and third row transition bis(arene)metal complexes require high-energy equipment, because of the high melting points of the metals. Two methods of vaporizing the metals are the resistive heating and electron-beam heating, which are commonly reported for molybdenum reactions. The research groups of Green,<sup>8</sup> Ittel,<sup>9</sup> and Andrews and Ozin<sup>10</sup> have synthesized a variety of bis(arene)molybdenum complexes using electron-beam heating method. Resistive heating method for molybdenum and tungsten complexes have been reported by Skell and coworkers.<sup>11</sup>

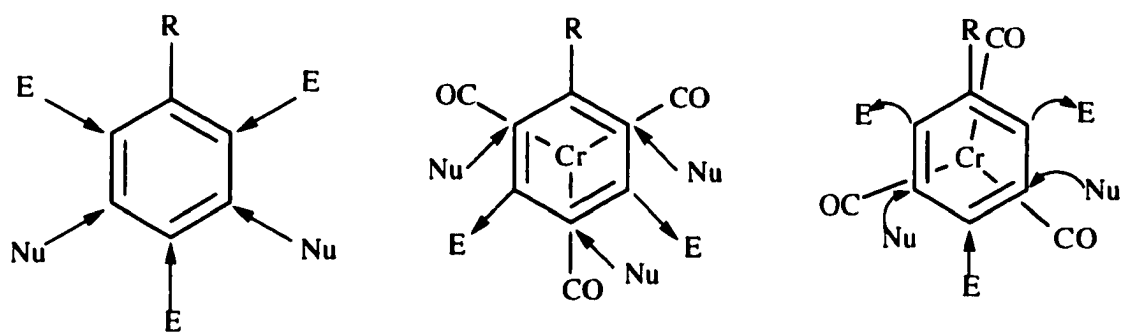
**Regiochemistry of Electrophilic Substitution.** The first known electrophilic substitution on an η<sup>6</sup>-arene complex is the Friedel-Crafts acylation of the (η<sup>6</sup>-C<sub>6</sub>H<sub>6</sub>)Cr(CO)<sub>3</sub> reported in 1959 by three independent groups.<sup>12-14</sup> Herberich and Fischer first reported the acylation of (η<sup>6</sup>-C<sub>6</sub>H<sub>5</sub>CH<sub>3</sub>)Cr(CO)<sub>3</sub> with *o*:*m*:*p* ratios of 43:17:40.<sup>15</sup> Researchers in the field have agreed that the arene is deactivated towards

electrophilic substitution based on acylation yields. The rates of electrophilic substitutions on  $(\eta^6\text{-arene})\text{Cr}(\text{CO})_3$  complexes were predicted to be slower than those of parent arenes by Brown using MO calculations.<sup>16</sup> Jackson and Jennings have studied the acylation of  $(\eta^6\text{-arene})\text{Cr}(\text{CO})_3$  (arene = alkylbenzenes) and reported the isomer ratios to be different from those of free arenes.<sup>17</sup> Their findings are summarized in Table 5.1. Meanwhile, Brown has carried out kinetic studies on the system and found the presence of  $\text{Cr}(\text{AlCl}_3)_2(\text{CS}_2)_2$ , which lead him to conclude that no theoretical predictions on relative reactivities of free arenes and metal bound arenes can be made regarding Friedel-Crafts acylations.<sup>18</sup> It is believed that in such acylations the low yields of ketone are due to the competing reaction of the Lewis acid attacking the metal center. However, Jackson has continued several studies on the  $(\eta^6\text{-arene})\text{Cr}(\text{CO})_3$  series (after addressing Brown's caution) and have proposed empirical predictions on the isomer ratios.<sup>19,20</sup> Using several electronic and steric arguments, the preferred sites (Scheme 5.1) of attack on the arene were reported.<sup>21</sup> The free arene is activated towards electrophilic substitution in the *ortho* and *para* position, while in the complexed arene it depends on the bulkiness of the R group. When the R is bulky, for example R = t-butyl, the electrophilic attack is in the *meta* position and for small R groups like methyl, the *ortho* and *para* isomers dominate as substitution products. This model predicts the isomeric ratio in the acetylation of  $(\eta^6\text{-1,1-dimethylindane})\text{Cr}(\text{CO})_3$ ,<sup>22,23</sup> Pinder and von Rosenberg have found increased yield conditions for the acetylation of  $(\eta^6\text{-arene})\text{Cr}(\text{CO})_3$  and have studied biphenyl complexes which show activation towards electrophilic substitution in the uncomplexed ring compared to the complexed ring.<sup>24</sup>

Since the mechanism of electrophilic aromatic protonation for  $(\eta^6\text{-arene})\text{Mo}(\text{TRIPOD})$  system is found to be different from that of  $(\eta^6\text{-arene})\text{Cr}(\text{CO})_3$ , it was decided that it would be interesting to study the regiochemistry of electrophilic substitutions in such systems and compare it to Jackson's predictions. The simplest electrophile, proton can be used to follow the regiochemistry because isotopic tracer provide an easy handle on the product.

Table 5.1. Isomer ratios for acetylations from Jackson and Jennings

| Arene                   | free arene <i>o:m:p</i> | areneCr(CO) <sub>3</sub> <i>o:m:p</i> |
|-------------------------|-------------------------|---------------------------------------|
| Toluene                 | 1.2:2:96.8              | 43: 17: 40                            |
| Ethylbenzene            | 0.4:2.9:96.7            | 24:33:43                              |
| <i>i</i> -propylbenzene | 0.1:3.4:96.5            | 5:59:36                               |
| <i>t</i> -Butylbenzene  | 0.0:4.3:95.7            | 0:87:13                               |



Scheme 5.1 Preferred sites of nucleophilic and electrophilic substitutions

Moreover, a proton would be a suitable electrophile for ( $\eta^6$ -arene)Mo(TRIPOD) because the hydride species can be isolated unlike in the ( $\eta^6$ -arene)Cr(CO)<sub>3</sub> case.

**Electrophilic Reactions of C<sub>6</sub>H<sub>5</sub>SiMe<sub>3</sub> and its Metal Complexes.** The silicon-carbon bond in C<sub>6</sub>H<sub>5</sub>SiMe<sub>3</sub> is known to be cleaved by many electrophiles.<sup>25</sup> These electrophilic aromatic desilylation reactions have been used as a synthetic strategy to introduce different substituents on the ring. The *ipso*-directing effect is large, and can direct addition to rather unusual sites.<sup>26</sup> A handful of metal complexes of C<sub>6</sub>H<sub>5</sub>SiMe<sub>3</sub> are known since the first complex, ( $\eta^6$ -C<sub>6</sub>H<sub>5</sub>SiMe<sub>3</sub>)Cr(CO)<sub>3</sub> was reported in 1960.<sup>27</sup> Elschenbroich and Koch synthesized ( $\eta^6$ -C<sub>6</sub>H<sub>5</sub>SiMe<sub>3</sub>)<sub>2</sub>Cr by the metal atom vapor method.<sup>28</sup> Green and coworkers reported the synthesis of ( $\eta^6$ -C<sub>6</sub>H<sub>5</sub>SiMe<sub>3</sub>)<sub>2</sub>Mo by solution route from ( $\eta^6$ -C<sub>6</sub>H<sub>6</sub>)<sub>2</sub>Mo precursor.<sup>29</sup> The synthesis of ( $\eta^6$ -C<sub>6</sub>H<sub>5</sub>SiMe<sub>3</sub>)Mo(CO)<sub>3</sub> and its crystal structure was reported.<sup>30</sup> Effenberger et al. have reacted ( $\eta^6$ -C<sub>6</sub>H<sub>5</sub>SiMe<sub>3</sub>)Cr(CO)<sub>3</sub> with aldehydes and ketones under basic conditions forming derivative trimethyl silyl ether complexes, which can be hydrolyzed to give substituted benzyl alcohol complexes.<sup>31,32</sup> The ( $\eta^6$ -C<sub>6</sub>H<sub>5</sub>SiMe<sub>3</sub>)Cr(CO)<sub>3</sub> was converted to ( $\eta^6$ -C<sub>6</sub>H<sub>5</sub>COR)Cr(CO)<sub>3</sub> (R = H, Ph) by reacting RCOR' (R' = NMe<sub>2</sub> or F) in the presence of CsF in HMPA as solvent. Complexes of Mn and Ru are also known. [( $\eta^6$ -C<sub>6</sub>H<sub>5</sub>SiMe<sub>3</sub>)Mn(CO)<sub>3</sub>]<sub>2</sub>BF<sub>4</sub> and [( $\eta^6$ -C<sub>6</sub>H<sub>5</sub>SiMe<sub>3</sub>)Ru(4-isopropyltoluene)](BF<sub>4</sub>)<sub>2</sub> were synthesized by Went and coworkers.<sup>33</sup> Hagen and Beck investigated acid reactions of ( $\eta^6$ -C<sub>6</sub>H<sub>5</sub>SiMe<sub>3</sub>)Cr(CO)<sub>3</sub> and free arene.<sup>34</sup>

### 5.3 SYNTHESIS

As pointed out in the literature overview section, the two known routes for the syntheses of bis(arene)metal complexes are the reduction route and metal atom vapor route. Complexes **26-30** are previously known in the literature. Complex **26** was synthesized both by reduction<sup>35</sup> and metal-atom<sup>36</sup> routes. Synthesis of **27** by the Friedel-Crafts reduction procedure is mentioned in the literature.<sup>37</sup> Synthesis and decomposition

properties of **28** were patented in 1966.<sup>38</sup> The patent describes a metal amalgam reduction procedure. Complex **29** was obtained by metal-atom vapor route.<sup>39</sup> In this project, bis(arene)molybdenum complexes, **26-29** were synthesized by arene displacement reaction of  $(\eta^6\text{-C}_6\text{H}_6)_2\text{Mo}$  with the appropriate arene by heating at 160 °C. Arene displacement reaction of  $(\eta^6\text{-C}_6\text{H}_6)_2\text{Mo}$  to give bis(arene)molybdenum compounds is a new route discovered during this study. The route is fairly simple and clean products are obtained without difficult workup procedures. The optimum temperature, pressure and time is crucial for the success of the reaction. The temperature at 160 °C, pressure at 0.1 torr and 48 hours duration are ideal for the completion of the reaction. At temperatures higher than 160 °C more decomposition of the starting material takes place as evidenced by the formation of a black metal deposit. Pressures lower than 0.1 torr were not attempted, although it is likely that lower pressures at 160 °C would lead to decomposition of the starting material. Shorter reaction times gave mono arene displaced products.

Syntheses of complexes **31-35** were accomplished following a procedure similar to that of the unsubstituted benzene complex, **1**. Melt reactions of the bis(arene)molybdenum and TRIPOD ligand works well, though the reaction in the appropriate arene as the solvent is preferred. Grinding the reagents with a mortar and pestle and loading into 8 mm tube attached to a Schlenk adapter constituted considerable waste of reagents and longer setting up time. Therefore, reactions were conducted in the appropriate arene as solvent in most of the cases. At 160 °C, the arene is labile enough for displacement by phosphines or other arenes. When an arene is used as the solvent, there is a large excess of the arene in the mixture. At the reaction temperature, the arene exchange is competing with arene displacement by TRIPOD ligand. It is believed that after the phosphines are attached to the metal, the arene and TRIPOD are not labile at the reaction temperature, which makes arene displacement by phosphines more favorable.

A single crystal X-ray structure (Figure 5.1) was obtained for **35**. The parameters are comparable to those of the unsubstituted complex, **1**. A notable feature is the position

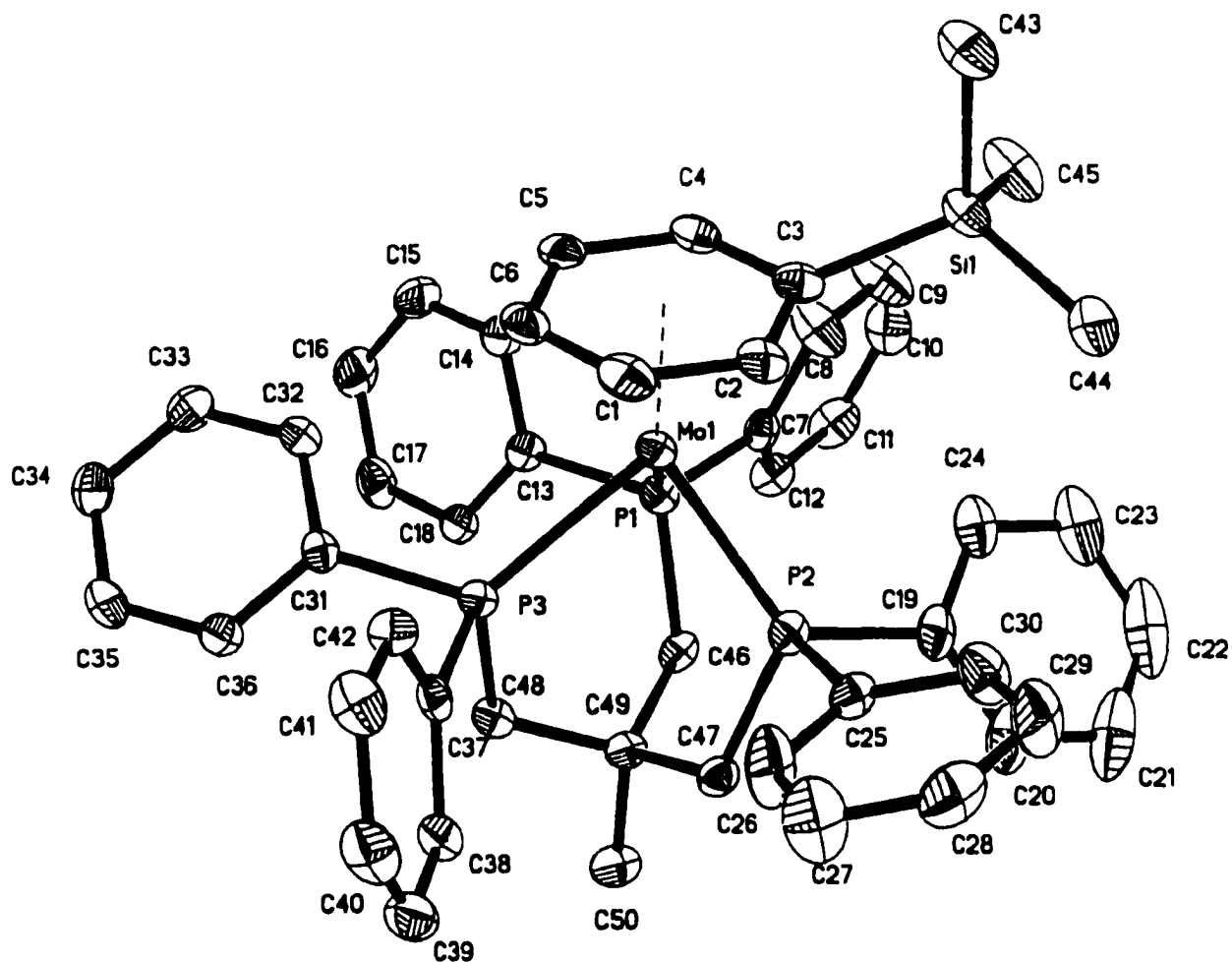


Figure 5.1. Thermal ellipsoid drawings (50% probability) of  $(C_6H_5SiMe_3)Mo(TRIPOD)$ .

Table 5.2. Selected interatomic distances (Å) and bond angles (deg) for **35** and **1**.

| Bond/Angle | <b>35</b> | <b>1</b>   |
|------------|-----------|------------|
| Mo-P1      | 2.4305(7) | 2.4118(13) |
| Mo-P2      | 2.4142(7) | 2.3856(10) |
| Mo-P3      | 2.4305(7) | 2.3846(10) |
| Mo-X       | 1.814(3)  | 1.816(5)   |
| P1-Mo-P2   | 82.92(2)  | 84.82(4)   |
| P2-Mo-P3   | 85.20(2)  | 83.12(4)   |
| P3-Mo-P1   | 82.60(2)  | 83.50(3)   |
| P1-Mo-X    | 136.3(1)  | 129.2(1)   |
| P2-Mo-X    | 128.0(1)  | 128.4(1)   |
| P3-Mo-X    | 124.6(1)  | 131.0(1)   |

X - centroid of the arene

of the TMS group that sits between the two P atoms of TRIPOD ligand. The C-Si bond is 0.65 Å above (with an angle of 29.7 deg) from the mean plane of the arene.

## 5.4 REACTIONS

The reaction of acids with  $(\eta^6\text{-C}_6\text{H}_5\text{Me})\text{Mo}(\text{TRIPOD})$  (**31**) was studied by nmr spectroscopy. Reaction of one equivalent of  $\text{CF}_3\text{SO}_3\text{D}$  with **31** gives  $[(\eta^6\text{-C}_6\text{H}_4\text{DMe})\text{MoH}(\text{TRIPOD})]^+$  with approximately equal distribution of *ortho*, *meta*, *para* isomers. Free toluene shows a very high preference for *para* electrophilic substitution. This preference is lost in **31**, which could be due to the disruption of the  $\pi$ -cloud of the arene when attached to metal. The inductive electronic effects in arenes are transmitted through  $\pi$ -bonds. Since the arenes in sandwich type complexes bond to the metal via  $\pi$ -cloud, the inductive effects are not transmitted effectively in these metal bound arenes. Such reduced effectiveness of the substituent electronic effect has been encountered in carboxylic acid complexes of  $\text{Cr}(\text{CO})_3$ .<sup>40</sup> The isotope tracer reactions were not performed on **32**, **33** and **34** because of the difficulty in obtaining pure compounds.

The reaction of acid with **35** gives  $[(\text{C}_6\text{H}_6)\text{MoH}(\text{TRIPOD})]^+$  (**3**) as the only product after workup. The first equivalent of acid attacks the nucleophilic C-Si bond, cleaving it to form **1**, which in turn is protonated by another equivalent of acid to give **3**. The reaction is similar to ones displayed by  $(\eta^6\text{-C}_6\text{H}_5\text{SiMe}_3)\text{Cr}(\text{CO})_3$  and its free arene. The Si atom in **35** is susceptible to nucleophilic attack by fluoride ions. The reaction of  $\text{Bu}_4\text{NF}$  in aqueous THF produces **1** as a clean product. The  $\text{F}^-$  ion cleaves the TMS group, creating a carbanion on the ring, which is protonated by water to yield **1**.

## 5.6 SUMMARY

Preliminary regiochemistry studies show no regiochemical preferences for **31**, indicating that the arene might have lost the directing effect upon complexation to the metal.

Based on reactions of **31** and **35**, the mechanism of protonation does not appear to be affected by the alkyl group on the ring. As seen for benzene complex **1**, the initial site of protonation is the arene for these complexes. Reaction of acid cleaves the C-Si bond in **35** similar to free arene.

## 5.6 BIBLIOGRAPHY

- (1) Fischer, E. O.; Stahl, H. O. *Chem. Ber.* **1956**, *89*, 1805-1808.
- (2) Silverthorn, W. E. *Inorg. Synth.* **1977**, *17*, 54.
- (3) March, J. *Advanced Organic Chemistry*; 4 ed.; John Wiley & Sons: New York, 1992.
- (4) Hawker, P. N.; Kundig, E. P.; Timms, P. L. *J. Chem. Soc. Chem. Commun.* **1978**, 730-731.
- (5) Thi, N. P. D.; Spichiger, S.; Paglia, P.; Bernardinelli, G.; Kundig, E. P.; Timms, P. L. *Helv. Chim. Acta* **1992**, *75*, 2593-2607.
- (6) Calderazzo, F.; Invernizzi, R.; Marchetti, F.; Masi, F.; Moalli, A.; Pampaloni, G.; Rocchi, L. *Gazz. Chim. Ital.* **1993**, *123*, 53-60.
- (7) Klabunde, K. J.; Timms, P. L.; Skell, P. S.; Ittel, S. D. *Inorg. Synth.* **1979**, *19*, 59-86.
- (8) Green, M. L. H. *J. Organomet. Chem.* **1980**, 119-132.
- (9) Ittel, S. D.; Van-Catledge, F. A.; Tolman, C. A. *Inorg. Chem.* **1985**, *24*, 62-65.
- (10) Ozin, G. A.; Andrews, M. P.; Francis, C. G.; Hüber, H. X.; Molnar, K. *Inorg. Chem.* **1990**, *29*, 1068-1073.
- (11) Silvon, M. P.; Van Dam, E. M.; Skell, P. S. *J. Am. Chem. Soc.*, **1973**, 1945-1946.
- (12) Nicholls, B.; Whiting, M. C. *J. Chem. Soc.* **1959**, 551-556.
- (13) Ercoli, R.; Calderazzo, F.; Mantica, E. *Chim. Ind. (Milan)* **1959**, *41*, 404.
- (14) Riemschnieder, R.; Becker, O.; Franz, K. *Monatsch. Chem.* **1959**, *90*, 571-572.
- (15) Herberich, G. E.; Fischer, E. O. *Chem. Ber.* **1962**, *95*, 2803-2809.
- (16) Brown, D. A. *J. Chem. Soc.* **1963**, 4329-4394.
- (17) Jackson, W. R.; Jennings, W. B. *J. Chem. Soc., Chem. Commun.* **1966**, 824-825.
- (18) Brown, D. A.; Hughes, F. J. *Inorg. Chim. Acta* **1967**, *1*, 448-450.
- (19) Jackson, W. R.; Jennings, W. B.; Rennison, S. C.; Spratt, R. *J. Chem. Soc., Sec. B* **1969**, 1214-1220.

- (20) Jackson, W. R.; Jennings, W. B. *J. Chem. Soc., Sec. B* **1969**, 1221-1228.
- (21) Jackson, W. R.; Wong, M. G.; Rae, I. D. *Aust. J. Chem.* **1986**, *39*, 303-315.
- (22) Gracey, D. E. F.; Jackson, W. R.; Jennings, W. B. *J. Chem. Soc., Chem. Commun.* **1968**, 366-367.
- (23) Jackson, W. R.; Rae, I. D.; Wong, M. G.; Semmelhack, M. F.; Garcia, J. N. *J. Chem. Soc., Chem. Commun.* **1982**, 1359-1360.
- (24) von Rosenberg, J. L.; Pinder, A. R. *J. Chem. Soc., Perkin Trans. I* **1987**, 747-752.
- (25) Bassindale, A. R.; Taylor, P. G. *Activating and Directive effects of Silicon*; Patai, S. and Rappoport, Z., Ed.; John Wiley: Chichester, 1989; Vol. 2, pp 907-959.
- (26) Colvin, E. *Silicon in Organic Synthesis*; Butterworths: London, 1981.
- (27) Seyferth, D.; Alleston, D. L. *Inorg. Chem.* **1963**, *2*, 417-418.
- (28) Elschenbroich, C.; Koch, J. *J. Organomet. Chem.* **1982**, *229*, 139-158.
- (29) Green, M. L. H.; Treurnicht, I. *J. Organomet. Chem.* **1986**, *306*, 145-165.
- (30) Alyea, E. C.; Ferguson, G.; Jain, V. K. *Acta Cryst. Sect. C.* **1994**, *50*, 491-493.
- (31) Effenberger, F.; Schollkopf, K. *Chem. Ber.* **1985**, *115*, 4356-4376.
- (32) Effenberger, F.; Schollkopf, K. *Chem. Ber.* **1985**, *115*, 4377-4384.
- (33) Wiseman, A. J.; Jones, R. G.; Went, M. J. *J. Organomet. Chem.* **1997**, *544*, 129-132.
- (34) Hagen, A. P.; Beck, H. W. *Inorg. Chem.* **1976**, *15*, 1512-1515.
- (35) Green, M. L. H.; Silverthorn, W. E. *J. Chem. Soc., Dalton Trans.* **1973**, 301-306.
- (36) Green, M. L. H. In *Chemistry of Molybdenum*; Green, M. L. H., Ed.; The Company: Golden, CO, 1982, pp 71-78.
- (37) Aleksandrov, Y. A.; Lunin, A. V.; Fomin, V. M.; Volchenkove, G. P. *Koord. Khim.* **1988**, *14*, 1405-1408.
- (38) Whaley, T. P.; Norman, V. *Carbonaceous Solid Bodies and Processes for their Manufacture*; U. S. Patent 3252824, 1966.
- (39) Wilburn, B. E.; Skell, P. S. *J. Am. Chem. Soc.*, **1981**, *104*, 6989-6994.
- (40) van Meurs, F.; Hoefnagel, A. J.; Wepster, B. M.; van Bekkum, H. *J. Organomet. Chem.* **1977**, *142*, 299.

## CHAPTER 6

### EXPERIMENTAL

#### 6.1 CHEMICALS AND SOLVENTS

All operations were carried out in Schlenk flasks under argon or nitrogen atmospheres and glove-box unless mentioned otherwise. All solvents were distilled and degassed by three freeze-pump-thaw cycles. Hydrocarbon solvents were distilled from sodium benzophenone ketal. THF was initially distilled from  $P_2O_5$ , stored over KOH and redistilled from sodium benzophenone ketal. Methylene chloride was distilled from  $CaH_2$ . MeI was dried over  $CaCl_2$  and vacuum distilled.  $BF_3$  etherate was freshly distilled before use.  $TMSCl$  was vacuum distilled before use.  $TMEDA$  was dried over KOH and distilled. Syntheses of  $(\eta^6-C_6H_6)Mo(CO)_3$ ,<sup>1</sup>  $(\eta^6-1,3,5-C_6H_3Me_3)Mo(CO)_3$ ,<sup>2</sup> and  $(\eta^6-C_6H_6)_2Mo^3$  were accomplished by slight modification of published procedures. All other reagents were used as received from commercial sources.

**Synthesis of  $(\eta^6-C_6H_6)_2Mo$ .** To a 300-mL Schlenk flask in the glove box were added  $MoCl_5$  (10 g, 0.03 mol),  $AlCl_3$  (22 g, 0.16 mol) and Al powder (1.4 g, 0.04 mol) and the mixture thoroughly shaken. The flask was connected to the Schlenk line and dry benzene (60 mL) was cannulated over, frozen, and evacuated. The black slurry was heated in an oil bath at 120 °C for 24 hours, shaking several times during the first one hour to avoid caking of the product. Later, excess benzene was vacuum transferred, the remaining black lumps washed with pentane (3x50 mL) and dried overnight under vacuum. To a 500 mL three necked flask fitted with a mechanical stirrer and argon adapter were added

degassed distilled water (350 mL) and KOH (171 g, 30 mol) and stirred. The flask is cooled with NaCl/ice bath, before the black lumps from the Schlenk flask were added to the basic solution under counter current of argon over a period of 1 hour. The bath is maintained at below -10 °C during the addition. A olive green fluffy precipitate was observed to float on the water while the mixture was stirred to reach ambient temperature. The precipitate was collected over Celite on a filter frit and dried under vacuum. The dry precipitate was extracted with hot benzene, filtered over Celite and cooling the green filtrate gave shiny green crystals of the product. Further product was recovered by removing the benzene from the filtrate and subliming the product (2.1 g, 36 %).  $^1\text{H NMR}$  ( $\text{C}_6\text{D}_6$ , 500 MHz, 20 °C)  $\delta$  4.54 (s, 6 H, arene)

**Synthesis of  $(\eta^6\text{-C}_6\text{H}_6)\text{Mo}(\text{TRIPOD})$  (1).**  $\text{Mo}(\eta^6\text{-C}_6\text{H}_6)_2$  (0.27 g, 1.1 mmol) and TRIPOD (0.62 g, 1.0 mmol) were mixed with a mortar and pestle in the glove box and loaded into a 8 mm tube connected a Schlenk adapter. The tube was evacuated, flame sealed, and heated in an oil bath at 160 °C for 36 hours to form a red colored solid. After completion of heating the tube was opened into a Schlenk flask and extracted with 30 ml of benzene and 60 mL of heptane. The red solution was filtered over Celite to rid it of a black precipitate. The volume was reduced to give 0.52 g (65%) of product as a red powder. Cooling the concentrated benzene/heptane solution at 5 °C for one week produced crystals of this compound.  $^1\text{H NMR}$  ( $\text{C}_6\text{D}_6$ , 500 MHz, 20 °C)  $\delta$  7.08 (m, 12 H, Ph) 6.96 (t, J = 7 Hz, 6 H, Ph), 6.85 (t, J = 7 Hz, 12 H, Ph), 4.41 (m, 6 H, arene), 2.17 (m, 6 H,  $\text{CH}_2$ ), 1.16 (m, 3 H,  $\text{CH}_3$ );  $^{31}\text{P}\{^1\text{H}\}\text{NMR}$  ( $\text{C}_6\text{D}_6$ , 202 MHz, 20 °C)  $\delta$  46.59 (s); Anal. Calcd. (found) for  $\text{C}_{47}\text{H}_{45}\text{P}_3\text{Mo}$  (798.74): C, 70.68 (70.44), H, 5.68 (5.74).

**Synthesis of  $[(\eta^6\text{-C}_6\text{H}_6)\text{Mo}(\text{TRIPOD})]\text{PF}_6$  ( $1\cdot\text{PF}_6$ ).**  $(\text{C}_6\text{H}_6)\text{Mo}(\text{TRIPOD})$  (0.19 g, 0.24 mmol) was weighed into a 100 mL Schlenk flask, dissolved in 10 mL of THF and stirred with  $\text{AgPF}_6$  (0.06 g, 0.24 mmol) for 10 minutes. The solution turns immediately from red to yellow forming a gray metallic silver precipitate, which was filtered. The THF solution was concentrated to ca. 2 mL and slow vapor diffusion of

pentane to yield 0.21 g (92%) of yellow-brown crystals. UV-vis spectral titration of **1** with  $\text{AgBF}_4$  and  $\text{FcBF}_4$  indicated that one equivalent of the oxidizing agent is consumed. EPR (THF, X-band, 4K)  $g_x = 2.050$ ,  $g_y = 2.038$ ,  $g_z = 1.990$ ;  $^{31}\text{P}$  hfc,  $a_{xx} = a_{yy} = 25$  G,  $a_{zz} = 29$  G;  $^1\text{H}$  hfc,  $a_{xx} = a_{yy} = a_{zz} = 5$  G;  $^{95}\text{Mo}/^{97}\text{Mo}$  hfc,  $a_{xx} = a_{yy} = a_{zz} \approx 1$  G (unresolved).

**Synthesis of  $[(\eta^6\text{-C}_6\text{H}_6)\text{MoH}(\text{TRIPOD})]\text{PF}_6$  (**3**· $\text{PF}_6$ ).** Precursor **1** (0.37 g, 0.46 mmol) was dissolved in  $\text{CH}_2\text{Cl}_2$  (10 mL) and  $\text{HPF}_6$  (60% in water, 0.5 mL) was added. After stirring 15 min, the solution was extracted with water (2x10 mL) and the organic layer was dried over  $\text{CaCl}_2$ . Evaporation yielded a red solid that was recrystallized from  $\text{CH}_2\text{Cl}_2/\text{Et}_2\text{O}$  to give **3**· $\text{PF}_6$  (0.24 g, 56%).  $^1\text{H}$  NMR ( $\text{CD}_2\text{Cl}_2$ , 20 °C, 500 MHz)  $\delta$  7.25 (t,  $J = 7$  Hz, 6 H, Ph), 7.11 (t,  $J = 7$  Hz, 12 H, Ph), 6.98 (br m, 12 H, Ph), 5.24 (s, 6 H, arene), 2.41 (br s, 6 H,  $\text{CH}_2$ ), 1.57 (br s, 3 H,  $\text{CH}_3$ ), -5.87 (q,  $J = 45$  Hz, 1 H, Mo-H);  $^{31}\text{P}\{^1\text{H}\}$  NMR ( $\text{CD}_2\text{Cl}_2\text{F}$ , 20 °C, 202 MHz)  $\delta$  37.89 (s, 3 P);  $^1\text{H}$  NMR ( $\text{CDCl}_2\text{F}$ , -125 °C, 500 MHz)  $\delta$  7.28 (m, 4 H, Ph), 7.20 (m, 4 H, Ph), 7.12 (m, 6 H, Ph), 7.01 (m, 8 H, Ph), 6.90 (m, 4 H, Ph), 6.63 (m, 4 H, Ph), 5.30 (s, 6 H,  $\text{C}_6\text{H}_6$ ), 2.31 (br s, 2H,  $\text{CH}_2$ ), 2.19, 2.65 (br m, 4 H, diastereotopic  $\text{CH}_2$ ), 1.54 (br s, 3 H,  $\text{CH}_3$ ), -6.36 (td,  $J_{\text{trans-H}} = 16$  Hz,  $J_{\text{cis-H}} = 62$  Hz, 1 H, Mo-H);  $^{31}\text{P}\{^1\text{H}\}$  NMR ( $\text{CDCl}_2\text{F}$ , -125 °C, 202 MHz)  $\delta$  43.23 (d, 2 P), 34.52 (t, 1 P,  $J_{\text{pp}} = 62$  Hz); Anal. Calcd. (found) for  $\text{C}_{47}\text{H}_{46}\text{P}_4\text{F}_6\text{Mo}$  (944.71): C 59.76 (59.48), H 4.91 (4.95).

**Synthesis of  $(\eta^6\text{-C}_6\text{H}_6)\text{Mo}(\text{TRIPHOS})$  (**4**).**  $(\eta^6\text{-C}_6\text{H}_6)_2\text{Mo}$  (0.20 g, 0.78 mmol) and TRIPHOS (0.40 g, 0.75 mmol) were loaded into a 100 mL Schlenk flask. And 10 mL of benzene was added to the mixture. The flask was frozen, evacuated and sealed before heating in an oil bath at 160 °C for 24 hours. Then methanol (30 mL) was layered over the red-brown solution and the flask was placed in the refrigerator at 5 °C for 12 hours to yield red-orange crystals of the product (0.31 g, 59%).  $^1\text{H}$  NMR ( $\text{CD}_2\text{Cl}_2$ , 500 MHz)  $\delta$  7.91 (m, 2 H, Ph), 7.54 (m, 2 H, Ph), 7.42 (m, 1 H, Ph), 7.25 (m, 4 H, Ph), 7.12 (m, 8 H, Ph), 7.00 (m, 8 H, Ph) 3.82 (m, 6 H, arene) 2.42 (m, 4 H,  $\text{CH}_2$ ) 1.73 (m, 2 H,  $\text{CH}_3$ ) 1.41 (m, 2 H,  $\text{CH}_2$ )  $^{31}\text{P}\{^1\text{H}\}$  NMR ( $\text{CD}_2\text{Cl}_2$ , 202 MHz)  $\delta$  104.92 (t, 1 P,  $J_{\text{p,p}} = 16$  Hz)

87.19 (d, 2 P,  $J_{p,p} = 16$  Hz) (s); Anal. Calcd (found) for  $C_{40}H_{39}P_3Mo$  (708.61): C 67.77 (67.23), H 5.54 (5.53).

**Synthesis of  $[(\eta^6-C_6H_6)MoH(TRIPHOS)]PF_6$  (**6**· $PF_6$ ).** Compound **4** (0.07 g, 0.10 mmol) was dissolved in  $CH_2Cl_2$  (15 mL) and  $HPF_6$  (60% in water, 0.5 mL) was added. After stirring 15 min, excess acid was washed off with water (3x10 mL), the aqueous layer was removed, and the organic layer dried over  $CaCl_2$ . Evaporation of  $CH_2Cl_2$  under argon yielded red crystals of the product (0.06 g, 70%).  $^1H$  NMR (500 MHz,  $CD_2Cl_2$ , 20 °C)  $\delta$  7.66 (t, 4 H, Ph), 7.58 (m, 1 H, Ph), 7.54 (t, 4 H, Ph), 7.39 (m, 8 H, Ph) 7.24 (m, 8 H, Ph) 4.63 (s, 6 H, arene) 2.87 (br m,  $CH_3$ , 2 H), 2.66 (br m,  $CH_3$ , 2 H), 2.0-2.2 (br m,  $CH_2$ , 4 H), -6.06 (dt,  $J_{trans-H} = 3.5$  Hz,  $J_{cis-H} = 50$  Hz, 1 H, Mo-H);  $^{31}P\{^1H\}$ NMR (202 MHz,  $CD_2Cl_2$ , 20 °C)  $\delta$  110.08 (t, 1 P,  $J_{p,p} = 32$  Hz) 89.86 (d, 2 P,  $J_{p,p} = 32$  Hz) -144.02 (septet, 1 P,  $J_{p,F} = 709$  Hz); Anal. Calcd (found) for  $C_{40}H_{40}P_4F_6Mo$  (854.58): C 56.21 (56.17), H 4.71 (4.82).

**General procedure for 7, 8 and 9.**  $(\eta^6-C_6H_6)_2Mo$  (0.15 g, 0.60 mmol) and phosphine (3 mmol) were loaded into a Schlenk flask along with 5 mL of benzene. The frozen flask was evacuated, sealed, and heated in an oil bath for 24 hours. The red solution was layered with 15 mL of methanol and allowed to sit overnight at 5 °C to yield red crystals of the product. Yields for **7**, **8** and **9** were 85%, 58% and 49%, respectively.  $(\eta^6-C_6H_6)Mo(PMePh_2)_3$  (**7**).  $^1H$  NMR ( $C_6D_6$ , 500 MHz, 20 °C)  $\delta$  6.97-7.17 (m, 30 H, Ph), 3.88 (q, 6 H, arene), 1.65 (s, 9 H,  $CH_3$ );  $^{31}P\{^1H\}$ NMR ( $C_6D_6$ , 202 MHz, 20 °C)  $\delta$  35.58 (s).

$(\eta^6-C_6H_6)Mo(PMe_2Ph)_3$  (**8**)  $^1H$  NMR ( $C_6D_6$ , 500 MHz, 20 °C)  $\delta$  7.42 (m, 6 H, Ph), 7.03-7.10 (m, 9 H, Ph), 3.86 (q, 6 H, arene), 1.29 (s, 18 H,  $CH_3$ );  $^{31}P\{^1H\}$ NMR ( $C_6D_6$ , 202 MHz, 20 °C)  $\delta$  18.06 (s).

$(\eta^6-C_6H_6)Mo(PMe_3)_3$  (**9**).  $^1H$  NMR ( $C_6D_6$ , 500 MHz, 20 °C)  $\delta$  3.66 (q, 6 H, arene), 1.13 (s, 27 H,  $CH_3$ );  $^{31}P\{^1H\}$ NMR ( $C_6D_6$ , 202 MHz, 20 °C)  $\delta$  3.4 (s).

$(\eta^6-C_6D_6)Mo(TRIPOD)$  (**1-d<sub>6</sub>**),  $(\eta^6-C_6D_6)Mo(TRIPHOS)$  (**4-d<sub>6</sub>**),

$(\eta^6\text{-C}_6\text{D}_6)\text{Mo}(\text{PMePh}_2)_3$  (**7-d<sub>6</sub>**),  $(\eta^6\text{-C}_6\text{D}_6)\text{Mo}(\text{PMe}_2\text{Ph})_3$  (**8-d<sub>6</sub>**) and  $(\eta^6\text{-C}_6\text{D}_6)\text{Mo}(\text{PMe}_3)_3$  (**9-d<sub>6</sub>**) were synthesized by analogous procedures using  $(\eta^6\text{-C}_6\text{D}_6)_2\text{Mo}$  as the starting material and  $\text{C}_6\text{D}_6$  as the reaction solvent. Characterization of the deuterio derivatives were carried out using  $^1\text{H}$ ,  $^2\text{H}$  and  $^{31}\text{P}$  NMR spectroscopy. All resonances are at the appropriate chemical shifts compared with the analogous proton derivatives.

**Synthesis of  $(\eta^6\text{-C}_6\text{H}_5\text{Me})_2\text{Mo}$  (**26**)** (Metal-atom vapor method) The apparatus that was used in this procedure is reported in the literature.<sup>4</sup> In a typical run, 3 g of Mo wire was heated and the vapor cocondensed with 50 mL of toluene over a period of 2 hours. Nearly 300-500 mg of the wire vaporizes during the reaction period to give 0.05 g of the isolated product.  $^1\text{H}$  NMR ( $\text{C}_6\text{D}_6$ , 500 MHz)  $\delta$  4.41 (m, 5 H,  $\text{C}_6\text{H}_5$ ), 1.85 (s, 3 H,  $\text{CH}_3$ );  $^{13}\text{C}\{^1\text{H}\}$  NMR ( $\text{C}_6\text{D}_6$ , 125 MHz)  $\delta$  89.65 (s, *ipso*), 78.68 (s, *ortho*), 76.02 (s, *para*), 75.08 (s, *meta*), 21.63 (s,  $\text{CH}_3$ )

**Synthesis of  $(\eta^6\text{-C}_6\text{H}_5\text{R})_2\text{Mo}$  (R = Et, i-Pr, or t-Bu)** In a typical reaction  $(\text{C}_6\text{H}_6)_2\text{Mo}$  (0.10 g, 0.40 mmol) was taken in a 100 mL Schlenk flask and 2 mL of the appropriate arene was added. The solution was frozen, evacuated and stopcock closed under vacuum. The flask was heated in an oil bath at 160 °C for 2 days. Excess solvent was removed by vacuum transfer and product recovered. Typical yields are around 60-70%.

$(\eta^6\text{-C}_6\text{H}_5\text{Et})_2\text{Mo}$  (**27**)  $^1\text{H}$  NMR ( $\text{C}_6\text{D}_6$ , 500 MHz)  $\delta$  4.57 (m, 5 H,  $\text{C}_6\text{H}_5$ ), 2.05 (q,  $J_{\text{H-H}} = 7.5$  Hz, 2 H,  $\text{CH}_2$ ), 1.02 (t,  $J_{\text{H-H}} = 6.5$  Hz, 3 H,  $\text{CH}_3$ );  $^{13}\text{C}\{^1\text{H}\}$  NMR ( $\text{C}_6\text{D}_6$ , 125 MHz)  $\delta$  97.54 (s, *ipso*), 77.73 (s, *ortho*), 76.04 (s, *para*), 75.24 (s, *meta*), 29.56 (s,  $\text{CH}_2$ ), 16.89 (s,  $\text{CH}_3$ )

$(\eta^6\text{-C}_6\text{H}_5\text{i-Pr})_2\text{Mo}$  (**28**)  $^1\text{H}$  NMR ( $\text{C}_6\text{D}_6$ , 500 MHz)  $\delta$  4.52 (m, br, 5 H,  $\text{C}_6\text{H}_5$ ), 2.20 (septet,  $J_{\text{H-H}} = 6.5$  Hz, 1 H, CH), 1.08 (d,  $J_{\text{H-H}} = 7.5$  Hz, 6 H,  $\text{CH}_3$ );  $^{13}\text{C}\{^1\text{H}\}$  NMR ( $\text{C}_6\text{D}_6$ , 125 MHz)  $\delta$  103.51 (s, *ipso*), 76.34 (s, *ortho*), 75.91 (s, *para*), 75.20 (s, *meta*), 34.17 (m, CH), 24.98 (s,  $\text{CH}_3$ )

$(\eta^6\text{-C}_6\text{H}_5\text{t-Bu})_2\text{Mo}$  (**29**)  $^1\text{H}$  NMR ( $\text{C}_6\text{D}_6$ , 500 MHz)  $\delta$  4.52 (m, br, 5 H,  $\text{C}_6\text{H}_5$ ), 1.12

(t, 9 H, CH<sub>3</sub>); <sup>13</sup>C{<sup>1</sup>H}NMR (C<sub>6</sub>D<sub>6</sub>, 125 MHz) δ 106.87 (s, *ipso*), 77.45 (s, *ortho*), 75.35 (s, *para*), 75.17 (s, *meta*), 32.03 (s, CH<sub>3</sub>)

**Synthesis of (η<sup>6</sup>-C<sub>6</sub>H<sub>5</sub>SiMe<sub>3</sub>)<sub>2</sub>Mo (30)** (η<sup>6</sup>-C<sub>6</sub>H<sub>6</sub>)<sub>2</sub>Mo (0.22 g, 0.90 mmol) was dissolved in 30 mL of cyclohexane and stirred in a Schlenk flask. To another 200 mL Schlenk flask cyclohexane (100 mL), 1.6 M n-BuLi (2.8 mL, 4.5 mmol) in hexanes and TMEDA (0.68 mL, 4.5 mmol) were mixed and stirred. The green (η<sup>6</sup>-C<sub>6</sub>H<sub>6</sub>)<sub>2</sub>Mo solution was cannula transferred to the lithiating mixture and stirred for 3 hours at 50 °C. The green mixture turns dark with brown precipitate was cooled to 0 °C before TMSCl (1.15 mL, 9.00 mmol) was added. After stirring the mixture overnight to become yellow-green in color, degassed water was added to quench any excess lithium reagent. The cyclohexane layer was separated, washed with 2x25 mL of water and solvent was removed. The green residue was redissolved in hexanes, filtered over Celite, concentrated and cooled to obtain (0.172 g, 67%) green crystals of the product. <sup>1</sup>H NMR (C<sub>6</sub>D<sub>6</sub>, 500 MHz) δ 4.63 (t, J<sub>H-H</sub> = 6 Hz, 1 H, *para* C<sub>6</sub>H<sub>3</sub>), 4.50 (t, J<sub>H-H</sub> = 7 Hz, 2 H, *ortho* C<sub>6</sub>H<sub>3</sub>), 4.42 (d, J<sub>H-H</sub> = 6.5 Hz, 2 H, *meta* C<sub>6</sub>H<sub>3</sub>), 0.10 (s, 9 H, CH<sub>3</sub>); <sup>13</sup>C{<sup>1</sup>H}NMR (C<sub>6</sub>D<sub>6</sub>, 125 MHz) δ 79.91 (s, *ortho*) 79.66 (s, *ipso*), 77.95 (s, *meta*), 75.58 (s, *para*), -0.20 (s, CH<sub>3</sub>)

**Synthesis of (η<sup>6</sup>-C<sub>6</sub>H<sub>5</sub>R)Mo(TRIPOD) (R = Me or SiMe<sub>3</sub>)** (η<sup>6</sup>-C<sub>6</sub>H<sub>3</sub>R)<sub>2</sub>Mo (1.35 mmol) and TRIPOD (0.760 g, 1.22 mmol) were heated in a sealed glass tube under vacuum at 160 °C for 2 days. The tube was opened under nitrogen, the contents were extracted with 1:1 benzene/heptane (~30 mL), and the extract was filtered. The red-orange product recrystallized from the solvent upon cooling to 5 °C. Typical yields are 40-60%.

**(η<sup>6</sup>-C<sub>6</sub>H<sub>5</sub>Me)Mo(TRIPOD) (31)** <sup>1</sup>H NMR (C<sub>6</sub>D<sub>6</sub>, 400 MHz) δ 7.05 (m, 12 H, Ph), 6.93 (t, J<sub>H-H</sub> = 7 Hz, 6 H, Ph), 6.83 (t, J<sub>H-H</sub> = 7.5 Hz, 12 H, Ph), 4.41 (br, 2 H, *ortho* C<sub>6</sub>H<sub>3</sub>), 4.36 (br, 2 H, *meta* C<sub>6</sub>H<sub>3</sub>), 4.26 (br, 1 H, *para* C<sub>6</sub>H<sub>3</sub>), 2.16 (s, 6 H, CH<sub>2</sub>), 1.86 (s, 3 H, CH<sub>3</sub>), 1.10 (s, 3 H, TRIPOD CH<sub>3</sub>); <sup>31</sup>P{<sup>1</sup>H}NMR (C<sub>6</sub>D<sub>6</sub>, 161 MHz) δ 48.58 (s); Anal. Calcd (found) for C<sub>48</sub>H<sub>47</sub>P<sub>3</sub>Mo (812.77): C, 70.93 (70.95), H, 5.83 (5.90).

( $\eta^6\text{-C}_6\text{H}_5\text{SiMe}_3$ )Mo(TRIPOD) (35)  $^1\text{H}$  NMR ( $\text{C}_6\text{D}_6$ , 400 MHz)  $\delta$  7.16 (m, 11 H, Ph), 7.03 (m, 1 H, Ph), 6.92 (t,  $J_{\text{H-H}} = 7$  Hz, 6 H, Ph), 6.85 (m,  $J_{\text{H-H}} = 7$  Hz, 12 H, Ph), 4.90 (d,  $J_{\text{H-H}} = 6$  Hz, 2 H, *ortho*  $\text{C}_6\text{H}_5$ ), 4.70 (m, 1 H, *para*  $\text{C}_6\text{H}_5$ ), 4.17 (t,  $J_{\text{H-H}} = 5$  Hz, 2 H, *meta*  $\text{C}_6\text{H}_5$ ), 2.20 (s, 6 H, TRIPOD  $\text{CH}_2$ ), 1.07 (s, 3 H, TRIPOD  $\text{CH}_3$ ), 0.11 (s, 9 H,  $\text{CH}_3$ );  $^{31}\text{P}\{^1\text{H}\}$ NMR ( $\text{C}_6\text{D}_6$ , 161 MHz)  $\delta$  46.20 (s); Anal. Calcd (found) for  $\text{C}_{50}\text{H}_{53}\text{P}_3\text{SiMo}$  (870.93): C, 68.95 (68.99), H, 6.13 (6.15).

**Attempted synthesis of ( $\eta^6\text{-C}_6\text{H}_5\text{R}$ )Mo(TRIPOD) (R = Et (32), *i*-Pr (33), or *t*-Bu (34))** An equimolar amounts of  $\text{Mo}(\eta^6\text{-C}_6\text{H}_5\text{R})_2$  and TRIPOD were loaded into a 100 mL Schlenk flask in the glove-box, and 2 mL of the appropriate arene was cannula transferred for the reaction solvent. The flask was cooled with liquid  $\text{N}_2$ , evacuated and stopcock sealed before heating at 160 °C for 2 days. The green solution turns red and solvent removed by vacuum transfer. The red residue was recrystallized from a mixture of benzene and heptane. Free TRIPOD ligand was found in the mixture after several recrystallization attempts.

## 6.2 INSTRUMENTS AND METHODS

Elemental analyses were performed by Atlantic Microlab, Norcross, GA.  $^1\text{H}$  and  $^{31}\text{P}$  NMR spectra were recorded on a Varian XL-500 spectrometer or Unity 400 spectrometer. Residual solvent peaks were used as internal standard in  $^1\text{H}$  NMR spectra and 85%  $\text{H}_3\text{PO}_4$  was used as an external reference at 0 ppm for  $^{31}\text{P}$  NMR spectra.

**Low-temperature NMR experiments.** (Section 3.5) Samples for the low-temperature reactions of the arene complexes with acids were prepared by the following method: The complex was dissolved in the solvent in a NMR tube with Schlenk adapter on the vacuum manifold. The solution is frozen with liquid  $\text{N}_2$  and the acid solution was syringed (using a gas-tight syringe) onto the frozen matrix under a positive  $\text{N}_2$  gas flow. Then the adapter was closed, vacuum was applied when the mixture remained frozen, and the tube was flame-sealed. The tube was transferred quickly to a *n*-pentane/liquid  $\text{N}_2$  bath

at -100 °C before inserting it into the pre-cooled spectrometer probe at -90 °C.

**Exchange of D<sub>2</sub> gas with [(η<sup>6</sup>-C<sub>6</sub>D<sub>6</sub>)Mo(H)<sub>2</sub>(TRIPHOS)]<sup>2+</sup> (5a).** To a CD<sub>2</sub>Cl<sub>2</sub> solution of **4** in an NMR tube attached to a Schlenk adapter on the manifold was added 3 equivalents of CF<sub>3</sub>SO<sub>3</sub>H (CD<sub>2</sub>Cl<sub>2</sub> solution) using a gas-tight syringe to form **5a**. The solution was frozen, tube evacuated, refilled with D<sub>2</sub> gas and solution thawed. This operation was repeated two more times. The solution was frozen and flame sealed under a low pressure of D<sub>2</sub> gas. The reaction was followed by <sup>1</sup>H and <sup>2</sup>H NMR spectroscopy.

**Electrophile reactions in NMR tube.** (Section 4.5) All NMR tube reactions were performed similarly. The tubes that had been glass-blown onto Schlenk adapters were connected to vacuum manifold, **1** was weighed out in the air and added to the tube and MeI was vacuum transferred onto the solid sample. All other reagents and electrophiles were added inside the glove box (using syringes in the case of liquids). The tubes with samples were frozen and flame sealed under vacuum. In the case of 50 °C reactions, the sealed tubes were heated in an oil bath.

**Monitoring the reaction of 1 and MeI with time.** (Section 4.4) Two different concentrations (0.16 M and 0.04 M) of **1** in MeI were made and divided into five NMR tubes each. All the ten tubes were frozen, stopcock sealed, evacuated and heated in an oil bath. One tube from each concentration was taken out of the oil bath at 0, 3, 6, 9, and 12 hours. The MeI was pumped off, and CD<sub>2</sub>Cl<sub>2</sub> introduced to obtain <sup>1</sup>H and <sup>31</sup>P NMR spectra.

**Photoelectron Spectra.** The photoelectron spectra were recorded using a McPherson ESCA36 instrument with a quartz excitation lamp that produces He I and He II radiation. (η<sup>6</sup>-C<sub>6</sub>H<sub>6</sub>)Mo(TRIPOD) sublimed cleanly at 270-285 °C at 10<sup>-4</sup> torr without any evidence of decomposition products as a solid residue or in the gas-phase. Both He I and He II data were recorded for (η<sup>6</sup>-C<sub>6</sub>H<sub>6</sub>)Mo(TRIPOD). The spectra of the free ligand TRIPOD were collected at 210-230 °C. Benzene and CO were seen as gas-phase contaminants in the spectrum of (η<sup>6</sup>-C<sub>6</sub>H<sub>6</sub>)Mo(CO)<sub>3</sub>. (η<sup>6</sup>-C<sub>6</sub>H<sub>6</sub>)Mo(CO)<sub>3</sub> sublimed at

60-70 °C leaving some black solid residue after completion. Ionizations arising from benzene and CO were spectrally subtracted to obtain the He I spectrum of  $(\eta^6\text{-C}_6\text{H}_6)\text{Mo}(\text{CO})_3$ . No effort was made to collect the He II spectrum of  $(\eta^6\text{-C}_6\text{H}_6)\text{Mo}(\text{CO})_3$ , due to the decomposition during sublimation.  $(\eta^6\text{-1,3,5-C}_6\text{H}_3\text{Me}_3)\text{Mo}(\text{CO})_3$  sublimed at 95-105 °C without any thermal decomposition, and He I and II spectra were recorded.

**Cyclic Voltammetry.** The cyclic voltammogram was measured using BAS CV-50W Electrochemical Analyzer with Ag/AgNO<sub>3</sub> reference electrode using a cell that has been described in the literature.<sup>5</sup> The measurement was made with 10<sup>-3</sup> M  $(\text{C}_6\text{H}_6)\text{Mo}(\text{TRIPOD})$  and 0.1 M Bu<sub>4</sub>NPF<sub>6</sub> as a supporting electrolyte in dry oxygen free CH<sub>2</sub>Cl<sub>2</sub> solvent at a scan rate was 25 mV/s. The formal potentials, E<sub>1/2</sub> values, were determined as the average of cathodic and anodic peak potentials, i.e. [(E<sub>p,c</sub> + E<sub>p,a</sub>)/2]. The ferrocene redox couple at 0.46 V versus SCE was used as an internal reference.<sup>6</sup>

**Electron Paramagnetic Resonance.** X-band EPR spectra were measured on a Bruker EMX spectrometer equipped with an ER 041 XG bridge, an ER 4102ST cavity, and an Oxford liquid helium cryostat. A Bruker ESP 300E spectrometer with an ER 051Q bridge, and ER 5106QT cavity was used to record Q-band EPR spectra. The EPR field calibration was checked by measuring the resonance of diphenylpicitylhydrazyl radical (dpph). THF solutions of  $[(\eta^6\text{-C}_6\text{H}_6)\text{Mo}(\text{TRIPOD})]^+$  were flash-frozen with liquid N<sub>2</sub> (to promote random orientation of the paramagnets) and evacuated before flame-sealing. The Zeeman modulation amplitude was set to approximately  $\sqrt{3}$  times the peak-to-peak line width. The influence of spectrometer amplifier gain was investigated and no additional features were observed at higher gain.

The X-band EPR spectrum was simulated using the program SimFonia. SimFonia uses the following spin Hamiltonian for simulating “powder” EPR spectra:

$$H = \mu_B \mathbf{B}_0 \cdot \mathbf{g}_e \cdot \mathbf{S} + \mathbf{S} \cdot \mathbf{D} \cdot \mathbf{S} + \mathbf{S} \cdot \mathbf{A} \cdot \mathbf{I} + \mathbf{I} \cdot \mathbf{P} \cdot \mathbf{I} + \mu_N \mathbf{B}_0 \cdot \mathbf{g}_n \cdot \mathbf{I}$$

where  $\mu_B$  is the Bohr magneton,  $B_0$  is the applied magnetic field,  $g$  is the unites g-factor,  $S$  is the effective spin angular momentum operator,  $D$  is the matrix of zero field splitting tensor,  $A$  is the nuclear hyperfine interaction tensor,  $I$  is the nuclear spin vector,  $P$  is the nuclear quadruple tensor, and  $\mu_N$  is the nuclear magneton.<sup>7</sup> Since only two of the six molybdenum isotopes have nuclear spins [<sup>95</sup>Mo (15.7%, I=5/2), <sup>97</sup>Mo (9.5%, I=5/2)], no significant metal hyperfine coupling is observed. Other four isotopes <sup>94</sup>Mo + <sup>96</sup>Mo + <sup>98</sup>Mo + <sup>100</sup>Mo are spin inactive (74.8%, I=0). Accordingly, ignoring the nuclear electric quadruple and nuclear Zeeman interactions the above equation reduces to

$$H = \mu_B B_0 g_e S + S A I$$

The simulated spectrum of Figure 2.6 was obtained using the values  $g_x = 2.050$ ,  $g_y = 2.038$ ,  $g_z = 1.990$ ; <sup>31</sup>P hfc,  $a_x = a_y = 25$  G,  $a_z = 29$  G; <sup>1</sup>H hfc,  $a_x = a_y = a_z = 5$  G; <sup>95</sup>Mo/<sup>97</sup>Mo hfc,  $a_x = a_y = a_z = 1$  G (unresolved). The line-widths were assumed to be isotropic and a 50:50 mixture of Lorentzian and Gaussian line-shapes with 1 G line-widths were employed.

**Theoretical Calculations.** Electronic structure calculations and geometry optimizations were carried out using a variety of theoretical models on several computers such as IBM RS/6000 590 and Silicon Graphics IRIS Indigo II Solid Impact. Geometry optimizations were performed using the BATCHMIN<sup>8</sup> program. The orbital and electron density figures were created using the SPARTAN 5.0 package. The semi-empirical, ab initio, and density functional electronic structure calculations were carried out using the SPARTAN 5.0 (PM3(tm) and pBP/DF\*)<sup>9,10</sup> GAUSSIAN 94 packages.<sup>11</sup>

Geometrical conformations of the free TRIPOD ligand were carried out by both Monte Carlo<sup>12</sup> and molecular dynamics methods (MM2 force field)<sup>13</sup>, and the results were analyzed with the aid of the MacroModel program. The geometries of ( $\eta^6$ -C<sub>6</sub>H<sub>6</sub>)Mo(CO)<sub>3</sub>, and ( $\eta^6$ -C<sub>6</sub>H<sub>6</sub>)Mo(PH<sub>3</sub>)<sub>3</sub>, and their monocations were optimized using the Merck molecular

force field (MMFF), then refined at the pBP/DF\* level using density-functional methods. The perturbative Becke-Perdew method (pBP) is analogous to the BP method, but the gradient correction is introduced only after convergence based on the local potential alone has been achieved. DN\* is a Gaussian basis set similar to 6-31G\* except five pure d-type functions are used instead of six second-order Gaussians.

More extensive ab initio and density functional electronic structure calculations for the free TRIPOD molecule and for  $(\eta^5\text{-C}_6\text{H}_6)\text{Mo}(\text{CO})_3$ ,  $(\eta^5\text{C}_6\text{H}_6)\text{Mo}(\text{PH}_3)_3$ , and their monocations were carried out. All of these calculations used the LanL2DZ basis set, which is the Dunning/Huzinaga full double zeta basis for first row atoms,<sup>14</sup> and the Los Alamos ECP plus DZ on other atoms.<sup>15-17</sup> Partial geometry optimizations were carried out using the B3PW91 model. Moller-Plesset correlation energy corrections, truncated at the second order for MP2, were carried out for some geometries as reported.

### 6.3 X-RAY DATA

**General procedure for X-ray analysis.** Data were collected at low temperature on a Siemens P4 diffractometer using Mo K $\alpha$  ( $\lambda = 0.71073 \text{ \AA}$ ) radiation. The data were corrected for Lorentz and Polarization effects; and empirical absorption correction based on PSI scans was applied. Structure was solved by the direct method using SHELXTL (Siemens) system and refined by full-matrix least squares on  $F^2$  using all reflections.

Table 6.1.1. Crystal data and structure refinement for  $[(\eta^6\text{-C}_6\text{H}_6)\text{Mo}(\text{TRIPOD})]\text{PF}_6$  ( $\mathbf{1}\cdot\text{PF}_6$ ).

|                                   |   |
|-----------------------------------|---|
| Empirical formula                 | $\text{C}_{47}\text{H}_{45}\text{F}_6\text{MoP}_4$  |
| Formula weight                    | 43.65   |
| Temperature                       | 188(2) K  |
| Wavelength                        | 0.71073 Å   |
| Crystal system                    | Monoclinic  |
| Space group                       | C2  |
| Unit cell dimensions              | $a = 18.323(4)$ Å $\alpha = 90$ deg.<br>$b = 24.491(5)$ Å $\beta = 91.28(3)$ deg.<br>$c = 10.434(2)$ Å $\gamma = 90$ deg. |
| Volume, Z                         | 4681(2) Å <sup>3</sup> , 4  |
| Density (calculated)              | 1.339 mg/m <sup>3</sup>   |
| Absorption coefficient            | 0.471 mm <sup>-1</sup>  |
| F(000)                            | 1932  |
| Crystal size                      | 0.12 x 0.36 x 0.36 mm   |
| Theta range for data collection   | 2.22 to 25.00 deg.  |
| Limiting indices                  | $0 \leq h \leq 21$ , $0 \leq k \leq 29$ , $-12 \leq l \leq 12$  |
| Reflections collected             | 4397  |
| Independent reflections           | 4219 [R(int) = 0.0520]  |
| Refinement method                 | Full-matrix least-squares on F <sup>2</sup>   |
| Data / restraints / parameters    | 4218 / 679 / 279  |
| Goodness-of-fit on F <sup>2</sup> | 1.038   |
| Final R indices [I > 2σ(I)]       | R1 = 0.1570, wR2 = 0.3761   |
| R indices (all data)              | R1 = 0.1998, wR2 = 0.4526   |
| Absolute structure parameter      | -0.5(2)   |
| Largest diff. peak and hole       | 4.488 and -1.149 e.Å <sup>-3</sup>  |

Table 6.1.2. Atomic coordinates ( $\times 10^4$ ) and equivalent isotropic displacement parameters ( $\text{\AA}^2 \times 10^3$ ) for  $1 \cdot \text{PF}_6$ .  $U(\text{eq})$  is defined as one third of the trace of the orthogonalized  $U_{ij}$  tensor.

|        | x        | y        | z          | $U(\text{eq})$ |
|--------|----------|----------|------------|----------------|
| Mo(1)  | 6773(1)  | 344(1)   | -8452(1)   | 43(1)          |
| P(1)   | 746(4)   | 343(2)   | -8388(8)   | 73(2)          |
| P(2)   | 7735(4)  | 1025(2)  | -8367(10)  | 77(2)          |
| P(3)   | 6945(3)  | 547(2)   | -6127(4)   | 36(1)          |
| C(7)   | 8372(12) | -170(9)  | -6895(22)  | 47(5)          |
| C(7')  | 8659(13) | 793(10)  | -7685(23)  | 54(5)          |
| C(7'') | 7913(11) | 628(8)   | -5635(19)  | 41(4)          |
| C(8)   | 7499(9)  | 361(10)  | -6544(16)  | 41(3)          |
| C(9)   | 9247(10) | 418(9)   | -5695(18)  | 44(4)          |
| C(1)   | 6347(10) | 489(5)   | -10464(15) | 60(6)          |
| C(2)   | 6004(10) | 859(6)   | -9634(16)  | 79(8)          |
| C(3)   | 5611(9)  | 655(5)   | -8562(14)  | 39(4)          |
| C(4)   | 5564(12) | 75(7)    | -8425(19)  | 79(8)          |
| C(5)   | 5942(11) | -270(6)  | -9250(18)  | 62(6)          |
| C(6)   | 6308(12) | -55(6)   | -10271(18) | 65(6)          |
| C(11)  | 7348(8)  | -999(6)  | -7505(20)  | 59(6)          |
| C(12)  | 6621(8)  | -1085(6) | -7217(18)  | 61(6)          |
| C(13)  | 6411(8)  | -1594(7) | -6736(24)  | 82(8)          |
| C(14)  | 6939(9)  | -2015(7) | -6576(34)  | 105(12)        |
| C(15)  | 7665(9)  | -1921(6) | -6963(30)  | 86(9)          |
| C(16)  | 7874(8)  | -1378(6) | -7221(24)  | 61(6)          |

Table 6.1.2 continued

|        |          |          |            |         |
|--------|----------|----------|------------|---------|
| C(11A) | 8180(7)  | -526(7)  | -9615(14)  | 45(4)   |
| C(12A) | 7763(8)  | -767(9)  | -10587(16) | 96(10)  |
| C(14A) | 8874(9)  | -865(10) | -11809(17) | 80(8)   |
| C(15A) | 9275(9)  | -626(13) | -10801(20) | 112(13) |
| C(16A) | 8911(8)  | -459(9)  | -9705(16)  | 57(5)   |
| C(21A) | 8263(10) | 1133(6)  | -10185(15) | 61(6)   |
| C(22A) | 8199(9)  | 706(6)   | -11066(15) | 67(7)   |
| C(23A) | 8585(11) | 728(7)   | 12206(16)  | 75(7)   |
| C(24A) | 9023(13) | 1194(8)  | -12465(17) | 88(9)   |
| C(25A) | 9107(12) | 1594(8)  | -11529(19) | 87(9)   |
| C(26A) | 8693(13) | 1571(7)  | -10415(18) | 76(8)   |
| C(31A) | 6535(10) | 1135(6)  | -5328(13)  | 49(5)   |
| C(32A) | 6447(11) | 1111(6)  | -3999(14)  | 76(8)   |
| C(33A) | 6137(12) | 1557(7)  | -3390(14)  | 65(7)   |
| C(34A) | 5914(14) | 2025(7)  | -4106(15)  | 77(8)   |
| C(35A) | 6021(12) | 2040(6)  | -5431(14)  | 56(5)   |
| C(36A) | 6350(11) | 1589(6)  | -6003(14)  | 50(5)   |
| C(31)  | 6622(7)  | -34(6)   | -5178(15)  | 40(4)   |
| C(32)  | 7073(8)  | -356(7)  | -4389(17)  | 60(6)   |
| C(33)  | 6781(9)  | -787(9)  | -3683(23)  | 116(14) |
| C(34)  | 6008(9)  | -872(8)  | -3694(22)  | 80(8)   |
| C(35)  | 5584(9)  | -572(9)  | -4600(27)  | 104(11) |
| C(36)  | 5888(8)  | -121(7)  | -5199(19)  | 55(5)   |
| C(21)  | 7717(11) | 1780(6)  | -8101(18)  | 73(7)   |
| C(22)  | 7217(11) | 2078(7)  | -8834(18)  | 84(9)   |
| C(23)  | 7067(14) | 2624(8)  | -8488(23)  | 156(20) |

Table 6.1.2 continued

|       |           |          |            |         |
|-------|-----------|----------|------------|---------|
| C(24) | 7440(16)  | 2852(8)  | -7415(28)  | 174(24) |
| C(25) | 7915(15)  | 2528(8)  | -6666(22)  | 99(11)  |
| C(26) | 8081(13)  | 2003(8)  | -7090(23)  | 89(10)  |
| P(4)  | 10160(4)  | 2167(3)  | -14755(8)  | 36(2)   |
| F(1)  | 10000     | 1562(6)  | -15000     | 139(10) |
| F(2)  | 10435(9)  | 2724(6)  | -14226(16) | 66(7)   |
| F(3)  | 10974(8)  | 2029(7)  | -15116(20) | 69(8)   |
| F(4)  | 9377(8)   | 2290(8)  | -14347(22) | 73(8)   |
| F(5)  | 10340(11) | 1930(6)  | -13344(12) | 49(5)   |
| F(6)  | 10034(14) | 2383(7)  | -16065(13) | 79(8)   |
| P(5)  | 10136(5)  | -1477(3) | -14816(8)  | 37(2)   |
| F(7)  | 10459(10) | -2024(6) | -14351(18) | 86(11)  |
| F(8)  | 9812(8)   | -936(6)  | -15317(14) | 40(5)   |
| F(9)  | 9361(7)   | -1657(7) | -14365(20) | 50(6)   |
| F(10) | 10910(7)  | -1295(7) | -15266(19) | 44(5)   |
| F(11) | 10004(13) | -1741(8) | -16181(16) | 79(10)  |
| F(12) | 10279(14) | -1219(8) | -13476(16) | 73(9)   |

---

Table 6.1.3. Anisotropic displacement parameters ( $\text{\AA}^2 \times 10^3$ ) for  $\mathbf{1} \cdot \mathbf{PF}_6$ . The anisotropic displacement factor exponent takes the form:  $-2 \pi^2 [ h^2 a^2 U_{11} + \dots + 2 h k a b U_{12} ]$

|       | $U_{11}$ | $U_{22}$ | $U_{33}$ | $U_{23}$ | $U_{13}$ | $U_{12}$ |
|-------|----------|----------|----------|----------|----------|----------|
| Mo(1) | 19(1)    | 82(1)    | 25(1)    | -1(1)    | -11(1)   | 2(1)     |
| P(1)  | 66(3)    | 26(3)    | 124(5)   | -1(3)    | -73(4)   | -4(2)    |
| P(2)  | 67(4)    | 18(2)    | 142(7)   | -7(3)    | -60(4)   | 3(3)     |
| P(3)  | 35(2)    | 39(2)    | 34(2)    | 1(2)     | -8(2)    | -4(2)    |

Table 6.2.1. Crystal data and structure refinement for ( $\eta^6$ -C<sub>6</sub>H<sub>6</sub>)Mo(TRIPHOS) (4).

|                                   |  |                      |
|-----------------------------------|--|----------------------|
| Empirical formula                 | C <sub>40</sub> H <sub>39</sub> MoP <sub>3</sub> |                      |
| Formula weight                    | 708.56   |                      |
| Temperature                       | 188(2) K   |                      |
| Wavelength                        | 0.71073 Å  |                      |
| Crystal system                    | Monoclinic                                       |                      |
| Space group                       | P2 <sub>1</sub> /n                               |                      |
| Unit cell dimensions              | a = 9.1830(10) Å                                 | α = 90 deg.          |
|                                   | b = 17.385(2) Å                                  | β = 101.830(10) deg. |
|                                   | c = 21.413(3) Å                                  | γ = 90 deg.          |
| Volume, Z                         | 3345.9(7) Å <sup>3</sup> , 4                     |                      |
| Density (calculated)              | 1.407 mg/m <sup>3</sup>                          |                      |
| Absorption coefficient            | 0.564 mm <sup>-1</sup>                           |                      |
| F(000)                            | 1464   |                      |
| Crystal size                      | 0.36 x 0.48 x 0.42 mm                            |                      |
| Theta range for data collection   | 1.94 to 26.00 deg.                               |                      |
| Limiting indices                  | 0 ≤ h ≤ 11, 0 ≤ k ≤ 21, -26 ≤ l ≤ 25             |                      |
| Reflections collected             | 7033   |                      |
| Independent reflections           | 6580 [R(int) = 0.0323]                           |                      |
| Absorption correction             | Semi-empirical from psi-scans                    |                      |
| Max. and min. transmission        | 0.9691 and 0.5949                                |                      |
| Refinement method                 | Full-matrix least-squares on F <sup>2</sup>      |                      |
| Data / restraints / parameters    | 6578 / 0 / 505                                   |                      |
| Goodness-of-fit on F <sup>2</sup> | 1.045  |                      |
| Final R indices [I > 2σ(I)]       | R1 = 0.0451, wR2 = 0.1095                        |                      |
| R indices (all data)              | R1 = 0.0614, wR2 = 0.1206                        |                      |
| Largest diff. peak and hole       | 1.480 and -0.723 e.Å <sup>-3</sup>               |                      |

Table 6.2.2 Atomic coordinates ( $\times 10^4$ ) and equivalent isotropic displacement parameters ( $\text{\AA}^2 \times 10^3$ ) for 4.  $U(\text{eq})$  is defined as one third of the trace of the orthogonalized  $U_{ij}$  tensor.

|       | x        | y       | z       | $U(\text{eq})$ |
|-------|----------|---------|---------|----------------|
| Mo(1) | 7998(1)  | 6288(1) | 2253(1) | 24(1)          |
| P(1)  | 9177(1)  | 5191(1) | 1927(1) | 39(1)          |
| P(2)  | 10496(1) | 6756(1) | 2337(1) | 35(1)          |
| P(3)  | 8625(1)  | 5610(1) | 3244(1) | 26(1)          |
| C(1)  | 5919(4)  | 6690(2) | 2558(2) | 65(1)          |
| C(2)  | 5517(4)  | 6062(3) | 2148(2) | 68(1)          |
| C(3)  | 5849(4)  | 6084(3) | 1550(2) | 65(1)          |
| C(4)  | 6493(4)  | 6753(2) | 1334(2) | 48(1)          |
| C(5)  | 6925(4)  | 7360(2) | 1750(2) | 43(1)          |
| C(6)  | 6621(4)  | 7345(2) | 2371(2) | 58(1)          |
| C(13) | 11065(3) | 7252(2) | 1650(2) | 36(1)          |
| C(14) | 10113(4) | 7290(2) | 1069(2) | 44(1)          |
| C(15) | 10542(5) | 7650(2) | 555(2)  | 58(1)          |
| C(16) | 11947(4) | 7955(2) | 622(2)  | 57(1)          |
| C(17) | 12925(4) | 7902(2) | 1195(2) | 51(1)          |
| C(18) | 12490(4) | 7558(2) | 1713(2) | 45(1)          |
| C(25) | 9780(3)  | 6022(2) | 3970(1) | 32(1)          |
| C(26) | 9682(4)  | 6810(2) | 4080(2) | 43(1)          |
| C(27) | 10479(5) | 7145(2) | 4631(2) | 54(1)          |
| C(28) | 11411(4) | 6704(2) | 5075(2) | 59(1)          |
| C(29) | 11546(4) | 5928(2) | 4976(2) | 55(1)          |

Table 6.2.2 continued

|        |           |         |         |       |
|--------|-----------|---------|---------|-------|
| C(30)  | 10708(4)  | 5586(2) | 4430(2) | 42(1) |
| C(31)  | 7012(3)   | 5295(2) | 3577(1) | 31(1) |
| C(32)  | 6477(4)   | 5730(2) | 4029(2) | 42(1) |
| C(33)  | 5187(4)   | 5521(2) | 4233(2) | 50(1) |
| C(34)  | 4426(4)   | 4872(2) | 3990(2) | 50(1) |
| C(35)  | 4922(4)   | 4438(2) | 3548(2) | 49(1) |
| C(36)  | 6206(4)   | 4642(2) | 3338(2) | 39(1) |
| C(37)  | 11186(4)  | 5336(2) | 1942(3) | 84(1) |
| C(38)  | 11806(4)  | 5934(2) | 2419(3) | 80(1) |
| C(39)  | 9599(3)   | 4681(2) | 3176(1) | 33(1) |
| C(40)  | 9240(4)   | 4383(2) | 2493(2) | 37(1) |
| C(7)   | 8878(9)   | 4776(4) | 1173(4) | 40(2) |
| C(8)   | 8017(12)  | 4140(6) | 1036(5) | 69(3) |
| C(9)   | 7608(15)  | 3834(8) | 422(6)  | 89(4) |
| C(10)  | 8070(13)  | 4197(6) | -65(4)  | 77(3) |
| C(11)  | 8974(12)  | 4849(6) | 49(4)   | 81(3) |
| C(12)  | 9335(12)  | 5140(5) | 657(4)  | 73(3) |
| C(7A)  | 8245(8)   | 4655(5) | 1145(4) | 37(2) |
| C(8A)  | 8364(9)   | 3881(4) | 1077(4) | 37(2) |
| C(9A)  | 7807(12)  | 3525(6) | 495(5)  | 57(3) |
| C(10A) | 7111(11)  | 3943(6) | -20(4)  | 68(3) |
| C(11A) | 7023(14)  | 4716(6) | 40(4)   | 92(4) |
| C(12A) | 7572(12)  | 5081(5) | 626(4)  | 70(3) |
| C(19)  | 11194(8)  | 7534(5) | 2986(4) | 36(2) |
| C(20)  | 10282(10) | 8179(5) | 3006(4) | 50(2) |
| C(21)  | 10713(13) | 8766(6) | 3444(5) | 76(3) |

Table 6.2.2 continued

|        |           |         |         |       |
|--------|-----------|---------|---------|-------|
| C(22)  | 12051(15) | 8724(7) | 3860(5) | 94(4) |
| C(23)  | 12962(14) | 8073(7) | 3868(5) | 84(4) |
| C(24)  | 12519(10) | 7494(6) | 3429(5) | 63(3) |
| C(19A) | 11502(10) | 7329(5) | 2927(4) | 37(2) |
| C(20A) | 10886(11) | 8060(6) | 2991(4) | 51(2) |
| C(21A) | 11594(14) | 8587(6) | 3449(5) | 78(3) |
| C(22A) | 12932(16) | 8387(7) | 3842(6) | 74(4) |
| C(23A) | 13531(12) | 7664(7) | 3789(4) | 79(3) |
| C(24A) | 12839(8)  | 7143(6) | 3336(4) | 50(2) |

---

Table 6.2.3. Anisotropic displacement parameters ( $\text{\AA}^2 \times 10^3$ ) for 4. The anisotropic displacement factor exponent takes the form:  $-2 \pi^2 [h^2 a^2 U_{11} + \dots + 2 h k a b U_{12}]$

|       | $U_{11}$ | $U_{22}$ | $U_{33}$ | $U_{23}$ | $U_{13}$ | $U_{12}$ |
|-------|----------|----------|----------|----------|----------|----------|
| Mo(1) | 27(1)    | 21(1)    | 26(1)    | 3(1)     | 7(1)     | 3(1)     |
| P(1)  | 64(1)    | 25(1)    | 35(1)    | 2(1)     | 24(1)    | 10(1)    |
| P(2)  | 29(1)    | 32(1)    | 42(1)    | 14(1)    | 5(1)     | -1(1)    |
| P(3)  | 33(1)    | 21(1)    | 26(1)    | 0(1)     | 8(1)     | 0(1)     |
| C(1)  | 46(2)    | 88(3)    | 71(2)    | 46(2)    | 36(2)    | 45(2)    |
| C(2)  | 28(2)    | 81(3)    | 95(3)    | 41(3)    | 11(2)    | -3(2)    |
| C(3)  | 50(2)    | 67(2)    | 66(3)    | 22(2)    | -16(2)   | -22(2)   |
| C(4)  | 40(2)    | 59(2)    | 41(2)    | 21(2)    | -4(1)    | -5(2)    |
| C(5)  | 45(2)    | 36(2)    | 48(2)    | 17(1)    | 10(2)    | 16(1)    |
| C(6)  | 70(2)    | 47(2)    | 61(2)    | 12(2)    | 23(2)    | 39(2)    |
| C(13) | 37(2)    | 27(1)    | 48(2)    | 10(1)    | 16(1)    | 2(1)     |
| C(14) | 42(2)    | 48(2)    | 45(2)    | 5(2)     | 14(1)    | -4(2)    |
| C(15) | 67(2)    | 67(3)    | 43(2)    | 6(2)     | 20(2)    | 4(2)     |
| C(16) | 71(2)    | 48(2)    | 64(2)    | 16(2)    | 44(2)    | 9(2)     |
| C(17) | 44(2)    | 38(2)    | 80(2)    | 15(2)    | 33(2)    | 2(2)     |
| C(18) | 36(2)    | 39(2)    | 62(2)    | 18(2)    | 15(2)    | 3(1)     |
| C(25) | 37(2)    | 34(2)    | 25(1)    | -2(1)    | 7(1)     | -4(1)    |
| C(26) | 56(2)    | 34(2)    | 38(2)    | -7(1)    | 10(2)    | -5(2)    |
| C(27) | 75(2)    | 44(2)    | 42(2)    | -14(2)   | 8(2)     | -11(2)   |
| C(28) | 65(2)    | 68(3)    | 42(2)    | -18(2)   | 5(2)     | -19(2)   |
| C(29) | 56(2)    | 70(2)    | 33(2)    | 1(2)     | -3(2)    | -2(2)    |
| C(30) | 49(2)    | 41(2)    | 32(2)    | 3(1)     | 3(1)     | -1(2)    |

Table 6.2.3 continued

|        |         |       |        |        |        |        |
|--------|---------|-------|--------|--------|--------|--------|
| C(31)  | 41(2)   | 27(1) | 28(1)  | 3(1)   | 11(1)  | -2(1)  |
| C(32)  | 53(2)   | 37(2) | 41(2)  | -6(1)  | 21(1)  | -6(2)  |
| C(33)  | 57(2)   | 52(2) | 50(2)  | 1(2)   | 31(2)  | 0(2)   |
| C(34)  | 8(2)    | 54(2) | 53(2)  | 10(2)  | 24(2)  | -8(2)  |
| C(35)  | 53(2)   | 42(2) | 55(2)  | 1(2)   | 19(2)  | -16(2) |
| C(36)  | 47(2)   | 35(2) | 37(2)  | -4(1)  | 15(1)  | -9(1)  |
| C(37)  | 84(2)   | 38(2) | 159(4) | 33(2)  | 95(2)  | 28(2)  |
| C(38)  | 28(2)   | 66(2) | 153(4) | 65(3)  | 36(2)  | 20(2)  |
| C(39)  | 42(2)   | 24(1) | 33(2)  | 9(1)   | 11(1)  | 8(1)   |
| C(40)  | 56(2)   | 21(1) | 35(2)  | 0(1)   | 13(1)  | 5(1)   |
| C(7)   | 58(4)   | 29(3) | 38(3)  | -4(3)  | 19(3)  | 9(3)   |
| C(8)   | 82(6)   | 75(7) | 67(7)  | -26(7) | 16(6)  | -17(7) |
| C(10)  | 124(8)  | 72(6) | 36(4)  | -13(4) | 18(5)  | 16(6)  |
| C(11)  | 142(8)  | 65(6) | 42(4)  | 0(4)   | 35(5)  | 18(6)  |
| C(12)  | 146(8)  | 40(4) | 41(4)  | 4(3)   | 39(5)  | 6(5)   |
| C(7A)  | 47(4)   | 32(4) | 33(3)  | -16(3) | 10(3)  | -11(3) |
| C(8A)  | 48(4)   | 32(4) | 31(3)  | -8(3)  | 7(3)   | -4(3)  |
| C(9A)  | 63(5)   | 51(5) | 54(5)  | -25(4) | 7(4)   | -3(4)  |
| C(10A) | 78(6)   | 74(6) | 42(4)  | -26(4) | -10(4) | -12(5) |
| C(11A) | 152(10) | 63(6) | 40(4)  | -12(4) | -34(5) | 20(6)  |
| C(12A) | 122(8)  | 42(4) | 35(4)  | 8(3)   | -14(4) | 14(5)  |
| C(19)  | 33(3)   | 30(4) | 44(4)  | 2(3)   | 8(3)   | -7(3)  |
| C(20)  | 63(5)   | 31(4) | 53(5)  | 4(3)   | 5(4)   | -13(4) |
| C(21)  | 101(8)  | 54(5) | 71(6)  | -9(4)  | 12(6)  | -30(5) |
| C(22)  | 126(9)  | 82(7) | 65(6)  | -12(6) | -1(7)  | -36(7) |
| C(23)  | 94(7)   | 86(8) | 52(6)  | 2(6)   | -31(5) | -44(6) |

**Table 6.2.3 continued**

|        |        |        |       |        |       |        |
|--------|--------|--------|-------|--------|-------|--------|
| C(24)  | 47(4)  | 74(6)  | 64(5) | 18(5)  | 4(4)  | 0(4)   |
| C(19A) | 45(4)  | 33(4)  | 34(4) | -2(3)  | 8(3)  | -9(3)  |
| C(20A) | 66(6)  | 49(5)  | 39(4) | -4(4)  | 10(4) | -20(5) |
| C(21A) | 128(9) | 61(6)  | 46(5) | -15(4) | 23(6) | -53(6) |
| C(22A) | 92(8)  | 71(8)  | 59(6) | -25(6) | 15(6) | -46(6) |
| C(23A) | 74(6)  | 125(9) | 35(4) | -22(5) | 4(4)  | -39(6) |
| C(24A) | 35(4)  | 81(6)  | 30(3) | -6(4)  | -1(3) | -12(4) |

---

Table 6.2.4. Hydrogen coordinates ( $\times 10^4$ ) and isotropic displacement parameters ( $\text{\AA}^2 \times 10^3$ ) for **4**.

|        | x        | y       | z       | U(eq) |
|--------|----------|---------|---------|-------|
| H(1A)  | 5713(4)  | 6672(2) | 2975(2) | 78    |
| H(2A)  | 5024(4)  | 5630(3) | 2280(2) | 82    |
| H(3A)  | 5729(4)  | 5608(3) | 1282(2) | 78    |
| H(4A)  | 6625(4)  | 6783(2) | 907(2)  | 58    |
| H(5A)  | 7429(4)  | 7788(2) | 1618(2) | 51    |
| H(6A)  | 6882(4)  | 7766(2) | 2654(2) | 69    |
| H(14A) | 9150(4)  | 7069(2) | 1016(2) | 53    |
| H(15A) | 9862(5)  | 7685(2) | 157(2)  | 70    |
| H(16A) | 12237(4) | 8203(2) | 271(2)  | 68    |
| H(17A) | 13905(4) | 8100(2) | 1239(2) | 62    |
| H(18A) | 13168(4) | 7532(2) | 2112(2) | 54    |
| H(26A) | 9057(4)  | 7120(2) | 3772(2) | 51    |
| H(27A) | 10383(5) | 7680(2) | 4702(2) | 65    |
| H(28A) | 11964(4) | 6937(2) | 5451(2) | 71    |
| H(29A) | 12207(4) | 5626(2) | 5279(2) | 65    |
| H(30A) | 10772(4) | 5046(2) | 4372(2) | 50    |
| H(32A) | 7004(4)  | 6177(2) | 4201(2) | 50    |
| H(33A) | 4836(4)  | 5826(2) | 4540(2) | 60    |
| H(34A) | 3550(4)  | 4726(2) | 4131(2) | 59    |
| H(35A) | 4386(4)  | 3991(2) | 3381(2) | 59    |
| H(36A) | 6537(4)  | 4333(2) | 3029(2) | 46    |
| H(37A) | 11727(4) | 4846(2) | 2052(3) | 100   |

Table 6.2.4 continued

|        |           |         |         |     |
|--------|-----------|---------|---------|-----|
| H(37B) | 11322(4)  | 5496(2) | 1514(3) | 100 |
| H(38A) | 12785(4)  | 6109(2) | 2347(3) | 96  |
| H(38B) | 11949(4)  | 5717(2) | 2855(3) | 96  |
| H(39A) | 10687(3)  | 4757(2) | 3311(1) | 39  |
| H(39B) | 9289(3)   | 4296(2) | 3464(1) | 39  |
| H(40A) | 8267(4)   | 4116(2) | 2413(2) | 44  |
| H(40B) | 10008(4)  | 4008(2) | 2429(2) | 44  |
| H(8A)  | 7674(12)  | 3892(6) | 1374(5) | 82  |
| H(9A)  | 7019(15)  | 3381(8) | 346(6)  | 106 |
| H(10A) | 7776(13)  | 4005(6) | -488(4) | 93  |
| H(11A) | 9333(12)  | 5088(6) | -289(4) | 97  |
| H(12A) | 9908(12)  | 5599(5) | 732(4)  | 87  |
| H(8AA) | 8834(9)   | 3579(4) | 1431(4) | 45  |
| H(9AA) | 7911(12)  | 2984(6) | 456(5)  | 68  |
| H(10B) | 6699(11)  | 3697(6) | -413(4) | 81  |
| H(11B) | 6582(14)  | 5016(6) | -319(4) | 111 |
| H(12B) | 7477(12)  | 5622(5) | 663(4)  | 84  |
| H(20A) | 9354(10)  | 8214(5) | 2714(4) | 60  |
| H(21A) | 10078(13) | 9196(6) | 3455(5) | 91  |
| H(22A) | 12369(15) | 9136(7) | 4147(5) | 113 |
| H(23A) | 13873(14) | 8033(7) | 4170(5) | 101 |
| H(24A) | 13139(10) | 7056(6) | 3432(5) | 76  |
| H(20B) | 9972(11)  | 8198(6) | 2719(4) | 62  |
| H(21B) | 11162(14) | 9076(6) | 3489(5) | 93  |
| H(22B) | 13437(16) | 8743(7) | 4147(6) | 89  |
| H(23B) | 14434(12) | 7524(7) | 4069(4) | 95  |

**Table 6.2.4 continued**

|               |                 |                |                |           |
|---------------|-----------------|----------------|----------------|-----------|
| <b>H(24B)</b> | <b>13279(8)</b> | <b>6654(6)</b> | <b>3304(4)</b> | <b>60</b> |
|---------------|-----------------|----------------|----------------|-----------|

Table 6.3.1. Crystal data and structure refinement for  $(\eta^6\text{-C}_6\text{H}_6)\text{Mo}(\text{PMePh}_2)_3$  (7).

|                                   |  |
|-----------------------------------|--|
| Empirical formula                 | $\text{C}_{45}\text{H}_{45}\text{MoP}_3$   |
| Formula weight                    | 774.66   |
| Temperature                       | 173(2) K   |
| Wavelength                        | 0.71073 Å  |
| Crystal system                    | Rhombohedral   |
| Space group                       | R3   |
| Unit cell dimensions              | a = 10.7703(5) Å $\alpha$ = 110.241(3) deg.<br>b = 10.7703(5) Å $\beta$ = 110.241(3) deg.<br>c = 10.7703(5) Å $\gamma$ = 110.241(3) deg. |
| Volume, Z                         | 933.33(8) Å <sup>3</sup> , 1   |
| Density (calculated)              | 1.378 mg/m <sup>3</sup>  |
| Absorption coefficient            | 0.512 mm <sup>-1</sup>   |
| F(000)                            | 402  |
| Crystal size                      | 0.52 x 0.62 x 0.58 mm  |
| Theta range for data collection   | 2.31 to 27.45 deg.   |
| Limiting indices                  | -13 ≤ h ≤ 13, -13 ≤ k ≤ 7, -8 ≤ l ≤ 13   |
| Reflections collected             | 3919   |
| Independent reflections           | 2738 [R(int) = 0.0295]   |
| Absorption correction             | Semi-empirical from psi-scans  |
| max. and min. transmission        | 0.5287 and 0.4949  |
| Refinement method                 | Full-matrix least-squares on F <sup>2</sup>  |
| Data / restraints / parameters    | 2736 / 1 / 151   |
| Goodness-of-fit on F <sup>2</sup> | 1.045  |
| Final R indices [I > 2σ(I)]       | R1 = 0.0224, wR2 = 0.0587  |
| R indices (all data)              | R1 = 0.0225, wR2 = 0.0595  |
| Largest diff. peak and hole       | 0.359 and -0.267 e.Å <sup>-3</sup>   |

Table 6.3.2. Atomic coordinates ( $\times 10^4$ ) and equivalent isotropic displacement parameters ( $\text{\AA}^2 \times 10^3$ ) for **7**.  $U(\text{eq})$  is defined as one third of the trace of the orthogonalized  $U_{ij}$  tensor.

|       | x        | y        | z        | $U(\text{eq})$ |
|-------|----------|----------|----------|----------------|
| Mo(1) | 9962     | 9962     | 9962     | 16(1)          |
| P(1)  | 10093(1) | 11313(1) | 12396(1) | 19(1)          |
| C(1)  | 8874(2)  | 10023(2) | 12813(2) | 22(1)          |
| C(2)  | 7289(2)  | 9509(2)  | 12196(2) | 26(1)          |
| C(3)  | 6372(3)  | 8469(3)  | 12446(3) | 33(1)          |
| C(4)  | 7016(3)  | 7919(3)  | 13313(3) | 35(1)          |
| C(5)  | 8576(3)  | 8422(3)  | 13936(2) | 33(1)          |
| C(6)  | 9498(2)  | 9464(2)  | 13696(2) | 27(1)          |
| C(7)  | 9326(2)  | 12624(2) | 12622(2) | 23(1)          |
| C(8)  | 9771(3)  | 13774(3) | 14077(3) | 35(1)          |
| C(9)  | 9052(3)  | 14625(3) | 14193(3) | 44(1)          |
| C(10) | 7886(3)  | 14347(3) | 12871(4) | 41(1)          |
| C(11) | 7437(3)  | 13217(3) | 11417(3) | 35(1)          |
| C(12) | 8152(2)  | 12360(2) | 11298(2) | 28(1)          |
| C(13) | 11949(2) | 12501(2) | 14291(2) | 30(1)          |
| C(14) | 7950(2)  | 7592(2)  | 9130(2)  | 26(1)          |
| C(15) | 8873(2)  | 7348(2)  | 8520(2)  | 26(1)          |

Table 6.3.3. Anisotropic displacement parameters ( $\text{Å}^2 \times 10^3$ ) for 7. The anisotropic displacement factor exponent takes the form:  $-2 \pi^2 [h^2 a^2 U_{11} + \dots + 2 h k a b U_{12}]$

|       | $U_{11}$ | $U_{22}$ | $U_{33}$ | $U_{23}$ | $U_{13}$ | $U_{12}$ |
|-------|----------|----------|----------|----------|----------|----------|
| Mo(1) | 16(1)    | 16(1)    | 16(1)    | 9(1)     | 9(1)     | 9(1)     |
| P(1)  | 20(1)    | 22(1)    | 17(1)    | 10(1)    | 10(1)    | 11(1)    |
| C(1)  | 28(1)    | 23(1)    | 18(1)    | 11(1)    | 14(1)    | 14(1)    |
| C(2)  | 27(1)    | 28(1)    | 26(1)    | 16(1)    | 14(1)    | 15(1)    |
| C(3)  | 29(1)    | 34(1)    | 31(1)    | 15(1)    | 19(1)    | 12(1)    |
| C(4)  | 44(1)    | 30(1)    | 30(1)    | 18(1)    | 23(1)    | 14(1)    |
| C(5)  | 47(1)    | 31(1)    | 26(1)    | 18(1)    | 20(1)    | 22(1)    |
| C(6)  | 33(1)    | 32(1)    | 23(1)    | 16(1)    | 16(1)    | 21(1)    |
| C(7)  | 26(1)    | 24(1)    | 28(1)    | 16(1)    | 19(1)    | 15(1)    |
| C(8)  | 43(1)    | 30(1)    | 30(1)    | 13(1)    | 20(1)    | 21(1)    |
| C(9)  | 55(2)    | 33(1)    | 50(1)    | 16(1)    | 35(1)    | 28(1)    |
| C(10) | 45(1)    | 29(1)    | 71(2)    | 30(1)    | 42(1)    | 26(1)    |
| C(11) | 32(1)    | 34(1)    | 51(1)    | 28(1)    | 24(1)    | 22(1)    |
| C(12) | 30(1)    | 28(1)    | 33(1)    | 18(1)    | 19(1)    | 18(1)    |
| C(13) | 25(1)    | 32(1)    | 21(1)    | 10(1)    | 8(1)     | 13(1)    |
| C(14) | 20(1)    | 22(1)    | 28(1)    | 13(1)    | 10(1)    | 6(1)     |
| C(15) | 25(1)    | 16(1)    | 28(1)    | 8(1)     | 11(1)    | 9(1)     |

Table 6.3.4. Hydrogen coordinates ( $\times 10^4$ ) and isotropic displacement parameters ( $\text{\AA}^2 \times 10^3$ ) for 7.

|        | x         | y         | z         | U(eq) |
|--------|-----------|-----------|-----------|-------|
| H(2A)  | 6836(2)   | 9877(2)   | 11598(2)  | 31    |
| H(3A)  | 5301(3)   | 8133(3)   | 12022(3)  | 39    |
| H(4A)  | 6387(3)   | 7201(3)   | 13478(3)  | 42    |
| H(5A)  | 9021(3)   | 8050(3)   | 14535(2)  | 39    |
| H(6A)  | 10571(2)  | 9804(2)   | 14138(2)  | 32    |
| H(8A)  | 10573(3)  | 13977(3)  | 14998(3)  | 42    |
| H(9A)  | 9366(3)   | 15405(3)  | 15191(3)  | 52    |
| H(10A) | 7394(3)   | 14927(3)  | 12957(4)  | 49    |
| H(11A) | 6641(3)   | 13026(3)  | 10501(3)  | 42    |
| H(12A) | 7833(2)   | 11583(2)  | 10297(2)  | 34    |
| H(13A) | 11742(3)  | 12758(20) | 15135(2)  | 44    |
| H(13B) | 12627(10) | 13465(11) | 14397(10) | 44    |
| H(13C) | 12464(12) | 11913(9)  | 14349(10) | 44    |
| H(14A) | 7736(2)   | 7139(2)   | 9704(2)   | 31    |
| H(15A) | 9326(2)   | 6774(2)   | 8735(2)   | 31    |

Table 6.4.1. Crystal data and structure refinement for  $(\eta^6\text{-C}_6\text{H}_6)\text{Mo}(\text{PPhMe}_2)_3$  (**8**).

|                                   |  |
|-----------------------------------|--|
| Empirical formula                 | $\text{C}_{30}\text{H}_{39}\text{MoP}_3$   |
| Formula weight                    | 588.46   |
| Temperature                       | 173(2) K   |
| Wavelength                        | 0.71073 Å  |
| Crystal system                    | Monoclinic   |
| Space group                       | $\text{P2}_1/\text{n}$   |
| Unit cell dimensions              | $a = 9.4393(8)$ Å $\alpha = 90$ deg.<br>$b = 9.4066(9)$ Å $\beta = 95.518(7)$ deg.<br>$c = 32.346(4)$ Å $\gamma = 90$ deg. |
| Volume, Z                         | $2858.7(5)$ Å <sup>3</sup> , 4   |
| Density (calculated)              | 1.367 mg/m <sup>3</sup>  |
| Absorption coefficient            | 0.644 mm <sup>-1</sup>   |
| F(000)                            | 1224   |
| Crystal size                      | 0.28 x 0.42 x 0.32 mm  |
| Theta range for data collection   | 2.20 to 26.00 deg.   |
| Limiting indices                  | $-2 \leq h \leq 11$ , $-11 \leq k \leq 11$ , $-39 \leq l \leq 39$  |
| Reflections collected             | 7252   |
| Independent reflections           | 5624 [R(int) = 0.0274]   |
| Absorption correction             | Semi-empirical from psi-scans  |
| Max. and min. transmission        | 0.2883 and 0.2702  |
| Refinement method                 | Full-matrix least-squares on F <sup>2</sup>  |
| Data / restraints / parameters    | 5619 / 0 / 308   |
| Goodness-of-fit on F <sup>2</sup> | 1.054  |
| Final R indices [I > 2σ(I)]       | R1 = 0.0297, wR2 = 0.0730  |
| R indices (all data)              | R1 = 0.0369, wR2 = 0.0788  |
| Largest diff. peak and hole       | 0.380 and -0.472 e.Å <sup>-3</sup>   |

Table 6.4.2. Atomic coordinates ( $\times 10^4$ ) and equivalent isotropic displacement parameters ( $\text{\AA}^2 \times 10^3$ ) for **8**.  $U(\text{eq})$  is defined as one third of the trace of the orthogonalized  $U_{ij}$  tensor.

|       | x        | y       | z       | U(eq) |
|-------|----------|---------|---------|-------|
| Mo(1) | 8711(1)  | 6116(1) | 1084(1) | 20(1) |
| P(1)  | 8188(1)  | 7151(1) | 1745(1) | 24(1) |
| P(2)  | 6376(1)  | 6773(1) | 747(1)  | 21(1) |
| P(3)  | 9771(1)  | 8354(1) | 886(1)  | 21(1) |
| C(1)  | 10421(3) | 4665(3) | 1401(1) | 36(1) |
| C(2)  | 9063(3)  | 4035(3) | 1430(1) | 39(1) |
| C(3)  | 8151(3)  | 3749(3) | 1065(1) | 39(1) |
| C(4)  | 8574(3)  | 4161(3) | 674(1)  | 39(1) |
| C(5)  | 9916(3)  | 4783(3) | 643(1)  | 36(1) |
| C(6)  | 10833(3) | 5051(3) | 1012(1) | 36(1) |
| C(7)  | 9552(3)  | 6815(4) | 2183(1) | 39(1) |
| C(8)  | 7949(3)  | 9070(3) | 1821(1) | 34(1) |
| C(9)  | 6624(3)  | 6472(3) | 1992(1) | 29(1) |
| C(10) | 6196(3)  | 7064(3) | 2358(1) | 37(1) |
| C(11) | 5015(3)  | 6539(4) | 2532(1) | 47(1) |
| C(12) | 4248(3)  | 5428(4) | 2345(1) | 53(1) |
| C(13) | 4667(3)  | 4829(4) | 1991(1) | 53(1) |
| C(14) | 5854(3)  | 5347(3) | 1815(1) | 40(1) |
| C(15) | 5288(3)  | 8106(3) | 982(1)  | 29(1) |
| C(16) | 5026(3)  | 5353(3) | 673(1)  | 35(1) |
| C(17) | 6250(2)  | 7388(2) | 199(1)  | 23(1) |

**Table 6.4.2 continued**

|       |          |          |         |       |
|-------|----------|----------|---------|-------|
| C(18) | 5034(3)  | 8041(3)  | 8(1)    | 27(1) |
| C(19) | 4971(3)  | 8486(3)  | -401(1) | 32(1) |
| C(20) | 6123(3)  | 8286(3)  | -629(1) | 30(1) |
| C(21) | 7327(3)  | 7606(3)  | -448(1) | 28(1) |
| C(22) | 7387(2)  | 7160(3)  | -38(1)  | 25(1) |
| C(23) | 8695(3)  | 9880(3)  | 691(1)  | 30(1) |
| C(24) | 10945(3) | 8259(3)  | 461(1)  | 34(1) |
| C(25) | 11058(2) | 9246(3)  | 1272(1) | 23(1) |
| C(26) | 11128(3) | 10716(3) | 1329(1) | 26(1) |
| C(27) | 12176(3) | 11318(3) | 1602(1) | 33(1) |
| C(28) | 13178(3) | 10475(3) | 1824(1) | 35(1) |
| C(29) | 13112(3) | 9019(3)  | 1777(1) | 35(1) |
| C(30) | 12057(3) | 8410(3)  | 1505(1) | 29(1) |

---

Table 6.4.3. Anisotropic displacement parameters ( $\text{\AA}^2 \times 10^3$ ) for **8**. The anisotropic displacement factor exponent takes the form:  $-2 \pi^2 [h^2 a^2 U_{11} + \dots + 2 h k a b U_{12}]$

|       | $U_{11}$ | $U_{22}$ | $U_{33}$ | $U_{23}$ | $U_{13}$ | $U_{12}$ |
|-------|----------|----------|----------|----------|----------|----------|
| Mo(1) | 20(1)    | 18(1)    | 21(1)    | -1(1)    | 1(1)     | 4(1)     |
| P(1)  | 23(1)    | 30(1)    | 20(1)    | -1(1)    | 2(1)     | -1(1)    |
| P(2)  | 18(1)    | 23(1)    | 22(1)    | -1(1)    | 2(1)     | 0(1)     |
| P(3)  | 16(1)    | 24(1)    | 23(1)    | 1(1)     | 1(1)     | 2(1)     |
| C(1)  | 40(2)    | 30(1)    | 37(1)    | -1(1)    | -7(1)    | 16(1)    |
| C(2)  | 48(2)    | 23(1)    | 44(2)    | 9(1)     | 2(1)     | 11(1)    |
| C(3)  | 43(2)    | 19(1)    | 54(2)    | 0(1)     | 0(1)     | 4(1)     |
| C(4)  | 46(2)    | 25(1)    | 43(2)    | -11(1)   | -5(1)    | 10(1)    |
| C(5)  | 43(2)    | 31(1)    | 33(1)    | -8(1)    | 3(1)     | 19(1)    |
| C(6)  | 32(1)    | 30(1)    | 44(2)    | -4(1)    | 2(1)     | 16(1)    |
| C(7)  | 30(1)    | 63(2)    | 23(1)    | -3(1)    | -3(1)    | 4(1)     |
| C(8)  | 39(2)    | 35(2)    | 30(1)    | -9(1)    | 9(1)     | -5(1)    |
| C(9)  | 25(1)    | 37(1)    | 25(1)    | 11(1)    | 2(1)     | 5(1)     |
| C(10) | 35(1)    | 46(2)    | 31(1)    | 12(1)    | 10(1)    | 10(1)    |
| C(11) | 44(2)    | 59(2)    | 40(2)    | 18(2)    | 18(1)    | 14(2)    |
| C(12) | 37(2)    | 69(2)    | 55(2)    | 30(2)    | 18(1)    | 4(2)     |
| C(13) | 46(2)    | 57(2)    | 55(2)    | 16(2)    | 4(2)     | -16(2)   |
| C(14) | 39(2)    | 45(2)    | 35(1)    | 8(1)     | 6(1)     | -8(1)    |
| C(15) | 23(1)    | 38(1)    | 27(1)    | -2(1)    | 5(1)     | 7(1)     |
| C(16) | 31(1)    | 36(2)    | 39(1)    | 4(1)     | (1)      | -12(1)   |
| C(17) | 22(1)    | 22(1)    | 23(1)    | -5(1)    | 0(1)     | -1(1)    |
| C(18) | 22(1)    | 31(1)    | 29(1)    | -3(1)    | 2(1)     | 5(1)     |

**Table 6.4.3 continued**

|       |       |       |       |       |       |       |
|-------|-------|-------|-------|-------|-------|-------|
| C(19) | 30(1) | 33(1) | 33(1) | 3(1)  | -2(1) | 10(1) |
| C(20) | 36(1) | 28(1) | 25(1) | 2(1)  | 2(1)  | 4(1)  |
| C(21) | 28(1) | 29(1) | 26(1) | -2(1) | 7(1)  | 1(1)  |
| C(22) | 22(1) | 25(1) | 28(1) | -4(1) | 1(1)  | 3(1)  |
| C(23) | 25(1) | 29(1) | 34(1) | 5(1)  | -7(1) | 0(1)  |
| C(24) | 27(1) | 47(2) | 27(1) | -2(1) | 7(1)  | -5(1) |
| C(25) | 16(1) | 32(1) | 22(1) | 0(1)  | 3(1)  | 0(1)  |
| C(26) | 23(1) | 29(1) | 27(1) | 0(1)  | 3(1)  | 0(1)  |
| C(27) | 33(1) | 35(1) | 33(1) | -6(1) | 4(1)  | -5(1) |
| C(28) | 27(1) | 52(2) | 27(1) | -7(1) | -1(1) | -5(1) |
| C(29) | 23(1) | 51(2) | 29(1) | -1(1) | -1(1) | 7(1)  |
| C(30) | 24(1) | 34(1) | 31(1) | 1(1)  | 1(1)  | 5(1)  |

---

Table 6.4.4. Hydrogen coordinates ( $\times 10^4$ ) and isotropic displacement parameters ( $\text{\AA}^2 \times 10^3$ ) for **8**.

|        | x        | y       | z       | U(eq) |
|--------|----------|---------|---------|-------|
| H(1A)  | 10997(3) | 4993(3) | 1659(1) | 44    |
| H(2A)  | 8699(3)  | 3917(3) | 1708(1) | 46    |
| H(3A)  | 7148(3)  | 443(3)  | 1089(1) | 47    |
| H(4A)  | 7864(3)  | 4134(3) | 424(1)  | 47    |
| H(5A)  | 10147(3) | 5196(3) | 372(1)  | 43    |
| H(6A)  | 11701(3) | 5650(3) | 996(1)  | 43    |
| H(7A)  | 9811(3)  | 5806(4) | 2188(1) | 59    |
| H(7B)  | 9172(3)  | 7071(4) | 2444(1) | 59    |
| H(7C)  | 10398(3) | 7391(4) | 2148(1) | 59    |
| H(8A)  | 7234(3)  | 9433(3) | 1607(1) | 52    |
| H(8B)  | 8855(3)  | 9560(3) | 1800(1) | 52    |
| H(8C)  | 7629(3)  | 9240(3) | 2096(1) | 52    |
| H(10A) | 6720(3)  | 7831(3) | 2488(1) | 44    |
| H(11A) | 4735(3)  | 6947(4) | 2780(1) | 56    |
| H(12A) | 3430(3)  | 5078(4) | 2462(1) | 63    |
| H(13A) | 4144(3)  | 4054(4) | 1865(1) | 63    |
| H(14A) | 6135(3)  | 4918(3) | 1570(1) | 47    |
| H(15A) | 5854(3)  | 8966(3) | 1044(1) | 43    |
| H(15B) | 4969(3)  | 7725(3) | 1239(1) | 43    |
| H(15C) | 4458(3)  | 8339(3) | 788(1)  | 43    |
| H(16A) | 5438(3)  | 4524(3) | 546(1)  | 53    |
| H(16B) | 4207(3)  | 5698(3) | 492(1)  | 53    |

**Table 6.4.4 continued**

|        |          |          |         |    |
|--------|----------|----------|---------|----|
| H(16C) | 4718(3)  | 5084(3)  | 943(1)  | 53 |
| H(18A) | 4236(3)  | 8183(3)  | 161(1)  | 33 |
| H(19A) | 4134(3)  | 8932(3)  | -525(1) | 39 |
| H(20A) | 6087(3)  | 8613(3)  | -907(1) | 36 |
| H(21A) | 8113(3)  | 7446(3)  | -605(1) | 33 |
| H(22A) | 8216(2)  | 6690(3)  | 83(1)   | 30 |
| H(23A) | 7984(3)  | 10095(3) | 884(1)  | 45 |
| H(23B) | 8212(3)  | 9652(3)  | 417(1)  | 45 |
| H(23C) | 9313(3)  | 10707(3) | 668(1)  | 45 |
| H(24A) | 11620(3) | 7474(3)  | 514(1)  | 50 |
| H(24B) | 11469(3) | 9155(3)  | 448(1)  | 50 |
| H(24C) | 10368(3) | 8100(3)  | 197(1)  | 50 |
| H(26A) | 10449(3) | 11310(3) | 1177(1) | 31 |
| H(27A) | 12208(3) | 12321(3) | 1637(1) | 40 |
| H(28A) | 13905(3) | 10895(3) | 2008(1) | 42 |
| H(29A) | 13789(3) | 8431(3)  | 1932(1) | 41 |
| H(30A) | 12016(3) | 7405(3)  | 1478(1) | 35 |

---

Table 6.5.1. Crystal data and structure refinement for  $[(\eta^6\text{-C}_6\text{H}_6)\text{MoH}(\text{TRIPHOS})]\text{PF}_6$   
( $6\cdot\text{PF}_6$ )

|                                   |  |
|-----------------------------------|--|
| Empirical formula                 | $\text{C}_{40}\text{H}_{40}\text{F}_6\text{MoP}_4$   |
| Formula weight                    | 854.54   |
| Temperature                       | 173(2) K   |
| Wavelength                        | 0.71073 Å  |
| Crystal system                    | Monoclinic   |
| Space group                       | $\text{P}2_1/c$  |
| Unit cell dimensions              | $a = 8.9180(10)$ Å $\alpha = 90$ deg.<br>$b = 36.908(3)$ Å $\beta = 97.930(10)$ deg.<br>$c = 11.0430(10)$ Å $\gamma = 90$ deg. |
| Volume, Z                         | $3600.0(6)$ Å <sup>3</sup> , 4   |
| Density (calculated)              | 1.577 mg/m <sup>3</sup>  |
| Absorption coefficient            | 0.604 mm <sup>-1</sup>   |
| F(000)                            | 1744   |
| Crystal size                      | 0.08 x 0.36 x 0.24 mm  |
| Theta range for data collection   | 1.94 to 25.00 deg.   |
| Limiting indices                  | $0 \leq h \leq 10$ , $-43 \leq k \leq 4$ , $-13 \leq l \leq 13$  |
| Reflections collected             | 7094   |
| Independent reflections           | 6337 [R(int) = 0.0227]   |
| Absorption correction             | Semi-empirical from psi-scans  |
| Refinement method                 | Full-matrix least-squares on F <sup>2</sup>  |
| Data / restraints / parameters    | 6330 / 0 / 463   |
| Goodness-of-fit on F <sup>2</sup> | 1.078  |
| Final R indices [I > 2σ(I)]       | R1 = 0.0573, wR2 = 0.1178  |
| R indices (all data)              | R1 = 0.1023, wR2 = 0.1433  |
| Largest diff. peak and hole       | 1.873 and -0.530 e.Å <sup>-3</sup>   |

Table 6.5.2. Atomic coordinates ( $\times 10^4$ ) and equivalent isotropic displacement parameters ( $\text{\AA}^2 \times 10^3$ ) for  $6\text{-PF}_6$ .  $U(\text{eq})$  is defined as one third of the trace of the orthogonalized  $U_{ij}$  tensor.

|       | x        | y       | z        | $U(\text{eq})$ |
|-------|----------|---------|----------|----------------|
| Mo(1) | 6605(1)  | 3760(1) | 4957(1)  | 20(1)          |
| P(1)  | 8274(2)  | 4092(1) | 6531(1)  | 25(1)          |
| P(2)  | 8616(2)  | 3943(1) | 3829(1)  | 23(1)          |
| P(3)  | 8038(2)  | 3273(1) | 6026(1)  | 21(1)          |
| P(4)  | 13611(2) | 3808(1) | -454(2)  | 36(1)          |
| F(1)  | 12142(5) | 3911(1) | 114(5)   | 83(2)          |
| F(2)  | 15115(4) | 3708(1) | -1032(4) | 51(1)          |
| F(3)  | 12716(5) | 3515(2) | -1295(5) | 89(2)          |
| F(4)  | 14556(6) | 4094(1) | 391(5)   | 76(2)          |
| F(5)  | 13218(6) | 4110(1) | -1482(5) | 84(2)          |
| F(6)  | 14053(5) | 3503(1) | 551(4)   | 67(1)          |
| C(1)  | 4456(6)  | 3652(2) | 3579(6)  | 37(2)          |
| C(2)  | 4363(6)  | 3464(2) | 4679(6)  | 35(2)          |
| C(3)  | 4329(7)  | 3649(2) | 5759(6)  | 38(2)          |
| C(4)  | 4556(6)  | 4021(2) | 5775(6)  | 35(2)          |
| C(5)  | 4824(7)  | 4211(2) | 4711(6)  | 39(2)          |
| C(6)  | 4704(6)  | 4025(2) | 3593(6)  | 37(2)          |
| C(7)  | 7632(6)  | 4506(2) | 7228(5)  | 28(1)          |
| C(8)  | 6757(7)  | 4476(2) | 8167(6)  | 40(2)          |
| C(9)  | 6208(8)  | 4777(2) | 8693(6)  | 47(2)          |
| C(10) | 6518(8)  | 5117(2) | 8267(7)  | 48(2)          |

Table 6.5.2 continued

|       |          |         |         |       |
|-------|----------|---------|---------|-------|
| C(11) | 7378(8)  | 5149(2) | 7334(7) | 46(2) |
| C(12) | 7915(7)  | 4848(2) | 6804(6) | 36(2) |
| C(13) | 8448(6)  | 4376(1) | 2986(5) | 26(1) |
| C(14) | 7720(7)  | 4668(2) | 3437(6) | 36(2) |
| C(15) | 7577(8)  | 4998(2) | 2818(7) | 49(2) |
| C(16) | 8191(9)  | 5037(2) | 1740(7) | 52(2) |
| C(17) | 8906(9)  | 4751(2) | 1290(7) | 57(2) |
| C(18) | 9051(8)  | 4420(2) | 1905(6) | 46(2) |
| C(19) | 9101(6)  | 3638(1) | 2648(5) | 22(1) |
| C(20) | 7956(7)  | 3540(2) | 1717(5) | 31(1) |
| C(21) | 8275(7)  | 3315(2) | 789(5)  | 34(2) |
| C(22) | 9697(8)  | 3178(2) | 780(5)  | 41(2) |
| C(23) | 10866(7) | 3277(2) | 1687(6) | 39(2) |
| C(24) | 10555(6) | 3507(2) | 2610(5) | 34(1) |
| C(25) | 9326(6)  | 2989(1) | 5257(5) | 25(1) |
| C(26) | 8815(6)  | 2852(1) | 4087(5) | 26(1) |
| C(27) | 9753(7)  | 2632(2) | 3485(5) | 29(1) |
| C(28) | 11194(7) | 2550(2) | 4025(6) | 34(1) |
| C(29) | 11711(7) | 2681(2) | 5175(6) | 36(2) |
| C(30) | 10771(6) | 2895(2) | 5791(6) | 30(1) |
| C(31) | 6871(6)  | 2925(1) | 6635(5) | 25(1) |
| C(32) | 6588(6)  | 2584(2) | 6128(5) | 29(1) |
| C(33) | 5619(6)  | 2344(2) | 6616(6) | 33(1) |
| C(34) | 4919(7)  | 2442(2) | 7611(6) | 33(1) |
| C(35) | 5184(7)  | 2784(2) | 8116(6) | 37(2) |
| C(36) | 6132(6)  | 3020(2) | 7646(5) | 30(1) |

**Table 6.5.2 continued**

|       |          |         |         |       |
|-------|----------|---------|---------|-------|
| C(37) | 10074(6) | 4221(2) | 5992(5) | 32(1) |
| C(38) | 10396(6) | 4001(2) | 4888(5) | 29(1) |
| C(39) | 9333(7)  | 3432(2) | 7394(5) | 29(1) |
| C(40) | 8823(7)  | 3793(2) | 7848(5) | 34(1) |

---

Table 6.5.3. Anisotropic displacement parameters ( $\text{\AA}^2 \times 10^3$ ) for  $6\text{-PF}_6$ . The anisotropic displacement factor exponent takes the form:  $-2 \pi^2 [h^2 a^2 U_{11} + \dots + 2 h k a b U_{12}]$

|       | $U_{11}$ | $U_{22}$ | $U_{33}$ | $U_{23}$ | $U_{13}$ | $U_{12}$ |
|-------|----------|----------|----------|----------|----------|----------|
| Mo(1) | 18(1)    | 23(1)    | 17(1)    | 0(1)     | 0(1)     | -1(1)    |
| P(1)  | 26(1)    | 24(1)    | 24(1)    | -3(1)    | -3(1)    | -1(1)    |
| P(2)  | 21(1)    | 24(1)    | 24(1)    | 2(1)     | 3(1)     | -1(1)    |
| P(3)  | 22(1)    | 23(1)    | 18(1)    | 0(1)     | 0(1)     | -1(1)    |
| P(4)  | 35(1)    | 42(1)    | 29(1)    | 2(1)     | 5(1)     | 5(1)     |
| F(1)  | 65(3)    | 94(4)    | 97(4)    | 21(3)    | 41(3)    | 24(3)    |
| F(2)  | 50(2)    | 54(2)    | 54(2)    | -4(2)    | 23(2)    | 7(2)     |
| F(3)  | 64(3)    | 95(4)    | 97(4)    | -27(3)   | -29(3)   | -14(3)   |
| F(4)  | 82(3)    | 66(3)    | 79(3)    | -39(3)   | 7(3)     | -1(3)    |
| F(5)  | 87(4)    | 92(3)    | 76(3)    | 45(3)    | 22(3)    | 35(3)    |
| F(6)  | 68(3)    | 75(3)    | 58(3)    | 30(2)    | 7(2)     | 10(2)    |
| C(1)  | 20(3)    | 60(4)    | 30(3)    | -12(3)   | -2(2)    | 4(3)     |
| C(2)  | 23(3)    | 26(3)    | 55(4)    | 0(3)     | 1(3)     | -10(2)   |
| C(3)  | 26(3)    | 59(4)    | 29(3)    | 8(3)     | 7(3)     | 2(3)     |
| C(4)  | 16(3)    | 57(4)    | 32(3)    | -19(3)   | 0(2)     | 5(3)     |
| C(5)  | 25(3)    | 29(3)    | 63(5)    | 5(3)     | 4(3)     | 6(3)     |
| C(6)  | 20(3)    | 60(4)    | 30(3)    | 20(3)    | -2(3)    | 2(3)     |
| C(7)  | 30(3)    | 26(3)    | 27(3)    | -10(2)   | 1(2)     | -2(2)    |
| C(8)  | 44(4)    | 33(3)    | 43(4)    | -9(3)    | 3(3)     | -4(3)    |
| C(9)  | 56(4)    | 44(4)    | 44(4)    | -11(3)   | 19(3)    | 6(3)     |
| C(10) | 59(4)    | 34(4)    | 48(4)    | -14(3)   | -2(4)    | 16(3)    |
| C(11) | 50(4)    | 26(3)    | 61(5)    | 1(3)     | 2(4)     | 4(3)     |

Table 6.5.3 continued

|       |       |       |       |       |        |        |
|-------|-------|-------|-------|-------|--------|--------|
| C(12) | 36(3) | 34(3) | 38(4) | 2(3)  | 5(3)   | -1(3)  |
| C(13) | 32(3) | 24(3) | 23(3) | 3(2)  | 5(2)   | -6(2)  |
| C(14) | 32(3) | 29(3) | 45(4) | 1(3)  | 2(3)   | -6(3)  |
| C(15) | 36(4) | 35(4) | 72(5) | 1(4)  | -11(4) | 0(3)   |
| C(16) | 65(5) | 29(3) | 56(5) | 15(3) | -15(4) | -11(3) |
| C(17) | 82(6) | 48(4) | 41(4) | 19(3) | 7(4)   | -17(4) |
| C(18) | 59(4) | 36(4) | 45(4) | 5(3)  | 11(3)  | -10(3) |
| C(19) | 25(3) | 21(3) | 22(3) | 6(2)  | 9(2)   | 0(2)   |
| C(20) | 31(3) | 39(3) | 23(3) | -1(3) | 5(2)   | -2(3)  |
| C(21) | 40(3) | 40(3) | 22(3) | -2(3) | 4(3)   | -7(3)  |
| C(22) | 66(5) | 39(4) | 21(3) | 0(3)  | 13(3)  | 3(3)   |
| C(23) | 37(3) | 45(4) | 39(4) | 6(3)  | 18(3)  | 9(3)   |
| C(24) | 26(3) | 43(3) | 32(3) | 2(3)  | 6(3)   | -4(3)  |
| C(25) | 26(3) | 23(3) | 25(3) | 5(2)  | 6(2)   | -3(2)  |
| C(26) | 26(3) | 24(3) | 28(3) | 5(2)  | 4(2)   | 1(2)   |
| C(27) | 38(3) | 24(3) | 27(3) | 1(2)  | 14(3)  | -2(3)  |
| C(28) | 30(3) | 29(3) | 44(4) | 1(3)  | 16(3)  | 2(3)   |
| C(29) | 22(3) | 44(3) | 44(4) | 10(3) | 4(3)   | 6(3)   |
| C(30) | 24(3) | 36(3) | 31(3) | 2(3)  | 2(3)   | -2(2)  |
| C(31) | 32(3) | 22(3) | 19(3) | 4(2)  | -1(2)  | 0(2)   |
| C(32) | 26(3) | 32(3) | 28(3) | -7(3) | 3(2)   | 5(2)   |
| C(33) | 30(3) | 28(3) | 39(3) | 1(3)  | 0(3)   | -3(3)  |
| C(34) | 28(3) | 35(3) | 37(3) | 14(3) | 7(3)   | 0(3)   |
| C(35) | 45(4) | 41(4) | 27(3) | 8(3)  | 8(3)   | 7(3)   |
| C(36) | 33(3) | 31(3) | 26(3) | -1(2) | 6(3)   | 1(3)   |
| C(37) | 27(3) | 33(3) | 34(3) | -4(3) | -2(3)  | -9(2)  |

**Table 6.5.3 continued**

|              |              |              |              |              |              |              |
|--------------|--------------|--------------|--------------|--------------|--------------|--------------|
| <b>C(38)</b> | <b>22(3)</b> | <b>33(3)</b> | <b>33(3)</b> | <b>3(3)</b>  | <b>2(2)</b>  | <b>-6(2)</b> |
| <b>C(39)</b> | <b>37(3)</b> | <b>28(3)</b> | <b>22(3)</b> | <b>-4(2)</b> | <b>1(2)</b>  | <b>0(3)</b>  |
| <b>C(40)</b> | <b>43(3)</b> | <b>29(3)</b> | <b>25(3)</b> | <b>-4(3)</b> | <b>-7(3)</b> | <b>3(3)</b>  |

---

Table 6.5.4. Hydrogen coordinates ( $\times 10^4$ ) and isotropic displacement parameters ( $\text{\AA}^2 \times 10^3$ ) for **6**·**PF<sub>6</sub>**.

|        | x        | y       | z       | U(eq) |
|--------|----------|---------|---------|-------|
| H(1A)  | 4351(6)  | 3526(2) | 2841(6) | 45    |
| H(2A)  | 4324(6)  | 3212(2) | 4676(6) | 42    |
| H(3A)  | 4158(7)  | 3527(2) | 6464(6) | 45    |
| H(4A)  | 4531(6)  | 4149(2) | 6499(6) | 42    |
| H(5A)  | 5076(7)  | 4455(2) | 4752(6) | 47    |
| H(6A)  | 4790(6)  | 4149(2) | 2872(6) | 45    |
| H(8A)  | 6535(7)  | 4247(2) | 8447(6) | 48    |
| H(9A)  | 5633(8)  | 4752(2) | 9329(6) | 56    |
| H(10A) | 6147(8)  | 5323(2) | 8610(7) | 58    |
| H(11A) | 7600(8)  | 5378(2) | 7056(7) | 56    |
| H(12A) | 8473(7)  | 4875(2) | 6157(6) | 43    |
| H(14A) | 7318(7)  | 4643(2) | 4166(6) | 43    |
| H(15A) | 7074(8)  | 5191(2) | 3127(7) | 59    |
| H(16A) | 8116(9)  | 5257(2) | 1326(7) | 63    |
| H(17A) | 9305(9)  | 4777(2) | 560(7)  | 68    |
| H(18A) | 9554(8)  | 4229(2) | 1588(6) | 55    |
| H(20A) | 6977(7)  | 3626(2) | 1721(5) | 37    |
| H(21A) | 7511(7)  | 3256(2) | 160(5)  | 41    |
| H(22A) | 9883(8)  | 3018(2) | 167(5)  | 49    |
| H(23A) | 11842(7) | 3190(2) | 1673(6) | 47    |
| H(24A) | 11333(6) | 3575(2) | 3216(5) | 40    |
| H(26A) | 7845(6)  | 2908(1) | 3709(5) | 31    |

Table 6.5.4 continued

|        |          |          |          |    |
|--------|----------|----------|----------|----|
| H(27A) | 9400(7)  | 2540(2)  | 2714(5)  | 35 |
| H(28A) | 11818(7) | 2406(2)  | 3616(6)  | 40 |
| H(29A) | 12688(7) | 2627(2)  | 5541(6)  | 44 |
| H(30A) | 11122(6) | 2976(2)  | 6577(6)  | 36 |
| H(32A) | 7048(6)  | 2514(2)  | 5458(5)  | 35 |
| H(33A) | 5440(6)  | 2116(2)  | 6269(6)  | 39 |
| H(34A) | 4279(7)  | 2281(2)  | 7936(6)  | 40 |
| H(35A) | 4713(7)  | 2852(2)  | 8780(6)  | 44 |
| H(36A) | 6296(6)  | 3249(2)  | 7997(5)  | 35 |
| H(37B) | 10036(6) | 4476(2)  | 5778(5)  | 38 |
| H(37A) | 10899(6) | 4187(2)  | 6653(5)  | 38 |
| H(38B) | 10803(6) | 3766(2)  | 5152(5)  | 35 |
| H(38A) | 11139(6) | 4126(2)  | 4475(5)  | 35 |
| H(39B) | 9356(7)  | 3253(2)  | 8040(5)  | 35 |
| H(39A) | 10350(7) | 3455(2)  | 7187(5)  | 35 |
| H(40B) | 9640(7)  | 3903(2)  | 8397(5)  | 40 |
| H(40A) | 7969(7)  | 3758(2)  | 8293(5)  | 40 |
| H(1)   | 6876(67) | 3389(15) | 4006(55) | 40 |

---

Table 6.6.1. Crystal data and structure refinement for ( $\eta^6$ -C<sub>6</sub>H<sub>5</sub>SiMe<sub>3</sub>)Mo(TRIPOD) (**35**).

|                                   |   |
|-----------------------------------|---|
| Empirical formula                 | C <sub>50</sub> H <sub>53</sub> MoP <sub>3</sub> Si   |
| Formula weight                    | 870.86  |
| Temperature                       | 188(2) K  |
| Wavelength                        | 0.71073 Å   |
| Crystal system                    | Monoclinic  |
| Space group                       | P2 <sub>1</sub> /n  |
| Unit cell dimensions              | a = 10.7247(13) Å    α = 90 deg.<br>b = 19.510(3) Å    β = 90.097(6) deg.<br>c = 20.433(3) Å    γ = 90 deg. |
| Volume, Z                         | 4275.4(10) Å <sup>3</sup> , 4   |
| Density (calculated)              | 1.353 mg/m <sup>3</sup>   |
| Absorption coefficient            | 0.482 mm <sup>-1</sup>  |
| F(000)                            | 1816  |
| Crystal size                      | 0.44 x 0.42 x 0.32 mm   |
| Theta range for data collection   | 1.99 to 25.00 deg.  |
| Limiting indices                  | 0 ≤ h ≤ 12, -23 ≤ k ≤ 0, -24 ≤ l ≤ 24   |
| Reflections collected             | 8267  |
| Independent reflections           | 7524 [R(int) = 0.0422]  |
| Absorption correction             | Semi-empirical from psi-scans   |
| Max. and min. transmission        | 0.2619 and 0.2385   |
| Refinement method                 | Full-matrix least-squares on F <sup>2</sup>   |
| Data / restraints / parameters    | 7515 / 0 / 496  |
| Goodness-of-fit on F <sup>2</sup> | 1.042   |
| Final R indices [I > 2σ(I)]       | R1 = 0.0378, wR2 = 0.0938   |
| R indices (all data)              | R1 = 0.0470, wR2 = 0.1013   |
| Largest diff. peak and hole       | 0.629 and -0.865 e.Å <sup>-3</sup>  |

Table 6.6.2. Atomic coordinates ( $\times 10^4$ ) and equivalent isotropic displacement parameters ( $\text{\AA}^2 \times 10^3$ ) for **35**.  $U(\text{eq})$  is defined as one third of the trace of the orthogonalized  $U_{ij}$  tensor.

|       | x        | y        | z       | U(eq) |
|-------|----------|----------|---------|-------|
| Mo(1) | -1374(1) | 7879(1)  | 764(1)  | 20(1) |
| P(1)  | -1997(1) | 8526(1)  | 5802(1) | 22(1) |
| P(2)  | 549(1)   | 8495(1)  | 6621(1) | 24(1) |
| P(3)  | -551(1)  | 7102(1)  | 5954(1) | 21(1) |
| Si(1) | -2247(1) | 9061(1)  | 8344(1) | 32(1) |
| C(1)  | -1068(3) | 7176(1)  | 7651(1) | 33(1) |
| C(2)  | -1050(3) | 7865(1)  | 7857(1) | 28(1) |
| C(3)  | -2106(3) | 8316(1)  | 7771(1) | 29(1) |
| C(4)  | -3124(3) | 8044(2)  | 7406(1) | 31(1) |
| C(5)  | -3144(3) | 7359(2)  | 7177(1) | 33(1) |
| C(6)  | -2107(3) | 6932(2)  | 7290(1) | 34(1) |
| C(7)  | -2833(2) | 9362(1)  | 5815(1) | 27(1) |
| C(8)  | -3497(3) | 9551(2)  | 6363(2) | 45(1) |
| C(9)  | -4217(4) | 10147(2) | 6368(2) | 56(1) |
| C(10) | -4291(3) | 10548(2) | 5827(2) | 48(1) |
| C(11) | -3650(3) | 10364(2) | 5269(2) | 42(1) |
| C(12) | -2925(3) | 9778(2)  | 5263(2) | 35(1) |
| C(13) | -3165(2) | 8121(1)  | 5253(1) | 26(1) |
| C(14) | -4326(3) | 7985(2)  | 5525(2) | 32(1) |
| C(15) | -5278(3) | 7702(2)  | 5153(2) | 40(1) |
| C(16) | -5086(3) | 7548(2)  | 4502(2) | 43(1) |

Table 6.6.2 continued

|       |          |          |         |       |
|-------|----------|----------|---------|-------|
| C(17) | -3946(3) | 7672(2)  | 4223(2) | 40(1) |
| C(18) | -2992(3) | 7963(1)  | 4592(1) | 30(1) |
| C(19) | 584(3)   | 9446(1)  | 6659(1) | 34(1) |
| C(20) | 1668(4)  | 9818(2)  | 6514(2) | 48(1) |
| C(21) | 1670(5)  | 10526(2) | 6544(2) | 68(1) |
| C(22) | 592(6)   | 10867(2) | 6713(2) | 75(2) |
| C(23) | -471(5)  | 10514(2) | 6861(2) | 62(1) |
| C(24) | -469(3)  | 9799(2)  | 6840(2) | 41(1) |
| C(25) | 1841(3)  | 8317(1)  | 7199(1) | 29(1) |
| C(26) | 2512(4)  | 7714(2)  | 7160(2) | 52(1) |
| C(27) | 3450(4)  | 7556(2)  | 7599(2) | 59(1) |
| C(28) | 3716(3)  | 7987(2)  | 8111(2) | 46(1) |
| C(29) | 3060(4)  | 8582(2)  | 8164(2) | 52(1) |
| C(30) | 2139(3)  | 8754(2)  | 7709(2) | 44(1) |
| C(31) | -1522(2) | 6424(1)  | 5573(1) | 23(1) |
| C(32) | -2814(3) | 6431(1)  | 5628(1) | 32(1) |
| C(33) | -3543(3) | 5970(2)  | 5287(2) | 38(1) |
| C(34) | -3001(3) | 5483(2)  | 4892(2) | 37(1) |
| C(35) | -1718(3) | 5459(1)  | 4832(1) | 33(1) |
| C(36) | -988(3)  | 5924(1)  | 5169(1) | 29(1) |
| C(37) | 782(2)   | 6542(1)  | 6187(1) | 25(1) |
| C(38) | 1951(3)  | 6557(1)  | 5896(1) | 31(1) |
| C(39) | 2920(3)  | 6147(2)  | 6129(2) | 40(1) |
| C(40) | 2736(3)  | 5706(2)  | 6646(2) | 42(1) |
| C(41) | 1567(3)  | 5667(2)  | 6923(2) | 39(1) |
| C(42) | 610(3)   | 6079(1)  | 6698(1) | 31(1) |

Table 6.6.2 continued

|       |          |         |         |       |
|-------|----------|---------|---------|-------|
| C(43) | -3006(3) | 8713(2) | 9094(2) | 48(1) |
| C(44) | -688(3)  | 9408(2) | 8577(2) | 50(1) |
| C(45) | -3261(4) | 9773(2) | 8058(2) | 55(1) |
| C(46) | -685(2)  | 8755(1) | 5246(1) | 25(1) |
| C(47) | 1327(2)  | 8368(1) | 5820(1) | 27(1) |
| C(48) | -1(2)    | 7499(1) | 5187(1) | 25(1) |
| C(49) | 434(2)   | 8251(1) | 5229(1) | 25(1) |
| C(50) | 1180(3)  | 8402(2) | 4603(1) | 33(1) |

---

Table 6.6.3. Anisotropic displacement parameters ( $\text{\AA}^2 \times 10^3$ ) for **35**. The anisotropic displacement factor exponent takes the form:  $-2 \pi^2 [h^2 a^2 U_{11} + \dots + 2 h k a b U_{12}]$

|       | $U_{11}$ | $U_{22}$ | $U_{33}$ | $U_{23}$ | $U_{13}$ | $U_{12}$ |
|-------|----------|----------|----------|----------|----------|----------|
| Mo(1) | 21(1)    | 22(1)    | 17(1)    | 0(1)     | 0(1)     | 2(1)     |
| P(1)  | 22(1)    | 24(1)    | 20(1)    | 0(1)     | -3(1)    | 2(1)     |
| P(2)  | 25(1)    | 26(1)    | 20(1)    | 0(1)     | -4(1)    | -2(1)    |
| P(3)  | 20(1)    | 23(1)    | 20(1)    | -1(1)    | 0(1)     | 1(1)     |
| Si(1) | 38(1)    | 34(1)    | 23(1)    | -4(1)    | 4(1)     | 5(1)     |
| C(1)  | 39(2)    | 35(2)    | 24(1)    | 9(1)     | 5(1)     | 6(1)     |
| C(2)  | 34(2)    | 36(2)    | 15(1)    | 1(1)     | 1(1)     | 4(1)     |
| C(3)  | 32(2)    | 34(1)    | 20(1)    | 2(1)     | 6(1)     | 2(1)     |
| C(4)  | 29(2)    | 38(2)    | 26(1)    | 1(1)     | 6(1)     | 4(1)     |
| C(5)  | 29(2)    | 41(2)    | 28(2)    | -3(1)    | 10(1)    | -6(1)    |
| C(6)  | 47(2)    | 28(1)    | 28(2)    | 1(1)     | 14(1)    | -2(1)    |
| C(7)  | 26(1)    | 25(1)    | 31(2)    | -1(1)    | -7(1)    | 2(1)     |
| C(8)  | 59(2)    | 43(2)    | 34(2)    | 1(1)     | 0(2)     | 22(2)    |
| C(9)  | 66(2)    | 56(2)    | 46(2)    | -3(2)    | 5(2)     | 33(2)    |
| C(10) | 45(2)    | 34(2)    | 64(2)    | -1(2)    | -11(2)   | 15(1)    |
| C(11) | 36(2)    | 34(2)    | 56(2)    | 15(2)    | -9(2)    | 1(1)     |
| C(12) | 33(2)    | 33(2)    | 39(2)    | 7(1)     | -3(1)    | 1(1)     |
| C(13) | 24(1)    | 28(1)    | 25(1)    | 1(1)     | -6(1)    | 1(1)     |
| C(14) | 28(2)    | 38(2)    | 29(2)    | -1(1)    | -1(1)    | 0(1)     |
| C(15) | 23(2)    | 46(2)    | 50(2)    | -2(2)    | -2(1)    | -2(1)    |
| C(16) | 34(2)    | 46(2)    | 47(2)    | -10(2)   | -15(1)   | -4(1)    |
| C(17) | 41(2)    | 46(2)    | 34(2)    | -13(1)   | -11(1)   | 3(1)     |

Table 6.6.3 continued

|       |        |       |       |        |        |        |
|-------|--------|-------|-------|--------|--------|--------|
| C(18) | 26(2)  | 36(2) | 28(2) | -3(1)  | 3(1)   | 1(1)   |
| C(19) | 51(2)  | 27(1) | 23(1) | -1(1)  | -11(1) | -6(1)  |
| C(20) | 71(2)  | 41(2) | 33(2) | 1(1)   | -9(2)  | -21(2) |
| C(21) | 121(4) | 43(2) | 39(2) | 11(2)  | -24(2) | -40(2) |
| C(22) | 154(5) | 29(2) | 43(2) | 3(2)   | -39(3) | -8(3)  |
| C(23) | 109(4) | 35(2) | 42(2) | -6(2)  | -21(2) | 17(2)  |
| C(24) | 62(2)  | 31(2) | 31(2) | 0(1)   | -13(2) | 7(2)   |
| C(25) | 24(1)  | 38(2) | 24(1) | 4(1)   | -4(1)  | -5(1)  |
| C(26) | 62(2)  | 43(2) | 51(2) | -10(2) | -30(2) | 9(2)   |
| C(28) | 33(2)  | 64(2) | 40(2) | 8(2)   | -16(1) | -3(2)  |
| C(29) | 57(2)  | 64(2) | 36(2) | -13(2) | -21(2) | -1(2)  |
| C(30) | 45(2)  | 51(2) | 34(2) | -10(1) | -13(1) | 7(2)   |
| C(31) | 26(1)  | 23(1) | 20(1) | 1(1)   | -3(1)  | 0(1)   |
| C(32) | 29(2)  | 29(1) | 37(2) | -3(1)  | 3(1)   | 2(1)   |
| C(33) | 25(2)  | 41(2) | 47(2) | -6(1)  | -1(1)  | -5(1)  |
| C(34) | 41(2)  | 32(2) | 38(2) | -4(1)  | -9(1)  | -5(1)  |
| C(35) | 39(2)  | 28(1) | 32(2) | -6(1)  | -3(1)  | 3(1)   |
| C(36) | 26(1)  | 34(2) | 28(1) | -3(1)  | 0(1)   | 3(1)   |
| C(37) | 26(1)  | 23(1) | 26(1) | -6(1)  | -5(1)  | 2(1)   |
| C(38) | 29(2)  | 34(2) | 31(2) | -3(1)  | 3(1)   | 3(1)   |
| C(39) | 27(2)  | 46(2) | 48(2) | -10(2) | 2(1)   | 7(1)   |
| C(40) | 35(2)  | 41(2) | 50(2) | -3(2)  | -11(1) | 16(1)  |
| C(41) | 46(2)  | 34(2) | 37(2) | 4(1)   | -1(1)  | 11(1)  |
| C(42) | 29(2)  | 31(1) | 33(2) | 2(1)   | 1(1)   | 3(1)   |
| C(43) | 58(2)  | 52(2) | 33(2) | -5(2)  | 13(2)  | 4(2)   |
| C(44) | 50(2)  | 56(2) | 43(2) | -18(2) | 3(2)   | -7(2)  |

**Table 6.6.3 continued**

|       |       |       |       |       |       |       |
|-------|-------|-------|-------|-------|-------|-------|
| C(45) | 74(3) | 49(2) | 42(2) | -4(2) | 3(2)  | 26(2) |
| C(46) | 25(1) | 28(1) | 22(1) | 3(1)  | -3(1) | -3(1) |
| C(47) | 22(1) | 34(1) | 25(1) | 0(1)  | -1(1) | -3(1) |
| C(48) | 26(1) | 30(1) | 18(1) | -1(1) | -1(1) | 2(1)  |
| C(49) | 23(1) | 31(1) | 20(1) | 2(1)  | 0(1)  | -2(1) |
| C(50) | 31(2) | 46(2) | 24(1) | 5(1)  | 2(1)  | -4(1) |

---

Table 6.6.4. Hydrogen coordinates ( $\times 10^4$ ) and isotropic displacement parameters ( $\text{\AA}^2 \times 10^3$ ) for **35**.

|        | x        | y        | z       | U(eq) |
|--------|----------|----------|---------|-------|
| H(1A)  | -294(3)  | 6892(1)  | 7683(1) | 39    |
| H(2A)  | -255(3)  | 8060(1)  | 8034(1) | 34    |
| H(4A)  | -3782(3) | 8367(2)  | 7247(1) | 37    |
| H(5A)  | -3819(3) | 7207(2)  | 6871(1) | 39    |
| H(6A)  | -2060(3) | 6475(2)  | 7070(1) | 41    |
| H(8A)  | -3464(3) | 9272(2)  | 6743(2) | 54    |
| H(9A)  | -4659(4) | 10272(2) | 6752(2) | 68    |
| H(10A) | -4781(3) | 10954(2) | 5833(2) | 57    |
| H(11A) | -3707(3) | 10640(2) | 4887(2) | 50    |
| H(12A) | -2485(3) | 9657(2)  | 4877(2) | 42    |
| H(14A) | -4470(3) | 8088(2)  | 5973(2) | 38    |
| H(15A) | 6066(3)  | 7615(2)  | 5347(2) | 48    |
| H(16A) | -5741(3) | 7355(2)  | 4248(2) | 51    |
| H(17A) | -3808(3) | 7560(2)  | 3777(2) | 48    |
| H(18A) | -2211(3) | 8055(1)  | 4393(1) | 36    |
| H(20A) | 2407(4)  | 9582(2)  | 6395(2) | 58    |
| H(21A) | 2408(5)  | 10775(2) | 6448(2) | 81    |
| H(22A) | 589(6)   | 11354(2) | 6728(2) | 90    |
| H(23A) | -1208(5) | 10755(2) | 6978(2) | 74    |
| H(24A) | -1204(3) | 9554(2)  | 6952(2) | 49    |
| H(26A) | 2323(4)  | 7397(2)  | 6821(2) | 62    |
| H(27A) | 3915(4)  | 7146(2)  | 7546(2) | 71    |

Table 6.6.4 continued

|        |          |          |         |    |
|--------|----------|----------|---------|----|
| H(28A) | 4344(3)  | 7874(2)  | 8421(2) | 55 |
| H(29A) | 3231(4)  | 8885(2)  | 8517(2) | 63 |
| H(30A) | 1710(3)  | 9177(2)  | 7750(2) | 52 |
| H(32A) | -3201(3) | 6759(1)  | 5905(1) | 38 |
| H(33A) | -4425(3) | 5989(2)  | 5325(2) | 45 |
| H(34A) | -3506(3) | 5164(2)  | 4662(2) | 44 |
| H(35A) | -1339(3) | 5124(1)  | 4560(1) | 40 |
| H(36A) | -107(3)  | 5905(1)  | 5126(1) | 35 |
| H(38A) | 2093(3)  | 6851(1)  | 5534(1) | 37 |
| H(39A) | 3717(3)  | 6172(2)  | 5928(2) | 48 |
| H(40A) | 3402(3)  | 5434(2)  | 6808(2) | 50 |
| H(41A) | 1419(3)  | 5355(2)  | 7272(2) | 46 |
| H(42A) | -188(3)  | 6046(1)  | 6898(1) | 37 |
| H(43A) | -2507(3) | 8333(2)  | 9268(2) | 71 |
| H(43B) | -3844(3) | 8548(2)  | 8985(2) | 71 |
| H(43C) | -3066(3) | 9075(2)  | 9425(2) | 71 |
| H(44A) | -153(3)  | 9033(2)  | 8728(2) | 74 |
| H(44B) | -787(3)  | 9745(2)  | 8929(2) | 74 |
| H(44C) | -306(3)  | 9630(2)  | 8196(2) | 74 |
| H(45A) | -4080(4) | 9591(2)  | 7935(2) | 82 |
| H(45B) | -2878(4) | 9994(2)  | 7677(2) | 82 |
| H(45C) | -3359(4) | 10110(2) | 8410(2) | 82 |
| H(46A) | -1021(2) | 8796(1)  | 4796(1) | 30 |
| H(46B) | -369(2)  | 9212(1)  | 5375(1) | 30 |
| H(47A) | 1848(2)  | 8776(1)  | 5728(1) | 32 |
| H(47B) | 1892(2)  | 7969(1)  | 5856(1) | 32 |

Table 6.6.4 continued

|        |         |         |         |    |
|--------|---------|---------|---------|----|
| H(48A) | 700(2)  | 7221(1) | 5017(1) | 30 |
| H(48B) | -684(2) | 7472(1) | 4861(1) | 30 |
| H(50A) | 1473(3) | 8878(2) | 4612(1) | 50 |
| H(50B) | 644(3)  | 8333(2) | 4220(1) | 50 |
| H(50C) | 1897(3) | 8092(2) | 4578(1) | 50 |

---

## 6.4 LIST OF NMR SPECTRA

S denotes solvent peak

\* denotes impurity peak

- Figure 6.1.  $^1\text{H}$  NMR spectrum of  $(\eta^6\text{-C}_6\text{D}_6)\text{Mo}(\text{TRIPOD}) + \text{CF}_3\text{SO}_3\text{H}$   
Figure 6.2.  $^2\text{H}$  NMR spectrum of  $(\eta^6\text{-C}_6\text{D}_6)\text{Mo}(\text{TRIPOD}) + \text{CF}_3\text{SO}_3\text{H}$   
Figure 6.3.  $^1\text{H}$  NMR spectrum of  $(\eta^6\text{-C}_6\text{D}_6)\text{Mo}(\text{TRIPHOS}) + \text{CF}_3\text{SO}_3\text{H}$   
Figure 6.4.  $^2\text{H}$  NMR spectrum of  $(\eta^6\text{-C}_6\text{D}_6)\text{Mo}(\text{TRIPHOS}) + \text{CF}_3\text{SO}_3\text{H}$   
Figure 6.5.  $^{31}\text{P}$  NMR spectrum of  $(\eta^6\text{-C}_6\text{D}_6)\text{Mo}(\text{TRIPHOS}) + \text{CF}_3\text{SO}_3\text{H}$   
Figure 6.6.  $^1\text{H}$  NMR spectrum of  $(\eta^6\text{-C}_6\text{D}_6)\text{Mo}(\text{PPh}_2\text{Me})_3 + \text{CF}_3\text{SO}_3\text{H}$   
Figure 6.7.  $^2\text{H}$  NMR spectrum of  $(\eta^6\text{-C}_6\text{D}_6)\text{Mo}(\text{PPh}_2\text{Me})_3 + \text{CF}_3\text{SO}_3\text{H}$   
Figure 6.8.  $^1\text{H}$  NMR spectrum of  $(\eta^6\text{-C}_6\text{D}_6)\text{Mo}(\text{PMe}_2\text{Ph})_3 + \text{CF}_3\text{SO}_3\text{H}$   
Figure 6.9.  $^2\text{H}$  NMR spectrum of  $(\eta^6\text{-C}_6\text{D}_6)\text{Mo}(\text{PMe}_2\text{Ph})_3 + \text{CF}_3\text{SO}_3\text{H}$   
Figure 6.10.  $^1\text{H}$  NMR spectrum of  $(\eta^6\text{-C}_6\text{D}_6)\text{Mo}(\text{PMe}_3)_3 + \text{CF}_3\text{SO}_3\text{H}$   
Figure 6.11.  $^2\text{H}$  NMR spectrum of  $(\eta^6\text{-C}_6\text{D}_6)\text{Mo}(\text{PMe}_3)_3 + \text{CF}_3\text{SO}_3\text{H}$   
Figure 6.12.  $^1\text{H}$  NMR spectrum of  $(\eta^6\text{-C}_6\text{H}_5\text{CH}_3)\text{Mo}(\text{TRIPOD})$   
Figure 6.13.  $^1\text{H}$  NMR spectrum of  $(\eta^6\text{-C}_6\text{H}_5\text{SiMe}_3)\text{Mo}(\text{TRIPOD})$

Figure 6.1.  $^1\text{H}$  NMR spectrum of  $(\eta^6\text{-C}_6\text{D}_6)\text{Mo}(\text{TRIPOD}) + \text{CF}_3\text{SO}_3\text{H}$  in  $\text{CD}_2\text{Cl}_2$  at  $20^\circ\text{C}$

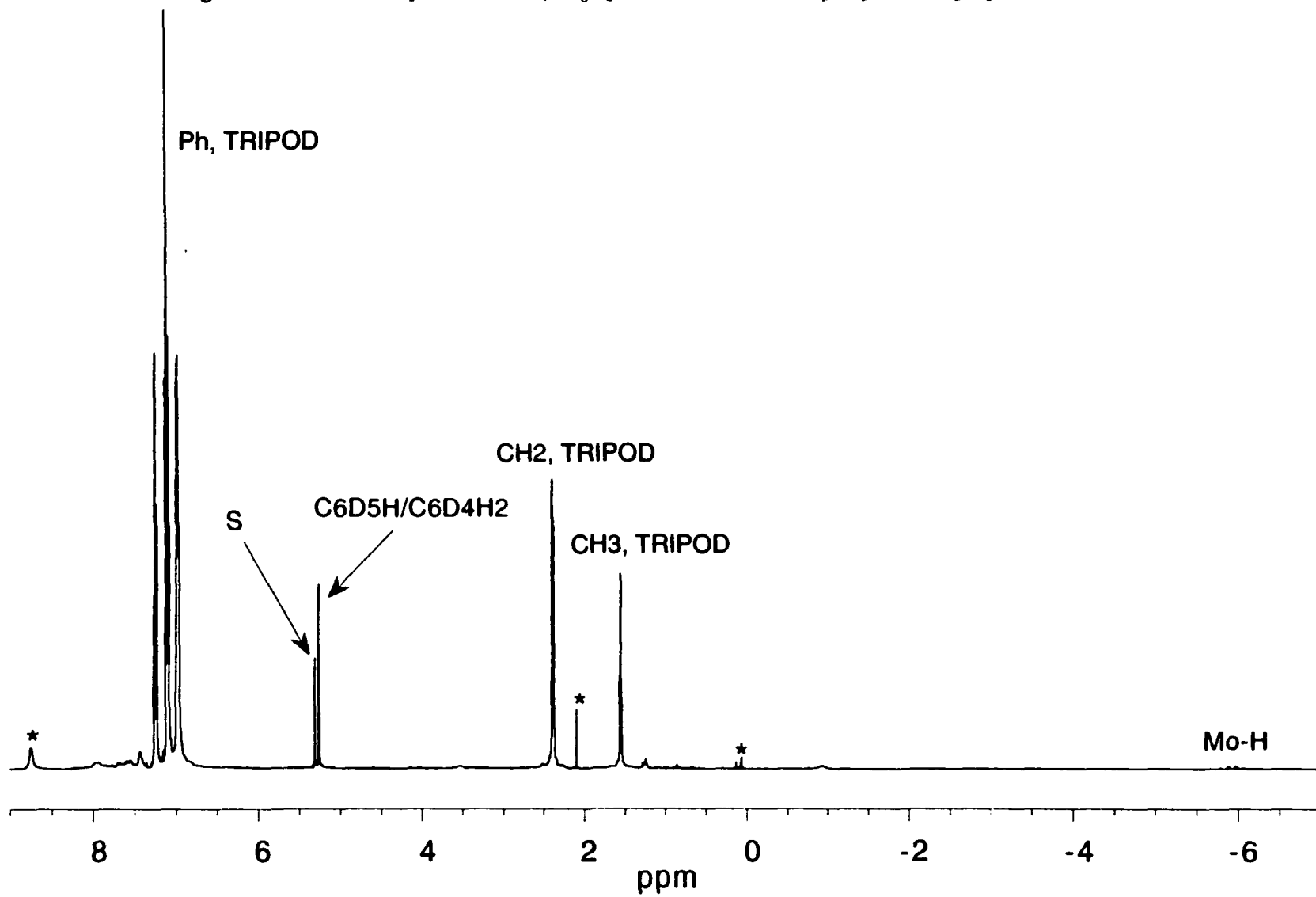


Figure 6.2.  $^2\text{H}$  NMR spectrum of  $(\eta^6\text{-C}_6\text{D}_6)\text{Mo}(\text{TRIPOD}) + \text{CF}_3\text{SO}_3\text{H}$  in  $\text{CH}_2\text{Cl}_2$  at  $20^\circ\text{C}$

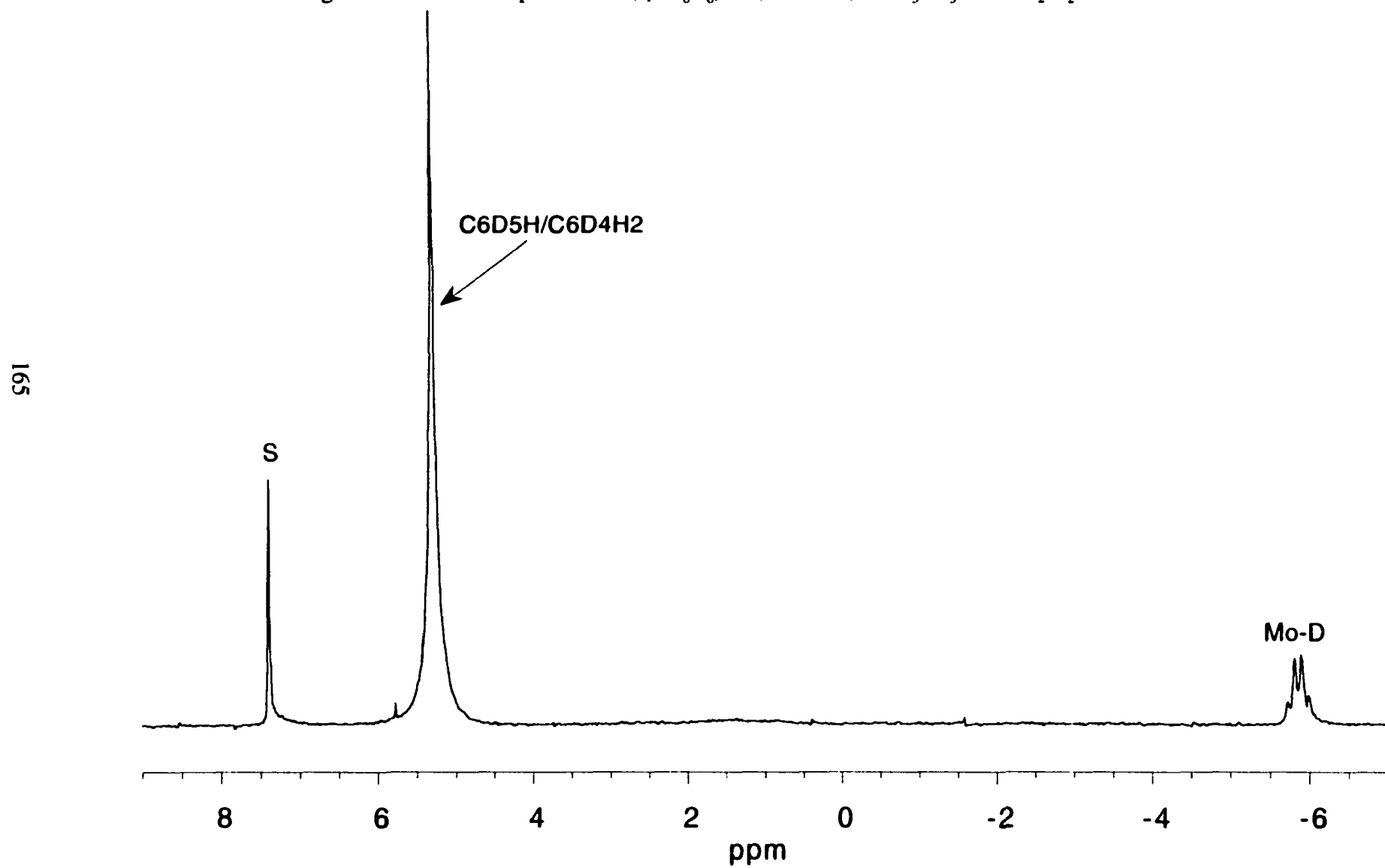


Figure 6.3.  $^1\text{H}$  NMR spectrum of  $(\eta^6\text{-C}_6\text{D}_6)\text{Mo}(\text{TRIPHOS}) + \text{CF}_3\text{SO}_3\text{H}$  in  $\text{CH}_2\text{Cl}_2$  at  $20^\circ\text{C}$

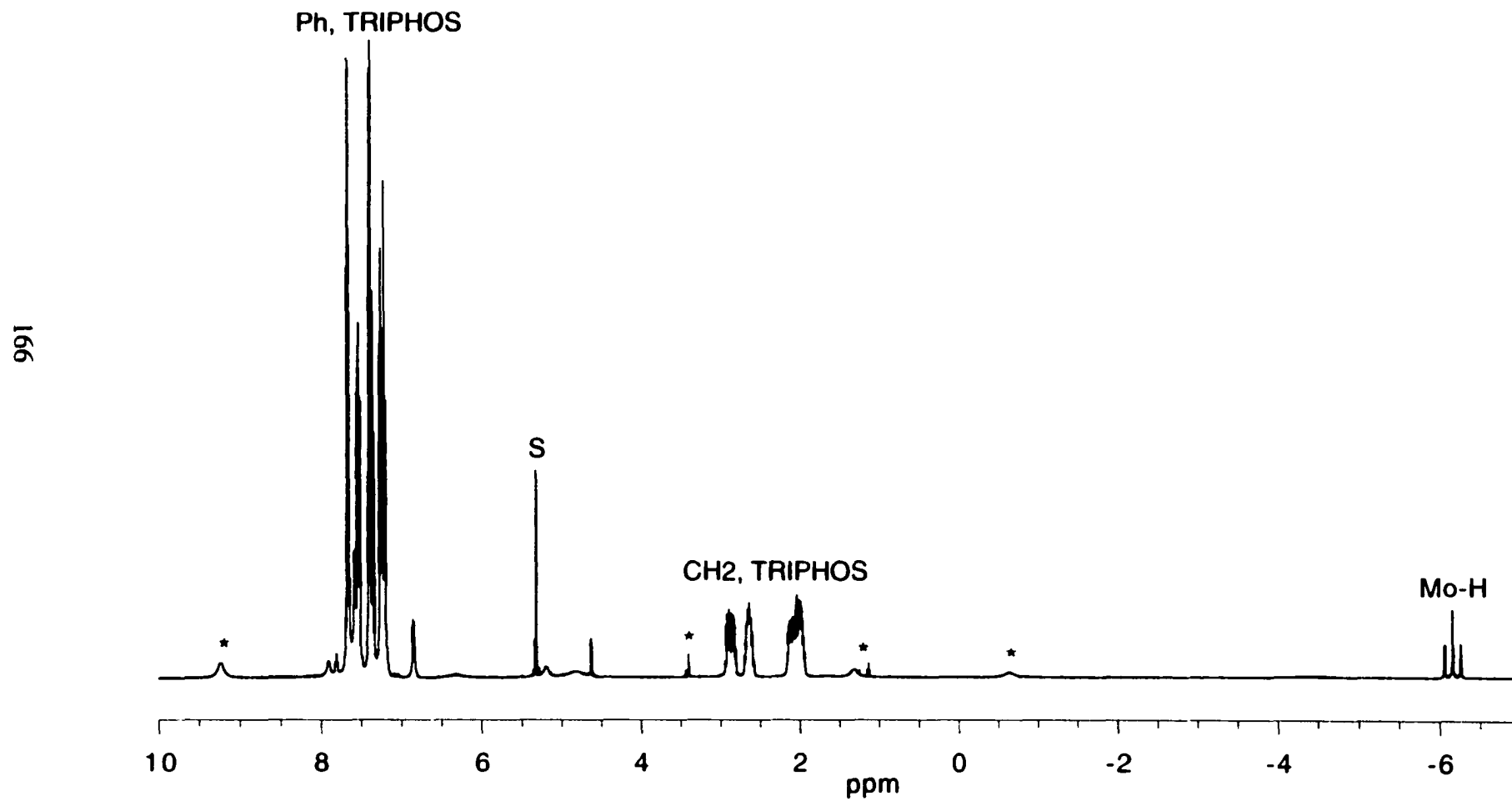


Figure 6.4.  $^3\text{H}$  NMR spectrum of  $(\eta^6\text{-C}_6\text{D}_6)\text{Mo}(\text{TRIPHOS}) + \text{CF}_3\text{SO}_3\text{H}$  in  $\text{CH}_2\text{Cl}_2$  at  $20^\circ\text{C}$

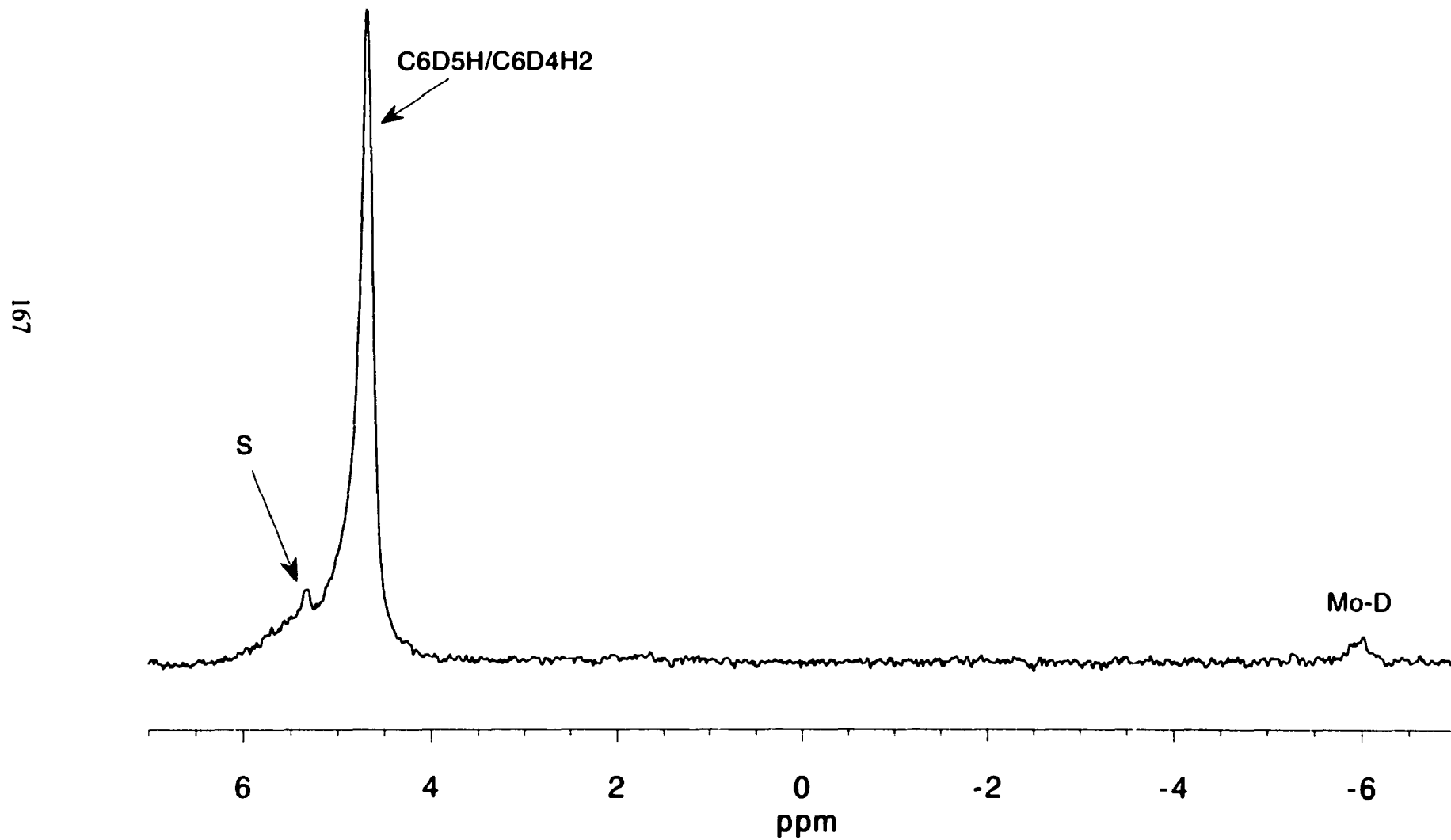


Figure 6.5.  $^{31}\text{P}$  NMR spectrum of  $(\eta^6\text{-C}_6\text{D}_6)\text{Mo}(\text{TRIPHOS}) + \text{CF}_3\text{SO}_3\text{H}$  in  $\text{CD}_2\text{Cl}_2$  at  $20^\circ\text{C}$

168

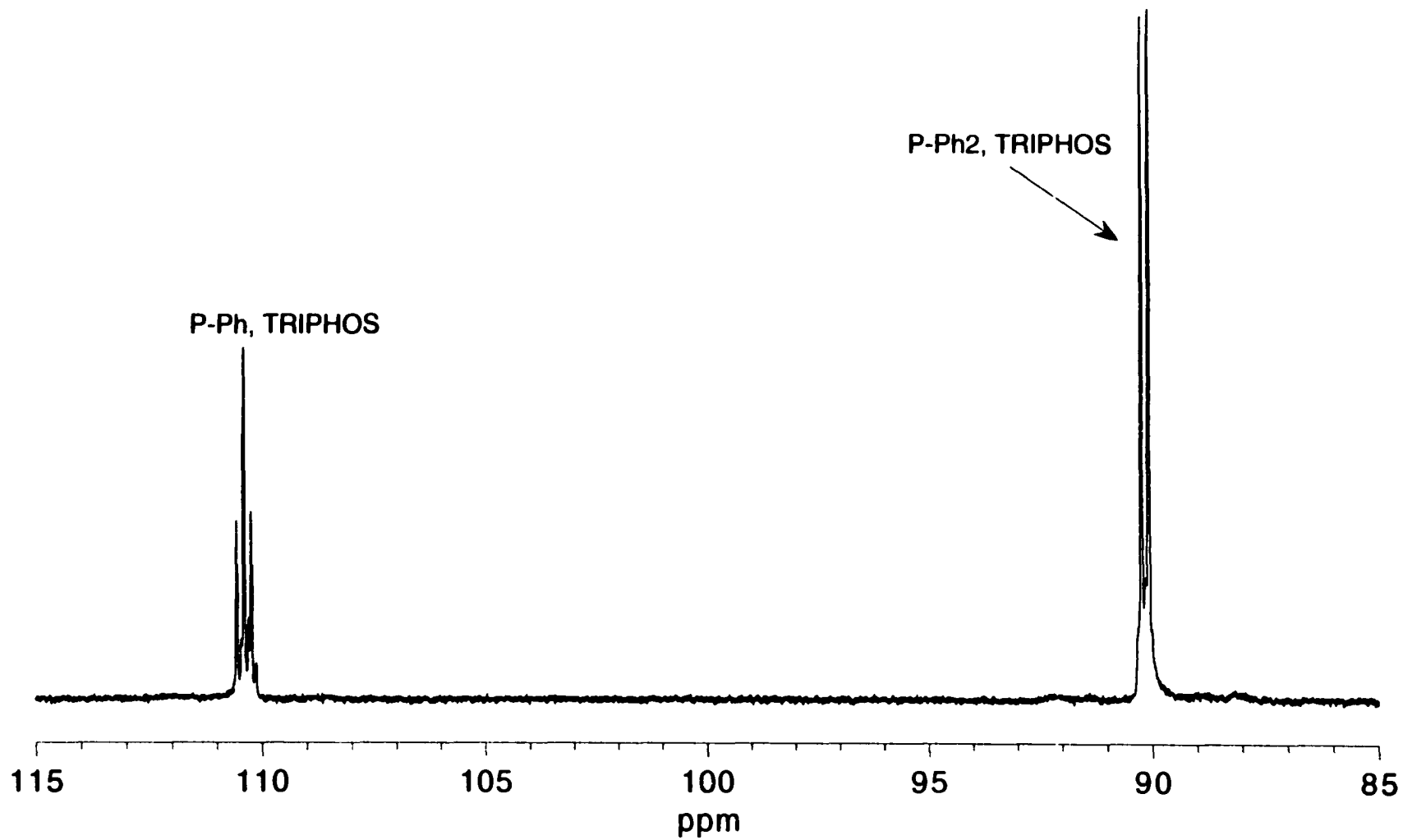


Figure 6.6.  $^1\text{H}$  NMR spectrum of  $(\eta^6\text{-C}_6\text{D}_6)\text{Mo}(\text{PPh}_2\text{Me})_3 + \text{CF}_3\text{SO}_3\text{H}$  in  $\text{CD}_2\text{Cl}_2$  at  $20^\circ\text{C}$

169

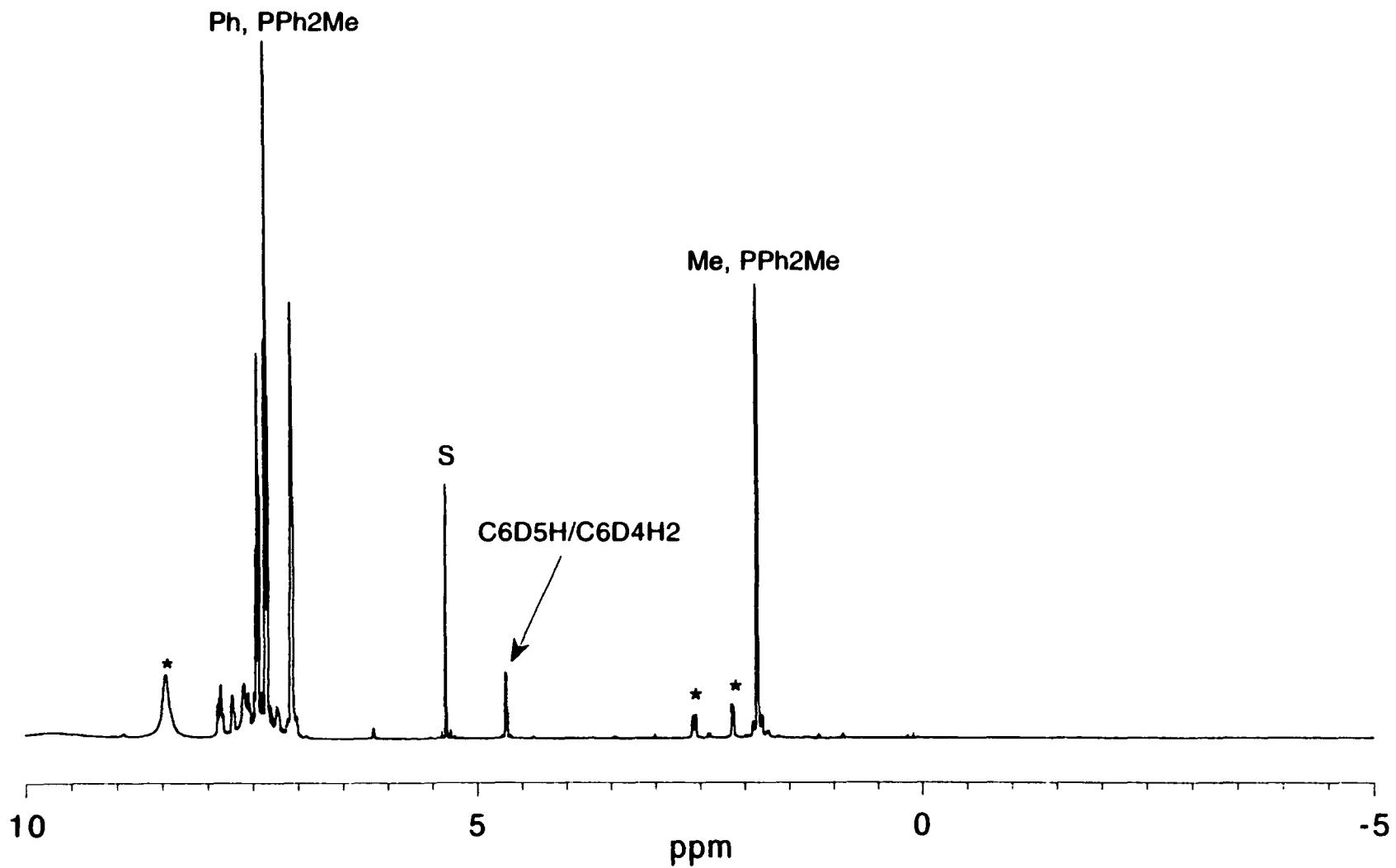


Figure 6.7.  $^2\text{H}$  NMR spectrum of  $(\eta^6\text{-C}_6\text{D}_6)\text{Mo}(\text{PPh}_2\text{Me})_3 + \text{CF}_3\text{SO}_3\text{H}$  in  $\text{CH}_2\text{Cl}_2$  at  $20^\circ\text{C}$

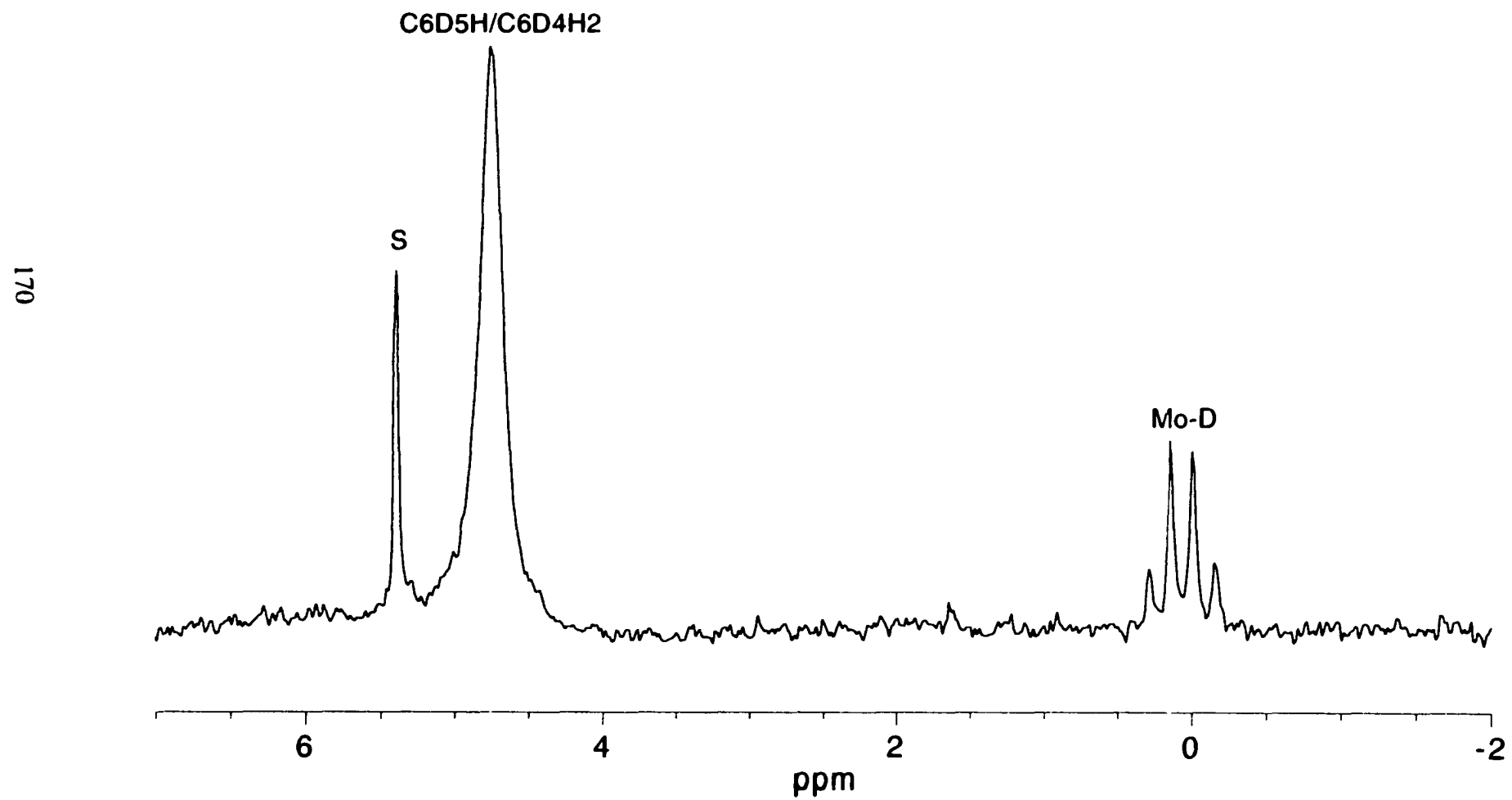


Figure 6.8.  $^1\text{H}$  NMR spectrum of  $(\eta^6\text{-C}_6\text{D}_6)\text{Mo}(\text{PMe}_2\text{Ph})_3 + \text{CF}_3\text{SO}_3\text{H}$  in  $\text{CD}_2\text{Cl}_2$  at  $20^\circ\text{C}$

171

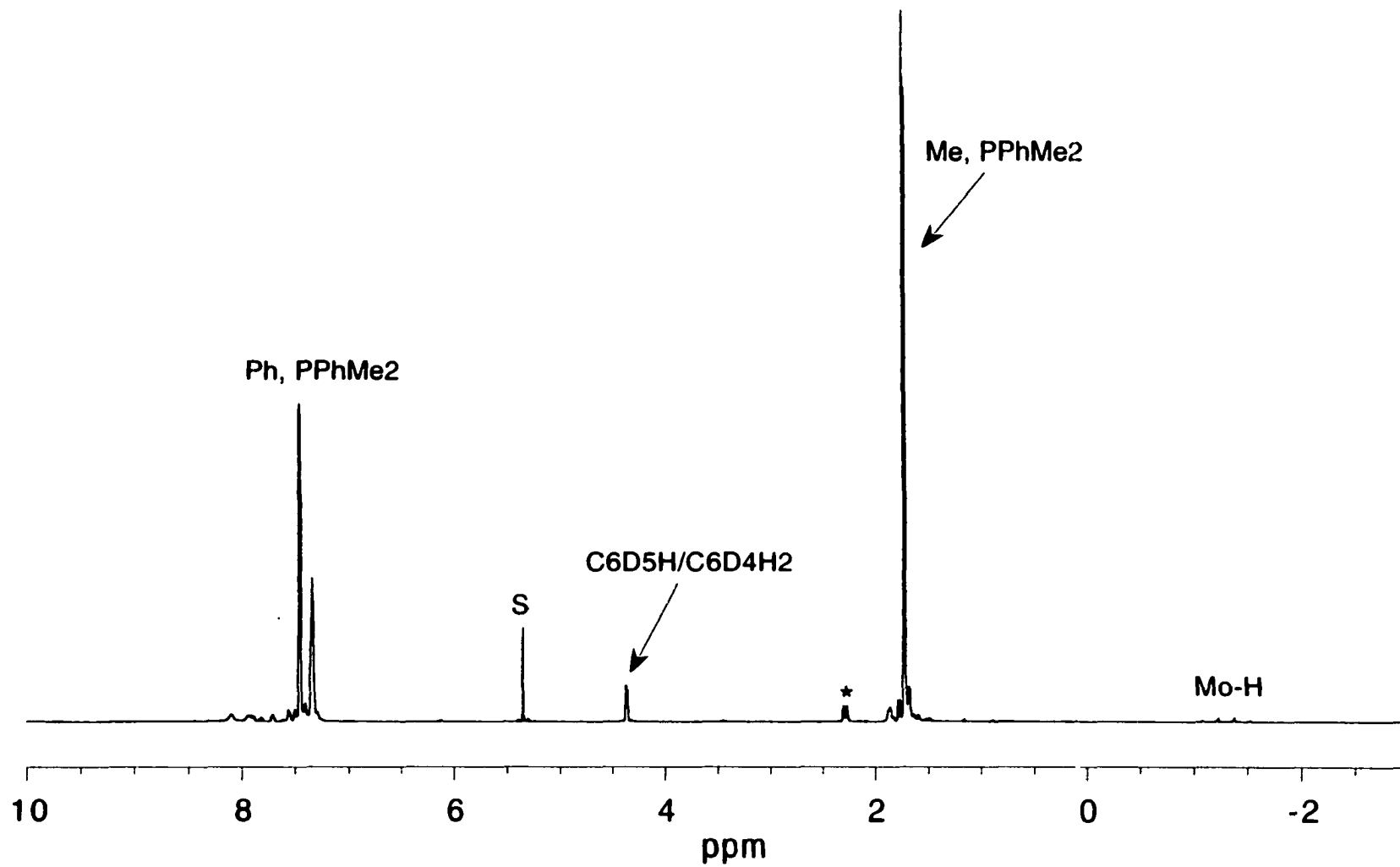


Figure 6.9.  $^2\text{H}$  NMR spectrum of  $(\eta^6\text{-C}_6\text{D}_6)\text{Mo}(\text{PMe}_2\text{Ph})_3 + \text{CF}_3\text{SO}_3\text{H}$  in  $\text{CH}_2\text{Cl}_2$  at  $20^\circ\text{C}$

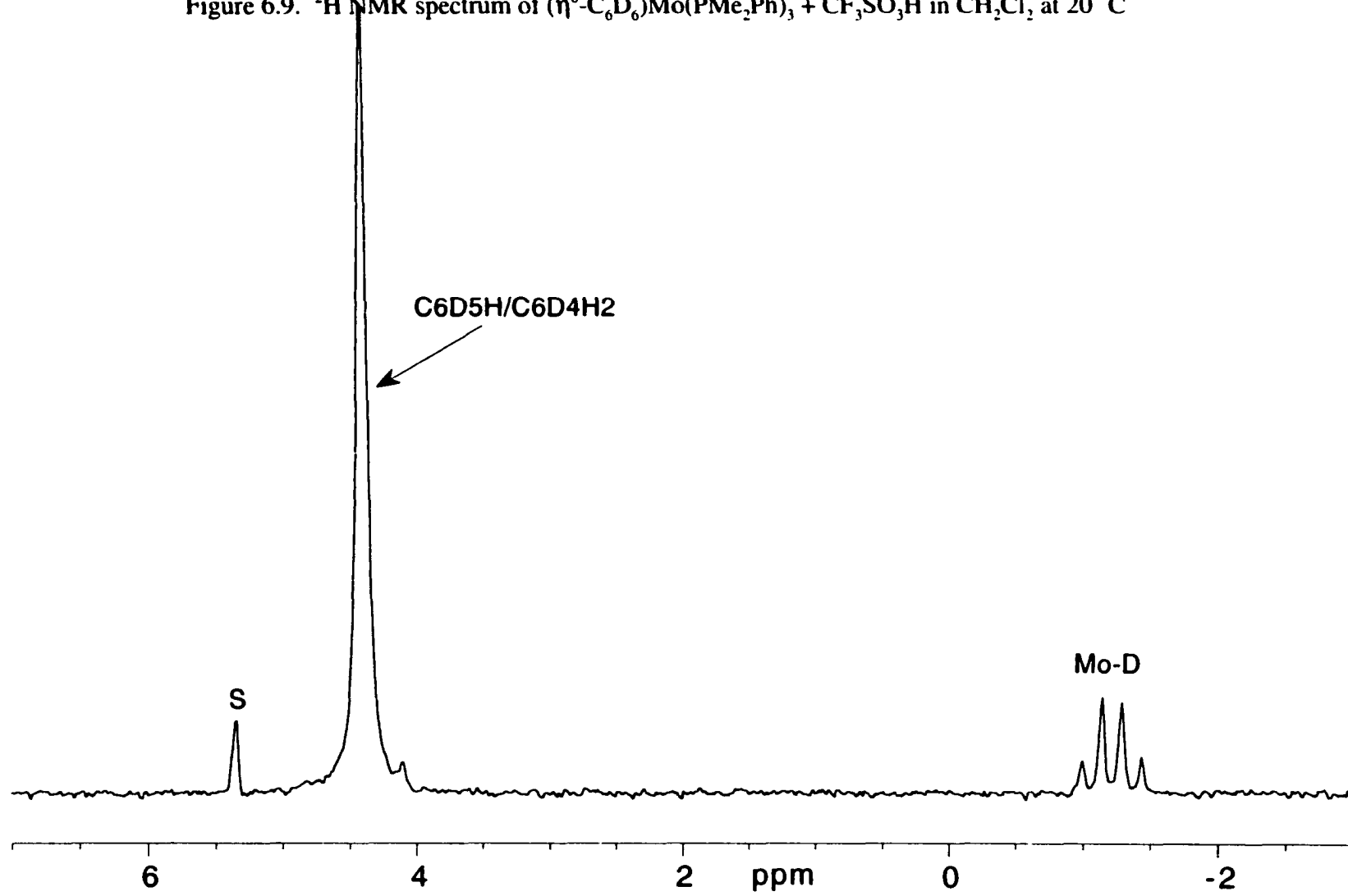


Figure 6.10.  $^1\text{H}$  NMR spectrum of  $(\eta^6\text{-C}_6\text{D}_6)\text{Mo}(\text{PMe}_3)_3 + \text{CF}_3\text{SO}_3\text{H}$  in  $\text{CD}_2\text{Cl}_2$  at  $20^\circ\text{C}$

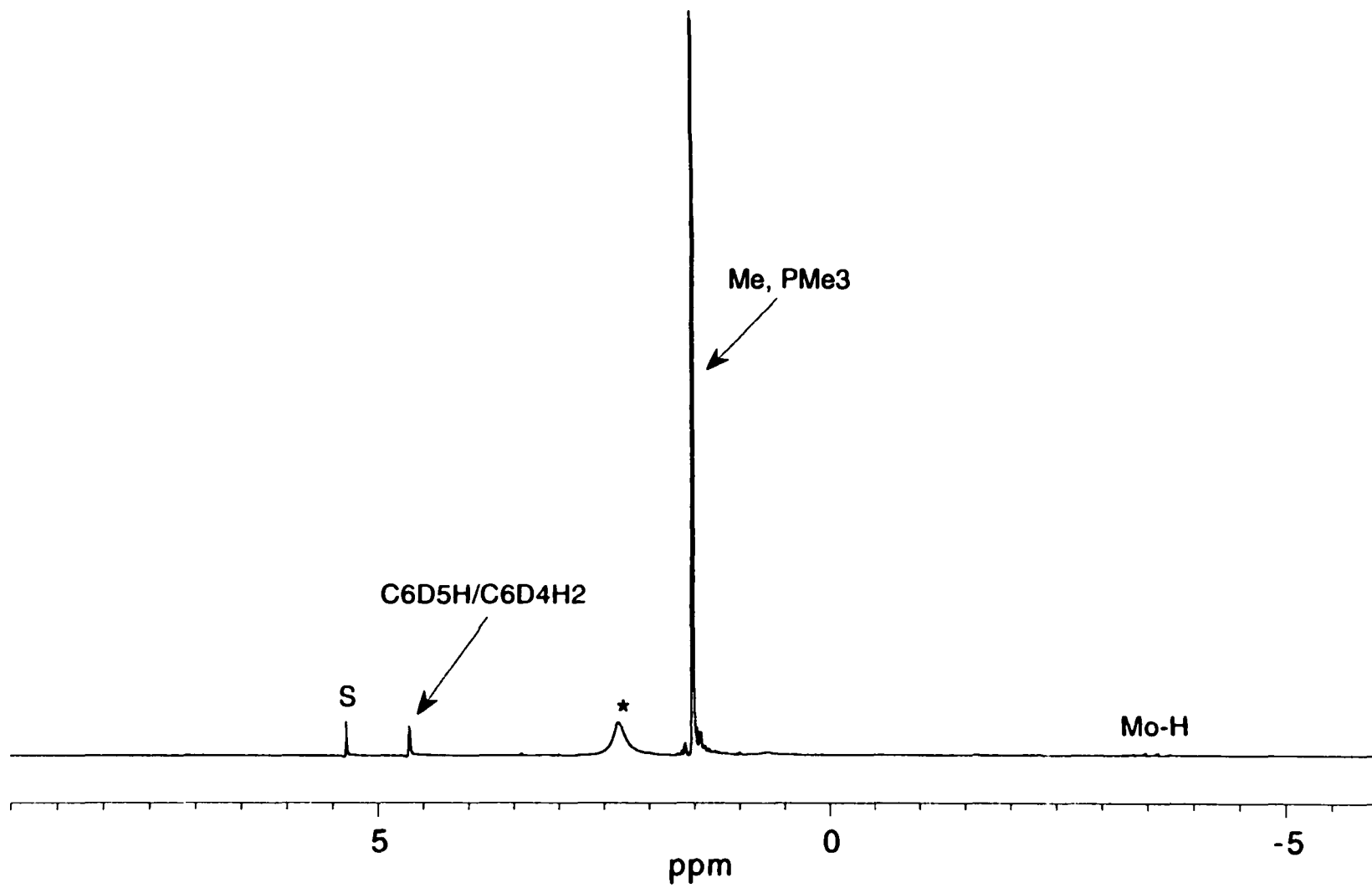


Figure 6.11.  $^2\text{H}$  NMR spectrum of  $(\eta^6\text{-C}_6\text{D}_6)\text{Mo}(\text{PMe}_3)_3 + \text{CF}_3\text{SO}_3\text{H}$  in  $\text{CH}_2\text{Cl}_2$  at  $20^\circ\text{C}$

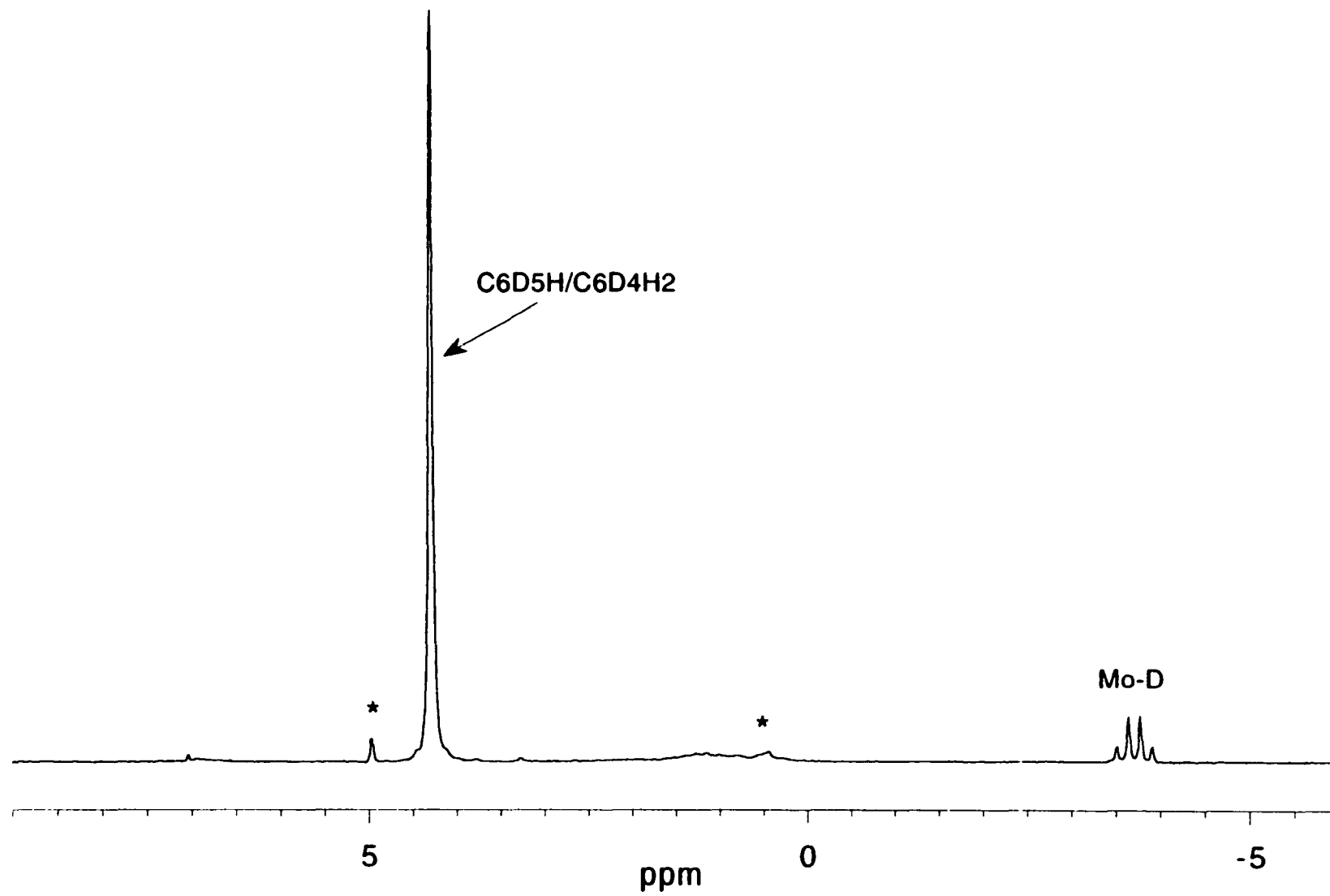


Figure 6.12.  $^1\text{H}$  NMR spectrum of  $(\eta^6\text{-C}_6\text{H}_5\text{CH}_3)\text{Mo}(\text{TRIPOD})$  in  $\text{C}_6\text{D}_6$  at  $20^\circ\text{C}$

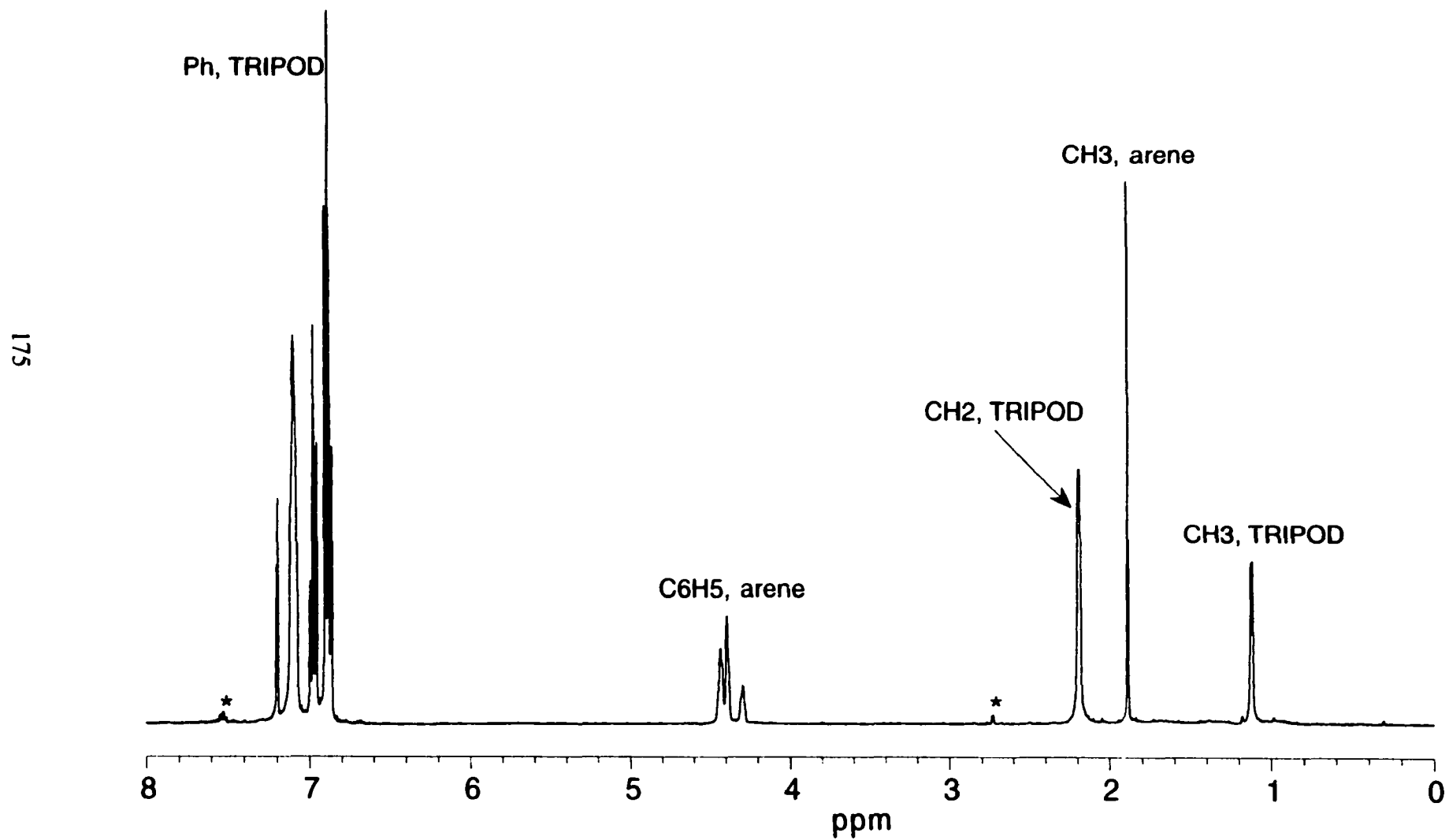
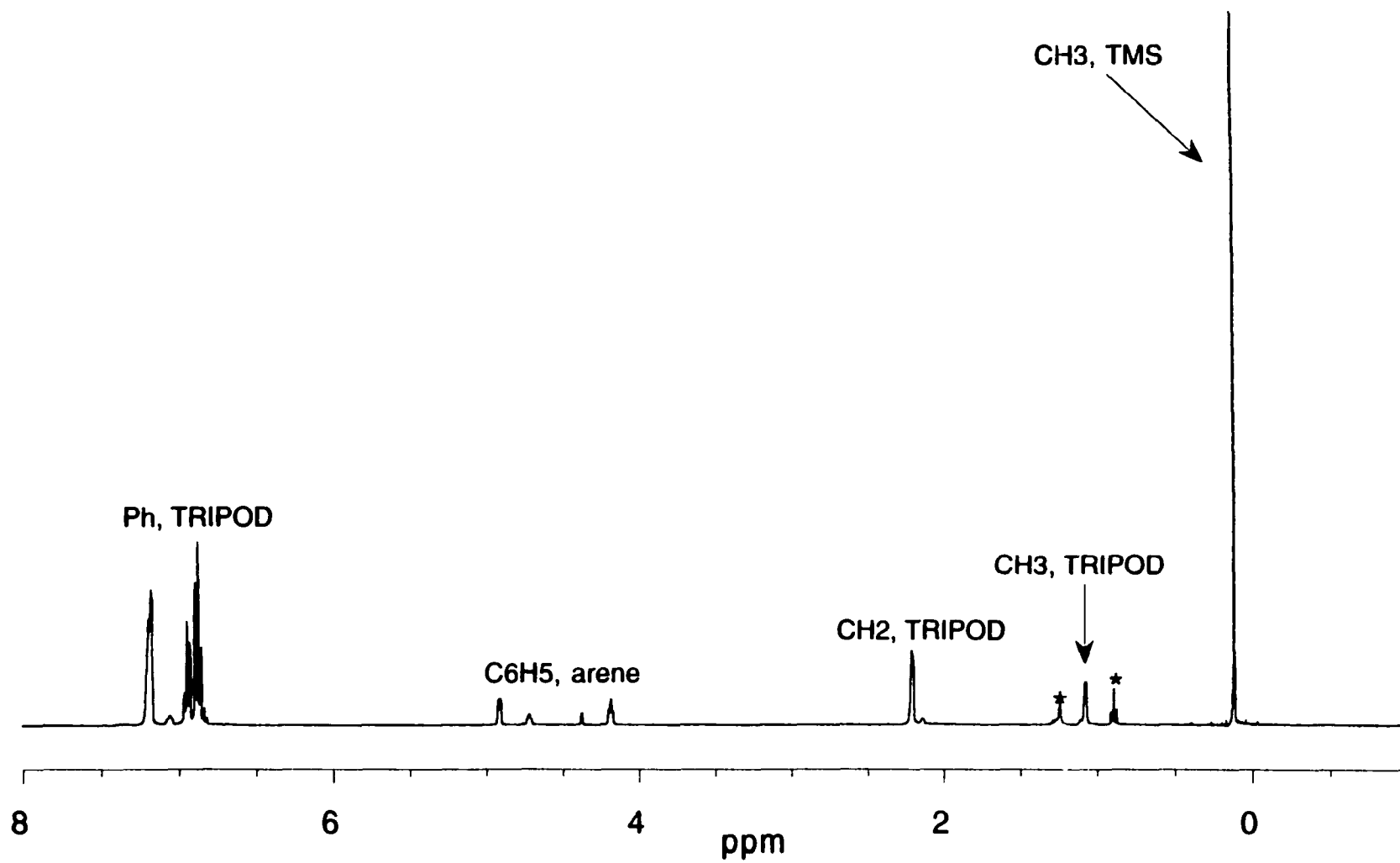


Figure 6.13.  $^1\text{H}$  NMR spectrum of  $(\eta^6\text{-C}_6\text{H}_5\text{SiMe}_3)\text{Mo}(\text{TRIPOD})$  in  $\text{C}_6\text{D}_6$  at  $20^\circ\text{C}$



## 6.5 BIBLIOGRAPHY

- (1) Nicholls, B.; Whiting, M. C. *J. Chem. Soc.* **1959**, 551-556.
- (2) Angelici, R. J. *Synthesis and Techniques in Inorganic Chemistry*; 2nd ed.; W. B. Saunders: Philadelphia, 1977.
- (3) Silverthorn, W. E. *Inorg. Synth.* **1977**, 17, 54.
- (4) Klabunde, K. J.; Timms, P. L.; Skell, P. S.; Ittel, S. D. *Inorg. Synth.* **1979**, 19, 59-86.
- (5) Herring, F. G.; Legzdins, P.; Richter-Addo, G. B. *Organometallics* **1989**, 8, 1485.
- (6) Connelly, N. G.; Geiger, W. E. *Chem. Rev.* **1996**, 96, 887.
- (7) Abragam, A.; Bleaney, B. *Electron Paramagnetic Resonance of Transition Metal Ions*; Clarendon Press: Oxford, 1970.
- (8) Mohamadi, F.; Richards, N. G.; Guida, W. C.; Liskamp, R.; Lipton, M.; Claufield, C.; Chang, G.; Hendrickson, T.; Still, W. C. *J. Comput. Chem.* **1990**, 11, 440.
- (9) Becke, A. D. *J. Chem. Phys.* **1993**, 98, 5648.
- (10) Perdew, J. P.; Wang, Y. *Phys. Rev.* **1992**, B45, 13244.
- (11) Frisch, M. J.; Trucks, G. W.; Schlegel, H. B.; Gill, W.; Johnson, B. G.; Robb, M. A.; Cheeseman, J. R.; Keith, T.; Peterson, G. A.; Montgomery, J. A.; Raghavachari, K.; Al-Laham, M. A.; Zakrzewski, V. G.; Ortiz, J. V.; Foresman, J. B.; Cioslowski, J.; Stefanov, W.; Andres, J. L.; Replogle, E. S.; Gomperts, R.; Martin, R. L.; Fox, D. J.; Binkley, J. S.; Gaussian94, Revision E.2; Gaussian, Inc.:Pittsburgh, Pa., 1995.
- (12) Chang, G.; Hendrickson, T.; Still, W. C. *J. Am. Chem. Soc.* **1989**, 111, 4379.
- (13) Allinger, N. L. *J. Am. Chem. Soc.* **1977**, 99, 8127.
- (14) Dunning, J. T., Jr.; Hay, P. J. *Methods of Electronic Structure Theory*; Schaefer, H. F., III, Ed.; Plenum: New York, 1976; Vol. 3, pp 1-27.
- (15) Hay, P. J.; Wadt, W. R. *J. Chem. Phys.* **1985**, 82, 270.
- (16) Wadt, W. R.; Hay, P. J. *J. Chem. Phys.* **1985**, 82, 284.
- (17) Hay, P. J.; Wadt, W. R. *J. Chem. Phys.* **1985**, 82, 299.

## CHAPTER 7

### CONCLUSIONS

#### 7.1 CONCLUSIONS

The mechanism of mono-protonation of  $(\eta^6\text{-C}_6\text{H}_6)\text{Mo}(\text{TRIPOD})$  (**1**) to give  $[(\eta^6\text{-C}_6\text{H}_6)\text{MoH}(\text{TRIPOD})]^+$  via a  $\eta^5$ -cyclohexadienyl intermediate was reported by Kowalski and Ashby in 1995.<sup>1</sup> The initial proton reaction at the arene though the metal is the thermodynamically favored site of protonation was a puzzle that led us to undertake this project. The basis of the protonation mechanism of **1** and related complexes was studied in detail using experimental and theoretical methods on **1**.<sup>2</sup> Our study of the electronic structure of **1** and related compounds by PES reveals that the HOMO of **1** is metal based with substantial arene character. The  $[(\eta^6\text{-C}_6\text{H}_6)\text{Mo}(\text{TRIPOD})]^+$  (**1**<sup>+</sup>) cation, the one-electron oxidized product of **1** can be generated by chemical and electrochemical methods. EPR spectra of **1**<sup>+</sup> and its deuterio derivative shows the evidence for an unpaired electron and arene hfc. The observation of arene hfc indicates that there is substantial arene character in the SOMO of **1**<sup>+</sup>. Calculations were performed on the structure and frontier orbitals of **1** and model compounds. The results of these calculations once more suggest that the frontier orbitals possess significant amount of arene character and the TRIPOD ligand is sterically demanding. The conclusion from PES, EPR, CV and computational studies is that the initial proton attack on the arene takes place at the same frontier orbital as the direct attack on the metal except on a different portion of the molecular orbital. The TRIPOD ligand, while rendering the metal electron-rich,

sterically protects the metal from direct attack by electrophiles. The necessary conditions for the proton to react at the arene are a steric protection at the metal, substantial arene character in the HOMO, and an electron rich metal center.

Unlike TRIPOD, some monodentate phosphines and other chelating phosphines do not sterically protect the metal center. This fact was verified by studying the protonation mechanism of  $(\eta^6\text{-C}_6\text{H}_6)\text{Mo}(\text{TRIPHOS})$  (**4**),  $(\eta^6\text{-C}_6\text{H}_6)\text{Mo}(\text{PMePh}_2)_3$  (**7**),  $(\eta^6\text{-C}_6\text{H}_6)\text{Mo}(\text{PMe}_2\text{Ph})_3$  (**8**), and  $(\eta^6\text{-C}_6\text{H}_6)\text{Mo}(\text{PMe}_3)_3$  (**9**).<sup>3</sup> Complexes **7**, **8**, **9** and **4** are protonated 0%, 22%, 37% and 88% respectively, at the metal. This trend was analyzed by mapping the frontier orbital of these complexes onto the surface electron density plots. The surface electron density plots were calculated from geometries obtained from crystal structures and semiempirical methods. The plots show the amount of metal electron density available for direct protonation. It is clear that steric factors play an important role in the mechanism of protonation of  $(\eta^6\text{-arene})\text{Mo}(\text{phosphine})_3$  complexes.

An effort was made to extend the mechanistic study to electrophiles other than proton. Methylation of **1** with different electrophilic reagents gives two products, the methylated and the unmethylated metal hydride complexes. Experimental conditions that minimized the likelihood of spurious proton still produced the unmethylated hydride. It is believed that the unmethylated complex is formed in the mechanism of methylation. The mechanisms of protonation and methylation appear to be different. Reactions of electrophiles such as EtI, *i*-PrI, *t*-BuI, and PhCH<sub>2</sub>Br gave a mixture of alkylated and unalkylated products, similar to methylation.  $[\text{CH}_2=\text{NMe}_2]\text{I}$  reacted with **1** to form the metal hydride complex,  $[(\eta^6\text{-C}_6\text{H}_5\text{CH}_2\text{NMe}_2)\text{MoH}(\text{TRIPOD})]\text{I}$  (**10**). Unlike the methylation reactions, only a single product is obtained in the reaction of  $[\text{CH}_2=\text{NMe}_2]\text{I}$  with **1**. Electrophiles such as Et<sub>3</sub>OBF<sub>4</sub>, Me<sub>3</sub>SiCl, CH<sub>3</sub>COCl, and CF<sub>3</sub>SO<sub>3</sub>SiMe<sub>3</sub> gave unalkylated hydride complex as the only product.

The precursors for tripodal complexes,  $(\eta^6\text{-alkylbenzene})_2\text{Mo}$  complexes, were synthesized by arene displacement reactions.<sup>4</sup> Heating  $(\eta^6\text{-C}_6\text{H}_6)_2\text{Mo}$  with C<sub>6</sub>H<sub>5</sub>R (R =

Me, Et, i-Pr, or t-Bu) at 160 °C and 0.1 torr for 48 hours gives  $(\eta^6\text{-C}_6\text{H}_5\text{R})_2\text{Mo}$ . This procedure had an advantage over the known Fischer-Hafner and metal-atom vapor methods. The limitation of Fischer-Hafner method is that the substituted benzenes are reactive in the presence of Al/AlCl<sub>3</sub>. Specialized equipment and poor yields limit the metal-atom vapor method.

Arene ring substituted derivatives of **1** were synthesized to study the effect of ring substitution in the mechanism of protonation.<sup>5</sup> Reaction of one equivalent of CF<sub>3</sub>SO<sub>3</sub>D with  $(\eta^6\text{-C}_6\text{H}_5\text{Me})\text{Mo}(\text{TRIPOD})$  (**31**) gives  $[(\eta^6\text{-C}_6\text{H}_4\text{DMe})\text{MoH}(\text{TRIPOD})]^+$  with approximately equal distribution of *ortho*, *meta*, *para* isomers. Free toluene shows a very high preference for *para* electrophilic substitution. This preference is lost in **31**, which could be due to the disruption of the  $\pi$ -cloud of the arene when attached to metal. The reaction of acid with  $(\eta^6\text{-C}_6\text{H}_5\text{SiMe}_3)\text{Mo}(\text{TRIPOD})$  (**35**) gives  $[(\text{C}_6\text{H}_6)\text{MoH}(\text{TRIPOD})]^+$  (**3**) as the only product after workup. The first equivalent of acid attacks the nucleophilic C-Si bond, cleaving it to form **1**, which in turn is protonated by another equivalent of acid to give **3**. The Si atom in **35** is reactive towards fluoride ions. The reaction of Bu<sub>4</sub>NF in aqueous THF produces **1** as a clean product. The F<sup>-</sup> ion cleaves the TMS group on the ring, which in turn is protonated by water to yield **1**.

## 7.2 FUTURE WORK

The mechanism of mono-protonation of **1** is well understood. We have made few attempts to study the di-protonation of **1**. Preliminary studies on the di-protonation mechanism suggest that the proton does not react at the ring. It appears that the second proton directly attacks the metal, possibly via  $\eta^2\text{-H}_2$  complex. The mechanistic studies have been affected by the difficulty in isolating the diprotonated species,  $[(\eta^6\text{-C}_6\text{H}_6)\text{Mo}(\text{TRIPOD})(\text{H})_2]^{2+}$ . Isolation and mechanism of the diprotonated species would be an interesting avenue to pursue.

Extension of the mechanistic study to complexes of different metals would also be interesting. The syntheses of  $(\eta^6\text{-C}_6\text{H}_6)\text{Cr}(\text{TRIPOD})$  and  $(\eta^6\text{-C}_6\text{H}_6)\text{W}(\text{TRIPOD})$  would be challenging. The synthesis of  $(\eta^6\text{-C}_6\text{H}_6)\text{Cr}(\text{TRIPOD})$  via the arene displacement route is not practical, owing to the inertness of  $(\eta^6\text{-C}_6\text{H}_6)_2\text{Cr}$  towards phosphines.  $(\eta^6\text{-C}_6\text{H}_6)\text{Cr}(\text{TRIPOD})$  may be accessible via the reduction route. Reduction of  $\text{Cl}_3\text{Cr}(\text{TRIPOD})$  in the presence of the benzene may yield  $(\eta^6\text{-C}_6\text{H}_6)\text{Cr}(\text{TRIPOD})$ . Tungsten complexes can be synthesized by the arene displacement procedure but the precursor synthesis is challenging.  $(\eta^6\text{-arene})_2\text{W}$  complexes are commonly prepared by the metal-atom vapor procedure.<sup>6,7</sup> The limitations to the syntheses of  $(\eta^6\text{-arene})_2\text{W}$  complexes are very high melting point of tungsten and very poor yields. The study could be extended to include complexes of metals such as titanium, vanadium and niobium as well.

### 7.3 BIBLIOGRAPHY

- (1) Kowalski, A. S.; Ashby, M. T. *J. Am. Chem. Soc.* **1995**, *117*, 12639-12640.
- (2) Asirvatham, V. S.; Gruhn, N. E.; Lichtenberger, D. L.; Ashby, M. T. *Organometallics* **2000**, *19*, 2215-2227.
- (3) Ashby, M. T.; Asirvatham, V. S.; Kowalski, A. S.; Khan, M. A. *Organometallics* **1999**, *18*, 5004-5016.
- (4) Asirvatham, V. S.; Ashby, M. T. *J. Chem. Soc. Chem. Commun.* accepted with revision
- (5) Asirvatham, V. S.; Khan, M. A.; Ashby, M. T. *manuscript in preparation*
- (6) Green, M. L. H.; Hughes, A. K.; Lincoln, P.; Martin-Polo, J. J.; Mountford, P.; Sella, A.; Wong, L.-L.; Bandy, J. A.; Banks, T. W.; Prout, K.; Watkin, D. J. *J. Chem. Soc., Dalton Trans.* **1992**, 2063-2069.
- (7) Fischer, E. O.; Scherer, F.; Stahl, H. O. *Chem. Ber.* **1960**, *93*, 2065-2074.